UNIVERSITY OF KWAZULU-NATAL

PLASMODIUM YOELII ACETYL-COA CARBOXYLASE: DETECTION AND CHARACTERISATION OF THE RECOMBINANT BIOTINOYL DOMAIN

IKECHUKWU A. ACHILONU

2008

PREFACE

The experimental studies described in this thesis was carried out in the Department of Biochemistry, School of Biochemistry, Genetics and Microbiology, University of KwaZulu-Natal, Pietermaritzburg from August 2004 to June 2008 under the supervision of **Prof. J. P. D. Goldring**. These studies represent original work by **Ikechukwu A. Achilonu** and have not been submitted in any other form to another University. Where use was made of the work by other authors it has been duly acknowledged in the text.

_____	_____
Ikechukwu A. Achilonu	Prof. J. P. D. Goldring
June 2008	June 2008

ABSTRACT

Human malaria, caused by four species of the intracellular protozoan parasite *Plasmodium*, is a major health and economic burden in the tropics where the disease is endemic. The biotin-dependent enzyme acetyl-CoA carboxylase catalyses the commitment step in *de novo* fatty acid biosynthesis in several organisms. Acetyl-CoA carboxylase is a target for anti-parasitic drug development due to its relevance in membrane biogenesis. This study describes the detection of acetyl-CoA carboxylase and the partial characterisation of the biotinoyl domain of the enzyme of the mouse malaria parasite, *Plasmodium yoelii*.

Acetyl-CoA carboxylase mRNA was detected by RT-PCR performed on total RNA isolated from *P. yoelii* 17XL-infected mouse erythrocytes using primers designed from PY01695 ORF of the Plasmodb-published MALPY00458 gene of *P. yoelii* 17XNL. The RT-PCR was confirmed by sequencing and comparative analysis of the sequenced RT-PCR cDNA products. Northern blot analysis performed on total RNA using probes designed from a 1 kb region of the gene showed that the transcript was greater than the predicted 8.7 kb ORF.

An immunogenic peptide corresponding to the *P. yoelii* theoretical acetyl-CoA carboxylase sequence was selected using epitope prediction and multiple sequence alignment algorithms. The immunogenic peptide was coupled to rabbit albumin carrier for immunisation in chickens and the affinity purified antibody titre was approximately 25 mg. The anti-peptide antibodies detected a 330 kD protein in *P. yoelii* lysate blot, which corresponds to the predicted size of the enzyme. The enzyme was also detected *in situ* by immunofluorescence microscopy using the anti-peptide antibodies.

A 1 kb region of the *P. yoelii* acetyl-CoA carboxylase gene containing the biotinoyl domain was cloned and expressed in *E. coli* as 66 kD GST-tag and 45 kD His-tag protein. Both recombinant biotinoyl proteins were shown to contain bound biotin using peroxidase-conjugated avidin-biotin detection system. This suggested *in vivo* biotinylation of the recombinant *P. yoelii* biotinoyl protein, possibly by the *E. coli* biotin protein ligase.

The Proscan™ and the NetPhos 2.0™ algorithms were used to predict protein kinase phosphorylation sites on the biotin carboxylase and the carboxyltransferase domains of the enzyme. The three-dimensional structure of the biotinoyl and the biotin carboxylase domains were predicted using the SWISS-MODEL™ homology modelling algorithm. Homology

modelling revealed a similarity in the 3D conformation of the predicted *P. yoelii* biotinoyl domain and the *E. coli* biotinoyl protein with negligible root mean square deviation. The model also revealed the possibility of inhibiting *P. yoelii* and *falciparum* acetyl-CoA carboxylases with soraphen A based on the similarity in conformation with *S. cerevisiae* biotin carboxylase and the stereochemical properties of the residues predicted to interact with soraphen A.

This study demonstrated that malaria parasite expresses acetyl-CoA carboxylase and, combined with data on other enzymes involved in fatty acid metabolism suggests that the parasite synthesizes fatty acids *de novo*. This enzyme could be a target for rational drug design.

ACKNOWLEDGMENTS

It is accomplished. Over 1.84×10^6 min of hard work in the lab, yet I still feel strong enough to do it all over again. It was not entirely my strength, but also the strength of those who laboured with me, even without knowing it. They were my source of inspiration and hope, and I will always remain grateful to them. I would like to extend my heartfelt thanks to the following people and organisations for their supports, encouragement and prayers for making this doctoral study possible.

Professor Dean Goldring, my supervisor and teacher, for giving me the freedom to work and develop my knowledge of science independently with the appropriate "controls". I deeply appreciate his enormous contribution to this study.

The **National Research Foundation** of South Africa, and University of KwaZulu-Natal **Special PhD Research Funds**, for their financial support.

Mematsepang Sephula, for her motherly role in my life as a student. I will always remain indebted to her for her financial support and encouragement.

Professor Theresa Coetzer, for her invaluable support, hospitality and guide to producing chicken antibodies used for this study. **Dr Alain Boulangé**, for his assistance in molecular biology techniques and wonderful entertainments.

Mum and **Dad**, your prayers and moral guidance, especially from the early stages of life have brought me through to where I am and the man I have become today. To my auntie, **Mrs. Moteane**, for her love, care and moral support.

Many colleagues enriched my life in the lab and stirred pleasurable working environments: **Mulinge**, it all began with your guide during my first ever PCR, thank you. **Bridgette,** for your help with reading some of my manuscripts and your good thoughts about my family. **Ramona,** for all the tasteful cups of coffee you made me and moment well spent. **Dave,** for providing me with recombinant *P. yoelii* copper transporter expression construct used for this study. **Phillia**, thanks for your care (even though you conceal it) and for "pinching" my marking pens. **Jacky**, for your hospitality and assistance when fetching egg from Ukulinga.

Davita and **Hlumani *"Pichia"* Ndlovu**, for your assistance with yeast expression studies. **Kangethe**, thank you for providing me with *Trypanosoma* RNA that was used for this study. **Yegan**, for your technical assistance, moral support and wonderful dinners. **Lorelle**, **Perina**, **Titos**, **Hermógenes**, **Mayuri** and **Cara**, I wish you guys all the best in your search for accomplished life in science, no matter how rough the road it may appear.

I did not spend all my time in the lab: I shared wonderful times with my friends and house mates at 71 St. Patricks road. **Fabian**, **Mehari**, **Irene**, **Terence**, **Kwesi** and **Brunhilda** thank you for the company and hilarious moments I shared with you guys. The quest for academia brought us together; I wish you guys the best in all your life's endeavour.

My brothers, **Chinonyerem**, **Chidozie** and **Chibunna**. I am forever grateful to God for having you guys around me. To all the students and staff of the School of Basic Studies Lesotho, I owe lots of appreciation to you.

CONTENTS

LIST OF TABLES

LIST OF FIGURES

ABBREVIATIONS AND SYMBOLS

3D	three dimensions
Å	Ångström unit (1 Ångström unit = 0.1 nm)
$A_{280\ nm}$	absorbance at 280 nm
ABC	ATP-binding cassette
ABTS	2, 2-azino-di-[3-ethylbenzthiazoline sulfonate]
ACP	acyl carrier protein
amp	ampicillin
AMPK	5'AMP-activated protein kinase
AT-rich	deoxyadenosine and deoxythymidine nucleotide-rich
BC	biotin carboxylase
BCCP	biotin carboxyl carrier protein
BLAST	basic local alignment search tool
bp	base pair
BSA	bovine serum albumin
cam	chloramphenicol
cDNA	copy DNA
CoA	Co-enzyme A
CoASH	Co-enzyme A-sulfhydryl
COO^-	carboxylate anion
CT	carboxyltransferase
C-terminal	carboxylic acid terminal
Da	dalton
DAPI	4', 6-diaminido-2-phenylindole
ddH_2O	deionised-distilled water
DDT	dichloro-diphenyl-trichloroethane
DEPC	diethylpyrocarbonate
dH_2O	distilled water
DMF	*N, N*-dimethylformamide
DMSO	dimethyl sulfoxide
DNA	deoxyribonucleic acid
dNTP	deoxynucleotide triphosphate
DTT	dithiothreitol

EC	enzyme commission
ECL	enhanced-chemiluminescence
EDTA	ethylenediamine-tetra-acetic acid
ELISA	enzyme-linked immunosorbent assay
FAS	fatty acid synthase
FCA	Freund's complete adjuvant
FIA	Freund's incomplete adjuvant
FITC	fluorescein isothiocyanate
FSB	frozen stock buffer
g	relative gravitational force
GST	glutathione s-transferase
GTE	glucose-Tris-EDTA
h	hour
HMW	high molecular weight
HRPO	horseradish peroxidase
IC_{50}	50% inhibitory concentration
IgG	immunoglobulin G
IgY	immunoglobulin Y
IPTG	isopropyl β-D-1-thiogalactopyranoside
kan	kanamycin
KAS	keto acyl carrier protein synthase
kb	kilobase
kD	kilodalton
kJ/mol	kilojoules per mole
LB	lysogeny broth
LSU	large subunit
mA	milliampere
MALDI-TOF	matrix-assisted laser desorption/ionization-time of flight
MBS	m-maleimidobenzoyl-*N*-hydroxysuccinimide ester
MCS	multiple cloning site
MEC	molecular exclusion chromatography
-mer	monomeric or monomer
MKM	methionine-lysine-methionine tripeptide
mRNA	messenger RNA

Mw	molecular weight
MWCO	molecular weight cut off
NCBI	National Centre for Biotechnology Information
NHS-biotin	*N*-hydroxysuccinimide-biotin
nm	nanometer
nM	nanomolar
NMR	nuclear magnetic resonance
N-terminal	amino terminal
OD	optical density
ORF	open reading frame
PAGE	polyacrylamide gel electrophoresis
pBLAST	protein-BLAST
PBS	phosphate buffered saline
PCR	polymerase chain reaction
PDB	Protein Data Bank
PEG	polyethylene glycol
PKA	protein kinase A
PKC	protein kinase C
PKG	protein kinase G
pLDH	*Plasmodium* lactate dehydrogenase
PMSF	phenymethylsulfonyl fluoride
pRBC	parasitised-red blood cell
PVDF	polyvinylidine fluoride
PyACC	*P. yoelii* acetyl-CoA carboxylase
PyBCCP	*P. yoelii* biotin carboxyl carrier protein (refers to the recombinant proteins)
RBC	red blood cells
RDT	rapid diagnostic test
RMSD	root mean square deviation
RNA	ribonucleic acid
rpm	revolution per minute
rRNA	ribosomal RNA
RT	room temperature (~ 25°C)
RT-PCR	reverse transcriptase-PCR
SAP	shrimp alkaline phosphatase

SDS	sodium dodecyl sulfate (or sodium lauryl sulfate)
SH	sulfhydryl
spdbv	SWISS-PDB viewer
SSC	saline sodium chloride
SSU	small subunit
TAE	Tris-acetate-EDTA
Taq	*Thermus aquaticus*
TBS	Tris-buffered saline
TCA	tricarboxylic acid
TEMED	*N, N, N', N'*-tetramethyl ethylene diamine
THS	Tris-buffer Hank's balanced salt solution
T_m	melting temperature
TPP	thiamine pyrophosphate (or thiamine diphosphate)
tRNA	transfer RNA
™	trademark
UKZN	University of KwaZulu-Natal
UTR	untranslated region
UV	ultraviolet
V	volts
v/v	volume per volume
w/v	weight per volume
WHO	World Health Organization
X-gal	5-bromo-4-chloro-3-indolyl-β-D-galactopyranoside
ε-amine	epsilon-amine
µl	microlitre
µm	micrometre
µM	micromolar
ϕ	phi
ψ	psi
ω	omega

CHAPTER 1
INTRODUCTION AND LITERATURE REVIEW

1.1 An overview of malaria

Malaria is caused by hematoprotozoa parasites of the genus *Plasmodium*. It is transmitted by the bite of the female anopheles mosquito. Four species of the *Plasmodium* parasite infect man namely: *Plasmodium falciparum, P. vivax, P. ovalae* and *P. malariae*. These four species show different clinical manifestations (Maegraith 1968; White 1992; Gilles 1997; Nosten *et al*. 1999). Generally malaria infections are characterised by fever, headache painful joints and weakness (Gilles, 1997; Van den Ende and Van Gompel, 1997; White, 1992). The majority of mortal cases of malaria in humans are caused by *falciparum* malaria and 1 – 2% of patients infected with *Plasmodium falciparum* die as a result of the infection. The major complications of a *falciparum* infection are cerebral malaria and placental malaria, often resulting in coma and pregnancy complications, respectively (Gilles, 1997; Hunt *et al*., 2006; Van den Ende and Van Gompel, 1997; White, 1992). 90% of the world malaria cases occur in the sub-Saharan regions of Africa. At the moment, clinical cases of malaria in the world are approaching 500 million infections and over 5 million deaths per year. More than three quarter of the deaths from the disease are infants below five years (McKean, 2002; WHO, 2003; WHO, 2005b). The symptoms of malaria appear about 9 to 14 days after a bite from an infected mosquito. In the absence of drug treatment, the infection can progress rapidly to become severe. Malaria parasites infect and destroy red blood cells causing anaemia and obstruct the blood capillaries by sequestering and attaching to the endothelial cells that carry blood to vital organs and the brain causing cerebral malaria (Gilles, 1997; Hunt *et al*., 2006; Van den Ende and Van Gompel, 1997; White, 1992). Malaria caused by the other species infecting humans is rarely fatal. *Plasmodium vivax* and *Plasmodium malariae* infections often reoccur if not properly treated. There are several drugs available to cure malaria. A major hindrance in malaria chemotherapy is drug resistant parasites. Quinine based drugs are commonly available and are still effectively used to treat the disease in malaria endemic regions of the world (Goldring *et al*., 1999; Gregson and Plowe, 2005; Menting *et al*., 1997; Wainwright and Amaral, 2005). The disease has a major economic impact in countries where it is endemic. It is estimated that an average of 1.3% is lost in annual economic growth due to reduced

productivity in countries where the disease is endemic (Sachs and Malaney, 2002; Sachs, 2002; WHO, 2003; WHO, 2005b).

1.2 Geographical distribution of human malaria

Figure 1.1 shows the geographical distribution of malaria in the world. Most malaria occurs between the Tropic of Cancer (latitude 23.5º North) and the Tropic of Capricorn (23.5º South). Infection is often seasonal with peak infections occurring during the rainy season when mosquitoes, the parasite vector, reproduce at an elevated rate. There are also cases of malaria outside these latitudes in Southern Africa, New Delhi (India) and in the Northern parts of Africa (WHO, 2003; WHO, 2005a; WHO, 2005b). Malaria is highly endemic in West Africa and Central Africa especially around the Congo basin. Most malaria cases in these parts of Africa are chloroquine resistant (WHO, 2005b). There are sparse cases of malaria infections in parts of Kenya's Rift valley that were previously thought to be too high above sea level for malaria transmission. Scientists believe that this may be because of human migration and climatic changes (WHO, 2003; WHO, 2005b).

Malaria is wide spread in other parts of the world including Asia, South America, Central America and Southern Mexico. Drug resistant *Plasmodium falciparum* is present in parts of Cambodia, Myannmar, Thailand and Laos (Rietveld and Kouznetsov, 1997; WHO, 2003; WHO, 2005b). *Plasmodium vivax* infection is also prevalent in these areas. Malaria has been eradicated in the Caribbean but there were reports of an outbreak of *falciparum* malaria in Haiti (Rietveld and Kouznetsov, 1997). The malaria eradication programmes of the 1940's and 1950's combined with widespread use of screening methods have proved to be successful in eliminating the disease in North America and Europe. However, human migration remains the possible threat to malaria eradication in the non-malaria regions of the world (Rietveld and Kouznetsov, 1997).

1.3 Treatment and management of malaria

The approaches currently being used in the treatment and management of malaria are vector control and anti-malarial drugs. Vector control has been successful over the years in controlling and managing malaria all over the world. In North America, malaria was eradicated in the 50s through the use of insecticides such as DDT (dichloro-diphenyl-trichloroethane) (Curtis and

Mnzava, 2000; Teklehaimanot *et al.*, 2007). In developing countries, the use of DDT has not being as successful as in North America. However, the use of household insecticides, insecticide-treated bed nets and removal of stagnant water around the house has been quite a success over the years (Curtis and Mnzava, 2000). In malaria endemic regions of Africa, homes are built with mosquito screens to prevent mosquitoes entering the building. The use of DDT has been discouraged and discontinued due to the environmental impact of this compound (Curtis and Mnzava, 2000).

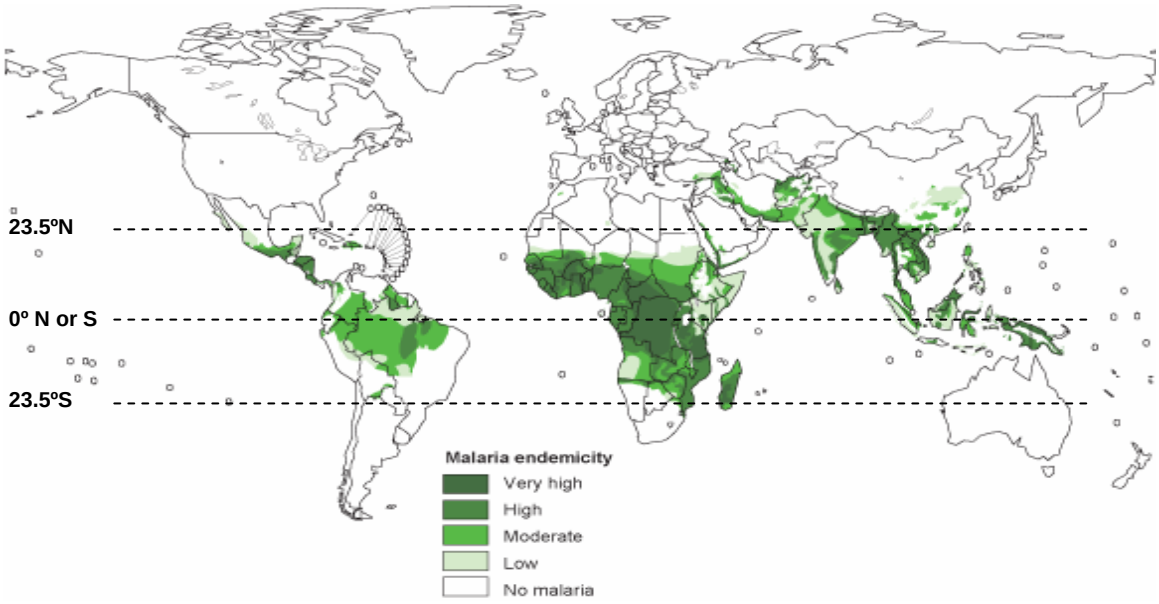

Figure 1.1 Geographical distribution of malaria. The broken lines represent the tropic of Cancer (23.5ºN), the equator (0ºN or S) and the tropic of Capricorn (23.5ºS). The area of dense malaria infection in Africa is between the tropics (Sachs, 2002; WHO, 2005b).

Malaria cases in South Africa are limited to regions below 1000 m above sea levels such as the Limpopo province, Mpumalanga province and the north-east of KwaZulu-Natal (RSA, 2004). The transmission of malaria in South Africa is seasonal just as in many malaria endemic regions. The transmission rate is believed to be minimal during the winter and dry seasons. Three drug regimes are currently recommended in South Africa namely: mefloquine (taken on weekly basis), doxycycline (taken on daily basis) and chloroquine (taken on weekly basis). Several

organizations have been set up by the health ministry to combat the disease, a web-based awareness site such as www.malaria.org.za and research funding institutions such as the South African Malaria Initiatives (SAMI, http://www.acgt.co.za/sami/) are part of governmental approach towards management of malaria in South Africa and the rest of Africa.

The use of drugs in the treatment of malaria dates back to 1891 when the dye, methylene blue [3, 7-bis (dimethylamino)-phenothiazinium chloride] was used to treat malaria infections (Brasseur *et al*., 1999; Gregson and Plowe, 2005; Wainwright and Amaral, 2005). This dye was initially used as a biological stain to stain DNA (Pearson, 1972). Although the precise mechanism of action of the dye was not understood, methylene blue and its analogue were predominantly used as malaria chemotherapy in the early days of malaria treatments (Färber *et al*., 1998). Since the discovery of anti-parasitic effects of methylene blue, the use of drugs to treat malaria infection has become wide spread and has proved to be very effective in controlling the disease (Wainwright and Amaral, 2005; White, 1992; White *et al*., 1999). Thus, case management relies only on the use compounds such as chloroquine, artemesinin, and pyrimethamine. Some of these drugs are cheap and widely available in malaria endemic regions. Chloroquine and quinoline derivatives are believed to inhibit the parasite's polymerisation of toxic heme to non-toxic hemozoin (Monti *et al*., 1999; Pandey *et al*., 1999). Quinine has also been found to be effective in reducing the expression of monocyte surface receptors to which malaria infected erythrocytes adhere to (Goldring and Nemaorani, 1999).

A major impediment in anti-malaria chemotherapy is the improper use of drugs against malaria infections (Peters, 1974; Peters, 1998; Ridley, 2002; White, 2004; White *et al*., 1999). This problem is very common in malaria endemic regions and has resulted in selection pressure on the human malaria parasite to develop resistance mechanisms to most anti-parasitic drugs (Gregson and Plowe, 2005; Menting *et al*., 1997; Wainwright and Amaral, 2005). The increase in malaria mortality amongst children in these regions is due to the evolution of drug resistant parasites. Chloroquine resistant strains of *Plasmodium vivax* and *falciparum* are predominant in some malaria endemic regions (Gregson and Plowe, 2005; Ridley, 2002; White, 2004; White *et al*., 1999). An effective strategy used to combat chloroquine-resistant malaria is through the use of combination of drugs to treat malaria cases (Wainwright and Amaral, 2005; White, 2004; White

et al., 1999). An example is the use of mefloquine (a quinoline derivative)-amodiaquine combination or sulfadoxine-pyrimethamine combination. There has not been any reported case of artimesinin-resistant *Plasmodium*; thus artemesinin has proved to be the best clinical choice to treat malaria cases (Brasseur *et al*., 1999; Goldring and Nemaorani, 1999).

1.4 The life cycle of malaria parasites

Malaria is transmitted through the bite of the female anopheles mosquito during a blood meal as illustrated in Figure 1.2. The insect picks up the parasite in the blood of an infected human. In the gut of the mosquito, the parasite reproduces sexually undergoing several morphological changes. The parasite migrates to the salivary glands of the mosquito (Matteelli *et al*., 1997; Meis and Verhave, 1988). The mosquito introduces the parasite back into humans during another blood meal. Therefore the *Plasmodium* parasite life cycle spans between human (and other malaria susceptible animals) and mosquito. In a single mosquito bite, approximately twenty sporozoites enter the human blood stream and immediately migrate to the liver (Matteelli *et al*., 1997; Meis and Verhave, 1988). The sporozoite will pass through several hepatocytes and eventually settling in just a single hepatocyte. This begins the liver stage of the parasite life cycle, which is also known as the pre-erythrocytic stage. The sporozoites develop into schizonts. In human malaria, the pre-erythrocytic stage varies between species. In *P. falciparum*, the pre-erythrocytic stage lasts 5 – 6 days post infection. The schizonts rupture the liver cell releasing the merozoites into the blood stream. The merozoites invade the red blood cells to start the erythrocytic stage. The clinical symptoms and pathology of malaria is experienced at this stage of the parasite life cycle (Gilles, 1997; Van den Ende and Van Gompel, 1997; White, 1992).

Most anti-malaaria drugs target the erythrocyte stage (Macreadie *et al*., 2000; Ridley, 2002; Wainwright and Amaral, 2005). The entry into the blood stream by merozoites is of immunological significance because the merozoites are exposed to the immune system and antibodies before invading new red blood cells (Maegraith, 1968; Matteelli *et al*., 1997). Once in the red blood cell, the merozoites begin a period of replicative asexual cycle in the erythrocytes. The merozoite transforms into the ring, trophozoite, and schizont stages. The time taken to go through these transformations varies between the different species of the *Plasmodium* parasites; 48 h for *P. vivax* and *P. falciparum*, 50 h for *P. ovalae* and 72 h for *P. malariae* (Matteelli *et al*.,

1997). The schizonts burst the erythrocytes and invade new erythrocytes or transform into gametocytes. The gametocytes taken up by mosquito during blood meal undergo fertilization in the gut of the mosquito to begin the insect stage of the parasite life cycle (Matteelli *et al*., 1997).

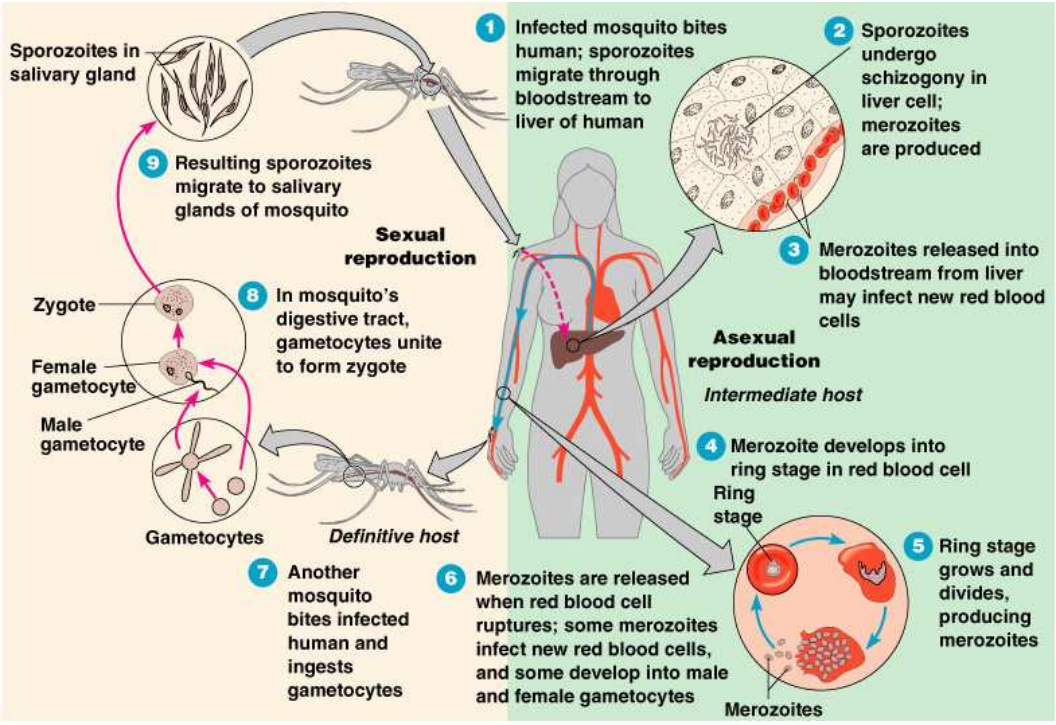

Figure 1.2 Life cycle of the *Plasmodium* parasite. The light brown portion on the figure represents the insect stage of the cycle and the light green portion represents the mammalian stage of the cycle. *Adapted from Pearson Education Inc. (2004). Published by Benjamin Cummings*

1.5 Diagnosis of malaria

Proper management of malaria cases is based on the accuracy of diagnosis of the disease. Most mortality cases are as a result of late and imprecise diagnosis of malaria (Bell and Peeling, 2006; Bell *et al*., 2006; Moody, 2002; Moody and Chiodini, 2002; Tomar *et al*., 2006). The gold standard for the detection and therefore diagnosis of malaria is the use of the light microscope to detect the blood stage of the parasite (Moody and Chiodini, 2002; Tomar *et al*., 2006). The red blood cells are not nucleated in mammals and so will not be stained by nucleic acid dyes such as methylene blue and azure-B. However, the presence of the parasite in the red blood cells will

result in the staining of the parasite in the red blood cell due to the parsite's nucleic acids. This method still remains the most accurate and standard serological method to detect and diagnose the disease. The method still faces numerous challenges such as ability to differentiate the infecting *Plasmodium* species and the lack of trained microscopists in malaria endemic regions (Moody, 2002; Moody and Chiodini, 2002).

These problems resulted in the development of immunochromatographic-based detection (Bell and Peeling, 2006; Moody, 2002; Moody and Chiodini, 2002) techniques called RDTs (rapid diagnostic tests). These techniques are quite easy and straight forward to use with very rapid results and it requires less technically qualified personnel. The most commonly available RDT is based on *Plasmodium* lactate dehydrogenase (pLDH), an enzyme that is relatively highly expressed by the parasite at the blood stage of the cycle for the parasite energy metabolism. Using immobilized and enzyme-labelled antibody directed against recombinant pLDH, the presence of pLDH could be detected for the diagnosis of malaria. The drawbacks of RDTs are false positive, false negative results and the short shelf life of the detection kit (Banoo *et al*., 2006; Bell and Peeling, 2006; Bell *et al*., 2006; Chiodini *et al*., 2007). Storage conditions have proved to be very important to the proper functioning of the detection kit and hence accurate diagnosis of the disease. This has been a subject of concern in impoverished malaria endemic regions of the world (Chiodini *et al*., 2007). Another approach towards antibody-mediated diagnosis employs the use of antibody directed against a synthetic peptide derived from a *Plasmodium* protein. Synthetic peptides deduced from molecules such as histidine-rich protein and lactate dehydrogenase have been used for the production of anti-peptide antibodies (Tomar *et al*., 2006). These antibodies are used in ELISA format to detect the presence of the native protein in the sera of infected patients.

Most recently, a quantitative real time PCR-based detection technique has been developed based on conserved nucleotide sequences on the *Plasmodium* 18S ribosomal RNA for detection of broad spectrum malaria infection as well as species-specific 18S ribosomal RNA for specie-specific detection (Bell and Ranford-Cartwright, 2002; Coleman *et al*., 2006). By using primers corresponding to conserved as well as specie-specific regions on the 18S subunit of the ribosomal RNA gene, a mixed infection and/or infection by particular specie of *Plasmodium* could be

diagnosed by PCR amplification (Bell and Ranford-Cartwright, 2002; Bell *et al*., 2006; Coleman *et al*., 2006; Mens *et al*., 2006).

1.6 The influence of the *Plasmodium* genomics projects on antimalarial drug discovery

The *Plasmodium* parasite's metabolic pathways were revealed after sequencing the genome of *P. falciparum* strain 3D7 and partial sequencing of other species of *Plasmodium.* Approximately 14% of the predicted proteins in the *P. falciparum* strain 3D7 genome were identified as enzymes and thus were assigned Enzyme Commission numbers (Gardner, 1999; Gardner *et al*., 2002a; Ginsburg, 2006; Kooij *et al*., 2006). It was envisaged that due to the AT richness of the genome some redundant proteins may be involved in unknown metabolic pathways (Ginsburg, 2006; Kooij *et al*., 2006). This may be due to the evolutionary distance between the parasite and other organisms whose genomes are well characterized. The analysis of the *P. falciparum* strain 3D7 genome revealed that the parasite possesses the metabolic "machinery" for a functional glycolytic pathway. There is no functional gluconeogenic pathway because genes coding for enzymes such as fructose bis-phosphatase and absence of trehalose, glycogen and storage forms of carbohydrate involved in this pathway were not identified in the parasite (Gardner, 1999; Gardner *et al*., 2002a; Gardner *et al*., 2002b). The genes coding for the enzymes of the TCA cycle were identified. However, it is not clear whether the TCA cycle performs the complete oxidation of products of glycolysis (Gardner, 1999; Gardner *et al*., 2002a; Gardner *et al*., 2002b). Genes coding for fatty acid biosynthesis in the *Plasmodium* parasite were identified. The ability of the parasite to carry out *de novo* fatty acid biosynthesis has been a subject of debate (Gardner, 1999; Gardner *et al*., 2002a; Gornicki, 2003). This will be discussed in full in Section 1.12.

The spread of drug resistant malaria strains requires the development of more effective anti-malaria drugs that the parasite cannot build up resistance to. The hunt for more effective anti-malaria drugs has been enhanced by the complete sequencing of the *P. falciparum* genome (Hammarton *et al*., 2003; Macreadie *et al*., 2000; Olliaro and Yuthavong, 1999). Functional genomics and a proteomics approach are currently applied in the validation of new anti-*Plasmodium* drug targets. Several synthetic and natural products have been screened for potential use to treat malaria. There are three major categories in which potential drugs against malaria parasites can be classified; they are (i) drugs targeting the cell cycle and signal transduction (ii)

drugs targeting the biochemical processes of the digestive food vacuole and (iii) drugs targeting macromolecular and metabolite biosynthesis (Di Girolamo *et al*., 2005; Ginsburg, 2006; Hoffman *et al*., 1998). Potential candidates for drug targets must be actively involved in the life cycle of the parasite and must differ significantly from the homologue of the host. There must be no salvage pathway to circumvent the inhibition of the target. The target must have low potential for resistance development and must be involved in committed and rate limiting biochemical processes (Hammarton *et al*., 2003; Macreadie *et al*., 2000; Olliaro and Yuthavong, 1999). Chloroquine, artemesisnin and quinine are inhibitors of hemozoin biosynthesis; an important detoxification pathway of the *Plasmodium* parasite (Monti *et al*., 1999; Pandey *et al*., 1999). Pyrymethamine, cycloguanyl and sulfonamide drugs inhibit folate biosynthesis. In the apicoplast, the proposed site of fatty acid synthesis, triclosan, thiolactomysisn and fosimidomysin inhibits fatty acid elongation pathways in other apicomplexan parasites. Therefore these drugs may be active against the malaria parasite (Perozzo *et al*., 2002; Surolia *et al*., 2004; Surolia and Surolia, 2001; Waller *et al*., 2003).

By and large, the complex nature of the *Plasmodium* life cycle has resulted in the slow identification of anti-*Plasmodium* drug targets. A good number of available anti-malaria drugs are against asexual blood stage of the parasite life cycle. The logical explanation to this is that most severe pathological conditions of malaria infection are experienced during the asexual life cycle of the parasite (Van den Ende and Van Gompel, 1997). The accessibility of the blood stage and the relative ease to which the asexual blood stage could be grown *in vitro* in laboratory cultures makes this stage very attractive for drug intervention studies. There are several approaches to target the hepatic stage of the parasite life cycle; especially in relapsing malaria. The transition by the parasite from asexual to sexual stage also has the potential for drug intervention (Hammarton *et al*., 2003; Olliaro and Yuthavong, 1999).

1.7 Overview apicomplexa fatty acid biosynthesis

Apicomplexa are parasitic protists that constitute a broad phylum of protozoa including *Plasmodium*, *Theileria*, *Babesia*, *Cryptosporidium* and *Toxoplasma*; which cause a wide range of infections in animals. They have a non-photosynthetic chloroplast-like organelle called the apicoplast or plastid (Carter *et al*., 1998; Gleeson, 2000; Menard, 2007; Ralph *et al*., 2004a;

Ralph *et al*., 2004b; Wilson, 2002). The origin of this organelle is not well understood, however, there is a general belief that the plastid in apicomplexa resulted from an evolutionarily distant endosymbiotic event (Carter *et al*., 1998; Gleeson, 2000; Ralph *et al*., 2004a; Ralph *et al*., 2004b). This event is postulated to be a sequence of endocyotosis that began by a cyanobacterium endocytosed by a eukaryote to form a common ancestor of modern day algae such as dinoflagellates. A second endocytosis occurred by an apicomplexa ancestor engulfing a photosynthetic eukaryote that previously engulfed a cyanobacterium (Carter *et al*., 1998; Gleeson, 2000; Ralph *et al*., 2004a; Ralph *et al*., 2004b). Studies have shown that a homology exists between the ORF of the plasmodial plastid genome and the plastid of red algae (Ralph *et al*., 2004a; Ralph *et al*., 2004b; Wilson, 2002). There is a difference of opinion on the number of membranes of a single plastid in an apicomplexan. Some authors stipulated that a plastid in *Plasmodium* is two (Carter *et al*., 1998; Gleeson, 2000; Ralph *et al*., 2004a; Ralph *et al*., 2004b) while others believe that the number is greater than two (Waller *et al.*, 2000).

The apicoplast of *Plasmodium* parasites comprises of a highly reduced genome made up of 68 genes on a 35 kb circular DNA (Gardner *et al*., 2002a) and has been shown to contain genes coding for ribosomal RNA, transfer RNA and RNA proteins. The *Plasmodium* plastid contains genes for approximately 17 ribosomal proteins, 16S ribosomal RNA, 23S ribosomal RNA, transfer RNAs, RNA polymerase and several proteins. This suggests that the apicoplast plastid is able to carry out protein synthesis (Gleeson, 2000; Ralph *et al*., 2004b; Wilson, 2002). Although not all genes necessary for protein synthesis are present in the plastid genome. The gene coding for ribosomal protein S9, vital for protein synthesis, is not present in the *Plasmodium* plastid genome but encoded in its nuclear genome (Ralph *et al*., 2004b; Wilson, 2002). Initially the function of the apicoplast was not well understood. After the sequencing of the *P. falciparum* genome, several apicoplast targeted genes and proteins were discovered to be related to fatty acid metabolism. Due to the evolutionary origin of the apicoplast, the organelle presents a range of metabolic pathways that differ significantly from the metabolic pathways of the host (Ralph *et al*., 2004b). In addition to apicoplast targeted proteins, ~ 551 nuclear encoded proteins may be targeted to the apicoplast based on bioinformatics and laboratory based studies. About 60% of the putative apicoplast-targeted proteins have no defined biological functions when compared to other organisms. This suggests that the apicoplast may possess unknown specialised functions

that could be unique to the apicomplexa parasites (Gardner *et al*., 2002a; Ralph *et al*., 2004b). Therefore the apicoplast offers numerous proteins and metabolic pathways that can be targeted for anti-parasitic chemotherapy (Gornicki, 2003; Hanada *et al*., 2002; Perozzo *et al*., 2002; Waller *et al*., 2003). By and large the plastid is believed to be involved in protein metabolism, haem biosynthesis, fatty acid metabolism, synthesis of essential amino acids, electron transport and isoprenoid biosynthesis (Gardner *et al*., 2002a; Gleeson, 2000; Ralph *et al*., 2004a; Ralph *et al*., 2004b; Zuegge *et al*., 2001).

Fatty acids in most biological systems are synthesised by two distinctly but related *de novo* fatty acid synthase (FAS) pathways namely; the Type I FAS pathway and the Type II FAS pathway. The Type I FAS is a large multifunctional enzymes with five enzyme domains found in the cytosol of fungi and other eukaryotic organism where it catalyses reactions of fatty acid chain elongation. The Type II FAS consist of separate and monofunctional enzymes. The chain initiation and elongation reaction of the Type II FAS is catalysed by discrete enzymes namely acyl carrier protein (ACP), β-ketoacyl-ACP synthase, β-ketoacyl-ACP reductase, β-hydroxyacyl-ACP dehydrase and enoyl-ACP reductase. This enzyme complex is found in bacteria and plant plastids (Gardner *et al*., 2002a; Ralph *et al*., 2004b). The *Plasmodium* genome encodes the genes for Type II fatty acid synthase (FAS).

The apicoplast was earlier proposed to be an organelle for fatty acid biosynthesis in apicomplexan parasites after the enzyme compenents of Type II FAS enzymes were identified in the organelle (Prigge *et al*., 2003; Ryall *et al*., 2003; Waller *et al*., 2003). This postulate was later strengthened after the *Plasmodium* genome was sequenced. These findings aroused early belief that the *Plasmodium* parasite is capable of *de novo* Type II fatty acid biosynthesis. Enzymes such as acyl carrier protein (ACP) and β-keto ACP synthase III are localized in the first chromosomes of the *Plasmodium* genome to be sequenced. These proteins have an N-terminal leader peptide targeted to the apicoplast. Similar observations were made in *Toxoplasma gondii* (Gardner *et al*., 2002a; Surolia and Surolia, 2001). Pyruvate present in the apicoplast of *Plasmodium falciparum* is thought to be the precursor of acetyl-CoA; the substrate that initiates *de novo* fatty acid synthesis. The pyruvate could have been formed from imported phosphoenolpyruvate by pyruvate kinase (Ralph *et al*., 2004b). Previous studies have demonstrated that *P. falciparum*

synthesises acyl carrier protein (ACP), β-keto ACP synthase III and malonyl-CoA of the Type II fatty acid synthase complex (Prigge *et al*., 2003), thus capable of initiating fatty acid biosynthesis *in vivo*. Figure 1.3 illustrates an overview of the proposed fatty acid biosynthesis pathway in apicomplexa parasites. The phosphoenolpyruvate is produced in the cyotosol by glycolysis and transported into the plastid through a membrane-bound phosphoenolpyruvate transport protein (Gleeson, 2000; Günther *et al*., 2007; Ke *et al*., 2000a; Ralph *et al*., 2004b).

The phosphoenol pyruvate is converted to pyruvate by the pyruvate dehydrogenase complex. Pyruvate is an important source of carbon in plastid fatty acid biosynthesis in plants (Ke *et al*., 2000a; Ke *et al*., 2000b; Ohlrogge *et al*., 2000). The plastid pyruvate dehydrogenase complex has evolutionary relationship with cyanobacteria. The cynobacteria-like pyruvate dehydrogenase complexes have been localised in *P. falciparum* and *Toxoplasma gondii*. Although *P. falciparum* seem to lack mitochondrial pyruvate dehydrogenase, the parasite does have mitochondrial-targeted subunits of keto-acid dehydrogenase and α-ketoglutarate dehydrogeanse complex (Ralph *et al*., 2004b; Waller *et al*., 2003). The pyruvate dehydrogenase complex is made up of four distinct subunits namely: E1α, E1β, E2 and E3. All enzymes and cofactors of the pyruvate dehydrogenase complex have been established to be present in the apicoplast of *P. falciparum* (Gardner *et al*., 2002a). Lipoic acid is synthesised from an octanoyl-ACP precursor by the enzyme lipoic acid synthase (LipA). A homologue of LipA is targeted to the apicoplast of the *P. falciparum* genome. Lipoic acid is attached to the E2 subunit of the pyruvate dehydrogenase complex to form a transient lipoic acid-E2 complex; a process catalysed by lipoate-protein ligase (LipB). LipB is found in both the mitochondria and plastid. In *P. falciparum*, LipB contains the apicoplast signal peptide, suggesting that the enzyme may be targeted to the apicoplast. In the next step, an acetyl group is attached to the lipoic acid-E2 complex; this is catalysed by E1-thyamine pyrophosphate complex (E1-TPP). The acetyl group is attached to coenzyme A (CoA) to form acetyl-CoA. The CoA is synthesised from dephospho-CoA by an enzyme called dephospho-CoA kinase. Other sources of CoA in the *Plasmodium* parasite are glycerol-phospholipid and sphingolipid pathways. The acetyl-CoA enters the *de novo* biosynthesis of fatty acids (Mitamura and Palacpac, 2003; Ralph *et al*., 2004b) where it is converted to malonyl-CoA by acetyl-CoA carboxylase. Malonyl-CoA enters the Type II FAS-mediated chain elongation (discussed in Section 1.13).

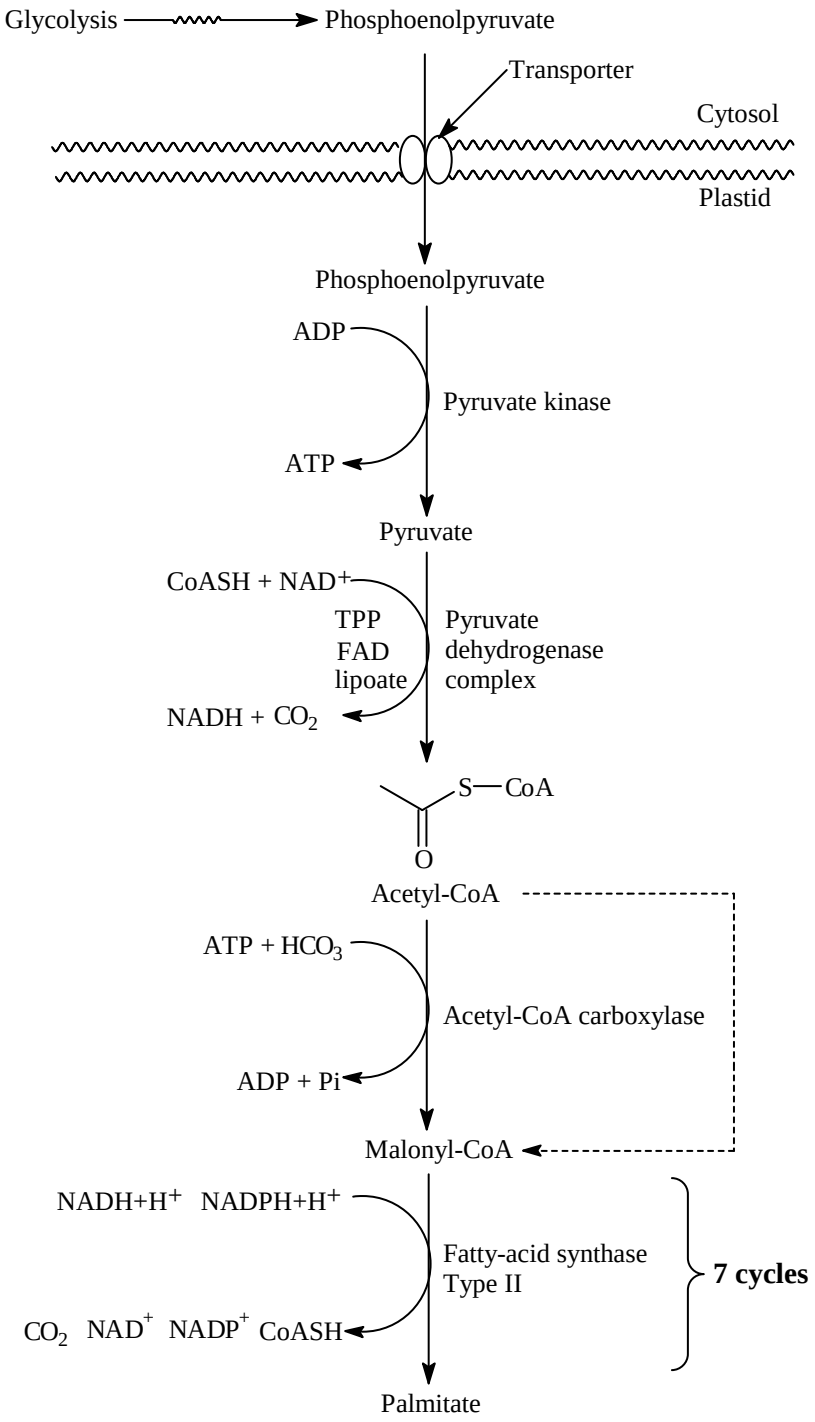

Figure 1.3 Overview of plastid fatty acid biosynthesis Simplified from the review by Wilson (2002). The broken arrow represents condensation of acetyl-CoA with malonyl-ACP.

1.8 Overview of acetyl-CoA carboxylase

Acetyl-CoA carboxylase (ACC) [EC 6.4.1.2] is an enzyme that catalyses the carboxylation of acetyl-CoA to form malonyl-CoA in the rate limiting step of *de novo* fatty acid biosynthesis. This reaction is driven by ATP hydrolysis (Abu-Elheiga *et al*., 2000; Abu-Elheiga *et al*., 1995; Al-Feel *et al*., 1992; Brownsey *et al*., 2006; Lu *et al*., 2005; Wakil *et al*., 1983). In addition to being involved in fatty acid biosynthesis, ACC may be involved in the synthesis of polyketides and possibly in yet unknown biosynthetic pathways leading to the production of unknown compounds (Al-Feel *et al*., 1992; Hopwood and Sherman, 1990; Sasaki *et al*., 1993). The product, malonyl-CoA, formed by ACC, becomes an important substrate for fatty acid synthesis in the liver and lactating mammary glands of animals. Malony-CoA is a substrate for the chain elongation system of enzymes in the endoplasmic reticulum and in many tissues with fatty acid chains greater than 20 subunits. Malonyl-CoA is involved in numerous cellular functions such as the synthesis of eicosanoid, glycolipids, sphingolopids and glycerolipids. Malonyl-CoA also plays an important function in the regulation of fatty acid oxidation by inhibiting palmitoyl-CoA transferase I (Brownsey *et al*., 2006). Therefore the availability of malonyl-CoA can alter the rate of fatty acid biosynthesis, β-oxidation and ketogenesis (McGarry, 2002). By and large, the role played by ACC in the production of malonyl-CoA emphasises the importance of ACC in carbon and energy metabolism in organisms expressing this enzyme.

Figure 1.4 illustrates the rate limiting step in fatty acid biosynthesis catalysed by ACC. The enzyme transfers a carboxylate ion (COO^-) to acetyl-CoA (Boone *et al*., 2000; Brownsey *et al*., 2006). The first step is the ATP-dependent phosphorylation of bicarbonate to carbamoyl phosphate. This step is catalysed by the carbamoyl phosphate synthatase sub-domain of the biotin carboxlase domain (Boone *et al*., 2000; Brownsey *et al*., 2006). In the second step, the phosphate-activated carboxylate ion is transferred to the biotin moiety in the biotinoyl domain to form carboxybiotinyl ACC. The carbondioxide is subsequently detached from the biotin molecule and transferred to acetyl-CoA in the final step. This step is catalysed by the carboxyl transferase domain (Boone *et al*., 2000; Brownsey *et al*., 2006).

In mammals, there are two isoforms of ACC namely ACC1 (ACC α) and ACC2 (ACC β), as illustrated in Figure 1.5. These two isoenzymes vary in their amino acid sequence suggesting

possible variation in function between these two isozymes. ACC1 is expressed in the lipogenic tissues as a ~ 265 kD monomeric protein, where it is involved in the rate limiting step of fatty acid biosynthesis. ACC2 is a 270 – 280 kD monomeric protein expressed in the skeletal and heart muscle where is it believed to play an important role in the regulation of fatty acid oxidation (Brownsey *et al*., 2006; Ha *et al*., 1996; Lu *et al*., 2005).

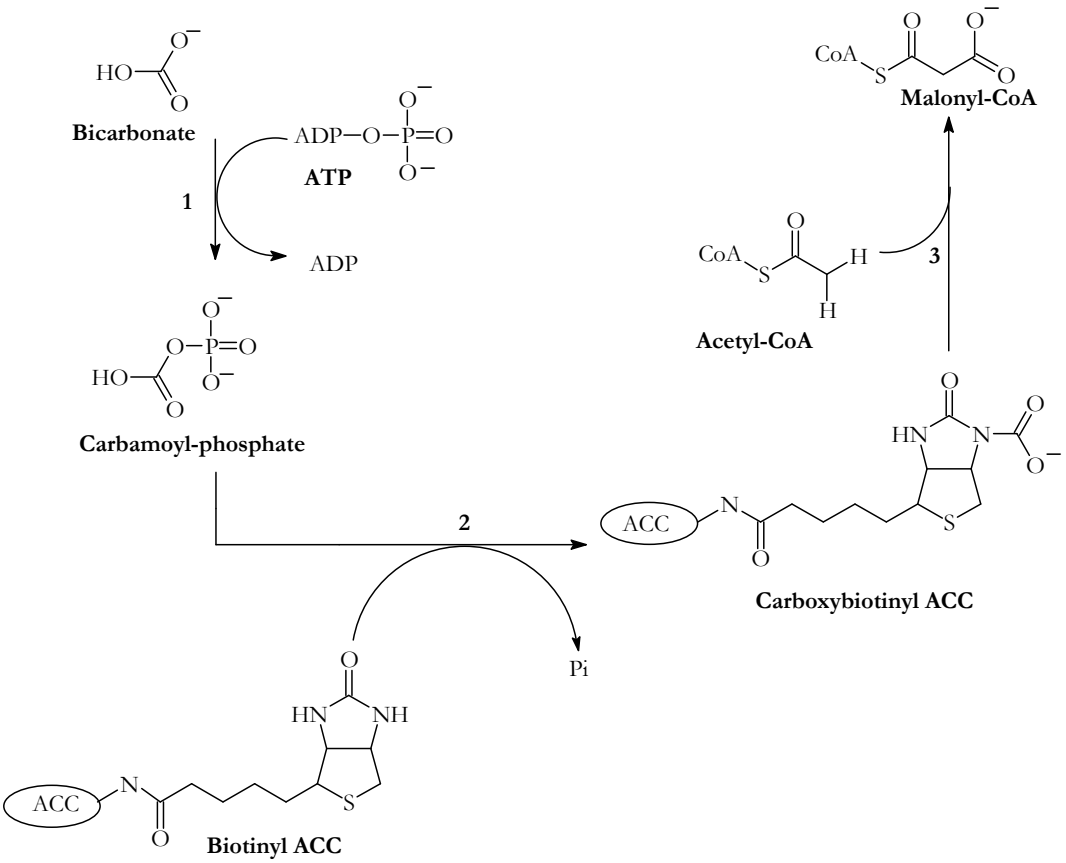

Figure 1.4 Formation of malonyl-CoA from acetyl-CoA and bicarbonate. Step 1 is the phosphorylation of the carboxylate ion to form carbamoylphosphate; Step 2 is the transfer of carbamoylphosphate to the biotin molecule on the biotinoyl domain to form carboxybiotinyl ACC; Step 3 is the transfer of carboxylate ion to acetyl-CoA to form malonyl-CoA. Steps 1 and 2 are catalysed by the biotin carboxylase domain (or subunit) and Step 3 is catalysed by the carboxyl transferase domain.

The complex structure of ACC may suggest the complex nature of its catalytic and regulatory properties. ACC found in higher animals, protozoa (*Toxoplasma gondii*), plants and yeasts have three protein domains. The biotin carboxylase domain is situated at the N-terminal region of the enzyme. The biotin/lipoyl binding domain (the biotin carboxyl carrier protein or biotinoyl domain) is situated closer to the biotin carboxylase domain at the N-terminal region of the enzyme. The carboxyltransferase domain is situated at the C-terminal region. In some organisms including mammals, the carboxyltransferase domain is further subdivided into an N-terminal transferase and a C-terminal transferase domain (Brownsey *et al*., 2006; Cronan and Waldrop, 2002; Ha *et al*., 1996; Lu *et al*., 2005). ACC exists in the form of a dimer or polymer of up to 4 000 Å unit (~ 400 nm in length). *In vitro* studies have shown that the dimeric form of ACC shows low catalytic activity while the polymeric form is more active (Brownsey *et al*., 2006).

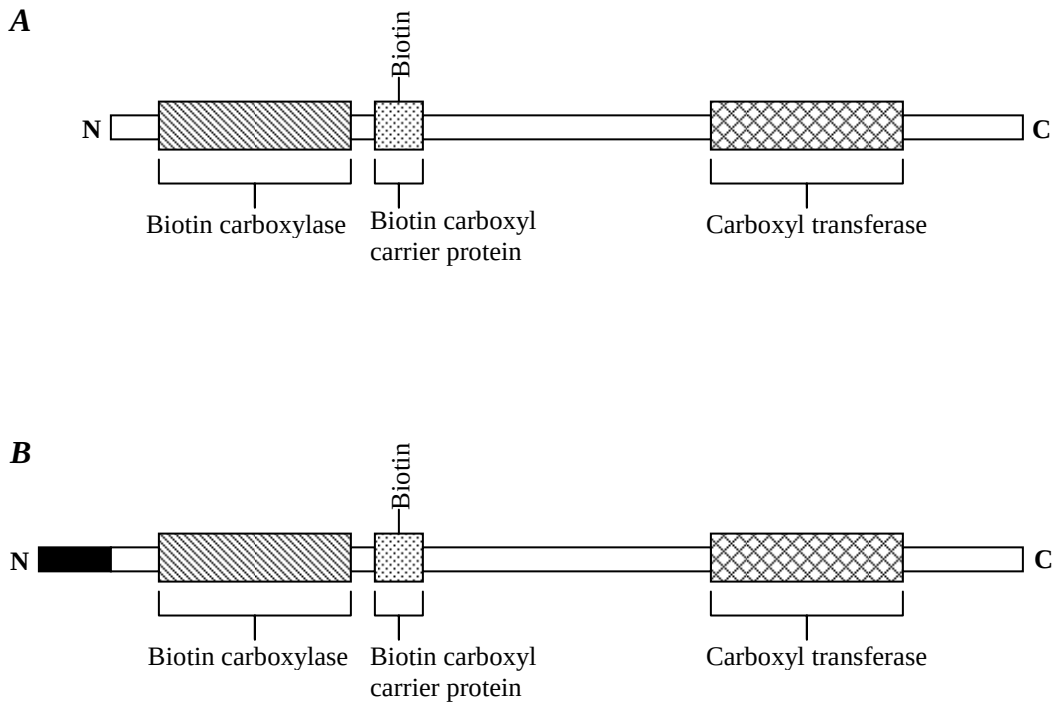

Figure 1.5 Domain organisation of the multi-enzyme domain acetyl-CoA carboxylase. (*A*) Acetyl-CoA carboxylase 1 (ACC 1) (*B*) Acetyl-CoA carboxylase 2 (ACC 2) with the mitochondrial signal sequence (filled box) at the N-terminal (Hardie and Pan, 2002).

ACC2 has a predicted molecular weight of 290 kD; larger than ACC1. ACC2 was first isolated from rat heart (Thampy, 1989; Thampy and Wakil, 1988a; Thampy and Wakil, 1988b). Sequence analysis of ACC2 showed that it has an N-terminal sequence extension. This sequence (not found in ACC1), which contains a mitochondrial targeting motif, differentiates ACC1 from ACC2. ACC is made up of an ATP binding motif, a protein kinase recognition site and other numerous catabolite binding sites that are involved in the regulation of the enzyme. Three dimensional structural studies have been reported for the biotin carboxyl carrier protein of *E. coli* and *Saccharomyces cerevisiae* (Roberts *et al*., 1999; Waldrop *et al*., 1994) as well as the carboxyl transferase domain of *Saccharomyces cerevisiae* (Zhang *et al*., 2003). To date, there is no resolved 3D structure for mammalian, plant and protozoan ACC domains. The important nature of this enzyme in various organisms as a "manager" of carbon and energy metabolism makes it attractive to resolve its three dimensional structure.

Some plants express both the multi-enzyme-domain type ACC as well as the multi-enzyme-subunit type ACC complex. The multi-enzyme-subunit type ACC complex form is localised in the plastid of plant cells where *de novo* fatty acid biosynthesis takes place, and the multi-enzyme-domain ACC is localised in the plant cell cytosol. *De novo* fatty acid biosynthesis found in plants is very similar to the pathway of yeast, and higher animals (Konishi *et al*., 1996; Sasaki *et al*., 1993; Zuther *et al*., 1999). The plant plastid multi-enzyme-subunit ACC complex (similar to those found in prokaryotes) dissociates into four protein subunits namely: the biotin carboxyl carrier protein (biotinoyl protein), biotin carboxylase, α-carboxyltransferase and β-carboxyltransferase (Figure 1.6). The plastid ACC is involved only in fatty acid biosynthesis, while the cytosolic ACC is involved in flavonoid, anthocyanin, malonated amino acids, very long chain fatty acid biosynthesis and other natural products found in plants (Sasaki and Nagano, 2004; Thelen *et al*., 2001).

Grass and some monocotyledonous plants lack the gene that codes for the multi-enzyme-domain ACC subunits complex, but encodes the multi-enzyme-domain ACC that is targeted to both the plastid and the cytosol. The lack of the multi-enzyme-subunit ACC complex in grasses confirms the sensitivity shown towards herbicides by these plants. Herbicides such as fenoxaprop, diclofop and sethoxydim (Figure 1.8) inhibit the activity of the multi-enzyme-domain ACC, while the

multi-enzyme-subunit ACC complex is insensitive to herbicides (Davis *et al*., 2000). There is no defined molecular weight of plant ACC. But studies have shown that the plant single multi-enzyme-domain ACC is in the form of a dimer ranging from about 210 kD to 250 kD. The observed size in pea ACC is about 650 – 700 kD (Sasaki and Nagano, 2004). The usual flow of carbon from photosynthesis to primary and secondary metabolites in plants is controlled by ACC. Therefore in plants, ACC and malonyl-CoA (product of ACC) are vital for the regulation of metabolite flux through the fatty acid biosynthetic and degradation pathways (Jelenska *et al*., 2001; Jelenska *et al*., 2002).

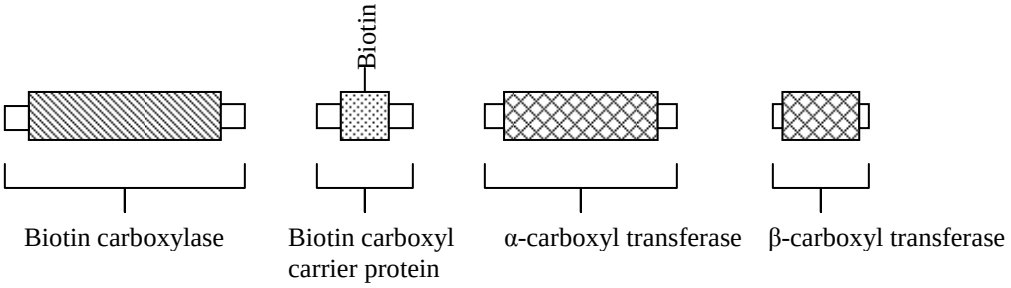

Figure 1.6 The multi-enzyme acetyl-CoA carboxylase complex (Sasaki and Nagano, 2004).

1.9 Transcriptional regulation of acetyl-CoA carboxylase

Eukaryotic ACC can be regulated at the level of transcription, regulated allosterically and covalently (Brownsey *et al*., 2006; Sasaki *et al*., 1993). In mammals, ACC1 expression is often controlled by the feeding state of the animal. The diet of animals used for isolation of tissue ACC is often controlled to enable high level expression of the enzyme (Song and Kim, 1981; Thampy and Wakil, 1988a). The hepatic expression of ACC is decreased during insulin deficiency and starvation, and restored by feeding a low fat diet or insulin treatment (Iritani, 1992; Thampy and Wakil, 1988b). Therefore hepatic ACC1 transcription is controlled by factors such as low blood glucose, insulin, thyroid hormone hormones involved in catabolism and transcriptional factors. The enzyme is expressed in high levels in lactating mammary glands, which is an indication of the inducible nature of this enzyme (Brownsey *et al*., 2006; Hardie and Pan, 2002). The most

significant transcriptional factors are the sterol-regulating elements binding-protein-1c and other lipogenic enzymes (Zhang *et al*., 2003).

The expression of ACC2 in mammals is increased during starvation, which is antagonistic to the ACC1 expression (Brownsey *et al*., 2006). This is because most fatty acid biosynthesis is incorporated into membrane synthesis and lipid storage. Thus fatty acid biosynthesis is required for early stages of cell growth and development. If these fatty acids are not exhausted, the *de novo* fatty acid biosynthesis decreases (feed back inhibition). The decrease and increase in fatty acid biosynthesis is therefore achieved by the expression of the key enzyme, ACC (Brownsey *et al*., 2006; Thampy and Wakil, 1988b). Eukaryotic organisms control ACC transcription by RNA editing. This process is universally known to affect gene regulation (Sasaki *et al*., 1993). ACC in plants is also believed to be post-translationally regulated by assembly and disassembly of the monomeric proteins of the heteromeric enzyme complex resulting to controlled activity of ACC (Sasaki and Nagano, 2004; Thelen *et al*., 2001).

1.10 Allosteric regulation of acetyl-CoA carboxylase

Allosteric regulation of ACC is achieved by the binding of citrate to the enzyme resulting in polymerization of the inactive dimeric form of the enzyme to the active filamentous polymer (Boone *et al*., 2000; Brownsey *et al*., 2006; Hardie and Pan, 2002; Munday, 2002). Other metabolites such as glutamate and other dicarboxylic acids activate ACC1; this indicates the possible effect of amino acid metabolism on ACC activity (Boone *et al*., 2000). The substrates of fatty acid biosynthetic pathways, including malonyl-CoA, free CoA and fatty-acyl CoA esters, have been shown to inhibit ACC1 (Boone *et al*., 2000; Moule *et al*., 1992). Mammalian ACC2 does not polymerize as readily as the ACC1, which suggests that both enzymes may have different allosteric regulators. ACC2 is however activated by citrate just as ACC1; a crucial process in skeletal muscles. Citrate is an important reagent used in most isolation procedures for ACC (Song and Kim, 1981; Thampy and Wakil, 1988a). The citrate binding site on ACC is yet to be identified (Boone *et al*., 2000; Hardie and Pan, 2002).

1.11 Regulation of acetyl-CoA carboxylase by phosphorylation

Most studies to date on the regulation of ACC by phosphorylation and de-phosphorylation have focused on mammalian (especially humans) and yeast ACC. There is also evidence that ACC is regulated by phosphorylation in *Drosophila melanogaster* (Pan and Hardie, 2002). The link between ACC and pathologies such as diabetes and obesity has encouraged the research on the "phospho-regulation" of ACC in human species. ACC is regulated by phosphorylation and de-phosphorylation by protein kinases and phosphatases (Brownsey *et al*., 2006; Davies *et al*., 1990; Hardie *et al*., 1998; Hardie and Pan, 2002).

5'AMP-activated protein kinase (AMPK) phosphorylates three serine residues of the mammalian ACC namely Ser^{79}, Ser^{1200} and Ser^{1215}. Ser^{79} lies on the N-terminal region of ACC1 before the biotin carboxylase domain. Ser^{1200} and Ser^{1215} lie on the central region of ACC1, between the biotin carboxyl carrier protein (BCCP) and the carboxyltransferase domain (Brownsey *et al*., 2006; Hardie and Pan, 2002). Phosphorylation of Ser^{79} occurs more rapidly than the other two residues; confirmed by site-directed mutagenesis. In ACC1, phosphorylation of Ser^{79} results in inactivation of ACC1, which is reversed by dephosphorylation by protein phosphatase-2C (PP2C) or by cleavage of the N-terminal 10 – 20 kD region of ACC1 containing the Ser^{79} residue (Brownsey *et al*., 2006; Hardie and Pan, 2002).

In vitro studies with AMPK confirmed that there are other possible phosphorylation sites on ACC1 that may be phosphorylated by other protein kinases (Hardie, 2003; Hardie *et al*., 1998; Hardie and Pan, 2002; Pan and Hardie, 2002). ACC1 can be phosphorylated by protein kinase A (PKA) at Ser^{77} and Ser^{1200} resulting in minimal inhibition of ACC1. However, there is no evidence for the *in vivo* phosphorylation of ACC1 by PKA. AMPK is the only protein kinase that has shown significant relationship to energy metabolism in terms of induced expression of the enzyme in various physiological conditions related to energy changes (Hardie and Pan, 2002). The regulation of ACC2 by AMPK in the mammalian system is still not well understood. ACC2 purified from rat muscle can be phosphorylated and inactivated *in vitro* by AMPK. Although the Ser^{79} residue found in ACC1 is absent in ACC2, Ser^{219} in ACC2 is thought to be the equivalent of the ACC1-Ser^{79} (based on the hydrophobic amino acid residues around Ser^{79}). ACC2-Ser^{219} is phosphorylated by AMPK (Hardie *et al*., 1998; Hardie and Pan, 2002).

1.12 The apicomplexa plastid acetyl-CoA carboxylase

Until recently, parasitic organisms such as *Plasmodium* were thought to be incapable of *de novo* fatty acid biosynthesis. This was based on the inability of *Plasmodium knowlesi* to incorporate a radio-labelled carbon precursor to its lipids synthesised *in vivo* (Holtz, 1977; Ralph *et al.*, 2004b). The malaria parasite was assumed to depend entirely on its host for fatty acid requirement and other lipid precursors for cell wall synthesis. Work carried out on the lipid composition and lipid turn over of malaria parasite-infected red blood cells showed that infected red blood cell exhibited a remarkable alteration in their lipid composition (Beaumelle and Vial, 1988a; Vial *et al*., 1984). Lipid precursors such as phosphatidylethanolamine, phosphatidylcholine, and phosphatidylserine are taken up by the parasite. This suggested that the *Plasmodium* parasite is capable of scavenging lipid precursors from the host. This uptake was shown to be enhanced by the presence of lipid transfer proteins (Beaumelle and Vial, 1988b; Beaumelle *et al*., 1988) and these lipids are incorporated into parasite membranes. Chloroquine was also shown to inhibit the uptake and assimilation of lipid precursors using radiolabelled inositol, 1-[^{14}C]-palmitoyl-lysophosphatidylcholine (Vial *et al*., 1988). However, this postulate was refuted after it was discovered that the malaria parasite expressed genes that code for *de novo* fatty acid biosynthesis as revealed by the malaria genome analysis. Work done by several authors have shown that *P. falciparum* is capable of incorporating acetate into its fatty acid synthesis (Gardner *et al*., 2002a; Mitamura and Palacpac, 2003; Ralph *et al*., 2004b; Surolia and Surolia, 2001; Waller *et al*., 2003).

In *Toxoplasma gondii*, ACC and the gene expressing ACC have been well characterised. Due to the relatedness of this parasite to the *Plasmodium* parasite, it is likely that there exists a correlation between the apparent functional similarities of the ACC gene and protein between these protozoan parasites (Gornicki, 2003; Mitamura and Palacpac, 2003). The *Toxoplasma gondii* genome encodes two copies of ACC genes (*ACC1* and *ACC2*) coding for the multi-enzyme-domain ACC (Jelenska *et al*., 2001; Jelenska *et al*., 2002). Both enzymes are biotin-dependent and they catalyse the first step in the *de novo* synthesis of fatty acids in the parasite (Jelenska *et al*., 2001; Jelenska *et al*., 2002; Lauer *et al*., 1995; Zuther *et al*., 1999). Studies using the *Toxoplasma* parasite lysates have shown ACC activity. The genes encoding the two ACC isoforms have multiple introns within their open reading frames; this is similar to the mammalian

and yeast ACC gene structure. Both mammalian and yeast ACC amino acid sequences share some common sequence motifs with the *Toxoplasma* ACC sequence especially in the enzyme domain regions. ACC1 is smaller than ACC2; a phenomenon common to the mammalian ACC. Jalenska *et al.* (2002) postulated that ACC1 is apicoplast-targeted and is involved in the *de novo* fatty acid biosynthesis. ACC2 is the cytosolic form. They observed that ACC1 is inhibited by plant herbicide such as aryloxyphenoxypropionates and clodinafops. This inhibitory effect on the parasite ACC by herbicides underlines the potential for targeting protozoan parasite fatty acid synthesis for anti-parasitic drug intervention.

1.13 Apicoplast Type II FAS-mediated chain elongation

Figure 1.7 illustrates the proposed reaction steps used by apicomplexa to produce palmitic acid (Ralph *et al*., 2004b; Surolia *et al*., 2004; Wilson, 2002). Malonyl-CoA is attached to acyl carrier protein (ACP) in a ping-pong reaction mechanism catalysed by malonyl-CoA:ACP transacylase. This enzyme has been cloned, expressed and characterised in *P. falciparum* (Prigge *et al*., 2003). Although this enzyme is necessary for parasite survival, its potential as an anti-parasitic agent is yet to be exploited (Surolia *et al*., 2004). Malonyl-ACP is the substrate that is continually added to the fatty acid chain, thus each cycle results in the addition of two carbon moieties from malonyl-ACP. The chain elongation step is divided into four distinct reaction steps namely: condensation, reduction, dehydration and reduction (Surolia *et al*., 2004).

The Type II FAS-catalysed chain elongation in the apicomplexa plastid begins with the condensation of acetyl-CoA with malonyl-ACP; unlike the Type I FAS chain elongation that uses acetyl-ACP as substrate for the condensation step (Surolia *et al*., 2004; Wilson, 2002).This first step is catalysed by β-ketoacyl-ACP synthase III (KAS III or FabH), while the subsequent condensation steps (cycles 2 – 7) are catalysed by a FabB/F (KAS I/II) isoezyme (Surolia *et al*., 2004; Wilson, 2002). FabH is annotated in *P. falciparum* (Plasmodb ID PFB0505c, located on chromosome 2), *vivax*, *knowlesi*, *berghei* and *chabaudi* as a beta-ketoacyl-ACP synthase III precursor. FabB/F is annotated in *P. falciparum* (Plasmodb ID PFF1275c, located on chromosome 6), *vivax*, *knowlesi*, *berghei*, *yoelii* and *chabaudi* as the beta-ketoacyl-ACP synthase III precursor. *P. falciparum* FabH is inhibited by 1,2, dithiole-3-one (an analogue of thiolactomycin) with an IC_{50} of 0.5 – 10 µM (Prigge *et al*., 2003). Thiolactomycin (Figure 1.8) is

a competitive inhibitor of bacterial and plant ketoacyl-ACP synthase (Sasaki and Nagano, 2004; Surolia *et al*., 2004) and has been shown to inhibit *P. falciparum* growth in human erythrocyte at concentrations less than 50 µM (Gornicki, 2003).

The second step in the Type II FAS chain elongation is the reduction of β-ketoacyl-ACP to β-hydroxyacyl-ACP. This reaction step is catalysed by NADP-dependent β-ketoacyl-ACP reductase (Surolia *et al*., 2004). This enzyme is annotated in *P. falciparum* as putative 3-oxoacyl-ACP reductase (Plasmodb ID: PFI1125c, located on chromosome 9), as well as in *vivax*, *knowlesi*, *berghei*, *yoelii* and *chabaudi* (Gornicki, 2003). No inhibitor of this enzyme has been identified. β-hydroxyacyl-ACP is dehydrated to enoyl-ACP by β-hydroxyacyl-ACP dehydrase (FabA/Z). The FabA isoenzyme is bifunctional, it catalyses the dehydration of β-hydroxyacyl-ACP and the trans-isomerisation of *trans*-enoyl-ACP to *cis*-enoyl-ACP. *Cis*-enoyl-ACP is channelled into the production of unsaturated fatty acids (Surolia *et al*., 2004; Surolia and Surolia, 2001). FabZ is characterised in *P. falciparum* (Plasmodb ID PF13_0128, located on chromosome 13) (Sharma *et al*., 2003). Orthologues of FabZ have been identified in *P. vivax*, *knowlesi*, *berghei*, *yoelii* and *chabaudi*; and annotated as the β-hydroxyacyl-ACP dehydrase precursor in the Plasmodb database. In the final elongation step, enoyl-ACP is reduced to butyryl-ACP by enoyl-ACP redcutase (FabI). This enzyme is NADH-dependent in apicomplexa Type II FAS as contrasting the NADPH-dependent homologue of the Type I FAS (Surolia *et al*., 2004; Surolia and Surolia, 2001). FabI is inhibited by triclosan (Figure 1.8) a broad spectrum antimicrobial agent (Suguna *et al*., 2001; Surolia *et al*., 2004; Surolia and Surolia, 2001). In *Plasmodium*, triclosan inhibits FabI (Plasmodb ID PFF0730c, located on Chromosome 6) with an IC_{50} of 0.2 – 1.2 µM. The FabI ortholgue has been annotated in *P. vaivax, knowlesi*, *berghei*, *yoelii* and *chabaudi*. The final product of the first elongation cycle (butyryl-ACP) enters the second cycle by condensing with malonyl-ACP catalysed by FabB/F. Cerulenin (Figure 1.8) is an inhibitor of FabB/F (Johnson *et al*., 1994; Lack *et al*., 2006). After the seventh cycle, the resulting product is a 16-carbon atom fatty acid called palmitioyl-ACP. This product is hydrolysed to palmitate (Surolia *et al*., 2004; Wilson, 2002).

In summary, fatty acid metabolism is vital to energy and membrane biogenesis. Acetyl-CoA carboxylase is central to *de novo* fatty acid metabolism. The two major types of acetyl-CoA

carboxylase are the multi-enzyme domain type found in humans, yeast and monocot plants and the multi-subunit enzyme complex found in bacteria and dicot plants. *De novo* fatty acid synthesis is initiated by the acetyl-CoA carboxylase-mediated carboxylation of acetyl-CoA to form malonyl-CoA. This reaction is the committed step in fatty acid synthesis and is ATP-dependent. Malonyl-CoA is elongated to palmitic acid via a series of repetitive steps of condensation, reduction and dehydration reactions catalysed by fatty acid synthase (FAS).

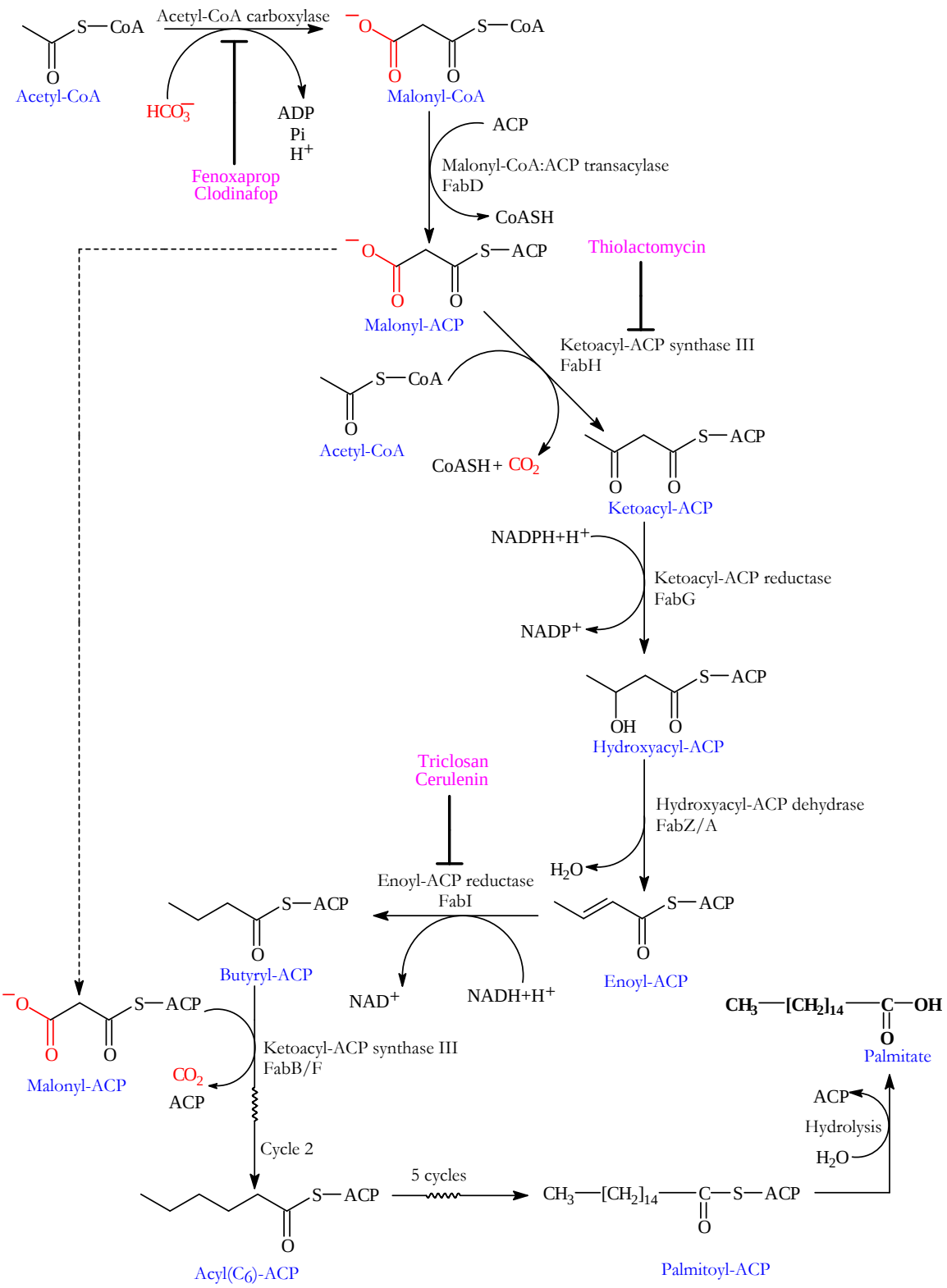

Figure 1.7 Type II fatty acid synthase-mediated synthesis of palmitate. Reaction products and intermediates are in blue and inhibitors are in magenta. Squiggle arrows indicate a multi-step and a broken arrow indicates second and subsequent condensation steps (Surolia *et al.*, 2004).

There are two types of FAS responsible for elongation of malonyl-CoA, namely the Type I FAS and Type II FAS. The type I FAS is a large multi-enzyme domain (multi-functional) polypeptide found in humans and fungi, while the Type II FAS is made up of discrete and mono-functional enzymes (complex) found in bacteria and plant chloroplasts. Apicomplexan parasites have been shown to express a nucleus-encoded acetyl-CoA carboxylase and Type II FAS, which are targeted to the apicoplast. However, *Cryptosporidium parvum* (an apicomplexa) has been shown to express cytoplasmic-targeted acetyl-CoA carboxylase and Type I FAS (Zhu, 2004; Zhu *et al*., 2004; Zhu *et al*., 2000). There are inhibitors of acetyl-CoA carboxylase and FAS. Fatty acid metabolism is targeted for anti-parasite chemotherapy due to the relevance of fatty acid metabolism to the survival of parasites.

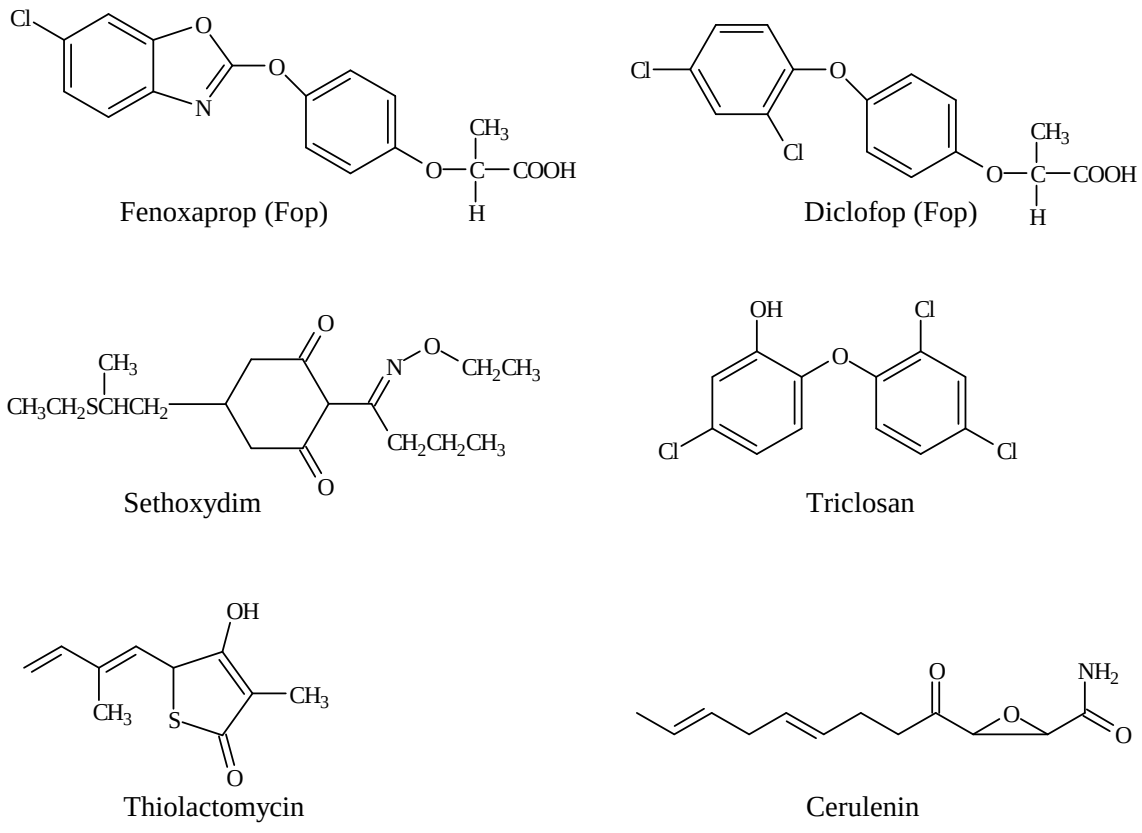

Figure 1.8 Inhibitors of acetyl-CoA carboxylase and Type II fatty acid synthase. (Jelenska *et al*., 2001; Jelenska *et al*., 2002; Surolia *et al*., 2004)

1.14 Aim and objectives of the study

There are no experimental data published to date suggesting that the *Plasmodium* parasites express functional acetyl-CoA carboxylase. However, there seem to be homologues of acetyl-CoA carboxylase in *P. falciparum* (Plasmodb-gene number PF14_0664), *Plasmodium yoelii yoelii* (Plasmodb-gene number PY01695), and *Plasmodium berghei* (Plasmodb-gene number PB000494.02.0) as a fragment and as hypothetically annotated proteins in *Plasmodium chabaudi* (Plasmodb-gene number PC000014.02.0). The identification of the gene that codes for acetyl-CoA carboxylase in the malaria parasite suggests that the *Plasmodium* parasite is capable of fatty-acid synthesis. However, there is no evidence that the gene coding for acetyl-CoA carboxylase is expressed as a functionally active enzyme capable of initiating the rate-limiting step of fatty acid synthesis. It is still unclear how the parasite metabolises fatty acids *in vivo*.

Lipid metabolism is elevated in *P. falciparum*-infected erythrocytes, when compared to non-infected erythrocytes in which fatty acid metabolism is almost non-existent (Hanada *et al*., 2002; Perozzo *et al*., 2002; Sherman, 1979; Waller *et al*., 2003). The majority of the lipids synthesised during the intra-erythrocytic stage of *Plasmodium* parasite cycle are channelled towards membrane biogenesis including organellar and tublovessicular membrane networks in the cytoplasm of infected erythrocytes (Hanada *et al*., 2002). Other findings (Beaumelle and Vial, 1988b; Moll *et al*., 1988) propose that *Plasmodium* parasites meet the demand for important lipids by simultaneously importing lipids from its hosts and employing *de novo* pathways. Perhaps this is a clever adaptation by the parasite to maximise cellular energy turnover, since *de novo* biosynthetic pathways are often energy consuming. Therefore, there is the possibility that *Plasmodium* parasites exhibit a well developed mechanism of lipid biosynthesis needed to meet its lipid demands for its atypical form of cell proliferation and survival in its host environment (Hanada *et al*., 2002; Lauer *et al*., 1995).

Based on the available data on *Plasmodium* lipid metabolism, much is yet to be understood about the *Plasmodium* fatty acid synthesis, the fate of acetyl-CoA carboxylase and how the parasite manages carbon and other energy sources. The significance of these biochemical processes for parasite survival can not be overlooked as potential pathways for anti-*Plasmodium* drug intervention. The gene encoding acetyl-CoA carboxylase in *P. yoelii* strain 17XNL has been sequenced and published (Plasmodb ID: PY01695). The ability of the parasite to synthesise fatty

acids *de novo* via the acetyl-CoA carboxylase-mediated commitment step of malonyl-CoA formation depends on the transcription of the gene and synthesis of the enzyme.

This study was aimed at establishing the presence of acetyl-CoA carboxylase and the mRNA transcript encoding the enzyme at the eythrocytic stage of *P. yoelii* strain 17XL propagated in BALB/c mice. Therefore the objectives are as follows:

1. The presence of the mRNA transcript will be established by RT-PCR using primers designed to amplify the region of the open reading frame. The RT-PCR cDNA products will be sequenced to confirm the RT-PCR results. The size of the transcript will be determined by Northern blot analysis.
2. Anti-peptide antibodies produced in chickens against *Plasmodium* proteins have shown to be an effective tool in the detection and characterisation of plasmodial proteins. Antibodies will be produced in chickens against an immunogenic region of the theoretical acetyl-CoA carboxylase amino acid sequence published in the Plasmodb database. The presence of the enzyme in parasite lysates and in a *P. yoelii*-infected-red blood cell will be evaluated using anti-peptide antibodies on a Western blot and by immunofluorescent microscopy.
3. The DNA coding for the predicted biotinoyl domain of the enzyme in *P. yoelii* 17XL will be cloned into *E. coli* expression systems. The expressed protein will be characterised for the presence of attached biotin.
4. Homology modelling of the *P. yoelii* acetyl-CoA carboxylase biotinoyl protein and biotin carboxylase domains will be carried out. Insights gained from the modelling will assist in possible identification of potential enzyme inhibitors.

CHAPTER 2
GENERAL MATERIALS AND METHODS

2.1 Introduction

This chapter describes several basic biochemical, immunochemical, parasitological and molecular biology techniques used in this study.

2.2 Materials

The following reagents and antibodies were purchased from Sigma-Aldrich-Fluka (Steinheim Germany) β-mercarptoethanol, 4-chloro-1-naphthol, acrylamide, agarose, ampicillin, avidin, Biomax® X-ray film, bisacrylamide, bromophenol blue, carbenicillin, chloramphenicol, Coomassie Brilliant Blue G-250, Coomassie Brilliant Blue R-250, diethyl pyrocarbonate (DEPC), Ellman's Reagent, Ficoll Type 400, formamide, Freund's complete adjuvant, Freund's incomplete adjuvant, Giemsa stain, glycine, guanidine thiocyanate, guanidine-HCl, Herring sperm DNA, isopropyl thioglucopyranoside (IPTG), L-cysteine kanamycin, maleimidobenzoyl-*N*-hydroxysuccinimide ester (MBS), molecular biology grade phenol, mouse monoclonal anti-biotin IgG, N-laurylsarcosine, ovalbumin, peroxidase-conjugated avidin, *p*-iodophenol, polyvinypyrrolidine, Ponceau S, rabbit serum albumin, saponin, Sephadex G-25, Sephadex G-10, Semi-dry blot unit, *N,N,N',N'*-tetramethyethylenediamine (TEMED), Triton X-100, tryptone, Tween-20, urea and yeast extract. Bovine serum albumin and Expand High Fidelity PCR® system were purchased from Roche (Mannheim, Germany). Equipment purchased from BioRad (California USA) were Poly Prep® affinity column, Mini Protean II™ vertical PAGE unit, III™ vertical PAGE unit and VesaDoc™ imaging system. The following were purchased from Fermentas (Vilinius, Lithuania): 10× T4 DNA ligase buffer, T4 DNA ligase, Biotin DecaLabel™ DNA labeling kit, dATP, DNA MassRuler™, dNTP mix, *EcoR*I, molecular biology grade DTT, *Not*I, Buffer O™, shrimp alkaline phosphatase (SAP) and PageRuler™ Unstained Protein Ladder. Single stranded RNA ladder was purchased from New England BioLabs. Molecular biology reagents were purchased from Solis Biodyne (Tartu Estonia) 10× PCR buffer ($MgCl_2$ and detergent-free) PCR $MgCl_2$ [25 mM] solution and *Taq* polymerase. Cells, plasmid and antibodies purchased from Novagen (Damstadt, Germany) were BL 21 cells (glycerol stock), JM109 cells (glycerol stock), and Rosetta (DE3) pLysS commercial competent cells, pET-28a and mouse

monoclonal anti-His-Tag IgG, peroxidase-conjugated sheep monoclonal anti mouse IgG. PEG 6000 was purchased from Merck Biosciences (Damstadt, Germany). G333c™ fixer and STRUCTURIX G128™ were purchased from AGFA® (Morstel, Belguim). ABTS was purchased from Boehringer (Mannheim, Germany). Orbital shaking incubator was purchased from New Brunswick Scientific (New Jersey USA). SulfoLink™ Coupling Gel and Snake skin™ dialysis membrane were purchased from Pierce Perbio Science (Erembodegem, Belgium). pGEX-4T-1, Hybond-C™ Extra nitrocellulose membrane, HMW protein standards and Ultrspec 2100*pro* UV/visible spectrophotometer were purchased from GE Healthcare (Buckinghamshire England). Biotin-conjugated monoclonal anti-GST antibody was purchased from Anaspec (California USA). Peroxidase-conjugated rabbit anti-IgY antibody and FITC-conjugated donkey anti-chicken-IgY were from Jackson Immunochemicals (Pennsylvania, USA). TALON® metal affinity resin was from Clontech (California, USA). Improm II® Reverse Transcription System was purchased from Promega (Wisconsin, USA). Oligonucleotide primers were synthesized by ProLigos™ (Paris, France). Synthetic pLDH peptide was synthesized by GeneScript (New Jersey, USA) while Synthetic PyACC peptide was synthesized by Auspep (Melbourne, Australia). VersaMax™ ELISA plate reader was purchased from Molecular Devices Corporation (California, USA). Nunc Maxi Sorp™ 96-well ELISA plate was from Nunc products (Roskilde Denmark). DNA purification kit was purchased from PEQLAB Biotechnologie (Erlangen, Germany). Avanti™ J-26 XPI centrifuge was from Beckman Coulter (California USA). GeneAmp™ PCR thermocyler was from Applied Biosystems (California USA). Virosonic™ cell disruptor was purchased from VirTis (New York, USA).

2.3 Biochemical and immunochemical techniques

This section describes routine biochemical and immunochemical techniques that were used in this study.

2.3.1 Sodium dodecyl sulfate polyacrylamide gel electrophoresis

The discontinuous Sodium dodecyl sulfate polyacrylamide gel electrophoresis (Laemmli, 1970) was used to anaylse (i) the purification profile of the anti-peptide IgY, (ii) recombinant protein expression and (iii) purification of recombinant proteins.

2.3.1.1 Materials

Monomer solution [30% (w/v) acrylamide, 2.7% (w/v) bis-acrylamide]. Acrylamide (73 g) and bis-acrylamide (2 g) were dissolved and made up to 250 ml with distilled water. The solution was stirred, filtered though Whatman No. 1 filter paper and stored in an amber bottle at 4°C.

Separating gel buffer [1.5 M Tris-HCl, pH 8.8]. Tris (45.37 g) was dissolved in 200 ml of distilled water, stirred, pH adjusted to 8.8 with HCl and the volume made up to 250 ml with distilled water. The solution was filtered with Whatman No. 1 filter paper and stored at 4ºC.

Stacking gel buffer [500 mM Tris-HCl, pH 6.8]. Tris (3 g) was dissolved in 40 ml of distilled water, adjusted to pH 6.8 with HCl, and the volume was made up to 50 ml with distilled water. The solution was filtered with Whatman No. 1 filter paper and stored at 4ºC.

10% (w/v) Sodium dodecylsulfate (SDS). SDS (10g) was dissolved in 100 ml of distilled water and stirred continuously until the detergent had dissolved and stored at RT.

Initiator reagent [10% (w/v) ammonium persulfate]. Ammonium persulfate (0.1 g) was dissolved in 1 ml of distilled water and stored at 4ºC.

Tank buffer [250 mM Tris-HCl, 192 mM glycine, 0.1% (w/v) SDS, pH 8.3]. Tris (15 g) and glycine (72 g) were dissolved in about 5 L of distilled water and stirred. Before use, SDS (1 g) was added to 1 L of the buffer.

Reducing sample buffer [125 mM Tris-HCl, 4% (w/v) SDS, 20 % (v/v) glycerol, 10% (v/v) β-mercaptoethanol, pH 6.8]. Stacking gel buffer (2.5 ml) was mixed 4 ml of 10% SDS, glycerol (2 ml) and β-mercaptoethanol (1 ml), mixed thoroughly and made up to 10 ml with distilled water. 35 μg of bromophenol blue was added as tracking dye and stored at RT.

Non-reducing sample buffer [125 mM Tris-HCl, 4% (w/v) SDS, 20 % (v/v) glycerol, pH 6.8]. Stacking gel buffer (2.5 ml), 4 ml of 10% SDS and glycerol (2 ml) were mixed thoroughly and

made up to 10 ml with distilled water. Bromophenol blue (35 μg) was added as tracking dye and stored at RT.

Coomassie stain solution [0.1 % (w/v) Coomassie dye in 1:5:4 (v/v/v) acetic acid-methanol-water solution]. Coomassie dye (0.1 g) was completely resusupended in 1:5:4 (v/v/v) acetic acid-methanol-water solution.

2.3.1.2 Method

Reducing or non-reducing SDS-PAGE was carried out as described by Laemmli (1970) using a Bio-Rad vertical slab electrophoresis apparatus. Running (separating) and stacking gels were prepared according to Table 2.1. Prior to casting of the gel mixture, the Bio-Rad Mini PROTEAN II® vertical slab electrophoresis accessory unit was pre-cleaned and rinsed with dH_2O. The unit was made up of a gel-casting stand with casting gaskets, two ten-well gel combs (1.5 mm thick), two 81.5 mm × 101.5 mm and 72.5 mm × 101.5 mm glass plates. The gel-casting unit was assembled according to the manufacturers' instructions.

Table 2.1 Recipe for two 72.5 × 101.5 × 1.5 mm^3 Laemmli SDS-polyacrylamide gels

Reagent	Separating gel			Stacking gel	
	12.5%	10.0%	5.5%	4%[a]	3%[b]
Monomer solution	6.25 ml	3.75 ml	2.75 ml	940 µl	720 µl
Separating gel buffer	3.75 ml	3.75 ml	3.75 ml	0	0
Stacking gel buffer	0	0	0	1.75 ml	1.75 ml
10% SDS	150 µl	150 µl	150 µl	70µl	70 µl
Distilled water	4.75 ml	7.25 ml	8.25 ml	4.3 ml	4.7 ml
Initiator reagent	75 µl	75 µl	75 µl	35µl	35 µl
TEMED	7.5 µl	7.5 µl	7.5 µl	15µl	15 µl

[a] Stacking gel for 12.5% and 10.0% separating gel

[b] Stacking gel for 5.5% separating gel.

Unpolymerised running gel solution were applied between the glass plates to a height of about 6 cm from the base and overlaid with water to prevent oxidative inhibition of polymerisation of the acrylamide. Once polymerised, the water overlay was removed and then the stacking gel

slurry was applied up to the brim of the glass plates and the gel comb was immediately inserted in the stacking gel and allowed to polymerise. Samples were loaded and the gel unit was immediately connected to a power pack. Electrophoresis was performed at 36 mA (18 mA per gel slab) until the dye front was about 0.5 cm from the bottom. The gels were immediately removed from the unit, stained with Coomassie Blue R 250 staining solution and destained. The electrophoregram was imaged using the BioRad VesaDoc^{TM} image documentation system. The molecular weight of the protein band was determined using the graph of Log molecular weight of standards against distance migrated (mm) into the running gel.

2.3.2 Western blot

Proteins resolved on SDS-PAGE gel and subsequently electro-transferred onto a membrane such as nitrocellulose, PVDF and nylon and are detected using antibodies or probes that recognize the blotted protein. The Western blot method used in this study was basically that of Towbin *et al.* (Towbin *et al.*, 1979). This technique was used in this work to detect recombinantly expressed protein in *E. coli* cell lysate resolved by SDS-PAGE and *in vivo* expressed protein in *Plasmodium* cell lysate resolved by SDS-PAGE.

2.3.2.1 Materials

Blotting solution [50 mM Tris, 0.2 M glycine, 20% (v/v) methanol, 0.1% (w/v) SDS]. Tris (6.05 g), glycine (15.01 g) and methanol (200 ml) were made up to 1 L with dH_2O and stored at 4ºC. Prior to use, SDS (1 g) was added.

Ponceau S reagent [0.2% (w/v) in 1% (v/v) acetic acid]. Ponceau S (20 mg) was resuspended in 1ml of glacial acetic acid. The volume was made up to 100 ml with dH_2O and stored at RT.

Tris buffered saline (TBS) [20 mM Tris-HCl, pH 7.4, 0.2 M NaCl]. Tris (2.42 g) and NaCl (11.69 g) were dissolved in 950 ml of dH_2O. The pH was adjusted to 7.4 with HCl and the volume made up to 1 L with dH_2O. The solution was stored at 4ºC.

Blocking solution [5% (w/v) non-fat powdered milk in TBS]. Locally sourced (Elite®) fat-free powdered milk (5 g) was suspended in 100 ml of TBS. This solution was prepared fresh.

BSA-TBS [0.5% (w/v) BSA in TBS]. BSA (0.25 g) was dissolved in 50 ml TBS. This solution was used fresh.

Substrate reagent [0.06% (w/v) 4-chloro-1-naphthol, 0.0015% (v/v) H_2O_2, 20% (v/v) methanol in TBS]. 4-chloro-1-naphthol (30 mg) was dissolved in methanol (10 ml). Four ml of this solution was made up to 20 ml with TBS and H_2O_2 (10 µl of a 30% solution) was added and kept away from light. This solution was used fresh.

2.3.2.2 Method

After SDS-PAGE, one of the duplicate gels was stained to display the protein band patterns and the other gel was used for blotting. Nitrocellulose membrane was cut to the dimension of the gel (7.2 cm × 10.5 cm) and six pieces of blotting paper were cut to the dimension of 8.2 cm × 10.5 cm. The gel was carefully placed on the nitrocellulose membrane from one side to avoid trapping air bubbles. The nitrocellulose membrane-gel was sandwiched between the six blotting papers (three on either side) and placed in between the electrode plates of the semi-dry blotting apparatus with the nitrocellulose membrane towards the anode. The semi-dry blotting apparatus was connected to a power supply unit {(7.0 V, 250 mA, 16 h) or (17.0 V, 250 mA, 1.5 h)}. After transfer, proteins on the nitrocellulose membrane were visualized with Ponceau S Reagent and the molecular weight marker proteins marked with a pencil. The nitrocellulose membrane paper was destained in dH_2O and blocked for 1 h with the Blocking Buffer. Subsequent steps were carried out on a “belly dancer”. The nitrocellulose membrane was then washed 3× (5 min/wash) with TBS and incubated for 2 h in the required dilution of the primary antibody or probe resuspended in BSA-TBS. The nitrocellulose membrane was washed 3× (5 min/wash) in TBS and incubated in the appropriate dilution of secondary antibody or probe diluted in BSA-TBS. The nitrocellulose membrane was washed 3× (5 min/wash) in TBS and incubated in the substrate reagent until the band suggestive of the detected protein appeared on the membrane. The image was captured with the VesaDoc imaging system and the blot stored.

2.3.3 Bradford standard protein assay

2.3.3.1 Materials

Bradford dye reagent [0.06% (w/v) Coomassie Brilliant Blue G-250 in 2% (v/v) perchloric acid]. Coomassie Brilliant Blue G-250 (0.3 g) was resuspended in 500 ml of 2% (v/v) perchloric acid in dH_2O. The solution was stirred for 1 h at RT, filtered with Whatman No.1 filter paper into a brown bottle and stored at RT.

Ovalbumin stock solution [0.5 mg/ml of buffer]. Ovalbumin (1 mg) was dissolved in 2 ml of the appropriate buffer. Different stock solutions were prepared for each experiment.

Protein standards [0 – 50 μg ovalbumin/100 μl of buffer]. Proteins standards were prepared by re-suspending 10 to 50 μg ovalbumin in 100 μl of buffer. Three independent working solutions were prepared for each experiment.

2.3.3.2 Method

Dye Reagent (0.9 ml) was mixed with the solution of the protein standards (0.1 ml) in a microfuge tube. The dye-protein solution was allowed to react at RT for 30 min and the absorbance value for each solution was read at 595 nm. The mean absorbance value for each protein concentration and for the two experiments was recorded. The absorbance value was plotted against the amount of protein in an *x-y* scatter. The solution with the unknown protein concentration was treated in a similar way and the protein concentration derived by interpolation on the standard curve.

2.3.4 Coupling synthetic peptides to rabbit albumin carrier for antibody production

Synthetic peptides derived from *P. yoelii* acetyl CoA carboxylase precursor related (Plasmodb ID: PY01695) and *P. yoelii* L-lactate dehydrogenase (Plasmodb ID PY03885) for anti-peptide antibody production in chickens were coupled to rabbit albumin carrier molecule. They are coupled to a carrier because the molecular weight of the peptides ranges from 1500 – 2000 Da and thus the peptides alone are unable to elicit an immunogenic reaction in the host. The peptides were designed and synthesized to have a terminal cystine residue that provided a functional sulfhydryl (SH) group that enabled the covalent attachment to the carrier and to the affinity

matrix. Prior to coupling, the cystine residue was reduced with DTT in order to acquire free terminal SH residues. The rabbit albumin carrier was activated with MBS; a hetero-bifunctional linker that links a primary amine fuctional group on one molecule to a sulfhydryl functional group on another molecule (Hermanson, 1996). Therefore activation of a protein molecule by MBS involves the covalent modification of the ε-amine groups of lysine residues on the protein molecule. The MBS-rabbit albumin complex was purified on Sephadex G-10 and Sephadex G-25 size chromatography columns (1.5 × 12.0 cm^2, linear flow rate of 8.5 cm/h) to separate coupled activated rabbit albumin from unreacted MBS and smaller reaction products.

2.3.4.1 Materials

Phosphate buffered saline (PBS), pH 7.2. NaCl (8 g), KCl (0.2 g), Na_2HPO_4 (1.15 g) and KH_2PO_4 (0.2 g) were dissolved in 1 L of dH_2O.

MEC Buffer [0.1 M $NaH_2PO_4.2H_2O$, pH 7.0, 0.02% (w/v) NaN_3, 1 mM Na_2-EDTA]. $NaH_2PO_4.2H_2O$ (15.6 g), Na_2-EDTA (0.3724 g) and sodium azide (0.2 g) were dissolved in 900 ml of dH_2O. The pH was adjusted to 7.0 with NaOH and the volume was made up to 1 L with dH_2O.

Peptide reducing buffer [0.1 M Tris-HCl, pH 8.0, 1 mM Na_2-EDTA]. Tris (2.24 g) and Na_2-EDTA (0.3724 g) were dissolved in 150 ml of dH_2O. The pH was adjusted to 8.0 with HCl and the volume was finally made up to 200 ml with dH_2O.

Ellman's reagent buffer [0.1 M Tris-HCl, pH 8.0, 1 mM Na_2-EDTA, 0.1% (w/v) SDS]. Tris (1.21 g), Na_2-EDTA (0.3724 g) and SDS (0.1 g) were dissolved in 90 ml of dH_2O. The pH was adjusted to 8.0 with HCl and the volume was finally made up to 100 ml with dH_2O.

Dithiothrietol [10 mM]. Dithiothrietol (7.71 mg) was dissolved in 5 ml of peptide reducing buffer.

2.3.4.2 Method

This laboratory had previously determined empirically that 4 mg of a synthetic peptide is enough to produce between 4 – 10 mg affinity purified polyclonal antibody in a chicken between 12 – 15 weeks of four immunisation schedules (Goldring and Coetzer, 2003).

Calculations

The peptide was coupled to the rabbit albumin carrier at 40:1 peptide-carrier ratio. The amount of rabbit albumin (carrier) to be coupled to 4 mg of synthetic peptide was determined by the formula:

$$68\,200 \times \frac{1}{40} \times \frac{4 \times 10^{-3}\, g\ (peptide)}{Mw(peptide)} \times 1000 = carrier\,(mg)$$

The molar mass of rabbit albumin in 68 200 Daltons.

The carrier was activated with MBS at 1:40 carrier-MBS ratio. The amount of MBS needed to activate the calculated amount of rabbit albumin (carrier) was determined by the formula:

$$314.26 \times 40 \times \frac{carrier\ (mg)}{68\,200} \times 1000 = MBS\,(mg)$$

Where 314.26 is the molar mass of MBS.

Activating the carrier with MBS

MBS (1 mg) was dissolved in 50 µl of DMF, made up to 200 µl with PBS and the volume of the solution containing the required molar quantity of MBS was added to 0.8 ml solution of the rabbit albumin (estimated amount) in PBS. The solution was mixed gently for 30 min at RT on a rotary mixer. The mixture was loaded onto Sephadex G-25 size exclusion chromatography column (1.5 cm × 12.5 cm) pre-equilibrated with the MEC buffer. The MBS-rabbit albumin complex was eluted with the MEC buffer by collecting fractions (1 ml). The $A_{280\ nm}$ of the eluate was determined for each fraction. The first set of fractions with $A_{280\ nm} > 0.5$ were pooled (~ 2 ml total volume).

Reducing the peptide with DTT

Peptide (4 mg) was initially resuspended in 50 μl of DMSO and the volume was made up to 0.5 ml with the peptide reducing buffer. DTT reagent (0.5 ml) was added to the peptide and allowed to react (1 h, 37ºC) with occasional mixing. The reduced peptide mixture was loaded onto Sephadex G-10 MEC column (1.5 cm × 11 cm) and eluted with the MEC buffer. Fractions of 1 ml were collected and a sample from each fraction was analysed for free –SH residue with the Ellman's Reagent (10 μl of fraction + 10 μl of Ellman's Reagent). The first set of fractions showing intense yellow colour compared to the first fractions were pooled (~ 2 ml total volume).

Reacting the reduced peptide with the MBS-activated carrier

The pooled MBS-rabbit albumin solution was mixed with the pooled reduced peptide solution. The mixture was incubated at RT overnight. The solution was aliquoted equally into four microfuge tubes and stored at –20ºC.

2.3.5 Preparation of immunogen for immunisation in chickens

The peptide-carrier complex used for production of anti-peptide antibody in chickens was mixed with Freund's complete (FCA) or incomplete adjuvant (FIA). The FCA is made up of heat attenuated and dried *Mycobacterium* mixed in mineral oil to elicit cell-mediated immunity that will result in production of antibody against the peptide as well as the carrier. The FIA is mineral oil without the *Mycobacterium* products.

2.3.5.1 Method

The peptide-carrier complex solution was allowed to thaw at RT and dispensed into a 20 ml scintillation vial containing equal volume of FCA or FIA. The mixture is triturated using a 2.5 ml syringe until an emulsion was formed and the emulsion was loaded into a 2.5 ml syringe. Chickens were immunised intra-muscularly on the large breast muscles with approximately 0.4 ml of the immunogen containing ~ 125 μg of the synthetic peptides. The first immunisation was carried out with FCA and the three subsequent booster immunisations were carried out with FIA at two-week interval with a similar dose. Eggs from each chicken were collected daily, labelled and stored at 4ºC until the isolation of antibody.

2.3.6 Isolation of immunoglobulin Y (IgY) from chicken egg yolk

The solubility of proteins in an aqueous environment depends largely on the surface availability of hydrophilic amino acids of the protein. These hydrophilic amino acids form hydrogen bonds with water molecules in the hydration shell (layer of water molecules surrounding an ion or molecule in an aqueous solution) of the protein molecules. Dextran and PEG are widely used as protein precipitation agents. These polymers (dextran and PEG) are preferentially excluded from the hydration shells around the proteins. This brings the protein solution to it solubility limit (Chun *et al*., 1967; Ingham, 1984; Polson *et al*., 1985). Polyethylene glycol (PEG) is a linear water-soluble non-ionic polymer with molecular weight varying from 0.2 kD to 20 kD depending on the extent of polymerization. It is widely used to extract proteins at room temperature without denaturation of the proteins (Ingham, 1984; Polson *et al*., 1985). PEG with MW 4 kD to 6 kD is routinely used in protein precipitation. Polymers larger than this offer no advantage, since their solutions are more viscous (Atha and Ingham, 1981; Ingham, 1984). By and large, the shorter time required for precipitation of proteins by PEG and little effect on the stability of the proteins makes PEG a molecule of choice for protein isolation compared to organic solvents and ammonium sulphate.

In this study, PEG 6000 (MW ~ 6 kD) extraction was used to isolate IgY from eggs collected from chickens immunised with the synthetic peptides-rabbit albumin complex using the method of Polson *et al.,* (1985). The buffer system was sodium dihydrogen phosphate buffer, pH 7.6 containing sodium azide as an anti-microbial preservative. Chickens were housed and cared for at the University of KwaZulu-Natal Farms at Ukulinga, Pietermaritzburg. The use of chickens for this study was approved by the University's Ethical Committee with ethical clearance project number: AE/GOLDRING/99/08 for 2001 and 025/04/Animal for 2008.

2.3.6.1 Materials

Isolation buffer [0.1 M $NaH_2PO_4.2H_2O$ pH 7.6, 0.02% (w/v) NaN_3]. $NaH_2PO_4.2H_2O$ (15.6 g) and 0.2g (NaN_3) were dissolved in 950 ml of dH_2O, titrated to pH 7.6 with NaOH and made up to 1 L with dH_2O.

IgY Storage Buffer [0.1 M $NaH_2PO_4.2H_2O$ pH 7.6, 0.1% (w/v) NaN_3]. $NaH_2PO_4.2H_2O$ (15.6 g) and 1g (NaN_3) were dissolved in 950 ml of dH_2O, titrated to pH 7.6 with NaOH and made up to 1 L with dH_2O.

2.3.6.2 Method

Egg yolks were separated from albumin and carefully washed under slow running tap water in order to remove traces of albumin. The yolk sacs were punctured and squeezed carefully into a measuring cylinder to determine the yolk volume. Two yolk volumes of the isolation buffer were added and stirred slowly to mix with the yolk. Solid PEG-6000 [3.5% (w/v)] was added and stirred continuously until the entire PEG-6000 dissolved. The precipitated vitellin fraction was removed by centrifuging (4420 *g*, 30 min, RT). The supernatant was filtered though a funnel packed with cotton wool. The volume of the filtrate was measured and PEG [8.5% (w/v)] was added to the filtrate and stirred thoroughly. The solution was centrifuged (4420 *g*, 10 min, RT) to pellet the precipitate. The supernatant was discarded and the pellet dissolved in a buffer volume equivalent to the original egg yolk volume. PEG-6000 [12% (w/v)] was added stirred thoroughly and centrifuged (4420 *g*, 10 min, RT). The final pellet was dissolved in the buffer with volume equivalent to $^1/_6$ the original yolk volume. The purification profile was analyzed by applying samples collected at each step of the isolation method on a reducing-SDS-PAGE (Laemmli, 1970). The final IgY concentration was determined using the extinction coefficient of $E^{1mg/ml}_{280nm} = 1.25$ (Coetzer *et al.*, 1985).

2.3.7 Preparing affinity chromatography matrices and purification of anti-peptide IgY

Affinity purification offers specificity-based separation of biomolecules based on unique biological interactions. The matrix consist of polyacrylamide, dextran or agarose polymerized beads. The matrix is insoluble and is usually commercially synthesized to acquire specific functional groups such as aldehyde, carboxylic acid, hydroxyl, amine and hydrazide. The ligand is immobilized on the matrix (solid) support by means of several coupling reactions. Molecules to be purified adsorb on the immobilized ligands when passed though the affinity column. The remaining components in the mixture are washed off the column. The column is washed with 5× the appropriate column buffer before eluting the adsorbed molecules. A buffer of low pH or high

ionic strength is often used to disrupt the affinity-based interaction between the adsorbed molecules and the ligand.

SulfoLink® Coupling Gel is a 6% beaded agarose that has been derivatized to have iodoacetyl group spaced by a 12-atom structure (Pierce SulfoLink manual). This enables the covalent bonding of molecules such as peptides and proteins ligands with free SH functional groups to the iodoacetyl functional group on the affinity support. The 12-atom spacer is designed to decrease steric hindrance between the coupled ligand and the affinity-bound molecule, enhancing the binding of the molecule to its ligand. The molecule to be coupled must be in monomeric units without a disulfide linkage. Thus, the molecule must be reduced with DTT to acquire free SH reactive functional group prior to coupling to the affinity support. The reducing agent (DTT) must be removed to prevent competing with the peptide for bonding on the iodoacetyl functional group on the affinity matrix. The SH group reacts with the iodide on the iodoacetyl functional group on the matrix to form a stable thioether bond.

2.3.7.1 Materials

Coupling buffer [0.05 M Tris-HCl, pH 8.5, 5 mM Na_2-EDTA]. Tris (6.5 g) and Na_2-EDTA (1.86 g) were dissolved in 900 ml of dH_2O. The pH was adjusted to 8.5 with HCl and the volume made up to 1 L.

Blocking buffer [0.05 M L-cysteine in coupling buffer]. L-cysteine (2.2 g) was dissolved in 250 ml of coupling buffer.

Wash solution [1 M NaCl]. NaCl (58.44 g) was dissolved in 1 L of dH_2O.

Equilibration buffer [0.1 M $NaH_2PO_4.2H_2O$, pH 7.6, 0.1% (w/v) NaN_3]. $NaH_2PO_4.2H_2O$ (15.6 g) and 1g (NaN_3) were dissolved in 950 ml of dH_2O. The pH was adjusted to 7.6 with NaOH and the volume made up to 1 L with dH_2O.

Affinity column-washing buffer [100 mM $NaH_2PO_4.2H_2O$, 0.02% (w/v) NaN_3, pH 6.5]. $NaH_2PO_4.2H_2O$ (15.6 g) and NaN_3 (0.2 g) were dissolved in 800 ml of dH_2O, stirred and adjusted to pH 6.5 with NaOH. The volume was made up to 1 L.

Elution buffer [100 mM glycine, 0.02% NaN_3 (w/v), pH 2.8]. Glycine (0.75 g) and NaN_3 (0.02 g) were dissolved in 80 ml of dH_2O, adjusted to pH 2.8 with HCl and the volume finally made up 100 ml.

Neutralizing buffer [1 M $NaH_2PO_4.2H_2O$, 0.02% NaN_3 (w/v), pH 8.5]. $NaH_2PO_4.2H_2O$ (15.6 g) and NaN_3 (0.02 g) were dissolved in 80 ml of dH_2O, stirred, adjusted to pH 8.5 with concentrated NaOH and the volume finally made up to 100 ml.

2.3.7.2 Method

Coupling of peptides to SulfoLink™ affinity matrix

For coupling of peptides to affinity matrix, 7.5 mg of the peptide was reduced as described in Section 2.3.4. SulfoLink™ matrix (3 ml of 50% slurry = 1.5 ml column volume) was dispensed into a BioRad Poly-Prep® affinity column. The matrix was equilibrated with 5 column volumes of coupling buffer. The buffer was allowed to flow through the matrix until the meniscus was just above the matrix. The reduced peptide solution was added to the matrix and the column was capped with the outlet closed. The suspension was mixed on a rotary mixer (15 min, RT), and was further incubated (30 min, RT) while standing. The cap and the outlet were opened to let the solution containing a reaction by-products and uncoupled peptides to elute. The matrix was washed with 5 column volumes of the coupling buffer, the outlet was closed and 1 ml of the blocking buffer was added to the matrix and capped. The suspension was mixed once again (15 min, RT) on a rotary mixer and the allowed to stand (30 min, RT). The column outlet and cap were opened allowing the buffer to drain out. The matrix was washed with 5 column volumes of the wash solution and equilibrated with 5 column volumes of the equilibration buffer. The affinity matrix was stored at 4ºC until use.

Affinity purification

The affinity column was first washed with 20 column volumes of washing buffer. The isolated IgY was filtered with Whatman No.1 filter paper to remove insoluble materials that may clog the affinity column. The filtrate was cycled through the column overnight (in a reverse direction) and the unbound antibodies were washed off the column with 20 column volumes of affinity column-washing buffer in the forward direction. The bound antibodies were eluted in the forward direction (flow rate of 200 μl/ min) up to 1 ml with the elution buffer into microfuge tubes containing 100 μl of the neutralizing buffer. The $A_{280\ nm}$ was read and then the elution profile was obtained by plotting the $A_{280\ nm}$ against elution volume. Fractions with $A_{280\ nm}$ >0.2 were pooled together. The affinity purified polyclonal anti-peptide IgY was stored at 4°C in a 100 mM sodium phosphate buffer, pH 7.2 containing 0.1% sodium azide.

2.3.8 Enzyme linked immunosorbent assay for anti-peptide IgY titre

Enzyme linked immunosorbent assay (ELISA) involves several parts that makes up a complete immunoassay system namely: a solid phase on which the antigen or antibody to be assayed is immobilized; antigen or antibody to be assayed; blocking molecule, which is usually protein that does not interfere with the assay; primary antibody, which interacts with the antigen or antibody immobilized on the solid phase. Depending on the ELISA format the primary antibody may be linked to the detecting enzyme in direct ELISA system. In an indirect ELISA system a secondary antibody that interacts with the primary antibody is linked to the detecting enzyme in the direct ELISA. Peroxidase, glucose oxidase and alkaline phosphatase are widely used as detecting enzymes in ELISA. These enzymes catalyse the conversion of colourless substrates or non-fluorescent molecules into coloured or fluorescent molecules that are quantified by spectrophotometry or fluorimetry. These substrates form part of the ELISA system (Nakamura *et al*., 1986). In this study, ELISA was used to determine the weekly anti-peptide IgY titre for each immunised chicken in an indirect ELISA technique.

2.3.8.1 Materials

Phosphate buffered saline (PBS). NaCl (8 g), KCl (0.2 g), Na_2HPO_4 (1.15 g) and KH_2PO_4 (0.2 g) were dissolved in 1 L of dH_2O.

Blocking solution [0.5% (w/v) bovine serum albumin-PBS]. BSA (0.5 g) was dissolved in 100 ml of PBS.

Tween-PBS washing solution [0.1% (v/v) Tween-PBS]. Tween-20 (1 ml) was made up to 1 L with PBS.

0.15 M citrate-phosphate buffer at pH 5.0. A solution of citric acid monohydrate (21 g/L) was titrated with a solution of $Na_2HPO_4.2H_2O$ (35.6 g/L) to pH 5.

Substrate solution [0.05% (w/v) ABTS and 0.0015% (v/v) H_2O_2 in citrate-phosphate buffer]. ABTS (7.5 mg) and H_2O_2 (7.5 µl) were dissolved in citrate-phosphate buffer at pH 5 (15 ml).

2.3.8.2 Method

A 96-well microtitre plate (Nunc Maxi Sorp™) was coated with 150 µl of 1 µg/ml of peptide in PBS over night at 4ºC. The following day, the plate was washed with Tween-PBS and blocked with 0.5% BSA-PBS (30 min, RT). After blocking, the plate was washed 3× with Tween-PBS. The plate was incubated with 150 µl (100 µg/ml) of crude IgY isolate or IgY isolated from pre-immune egg as control as primary antibody (2 h, 37ºC), washed 3× with Tween-PBS. The rabbit-anti-chicken-HRPO secondary antibody (150 µl of 1:20 000 dilution) was added to each well and incubated (1 h, 37ºC). After incubation, the plate was washed 3× with Tween-PBS and 150 µl of substrate solution was added to each well. The plate was incubated at RT until the colour developed and the absorbance was read at 405 nm with the VersaMax™ ELISA plate reader.

2.4 Parasitological techniques

Rodent malaria parasites including *P. yoelii*, *P. berghei*, *P. vinckei* and *P. chabaudi* are adapted for laboratory studies. All four rodent malaria parasites infect mice. The study of interaction between the host and the erythrocytic stage of the malaria parasite makes the mouse a very useful host for malaria infection models to study immunological, molecular and biochemical aspects of the parasite (Sanni *et al.*, 2002). There is a degree of variation in virulence in various mouse malaria model species and strains. There are strains of *P. yoelii* that are lethal in mice whereas some other *P. yoelii* strains are non-virulent in mice.

This section describes several techniques used in the propagation, isolation and purification of *P. yoelii*; a rodent malaria parasite. In this study, the lethal *P. yoelii* stain 17XL was used. Parasites were propagated in 6 – 8 weeks old male BALB/c mice through intraperitoneal injection of 100 µl of 10^7 parasitized red blood cells. Mice used in this study were kept in the University Animal housing facility in a temperature range of 19 – 22ºC. Each animal was kept in a single cage with a plastic bottom and steel mesh. Cages, saw dust, water and food were autoclaved prior to use. Food and water were available *ad libitum.* Parasitemia was monitored daily through thin blood smear made from the tail blood.

2.4.1 Propagation of *P. yoelii* parasite in BALB/c mice and cryo-preservation

2.4.1.1 Materials

Phosphate buffered saline (PBS), pH 7.2. NaCl (8 g), KCl (0.2 g), Na_2HPO_4 (1.15 g) and KH_2PO_4 (0.2 g) were dissolved in 1 L of dH_2O.

Cryo-preservative [10% (v/v) glycerol-PBS]. Glycerol (1 ml) was added to 9 ml of PBS. The solution was stirred and autoclaved.

2.4.1.2 Method

Parasites were propagated in male BALB/c mice by intra-peritoneal injection of parasite stabilate (10^7 parasitized red blood cells). The lower abdomen was cleaned with 70% ethanol and the mouse held upside down for the organs to partially drop. The syringe (insulin syringe, 1 cc) was inserted ~ 0.5 cm into the skin and the stabilate slowly released into the mouse. The syringe was slowly withdrawn to prevent exuding of the stabilate after injection. The mouse was immediately release into its cage and monitored for 5 – 10 min post injection. Parasitemia was monitored with daily thin smear of tail blood. The thin smear was air-dried and fixed in methanol for 1 min at RT and was allowed to dry at RT. The smear was stained with Giemsa stain for 20 – 30 min at RT, washed under slow running water and air-dried and viewed at 1000× magnification (oil immersion). The number of infected RBC was expressed as a percentage of total RBC. The parasites were preserved in 10%-glycerol-PBS at 10^7 parasitized-RBC (pRBC) per 100 µl of stabilate. The stabilate was immediately stored in liquid nitrogen.

2.4.2 Isolation of *P. yoelii* parasites from infected mouse red blood cells

2.4.2.1 Materials

Phosphate buffered saline (PBS), pH 7.2. NaCl (8 g), KCl (0.2 g), Na_2HPO_4 (1.15 g) and KH_2PO_4 (0.2 g) were dissolved in 1 L of dH_2O.

Saponin-PBS [0.05% (w/v) saponin in PBS]. Saponin (5 mg) is dissolved in 10 ml of PBS. This reagent is kept on ice prior to use.

Plasmodipur®

Heparinzed vacuum tubes

2.4.2.2 Method

At 30 – 40% parasitemia, the infected mouse was sacrificed. The blood was dispensed into a heparinzed vacuum tube and kept on ice. The blood was diluted (1:4) with ice cold PBS and filtered with Plasmodipur® according to the manufacturer's instructions to remove host white blood cells. The filtrate was centrifuged (700 *g*, 15 min at 4ºC) to pellet the infected RBC. The cells were washed 3× with ice cold PBS (5 volumes of the original blood volume) and re-suspended in 5 volumes of saponin-PBS. The cell suspension was incubated at RT for 30 min for complete hemolysis. A dark red colour indicates hemolysis of the RBC. The suspension was centrifuged (3500 *g*, 15 min at 4ºC) to pellet the released parasites. The supernatant was removed carefully leaving behind a small volume of the supernatant in order not to disturb the parasite pellet. The parasite pellet was washed 2× with 5 volumes of PBS.

2.4.3 Immunofluorescence microscopy

2.4.3.1 Materials

Fixing reagent [4% (w/v) paraformaldehyde-0.0075% (w/v) glutaraldehyde]. Paraformaldehyde (0.4 g) was suspended in 9 ml of ddH_2O. Drops of 1M NaOH were added while stirring in a boling water bath. The solution was made up to 10 ml with ddH_2O. Glutaraldehyde (1.5 µl of 50% solution) was added. The solution was filtered through a 0.22 µm syringe filter.

Quenching solution (0.1 mg/ml $NaCNBH_4$ in PBS). $NaCNBH_4$ (1.0 mg) was dissolved in 10 ml of PBS. The solution was filtered through a 0.22 µm syringe filter.

Phosphate buffered saline (PBS). NaCl (8 g), KCl (0.2 g), Na_2HPO_4 (1.15 g) and KH_2PO_4 (0.2 g) were dissolved in 1 L of dH_2O. The solution was filtered through a 0.22 µm syringe filter.

Permeabilizing solution (0.1% Triton X-100 in PBS). Triton X-100 (10 µl) was made up to 10 ml with PBS. The solution was filtered through a 0.22 µm syringe filter.

Saline solution. NaCl, (0.9 g) was made up to 10 ml with dH_2O. The solution was sterilized by filtration (0.22 µm syringe filter). The solution was filtered through a 0.22 µm syringe filter.

BSA-PBS solution [3% (w/v) BSA in PBS]. BSA (0.3 g) was dissolved in PBS (10 ml). The solution was filtered through a 0.22 µm syringe filter.

BSA-PBS solution [5% (w/v) BSA in PBS]. BSA (0.5 g) was dissolved in PBS (10 ml). The solution was filtered through a 0.22 µm syringe filter.

DAPI solution [5 µg/ml in PBS]. DAPI (2.5 µl of a 2 mg/ml solution) was made up to 1 ml with PBS. The solution was filtered through a 0.22 µm syringe filter.

2.4.3.2 Method

P. yoelii-infected mouse blood (300 µl) collected in a heparinised-tube was centrifuged (700 *g*, 10 min, 4ºC), the plasma was discarded and packed cells were resuspended in 1 ml of PBS and washed 5× with PBS (800 *g*, 10 min, 4ºC) until the supernatant became very clear. The packed cells were resuspended to 2× original blood volume (600 µl) with the Fixing reagent and incubated on ice for 30 min. The cells were washed 5× (800 *g*, 5 min, 4ºC) with saline solution, resuspended in the quenching reagent (0.5 ml) for 10 min on ice and washed 5× (800 *g*, 5 min, 4ºC) with saline solution. The cell were incubated in the permibilizing reagent (0.5 ml) for 10 min and washed 3× (800 *g*, 5 min, RT) with saline solution. The cells were blocked with 0.5 ml of BSA-PBS reagent (1 h, RT); aliquots of 100 µl were transferred to fresh microfuge tubes

and cells were pelleted (800 *g*, 5 min, RT). The cells were incubated in 5 – 20 µg/ml primary antibody in 3% BSA-PBS (overnight and 4ºC). The cells were equilibrated to room temperature (1 – 2 h), washed 5× (800 *g*, 5 min, RT) with saline solution and incubated with donkey anti-IgY-FITC secondary antibody ($^{1}/_{50}$ in 5% BSA-PBS) for 1 h at RT (away from light). The cells were washed 5× (800 *g*, 5 min, RT) with saline solution, stained with DAPI solution (away from light), washed 5× (800 *g*, 5 min, RT) with saline solution and resuspended to approximately 50 µl with PBS. A thin smear was made on a microscope slide and cells were allowed to dry overnight in a desiccated vacuum chamber away from light and mounted with SlowFade using coverslip. The edges of the cover slip were sealed with clear nail varnish. There was 5 min incubation period between each wash steps. The cells were viewed with Olympus AX70 fluorescent microscope using a green and UV filters for FITC and DAPI, respectively. Images were captured with CC12 Soft Imaging System™ colour camera and processed with the analySIS™ software.

2.5 Molecular biology methods

This section describes several methods that were used to obtain parasite nucleic acids used for downstream applications such as PCR, ligation, cloning, subcloning, analysis of expression by RT-PCR, Northern blot and expression of recombinant *P. yoelii* proteins. The design of oligonucleotides used for cloning and expression are based on sequences published on the plasmodb web site (www.plasmodb.org). Molecular grade reagents were used to ensure quality of the products.

2.5.1 Agarose gel electrophoresis

2.5.1.1 Materials

Na_2EDTA [0.5 M]. Na_2EDTA (18.6 g) was dissolved in 80 ml of dH_2O, pH was adjusted to 8 and the volume was made up to 100 ml with dH_2O.

50× TAE electrophoresis buffer. Tris (242 g) was dissolved in 500 ml of dH_2O, 100 ml of 0.5 M Na_2EDTA solution (pH 8) and glacial acetic acid (57.1 ml) were added. The solution was made up to 1 L with dH_2O and stored at RT.

Ethidium bromide staining reagent [10 mg/ml in 1× TAE]. Ethidium bromide (0.1 g) was resuspended in 1× TAE (10 ml) and stirred at RT for 30 min. The dye solution was filtered with Whatman No.1 filter paper and stored in an amber bottle at RT.

10× sample loading buffer. Bromophenol blue (0.25 g) was resuspended in 33 ml of 1× TAE and glycerol (60 ml) was added and the solution made up to 100 ml with 1× TAE. The reagent was stored at RT.

2.5.1.2 Method

The required amount of agarose was weighed and resuspended in the required amount of 1× TAE, heated in a microwave oven and removed from the oven after complete melting of the agarose powder granules. Ethidium bromide reagent was added to a final concentration of 0.5 µg/ml of agarose gel. The gel was poured into the casting tray and allowed to solidify at RT. The sample was mixed (9:1 sample-sample loading buffer ratio) with the loading buffer and loaded into the wells. The image of the electrophoregram was captured with the VesaDoc™ gel documentation system under UV light. The size of the DNA bands were interpolated from the graph of Log DNA standards (bp) against distance migrated (mm) from the well.

2.5.2 Isolation of *Plasmodium yoelii* total RNA

2.5.2.1 Materials

Sodium citrate buffer [0.75 M, pH 7]. Tri-Na citrate (9.7 g) was dissolved in 40 ml of ddH_2O and the pH was adjusted to 7 with 1 M citric acid solution. The volume was made up to 50 ml with ddH_2O.

10% (w/v) N-laurylsarcosine. N-laurylsarcosine (1 g) was dissolved in ddH_2O and the volume made up to 10 ml with ddH_2O.

RNA extraction buffer [4 M guanidine thiocyanate, 45 mM sodium citrate (pH 7), 0.9% (w/v) N-laurylsarcosine, 0.7% (v/v) 2-mercaptoethanol]. Stock reagent of 100 ml was prepared by mixing guanidine thiocyanate (47.3 g), 0.75 M citrate buffer (6 ml) and 10% N-laurylsarcosine (9 ml) in

50 ml of ddH_2O and stirred. The volume was made up to 100 ml with ddH_2O. β-mercaptoethanol (70 µl) was added to 10 ml of the stock reagent before use.

Sodium acetate [2 M, pH 4]. Anhydrous sodium acetate (16.4 g) was dissolved in 40 ml of ddH_2O and the pH was adjusted to 4 with acetic acid.

Water-saturated-acidic phenol. Molecular grade phenol (carbolic acid) was mixed with equal volume of ddH_2O and stirred continuously for 30 min. The mixture was transferred into a separation funnel and allowed to stand for more than four hours at RT until the mixture separates into two phases. The lower phenol phase was carefully removed and stored in 1 ml aliquots at –20ºC, away from light.

Chloroform-isoamylalcohol [49:1]. Chloroform (49 ml) was mixed with isoamylalcohol (1 ml) and stored at –20ºC.

DEPC-treated ddH_2O. DEPC was mixed to a final concentration of 0.1% (v/v) with ddH_2O. The mixture was incubated overnight at 37ºC and then autoclaved to remove residual DEPC.

70% ethanol in DEPC-ddH_2O. Absolute ethanol (35 ml) was made up to 50 ml with DEPC-treated ddH_2O in a sterile atmosphere.

DEPC-treated TE buffer [10 mM Tris (pH 8), 1 mM EDTA (pH 8)]. Tris (10 ml of 1 M solution at pH 8) was mixed with EDTA (2ml of 0.5 M solution at pH 8). The volume was made up to 1 L with ddH_2O. DEPC was added to 0.1% (v/v), incubated at 37ºC overnight and autoclaved.

Formamide gel-loading buffer. Formamide (160 µl) was mixed with DEPC-treated TE buffer (40 µl) and bromophenol blue dye was added.

2.5.2.2 Method

In this method (Voss, 2002), the packed cell volume was 1.2 ml and the parasitemia was approximately 45%. The parasite was isolated from whole blood as described earlier in Section

2.4.2. The parasite pellet was resuspended in 2.4 ml (2 packed cell volumes) of the RNA extraction buffer and mixed rapidly to completely resuspend and lyse the parasites. Na-acetate (0.2 ml) was added and gently mixed by inverting the tube 20×. Water-saturated acidic phenol reagent (2.4 ml) was added and the tube inverted gently 20× to mix properly. Chloroform-isoamylalcohol (1.6 ml) was added and the tube inverted 20× to mix. The tube was incubated on ice for 5 min and centrifuged (3500 *g*, 4ºC, 30 min). The upper aqueous layer (0.8 ml/tube) was carefully removed and transferred into RNase-free microfuge tube containing 0.7 ml of propan-2-ol, and the tube was incubated at –20ºC for 1 h to precipitate RNA. The tube was centrifuged (15 000 *g*, 4ºC, 20 min) to pellet the RNA. The supernatant was carefully removed and the tube dried for 5 min by inverting on filter paper. The RNA pellet was resuspended in 0.45 ml of the RNA extraction buffer, 50 µl of 2 M Na-acetate and 0.5 ml of water-saturated acidic phenol were added and mixed properly by inverting 20×. Chloroform-isoamylalcohol (0.33 ml) was added and mixed by inverting the tube 20×. The mixture was centrifuged (15 000 *g*, 4ºC, 10 min). The upper aqueous layer was transferred into a fresh RNase-free microfuge tube containing 0.9× the volume of the aqueous supernatant and the RNA precipitated at –20ºC for 1 h. The supernatant was carefully removed and the pellet washed with 1 ml of 70% ethanol-DEPC treated water and centrifuged (15 000 *g*, 4ºC, 5 min). The supernatant was gently removed and the pellet dried for 5 min, The RNA pellet was resuspended in 50 µl of formamide (for Northern blot analysis) or 50 µl of DEPC-treated water (for RT-PCR).

The purity of the RNA was analysed by electrophoresis on a 1.2% agarose gel. The RNA sample (5µl) was mixed with the formamide gel-loading buffer (10 µl) and the sample incubated at 65ºC for 10 min to denature the RNA. Agarose gel electrophoresis was performed. After electrophoresis the gel was viewed under UV and the image was captured. The concentration of RNA was determined spectophotometrically at 260 nm.

2.5.3 Isolation of *Plasmodium yoelii* genomic DNA

In this study, genomic DNA was isolated for molecular cloning of PCR-amplified fragment. Thus the Fermentas^{TM} DNA purification kit was used with modification to ensure higher DNA yields. This kit is designed to isolate genomic DNA from various materials such as whole blood, cell and tissue culture and bacterial culture. The kit is based on one step lysis and selective precipitation

of genomic DNA in alkali conditions. Although the kit specifies extraction of DNA from whole blood, rather purified parasites (150 µl) was used instead. The blood was collected in a microfuge tube containing 0.5 ml of PBS instead of a heparinized tube according to the manufacturer's instruction. The blood cells were washed 3× with PBS before isolating the parasite. Moreover, the precipitation step was prolonged by cooling at –20ºC for 30 min to enhance DNA precipitation. The DNA pellet was resuspended in sterile ddH_2O and stored in aliquots at –70ºC. DNA yield and purity were analysed by spectrophotometry and standard 0.5% agarose gel electrophoresis

2.5.4 Primers for RT-PCR of PY01695, cloning and subcloning of *PyBCCP* cDNA

Primers were derived from published sequences from the partially sequenced *P. yoelii* genome in the plasmodb^{TM} database. An internet software (www.basic.northwestern.edu/biotools/oligocalc) was used for designing primers with engineered restriction sites for cloning and expression. Secondary structures such as hair pin formation were avoided when designing these primers. Table 2.2 shows the primers used in the study.

Table 2.2 Primers used in the study

Single and double underlines represent added *Eco*RI and *Not*I restriction sites for cloning. Lower case italics are extra bases added to the primers.

Primer name	Sequence (5'→3')	Derived from (Plasmodb ID)	Application
PyACCBC-fwd	GCTAATAATGGTATGGCTGCATTAAAATGTATATTGTC	PY01695	RT-PCR analysis of the expression of PY01695 mRNA. Expected size of amplicon is 1424 bp. Production of probe for Northern blot analysis
PyACCBC-rev	GCAATTTCTCTTGTTTCCCCTTTTGCAAATATATGGCC	PY01695	
PyACCntCxT-fwd	GGAAATAGGACAAAATAAAATGAGCGTAATCGG	PY01695	RT-PCR analysis of the expression of PY01695 mRNA. Expected size of amplicon is 699 bp
PyACCntCxT-rev	GAGATATTCCATTTTTCATCATAATATTTACACCTCC	PY01695	
PyACCctCxT-fwd	GATGTTCTTGGGGAATCAACAAAATCATTTCAC	PY01695	RT-PCR analysis of the expression of PY01695 mRNA. Expected size of amplicon is 1128 bp
PyACCctCxT-rev	CTCCTTCATACATGATGATACATCATGTAGATCTGC	PY01695	
PyBCCP-Fwd	*ga*GAATTCACGGAAGATAGCCTAAATAGGGAAG	PY01695	Cloning and expression of PyACC-BCCP domain and production of probe for Northern blot analysis. Expected size of amplicon is 1041bp.
PyBCCP-Rev	*tt*GCGGCCGCATCTCTGGAGTTACTTTCTATATTCG	PY01695	
PyLDH-fwd	GGATCTGGTATGATTGGAGGTGTTATGGCC	PY03885	Positive control in PCR, RT-PCR and Northern blot analysis. Expected size of amplicon is 850 bp.
PyLDH-rev	TTCGATTACTTGTTCTACACCATTACCACC	PY03885	

2.5.5 Polymerase chain reaction (PCR)

Taq polymerase was used for routine PCR such as expression analysis and colony PCR. But due to mutational errors often introduced by *Taq* polymerase, Expand High Fidelity^{TM} PCR system containing a blend of *Pwo* and *Taq* DNA polymerases was used to limit potential mutations in the PCR-amplified DNA fragment used for cloning and expression. PCR was optimized for each set of primers. Parameters such as annealing temperature, $MgCl_2$ concentration (especially after the reverse transcription reaction) and cycle number (limited to 35 cycles) were varied during optimization. The initial denaturation temperature was 94ºC; extension temperature of 60ºC was used throughout the study as against 72ºC standard PCR extension temperature. The final elongation temperature was 72 ºC. Table 2.3 illustrates the various primers and specific conditions with which those primers were used. The 10× PCR buffer used was detergent and $MgCl_2$ free. PCR products used for cloning were purified from agarose gel (Section 2.5.7) before cloning.

Table 2.3 Primer properties, $MgCl_2$ concentration and thermo cycle condition for PCR

Primer name	T_m (ºC)	[Primer] (µM)	[$MgCl_2$] (µM)	PCR cycle conditions [ºC (time)]	No. of Cycle
PyACCBC-fwd	63	0.5	2.5	94 (30 s)→55 (30 s) →60 (2 min)	35
PyACCBC-rev	71	0.5			
PyACCntCxT-fwd	64	0.5	2.5	94 (30 s) →55 (30 s) →60 (2 min)	35
PyACCntCxT-rev	62	0.5			
PyACCctCxT-fwd	66	0.5	2.5	94 (30 s) →55 (30 s) →60 (2 min)	35
PyACCctCxT-rev	64	0.5			
PyBCCP-Fwd	63	0.8	2.5	94 (30 s) →55 (1 min) →60 (2 min)	30
PyBCCP-Rev	72	0.8			
PyLDH-fwd	65	0.5	2.5	94 (30 s) →55 (30 s) →60 (2 min)	25
PyLDH-rev	67	0.5			

2.5.6 Reverse transcriptase polymerase chain reaction for PY01695 expression analysis

Reverse transcriptase polymerase chain reaction (RT-PCR) was carried out with Improm II^{TM} (Promega) Reverse Transcription System kit according the manufacturer's instruction. *P. yoelii* total RNA isolated from purified parasite (Section 2.4.2) was used as template. The first strand synthesis was amplified with oligodT, or random oligonucleotide hexamers provided by the kit, according to the manufacturer's instructions. The reverse transcriptase product from both oligodT and random oligonucleotide hexamers were subsequently used for PCR

amplification using the following primers: PyACCBC-fwd, PyACCBC-rev, PyACCntCxT-fwd, PyACCntCxT-rev, PyACCctCxT-fwd, PyACCctCxT-rev, PyLDH-fwd and PyLDH-rev (Table 2.2). The conditions for PCR have already been described in Section 2.5.5 and Table 2.3. The amplified PCR product was resolved on a 1% agarose gel and the image captured with VesaDoc™ image documentation system.

2.5.7 Purification of DNA from agarose gel

In this study, purification of cDNA and plasmids was carried out with the peQLab™ gel purification kit. Both kits were designed to rapidly purify a DNA fragment of 100 bp – 10 kb that has been previously resolved on an agarose gel using mini-spin columns with a silica membrane. The kit is based on the capability of guanidine thiocyanate to denature agarose gel at 60 – 65ºC and extract the DNA fragment, which binds tightly to the silica membrane and reaction by-products, buffer ions in the agarose gel flow through the membrane. Using TE or sterile deionised water, the DNA fragment is eluted and concentrated into small volumes in purer form after several washes with an ethanol-based washing solution. DNA purification was carried out according to the manufacturer's instructions. The sample containing the DNA fragment was initially resolved on agarose gel as described in Section 2.5.1. The band that corresponded to the wanted DNA fragment was excised from the gel under UV light in 10 sec exposure to prevent UV-mediated cutting of DNA fragment. Aliquots of the samples before and after purification were kept for agarose gel analysis.

2.5.8 *PyBCCP* cDNA ligation using T4 ligase

DNA ligation is a biochemical reaction catalysed by DNA ligase; an enzyme that forms covalent phosphodiester bonds between 3' hydroxyl end of one nucleotide to the 5' phosphate end of another nucleotide. This technique thus enables successful cloning of DNA fragments obtained by PCR or excised from genomic DNA into plasmid vectors for creation of a cDNA library or for recombinant expression of the protein encoded by the DNA fragment (Sambrook, 1989a). T4 DNA ligase is widely used in molecular biology for ligation reactions. This enzyme originates from bacteriophage T4 but recombinantly expressed in *E. coli*. T4 DNA ligase and 10× T4 DNA ligase buffer were obtained from Fermentas™.

2.5.8.1 Materials

10× T4 buffer (Fermentas #EL0016), T4 ligase (Fermentas #EL0016), cDNA insert, linear DNA plasmid and sterile ddH_2O.

2.5.8.2 Method

All the processes were carried out on ice. cDNA from PCR or after restriction digestion or restriction endonuclease-digested plasmid was initially purified from agarose gel as described in Section 2.5.7. The approximate amount of the DNA was determined using the Fermentas DNA MassRuler^{TM} or by absorbance at 260 nm. The ligation reaction volume was 10 µl. The insert DNA and the plasmid DNA were added at 4:1 insert-plasmid ratio. The ligation reaction components were added as illustrated in Table 2.4 and the volume made up to 10 µl with sterile ddH_2O. The reaction mix was vortexed gently briefly centrifuged and incubated (4ºC, 16 h). The reaction mix was used directly for transformation of *E. coli* without deactivation of the enzyme.

Table 2.4 T4 Ligase reaction parameters

Components	Quantity
10× T4 ligase buffer	1.0 µl
Insert DNA	4× [plasmid]
Plasmid	0.25× [insert DNA]
T4 ligase	2.5 U
Sterile ddH_2O	Variable
Total volume	10 µl

2.5.9 Cloning of *PyBCCP* cDNA fragment into pJET1® blunt end cloning plasmid

pJET1 cloning vector (Figure 2.1) is a 3.128 kb linear plasmid DNA that has been designed to clone blunt end PCR fragments generated by DNA polymerases with a 3' → 5' exonuclease (proof reading) activity. The vector encodes a multiple cloning site (MCS) with an upstream P_{lacUV5} promoter region. The insert position interrupts a gene *eco47*IR (GeneBank ID: X82105), which codes for a restriction endonuclease lethal to most *E. coli* strains used for cloning. Thus only cells with the recombinant plasmid will grow. pJET1 also codes for an ampicillin resistance gene *bla* (β-lactamase). The recombinant plasmid can be digested with the restriction enzymes encoded by the cloned fragment to excise the fragment (GeneJET™ cloning technical manual, www.fermentas.com). In this study, blunt end PY01695 gene fragment derived from PCR amplification of *P. yoelii* genomic DNA using PyBCCP-Fwd, PyBCCP-Rev encoding an *EcoR*I and a *Not*I sites was cloned into pJET1 to produce pJET-PyBCCP recombinant plasmid. The gene of interest was subsequently excised from the

recombinant pJET1-PyBCCP plasmid with *EcoR*I and *Not*I restriction enzymes to generate gene fragments with sticky non-complementary ends used for subcloning into pET-28a and pGEX-4T-1 expression vectors (Section 2.5.11).

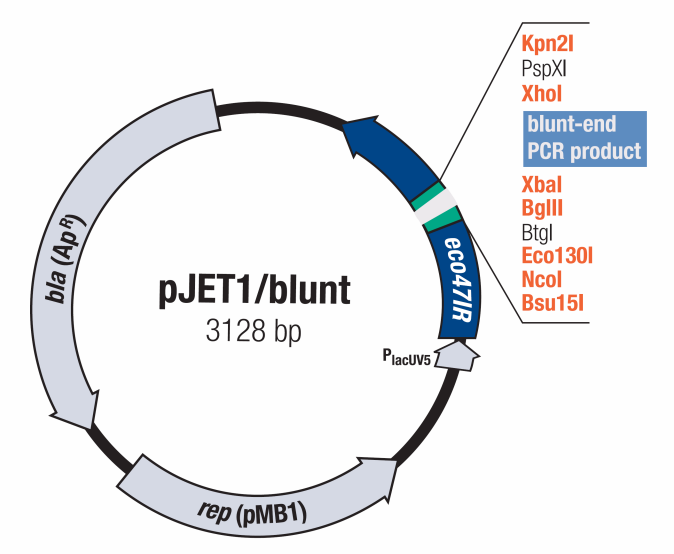

Figure 2.1 A map of the pJET1 blunt end cloning vector. The plasmid encodes a toxic gene *eco47IR* that is lethal to host cells with circularized plasmid without insert. The insert is cloned into the region between *Xho*I and *Xba*I (Fermentas, 2006).

2.5.10 Plasmid isolation

In this study, plasmid was isolated by the phenol-chloroform-isoamyl method (Sambrook, 1989b). The method is based on the underlying principles of differential precipitation between chromosomal DNA and plasmid DNA in a bacterial lysate. Purity of the isolated plasmid was evaluated by agarose gel electrophoresis.

2.5.10.1 Materials

GTE solution [50 mM glucose, 25 mM Tris-HCl pH 8, 10 mM di-Na-EDTA]. Glucose (1 g), Tris (0.3 g) and di-Na-EDTA (0.37 g) was dissolved in 80 ml of dH_2O, pH was adjusted to 8 with HCl and volume made up to 100 ml with dH_2O. The solution was autoclaved and stored at 4ºC.

Lysis reagent [1% (w/v) SDS, 0.2 M NaOH]. NaOH (0.08 g) and SDS (0.1 g) was dissolved in 10 ml of dH_2O. This solution was store at 4ºC for 1 week.

Potassium acetate [3 M KOH pH 4.8]. KOH pellet (16.8 g) was dissolved in 25 ml of acetic acid. The pH was checked after neutralisation and subsequently adjusted to 4.8 with acetic acid. The volume was made up to 100 ml with dH_2O and stored at 4ºC.

Phenol-chloroform-isoamyl alcohol [25:24:1 (v/v)]. Liquefied phenol (50 ml), chloroform (48 ml) and isoamyl alcohol (2 ml) was mixed and stored at RT in an amber bottle.

Chloroform-isoamyl alcohol [24:1 (v/v)]. Chloroform (48 ml) and isoamyl alcohol (2 ml) was mixed and stored at RT.

Sodium acetate [3 M NaOH pH 5.5]. NaOH pellet (12 g) was dissolved in 25 ml of acetic acid. The pH was checked after neutralization and subsequently adjusted to 5.5 with acetic acid. The volume was made up to 100 ml with dH_2O and stored at 4ºC.

70% (v/v) ethanol in dH_2O. Absolute ethanol (70 ml) was made up to 100 ml with dH_2O and stored at –20ºC.

2.5.10.2 Method

This method was adapted for the isolation of plasmid from a 50 ml overnight *E. coli* culture and was carried out in a 15 ml Falcon tube (RNase and DNase free). The culture was centrifuged (3500 *g*, 15 min, 4ºC) to pellet the cells. The cell pellet was resuspended in $1/100^{th}$ the culture volume (0.5 ml) with GTE, RNase A was added (10 U/1 ml) to the cell suspension and transferred to a 15 ml Falcon tube. Lysis reagent (0.5 ml) was added and the cells were mixed until the cells were completely lysed. Potassium acetate (1 ml) was added and mixed for 5 min and centrifuged (11 500 *g*, 30 min, RT). The supernatant containing the plasmid was carefully removed without carrying over the white pellet into a fresh 15 ml falcon tube. An equal volume of phenol-chloroform-isoamyl alcohol was added to the supernatant and mixed gently for 5 min. The mixture was centrifuged (11 500 *g*, 30 min, RT); the upper aqueous phase was gently transferred into a fresh 15 ml falcon tube and mixed with equal volume of chloroform-isoamyl alcohol for 2 min at RT. The mixture was centrifuged (11 500 *g*, 30 min, RT); the upper aqueous phase was gently transferred into a fresh 15 ml

falcon tube. Sodium acetate (1/10th the volume of aqueous supernatant) and ice-cold 100% ethanol (2.5 volume of the aqueous supernatant), mixed and incubated at –20ºC for 1 h. The precipitated plasmid was pelleted (11 500 *g*, 30 min, 4ºC), washed twice with ice-cold 70% ethanol and resuspended in sterile 1× TE buffer. The plasmid resolved on a 1% agarose gel for purity evaluation.

2.5.11 Expression plasmids used in the study

pET-28a

In this study, pET-28a (Figure 2.2) was used to express recombinant *P. yoelii* biotin carboxyl carrier protein (PyBCCP). The 1 kb gene fragment containing the BCCP domain was cloned into the vector at the *Eco*RI and *Not*I site. The product was expected to have an additional 48 to 50 amino acid residue as a result of the insert position relative to the start codon (bp 296 on the plasmid) situated at the *Nco*I site. The host strain used for pET-28a expression in this study was *E. coli* Rosetta (DE3) pLysS strain. The construct and the recombinant cells will be referred to as pT-PyBCCP and Rosetta-pT-PyBCCP respectively.

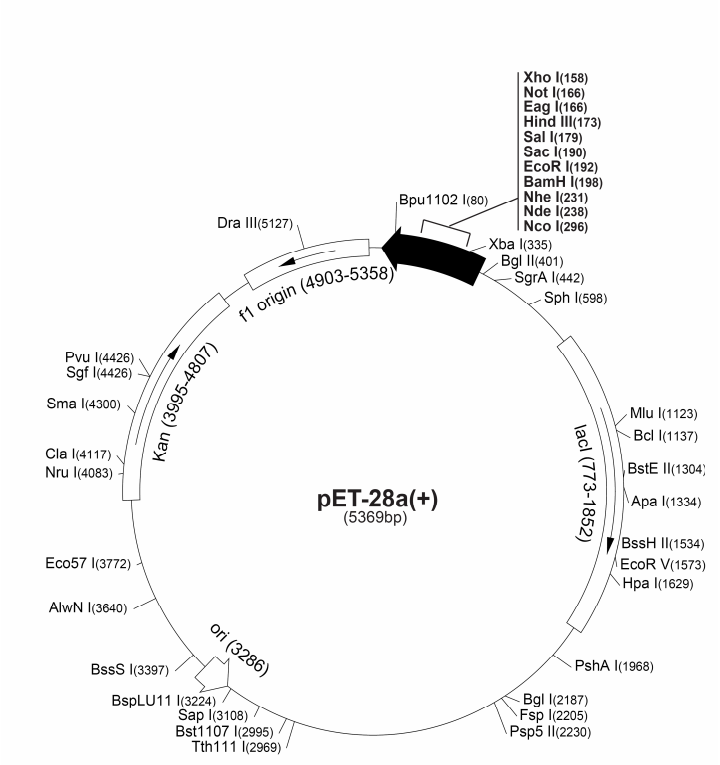

Figure 2.2 A map of the pET-28a expression plasmid. The figure illustrates restriction sites and important features of the pET-28a plasmid including the kanamycin resistant gene (kan) and the multiple cloning region. The gene of interest was inserted in the *Not*I and *Eco*RI sites, in frame with the N-terminal His_6-tag (pET-28a-c(+) and Vectors, 1998).

pGEX-4T-1

pGEX-4T-1 (Figure 2.3) was used to express recombinant GST-PyBCCP. The 1 kb gene fragment containing the biotin carboxyl carrier protein (or biotinoyl) domain was cloned into the vector at the *Eco*RI and *Not*I sites in frame with the N-terminal GST-tag protein. The host strain used was *E. coli* BL21. The construct and the recombinant cells will be referred to as pGX-PyBCCP and BL21-pGX-PyBCCP respectively.

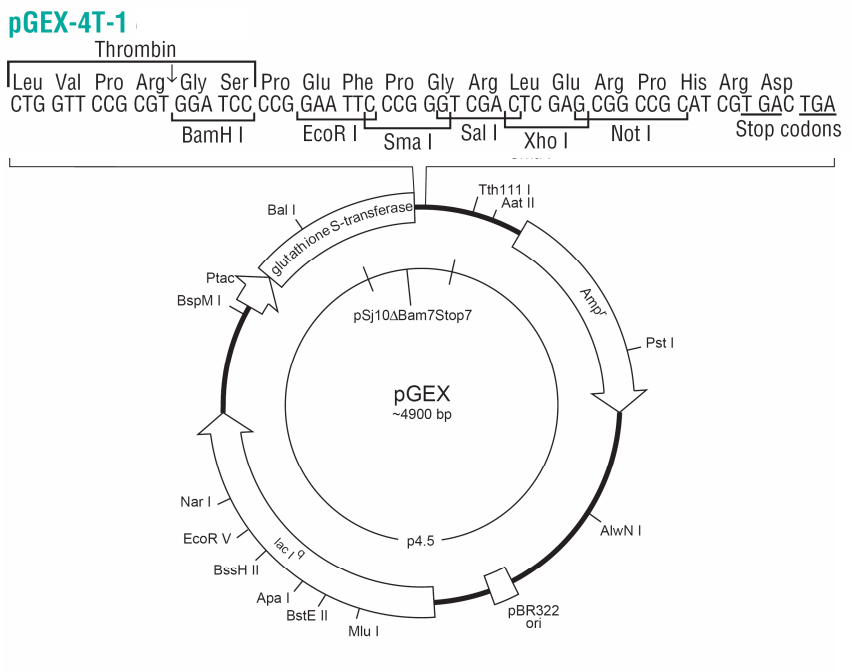

Figure 2.3 A map of pGEX-4T-1 expression plasmid. The figure illustrates restriction sites and important features of the plasmid including the glutathione S-transferase (GST) gene, the ampicillin resistant gene (Amp^r), the inducible P_{tac} promoter and the multiple cloning region. The gene of interest was inserted in the *Not*I and *Eco*RI sites, in frame with the GST gene (AmershamBiosciences, 2002).

2.5.12 Restriction endonuclease digestion of plasmids

The expression plasmids used in this study encoded an *EcoR*I site and a *Not*I site in their multiple cloning sites. Therefore the forward primers were designed to encode an *EcoR*I site (5'GAATTC3') while the reverse primers were designed to encode the palindromic *Not*I site (5'GCGGCCGC3'). The primer design allowed for cloning of the cDNA as fusion protein in pGEX-4T-1 (GST-fusion) and pET-28a (His_6-T_7-tagged). To prepare the plasmids for ligation and cloning of the cDNA it was necessary to digest the expression plasmid with *EcoR*I and

*Not*I to create non-complementary sticky ends for the ligation of gene of interest. The presence of a 5'-phosphate group may result in circularization of the plasmid and was avoided by dephosphorylation of the digested plasmid with shrimp alkaline phosphatase (SAP). The digestion was analysed on an agarose gel (1%). The digested plasmids was purified from agarose gel to eliminate nucleic acid fragments, buffer components, enzymes and nucleotides that may compromise the cloning of the target gene into the plasmid. The insert DNA to be subcloned into an expression plasmid was initially cloned into pJET1 for propagation in *E. coli*. This strategy reduces the likelihood of PCR-introduced mutations when PCR product is cloned directly into an expression vector. The inserts were cut out of the vector using *Eco*RI and *Not*I restriction enzymes and purified from the agarose gel.

2.5.12.1 Materials

*Eco*RI restriction enzyme, *Not*I restriction enzyme, shrimp alkaline phosphatatse (SAP), Fermentas 10× Orange Buffer™ (Buffer O) and recombinant/non-recombinant super coiled plasmid DNA

2.5.12.2 Method

E. coli cells containing a recombinant (with insert DNA) cloning or expression plasmid in glycerol stock was streaked on LB-agar plate containing the appropriate antibiotic and incubated (37°C, overnight). The following day, a single colony was picked with a sterile toothpick and used to inoculate 10 ml of 2×YT with the antibiotic and grown with shaking (37°C, 250 rpm, overnight). The culture was transferred into a 15 ml falcon tube and the cells pelleted by centrifugation (3500 *g*, 15 min, 25°C). Plasmid isolation was carried out as described in Section 2.5.10. A 100 µl reaction volume was set up in the following order: 10× Buffer O (10 µl), plasmid (89 µl), first (*Eco*RI) restriction enzyme (1 µl). The reaction mix was vortexed gently, centrifuged briefly to collect the mix at the bottom of the tube and incubated (30°C, 5 h). The first enzyme was deactivated (65°C, 20 min) and the tube chilled on ice. 2 µl of the mix was analysed by agarose gel electrophoresis (Section 2.5.1) before the next restriction digestion step. Thereafter 1 µl of the second enzyme (*Not*I) was added directly to the mix and incubated (RT, overnight). After incubation, the enzyme was deactivated (85°C, 15 min) and chilled on ice. 2 µl of the mix was analysed on agarose gel prior to dephosphorylation of the plasmid. SAP (1.5 µl) was added to the plasmid digestion mix and immediately incubated (37°C, 2.5 h). The cDNA fragment restricted from the cloning

plasmids was not dephosphorylated. The dephosphorylated plasmid and the cDNA fragment were purified from agarose gel (Section 2.5.7) before the ligation reaction.

2.5.13 *E. coli* hosts used for cloning and expression of recombinant proteins

Table 2.5 *E. coli* hosts used for cloning and expression of recombinant proteins

E. coli strain	Genotype	Application
JM109	F´ *traD36 proA$^+$B$^+$ lacI^q Δ(lacZ)M15/ Δ(lac-proAB) glnV44 e14$^-$ gyrA96 recA1 relA1 ndA1 thi hsdR17*	Maintenance and propagation of recombinant plasmids for transformation into expression cells
BL21^p	*F$^-$ ompT hsdS$_B$ (r$_B^-$ m$_B^-$)gal dcm*	Expression of recombinant pGEX-4T-1
Rosetta (DE3) pLysS$^{TM\ p}$	*F$^-$ ompT hsdS$_B$ (r$_B^-$ m$_B^-$)gal dcm (DE3) pLysS RARE26 (CamR)*	Expression of recombinant pET-28a vectors

^{p} deficient in lon protease

2.5.14 Transformation and culturing of *E. coli* transformants

2.5.14.1 Materials

$MgCl_2.6H_2O$ [1 M]. $MgCl_2.6H_2O$ (2.03 g) was dissolved in a final volume of 10 ml with ddH_2O and filter sterilised with a 0.2 µm syringe filter. The solution was used for SOC media.

$MgSO_4$ [1 M]. MgSO4 (1.2 g) was dissolved in a final volume of 10 ml with ddH_2O and filter sterilised with a 0.2 µM syringe filter. The solution was used for SOC media.

Glucose monohydrate [1 M]. Glucose monohydrate (1.98 g) was dissolved in a final volume of 10 ml with ddH_2O and filter sterilised with a 0.2 µM syringe filter. The solution was used for SOC media.

SOC Medium[2% (w/v) tryptone, 0.5% (w/v) yeast extract, 10 mM NaCl, 2.5 mM $MgCl_2$, 10 mM $MgSO_4$ and 20 mM Glucose].Tryptone (0.5 g), NaCl (0.015 g) and yeast extracts (0.125 g) were suspended in 25 ml of dH_2O and autoclaved. The media was cooled to ~ 55°C. $MgCl_2.6H_2O$ (125 µl), $MgSO_4$ (500 µl) and glucose (1 ml) were added to the media and the volume was made up to 50 ml with sterile (autoclaved) ddH_2O. The media was aliquoted into sterile microfuge tubes and stored at –20°C.

LB-agar [1% (w/v) tryptone, 0.5% (w/v) yeast extracts, 1.5% (w/v) agar, 10% (w/v) NaCl, pH 7.4]. Tryptone (10 g), yeast extracts (5 g) and NaCl (10 g) were completely resuspended in 900 ml of dH_2O with continuous stirring. The pH was adjusted to 7.4 with NaOH, agar (15 g) was added and the volume made up to 1 L with dH_2O. The media was autoclaved (121ºC, 20 min), cooled to ~ 55ºC and antibiotics added as illustrated in Table 2.6 depending on the requirement of the *E. coli* to be cultivated. The media was dispensed into sterile plastic culture plates, allowed to solidify and sealed with Parafilm™. Plates were stored at 4ºC.

2×YT [1.6% (w/v) tryptone, 1% (w/v) yeast extracts and 0.5% (w/v) NaCl, pH 7.4]. Tryptone (16 g), yeast extracts (10 g) and NaCl (5 g) were completely resuspended in 900 ml dH_2O with continuous stirring and the pH was adjusted to 7.4 with NaOH. The media was autoclaved, allowed to cool to RT and required amount of antibiotics added (see Table 2.6).

Potassium acetate [1 M, pH 7.5]. Potassium acetate (9.8 g) was dissolved 60 ml of ddH_2O, pH adjusted to 7.5 with KOH and volume made up to 100 ml with of ddH_2O. The solution was sterilised by filtration through a 0.22 µm syringe filter. This reagent was used in FSB and DTT-DMSO reagents.

Frozen stock buffer (FSB) [100 mM KCl, 45 mM $MnCl_2.4H_2O$, 10 mM $CaCl_2.2H_2O$, 3 mM hexamine cobalt chloride ($HACoCl_3$) 10 mM potassium acetate and 10% (w/v) glycerol, pH 6.2]. K-acetate (1 ml), KCl (0.74 g), $MnCl_2.4H_2O$ (0.98 g), $CaCl_2.2H_2O$ (0.15 g), $HACoCl_3$ (80 mg) and glycerol (10 g) were dissolved in 80 ml of ddH2O, pH adjusted to 6.2 and volume made up to 100 ml with ddH2O. The buffer was sterilised by filtration through a 0.22 µm syringe filter and used immediately to prepare competent *E. coli* cells.

DTT-DMSO [1 M DTT, 10 mM potassium acetate and 90% (v/v) DMSO]. Molecular biology grade DTT (1.54 g), K-acetate (0.1 ml) and DMSO (9 ml) were made up to 10 ml with sterile ddH_2O. This reagent was used immediately or stored at –20°C.

2.5.14.2 Method

Preparation of competent cells

An overnight culture made from a single *E. coli* colony was diluted 1/10 with fresh media and grown to $OD_{600\ nm} \approx 0.6$ at 30ºC shaking. The cells were pelleted (1000 *g*, 15 min, 4 ºC),

drained thoroughly and resuspended in $^{1}/_{10}^{th}$ the culture volume with cold FSB. The cell suspension was incubated on ice for 15 min and pelleted (1000 *g*, 15 min, 4 ºC). The cells were resuspended in 1/50th the culture volume with cold FSB, 17.5 µl of DTT-DMSO was added, mixed gently and incubated on ice for 10 min. 17.5 µl of DTT-DMSO was added the second time, mixed gently and incubated on ice for 20 min. 100 µl of the cell suspension was aliquoted into cold sterile microfuge tubes using chilled sterile pipette tips. The cells were quick-frozen in liquid nitrogen (5 min) and stored at –70ºC until use.

Transformation of competent *E. coli* cells

Ligation mix (5 µl) was added directly to the competent cells, the transformation mix was incubated on ice for 60 min and heat shocked at 42ºC for 90 sec. The cells were incubated on ice for 2 min, SOC (200 µl) was added to the cells and incubated at 37ºC for 60 min shaking. The cells were plated on LB-amp plates (ampicillin resistant encoded plasmids) and incubated at 37ºC.

2.5.15 Antibiotics used for positive selection and maintenance of *E. coli* transformants

Stock solutions of the antibiotics were prepared in ddH_2O or methanol and sterilized by filtration through a 0.22 µm syringe filter into sterile microfuge tubes in a sterile environment and stored an –20°C. Chloramphenicol was dissolved in methanol because it is insoluble in water and stored at –20°C. Table 2.6 illustrates the applications, concentration of stock and working solutions of antibiotics used in this study.

Table 2.6 Selective antibiotic: concentrations and applications

Antibiotic	[Stock] (mg/ml)	[Working] (µg/ml)	Application
Ampicillin	50	100	Used in LB-agar plates for selection of *E. coli* with ampicillin-encoded pJET1 and pGEX-4T-1.
Carbenicillin	50	100	Used for overnight culture, out growth and induction of expression in *E. coli* with ampicillin resistant pGEX-4T-1 expression plasmid. A more stable β-lactam analogue of ampicillin.
Chloramphenicol	30[a]	30	Used in LB-agar plates and 2×YT broth for selection of Rosetta (DE3) pLysS™ *E. coli* strains with the pLysS encoded plasmid for tight regulation of IPTG-expression.
Kanamycin	34	34	Used in LB-agar plates and 2×YT broth for selection of transformed Rosetta (DE3) pLysS™ *E. coli* strains with recombinant pET-28a for expression.

[a] Stock solution prepared in 100% methanol

2.5.16 Preparation of probes for Northern blot analysis

Probes for Northern blot analysis were prepared with Biotin DecaLabel™ DNA labeling kit according to the manufacturers instruction. PCR product from amplification of PyBCCP using PyBCCP-fwd and PyBCCP-rev and PyLDH using PyLDH-fwd PyLDH-rev were used as DNA template. PCR products were purified from agarose gel as described in Section 2.5.7 prior to labelling.

2.5.17 Northern blotting, hybridisation and enhanced chemiluminescence detection

2.5.17.1 Materials

DEPC-treated TE buffer (Section 2.5.2.1).

Formamide gel-loading buffer (Section 2.5.2.1).

5× SSC [0.75 M NaCl, 0.1M citric acid, pH 7]. NaCl (43.8 g) and citric acid (20.5 g) dissolved in 800 ml of ddH_2O, pH adjusted to 7 and volume made up to 1 L. The buffer treated with 0.1% DEPC and autoclaved.

Transfer buffer [5× SSC, 10 mM NaOH]. 1 ml of 1 M NaOH was added to 99 ml of 5× SCC.

5× SSC-NaH_2PO_4 [50 mM NaH_2PO_4, 0.75 M NaCl, 0.1 M citric acid, pH 6.5]. NaCl (4.38 g), citric acid (2.05 g) and NaH_2PO_4 (0.6 g) were dissolved in 80 ml of de-ionised dH_2O, pH adjusted to 6.5 and volume made up to 100 ml. The buffer treated with 0.1% DEPC and autoclaved.

50× Denhardt solution [BSA (1% w/v), polyvinylpyrrolidone 40 000 (1% w/v) and ficoll 400 (1% w/v)]. BSA (1 g), polyvinylpyrrolidone (1 g) and ficoll (1 g) were dissolved in 80 ml of DEPC-treated ddH_2O, made up to 100 ml with DEPC-treated ddH_2O and filter-sterilised. The solution was stored at –20ºC.

Pre-hybridisation buffer. Formamide (25 ml), 50× Denhardt solution (0.5 ml), herring sperm DNA (0.25 g) were made up to 50 ml with 5× SSC-50 mM NaH_2PO_4.

Hybridisation buffer. Biotinylated DNA probe (0.1 µg) was denatured at 100ºC for 10 min, cooled on ice and added to the pre-hybridisation buffer.

2× SSC-Tween (wash solution 1). 5× SSC (40 ml) was mixed with Tween-20 (1 ml) and the volume was made up to 100 ml with DEPC-treated ddH_2O.

0.1× SSC-Tween (wash solution 2). 5× SSC (2 ml) was mixed with Tween-20 (1 ml) and the volume was made up to 100 ml with DEPC-treated ddH_2O.

0.1 M Tris-HCl, pH 7.5. Tris (1.21 g) was dissolved in DEPC-treated ddH_2O, pH adjusted to 7.5 with HCl and volume made up to 100 ml with DEPC-treated ddH_2O.

BSA-Tris-HCl. BSA (0.5 g) was dissolved in 100 ml of 0.1 M Tris-HCl, pH 7.5.

Avidin-peroxidase solution. 1/500 dilution of avidin-peroxidase was prepared in BSA-Tris-HCl.

Stock luminol solution [40 mg/ml]. Luminol (40 mg) was dissolved in DMSO (1 ml) and stored at –20ºC for up to 6 months.

Stock *p*-iodophenol solution [0.1 M]. *p*-iodophenol (22 mg) was dissolved in DMSO (1 ml) and stored at –20ºC for 6 months.

ECL reagent. Luminol stock (50 µl), *p*-iodophenol stock (25 µl) and 30% H_2O_2 (25 µl) were made up to 10 ml with 0.1 M Tris-HCl buffer. The reagent was stored on ice away from light until use.

2.5.17.2 Method

Separation of total RNA by agarose gel electrophoresis

The RNA sample was prepared by mixing an appropriate amount (25 µg) with formamide gel-loading buffer (20 µl). The sample was incubated at 65ºC for 10 min. The sample was loaded onto 1.2% agarose gel (ethidium bromide concentration at 0.01 mg/ml). Electrophoresis was performed at 25 V for 8 cm long gel (3 – 4 V/cm gel). After electrophoresis, the gel was incubated in 7% (v/v) formamide for 10 min to enhance transfer of the resolved RNA onto a nitrocellulose membrane (Pélle and Murphy, 1993). A single stranded RNA marker was used to estimate the size of the RNA band on the gel using the graph of Log RNA base pair (bp) against distance migrated (mm) from the well.

Transfer to nitrocellulose membrane and cross linking of RNA to membrane

The blotting papers and the nitrocellulose membrane were wet with the transfer buffer to avoid trapping air bubbles between the membrane and the blotting paper. The bottom of the gel was also wet with the transfer buffer and the membrane was carefully laid over the gel placed upside down avoiding trapping of air bubbles between the gel and the membrane. The transfer was allowed to proceed overnight at RT without disturbing the assembly. The membrane is removed and pictured under UV to establish transfer of RNA. The blot was dried and baked at 80ºC for 2 h to cross-link the blotted RNA to the nitrocellulose membrane. The position of the molecular weight markers on the membrane was marked with pencil under UV.

Pre-hybridisation and hybridisation

The nitrocellulose membrane was incubated with minimal volume of prehybridisation buffer (enough to cover the membrane) in an RNase free Tupper ware container with lid in a water bath (42ºC for 20 h). This was followed with the hybridization buffer (42ºC for 24 h). The

membrane was washed 4× with wash solution 1 (5 min each at RT), followed by 2× with wash solution 2 (15 min each at 50ºC).

Avidin-peroxidase labeling and enhanced chemiluminescence detection

The nitrocellulose membrane was equilibrated by washing the nitrocellulose membrane in BSA-Tris (3×, 10 min each). The nitrocellulose membrane was incubated in avidin-peroxidase reagent overnight at 4ºC on a slow rocker, washed 5× with 0.1 M Tris-HCl, pH 7.5 (RT, 5 min per wash) and the ECL reagent applied on the nitrocellulose membrane; just enough to cover the entire membrane. The nitrocellulose membrane was covered with a cling wrap film avoiding trapping air bubbles. An X-ray film was placed over the membrane aligning the cut out sections on both the nitrocellulose membrane and the X-ray film and incubated placed in a film cassette for 35 min at RT.

Developing the X-ray film

Prior to exposure to exposure of the membrane to the X-ray film, the developer (STRUCTURIX G128™) and the fixer (G333c™) were diluted 1/3 and 1/4, respectively, with ddH_2O in separate baths. Immediately after exposure, the X-ray film was immersed in the developer for 5 min and transferred in the fixing solution for 2 min (in a dark room). The X-ray film was washed with tap water (under light) and allowed to dry while hanging.

2.6 Recombinant protein techniques

This section describes all techniques that were employed for the expression of recombinant PyBCCP from pT-PyBCCP and pGX-PyBCCP (pET-28a and pGEX-4T-1 constructs respectively). Biotinylation of rabbit albumin as a control for the biotinylation study is also described. SDS-PAGE analysis and Western blotting techniques had been described in Sections 2.3.1 and 2.3.2, respectively.

2.6.1 Expression of His_6-PyBCCP and GST-PyBCCP

2.6.1.1 Materials

Cell resuspension buffer [0.02 M Tris-HCl, 0.25 M NaCl, 0.1% (w/v) NaN_3, 1 mM DTT, 5% (v/v) glycerol, 0.5 mM PMSF, pH 7]. Tris (0.24 g), NaCl (1.5 g), PMSF (8.7 mg), NaN_3 (0.1 g), DTT (15 mg) and glycerol (5 ml) were completely dissolved in 85 ml of dH_2O, pH adjusted to 8 with HCl and volume made up to 100 ml with dH_2O.

2.6.1.2 Method

Expression of His_6-PyBCCP

Three-way streak of cells containing the recombinant plasmid (pT-PyBCCP in Rosetta (DE3) pLysS) was made on 2×YT-agar plate supplemented with kanamycin (34 µg/ml) and chloramphenicol (30 µg/ml) and incubated (37ºC, 16 h). A single colony was used to inoculate 2×YT-media (5 ml) supplemented with kanamycin and chloramphenicol (2×YT-kan-cam) and the culture was incubated (37ºC, 16 h). The culture was diluted 1/100 with fresh 2×YT-kan-cam and incubated at 37ºC until the culture had an OD of 0.6 (at 600 nm) after which the culture was induced with or without IPTG (0.5 mM) and incubated (37ºC, 5 h or 18ºC, 16 h). Cells were harvested by centrifugation (3500 *g*, 15 min, 4ºC) and suspended in $1/100^{th}$ of the culture volume with cell resuspension buffer. The cell suspension was subjected to three freeze-thaw cycles between 37ºC and –196ºC (liquid nitrogen for 2 min) and further disrupted by sonication on ice (10 cycles, 5 sec/burst, 1 min between bursts). The total cell lysate was analysed for expression by SDS-PAGE and Western blotting using monoclonal anti-His-tag antibody.

Expression of GST-PyBCCP

Three-way streak of cells containing the recombinant plasmid (pGX-PyBCCP in BL21) was made on 2×YT-agar plate supplemented with ampicillin (100 µg/ml) and incubated (37ºC, 16 h). A single colony was used to inoculate 2×YT-media (5 ml) supplemented with ampicillin 2×YT-amp) and the culture was incubated (37ºC, 16h). The cells were washed 2× (1000 *g*, 5 min, RT) with fresh media to reduce the effect of β-lactamase secreted into the media by the cells. The culture was diluted 1/100 with fresh 2×YT-amp and incubated at 37ºC until $OD_{600\ nm}$ of the culture was approximately 0.6 after which the culture was induced with or without IPTG (0.5 mM) and incubated (37ºC, 5 h). The culture was continuously supplemented with ampicillin (100 µg/ml) every hour during expression. For prolonged expression (18ºC, 16 h), the 2×YT media was supplemented with carbenicillin (100 µg/ml). Cells were harvested by centrifugation (3500 *g*, 15 min, 4ºC) and suspended in $1/100^{th}$ of the culture volume with cell resuspension buffer containing egg white lysozyme (1 mg/ml) and incubated (37ºC, 20 min). The cell suspension was subjected to three cycles of freeze thaw between 37ºC and –196ºC (liquid nitrogen for 2 min) and further disrupted by sonication on ice (10 cycles, 5 sec/burst, 1 min between bursts). The total cell lysate was analysed for expression by SDS-PAGE and Western blotting using monoclonal anti-GST antibody.

2.6.2 Purification and refolding of His_6-PyBCCP

2.6.2.1 Materials

TALON® metal affinity resin (1.5 ml matrix volume).

Pellet wash buffer [2 M Urea, 0.02 M Tris-HCl, 2.5% (v/v) Triton X-100, pH 8]. Urea (60 g), Tris (1.2 g) and Triton X-100 (12.5 ml) were completely dissolved in 350 ml of dH_2O, pH adjusted to 8 with HCl and volume made up to 500 ml with dH_2O. The buffer was stored at RT.

Solubilisation buffer [6 M guanidine-HCl, 0.02 M Tris-HCl, 0.25 M NaCl, 0.02 M imidazole, pH 8]. Guanidine-HCl (57.3 g), Tris (0.24 g), NaCl (1.5 g), and imidazole (1.4 g) were completely dissolved in ~ 25 ml of dH_2O, pH adjusted to 8 with HCl and volume made up to 100 ml with dH_2O. The buffer was stored at RT.

Wash buffer 1 [8 M urea, 0.02 M Tris-HCl, 0.5 M NaCl, pH 8]. Urea (24 g), Tris (0.12 g) and NaCl (1.45 g) were completely dissolved in ~ 10 ml of dH_2O, pH adjusted to 8 with HCl and volume made up to 50 ml with dH_2O. The buffer was stored at RT.

Wash buffer 2 [8 M urea, 0.02 M Tris-HCl, 0.03 M imidazole, pH 8.0]. Urea (24 g), Tris (0.12 g) and imidazole (0.1 g) were completely dissolved in ~ 10 ml of dH_2O, pH adjusted to 8 with HCl and volume made up to 50 ml with dH_2O. The buffer was stored at RT.

Elution buffer [8 M urea, 0.02 M Tris-HCl, 1 M imidazole, pH 8]. Urea (24 g), Tris (0.12 g) and imidazole (3.4 g) were completely dissolved in ~ 10 ml of dH_2O, pH adjusted to 8 with HCl and volume made up to 50 ml with dH_2O. The buffer was stored at RT.

Dialysis buffer 1 [4 M urea, 0.02 M Tris-HCl, 0.25 M L-arginine, 5% (v/v) glycerol, pH 8]. Urea (120 g), Tris (1.21 g), L-arginine (21.8 g) and glycerol (25 ml) were completely dissolved in 250 ml of dH_2O, pH adjusted to 8 with HCl and volume made up to 500 ml with dH_2O.

Dialysis buffer 2 [2 M urea, 0.02 M Tris-HCl, 0.25 M L-arginine, 10% (v/v) glycerol, pH 8]. Urea (120 g), Tris (2.4 g), L-arginine (43.6 g) and glycerol (100 ml) were completely

dissolved in 850 ml of dH_2O, pH adjusted to 8 with HCl and volume made up to 1 L with dH_2O.

Dialysis buffer 3 [1 M urea, 0.02 M Tris-HCl, 0.25 M L-arginine, 15% (v/v) glycerol, pH 8]. Urea (60 g), Tris (2.4 g), L-arginine (43.6 g) and glycerol (150 ml) were completely dissolved in 750 ml of dH_2O, pH adjusted to 8 with HCl and volume made up to 1 L with dH_2O.

Dialysis buffer 4 [0.5 M urea, 0.02 M Tris-HCl, 0.25 M L-arginine, 20% (v/v) glycerol, pH 8]. Urea (30 g), Tris (2.4 g), L-arginine (43.6 g) and glycerol (200 ml) were completely dissolved in 650 ml of dH_2O, pH adjusted to 8.0 with HCl and volume made up to 1 L with dH_2O.

Equilibration buffer [0.02 M Tris-HCl, 0.25 M L-arginine, 0.5 mM PMSF, 0.1% (w/v) NaN_3 20% (v/v) glycerol, pH 8]. Tris (2.4 g), L-arginine (43.6 g), PMSF (87 mg), NaN_3 (1 g) and glycerol (200 ml) were completely dissolved in 650 ml of dH_2O, pH adjusted to 8 with HCl and volume made up to 1 L with dH_2O.

2.6.2.2 Method

Purification of insoluble recombinant His_6-PyBCCP

TALON resin slurry (3 ml) containing ~ 1.5 ml of resin was placed into a BioRad affinity column washed with 10 column volumes (15 ml) of Solubilisation buffer. Insoluble protein pellet obtained from large scale expression (5 L) was washed 3 times with pellet wash buffer (12 000 *g*, 30 min, 4ºC). The protein pellet was dissolved in 50 ml of Solubilisation buffer and centrifuged (12 000 *g*, 30 min, 4ºC) to remove insoluble materials that may block the affinity column. The protein sample was continuously circulated over the affinity matrix (16 h, RT, 0.25 ml/min) in a reverse direction. The matrix was washed with 10 column volume of the following in this order: Solubilisation buffer, wash buffer 1 and wash buffer 2. Bound proteins were eluted from the matrix with the elution buffer (0.25 ml/min, 1 ml/fraction, 15 ml) and $A_{280\ nm}$ of each fraction was recorded. Fractions with $A_{280\ nm} > 0.5$ were pooled and the purification profile was analysed by SDS-PAGE (Section 2.3.1).

Refolding of recombinant His_6-PyBCCP

Dialysis membrane (10 kD MWCO) was washed; the eluted protein sample (2 ml) was placed in the dialysis bag and sealed. The protein was dialysed by continuous stirring against the buffers as illustrated in Table 2.7.

Table 2.7 Dialysis schedule for refolding of His_6-PyBCCP

Buffer	Vol (ml)	Time (h)	Temp	Number of changes	[Urea] (M)	Estimated [urea] (mM) at equilibrium
Dialysis buffer 1	250	6	RT	2	4.0	32.0
Dialysis buffer 2	1000	18	RT	1	2.0	0.064
Dialysis buffer 3	500	6	RT	2	1.0	1.28×10^{-4}
Dialysis buffer 4	1000	6	4ºC	2	0.5	1.28×10^{-7}
Equilibration buffer 1	1000	6	4ºC	3	0	8.53×10^{-11}

The final protein sample was concentrated with Centricon™ (30 kD MWCO) to a final volume of 0.85 ml and stored at –20 ºC. The refolding profile was analysed with SDS-PAGE and final protein concentration estimated by Bradford (Section 2.3.3).

2.6.3 Biotinylation of rabbit albumin

2.6.3.1 Materials

Reaction buffer [0.1 M $NaH_2PO_4.2H_2O$, 0.15 M NaCl, 0.1% (w/v) NaN_3, pH 7.5]. $NaH_2PO_4.2H_2O$ (7.8 g), NaCl (4.4 g) and NaN_3 (0.5 g) were dissolved in 450 ml of dH_2O, pH was adjusted to 7.5 and the volume was made up to 500 ml with dH_2O.

NHS-biotin solution [10 mg/ml]. NHS-biotin (1 mg) was dissolved in DMSO (100 µl).

Rabbit albumin solution [20 mg/ml]. Rabbit albumin (10 mg) was dissolved in 500 ml of reaction buffer.

2.6.3.2 Method

The amount of NHS-biotin (MW 341.38) to be coupled to 10 mg of rabbit albumin at a ratio of 20:1 NHS-biotin is to rabbit albumin was derived to be 1 mg of NHS-biotin/10 mg rabbit albumin. The reaction was initiated by mixing NHS-biotin solution (100 µl) with rabbit

albumin solution (400 µl) and incubating on a rotary mixer (1h, RT). The mixture was loaded onto Sephadex G-25 size exclusion chromatography column pre-equilibrated with the reaction buffer (10 column volumes). The biotin-rabbit albumin complex was eluted with the reaction buffer by collecting fractions (1 ml). The $A_{280\ nm}$ of the eluted fractions was determined for each fraction. The first set of fractions with $A_{280\ nm} > 0.5$ were pooled together (~ 4 ml total volume).

2.6.4 Biotinylation analysis of recombinant His_6-PyBCCP and GST-PyBCCP

2.6.4.1 Materials

D-biotin solution [100 mM in 0.01 M NaOH]. D-biotin (0.24 g) was dissolved in 10 mM NaOH solution and sterilised by filtration through a 0.22 µm syringe filter. The solution was stored at –20ºC.

2×YT-D-biotin-kan-cam. 2×YT was prepared as described in Section 2.5.14.1. D-biotin, kanamycin and chloramphenicol were added to a final concentration of 0.2 mM, 34 µg/ml and 30 µg/ml respectively after autoclaving for Rosetta-pT-PyBCCP cells.

2×YT-D-biotin-amp. 2×YT was prepared as described in Section 2.5.14.1. D-biotin and ampicillin were added to a final concentration of 0.2 mM and 100 µg/ml respectively after autoclaving for BL21-pGX-PyBCCP cells and *P. yoelii* putative copper transporter gene fragment cloned into pGEX-4T-1 in BL21 *E. coli* strain.

2.6.4.2 Method

A similar expression protocol described in Section 2.6.1.2 was employed for this study except that the out-growth 2×YT media was used with or without 0.2 mM D-biotin. The overnight culture was grown to $OD_{600\ nm}$ of approximately 0.6 in 2×YT ± 0.2 mM D-biotin containing the appropriate selective antibiotics (12 ml) and further split into two cultures (5 ml). One of the two was induced with IPTG (0.5 mM) and incubated (37ºC, 5 h or 18ºC, 16 h). For a negative control experiment, *P. yoelii* putative copper transporter gene fragment cloned into pGEX-4T-1 in BL21 *E. coli* strain was expressed using the same conditions as BL21-pGX-PyBCCP. Table 2.8 illustrates the conditions used.

Table 2.8 Culture treatment for biotinylation study

Culture set	1	2	3	4
0.5 mM IPTG	–	+	–	+
0.2 mM D-biotin	–	–	+	+

The cells were harvested as described in Section 2.6.1.2. The total cell lysate was resolved on 10% acrylamide gel by SDS-PAGE (Section 2.3.1) and electro-blotted onto nitrocellulose membrane (Section 2.3.2). The blot was blocked with fresh 5% (w/v) fat-free milk in TBS (Section 2.3.2.1), incubated with or without avidin-peroxidase or monoclonal anti-biotin IgG in the presence or absence of D-biotin (10 mM) or avidin (10 µg/ml) as negative control.

2.7 Bioinformatics methods

2.7.1 Sequence analysis

Sequences for acetyl-CoA carboxylase were extracted from the NCBI (National Centre for Biotechnology Information), swissprot/TrEMBL™ and the Plasmodb™ database. The sequences were saved as text files in FASTA format. The molecular mass and pI values were computed using the ProtParam (Gasteiger *et al*., 2005) programme on the expasy web site (www.expasy.org). The ScanProsite™ (de Castro *et al*., 2006; Gattiker *et al*., 2002) and InterPro Scan™ (Mulder *et al*., 2002) were used to obtain the amino acid sequence domains corresponding to the biotin carboxylase, biotinoyl (or biotin carboxyl carrier protein), the N-terminal carboxyl transferase and the C-terminal carboxyl transferase. This programme has a web interface with the Prosite™ (Falquet *et al*., 2002; Hulo *et al*., 2006; Sigrist *et al*., 2002) database containing families of proteins. The Prosite Scan™ (Proscan™) (Bairoch *et al*., 1997) and the NetPhos 2.0™ (Blom *et al*., 1999) programmes were used to predict protein kinase phosphorylation sites on the biotin carboxylase, biotinoyl and the carboxyl transferase (N and C terminal) amino acid sequences. Sequence similarity serach was carried out by protein-protein basic local alignment search tool (pBLAST) on the NCBI web site using default parameters (Altschul *et al*., 1997) and aligned with ClustalW algorithm implemented on the BioEdit™ editor programme (v 7.0.9.0) using 1000 bootstrap analysis with the Neighbor Joining algorithm (BioEdit™ v 7.0.9.0). Both alignment programmes run on the ClustalW™ algorithm (Thompson *et al*., 1994).

2.7.2 Three-dimensional homology modelling

A three-dimensional (3D) model for the *P. yoelii* 17XNL biotin carboxylase and carboxyl transferase domains, as well as the *P. yoelii* 17XL biotinoyl domains were constructed by comparative (homology) modelling using the SWISS-MODEL™ automated server (Kopp and Schwede, 2004). The biotin carboxylase and the carboxylase transferase 3D models were built using the crystal structure of *Saccharomyses cerevisiae* acetyl-CoA carboxylase biotin carboxylase domain (PDB ID: 1w93, 2.5 Å resolution, resolved by X-ray diffraction; (Zhang *et al*., 2004; Zhang *et al*., 2003) and acetyl-CoA carboxylase carboxyl transferase domain (PDB ID: 1bdo, 2.7 Å resolution, resolved by X-ray diffraction; (Shen *et al*., 2004) as templates, respectively. The 3D structure of the biotinoyl domain was built using the *E. coli* acetyl-CoA carboxylase biotinoyl protein as template (PDB ID: 1bdo, 1.8 Å resolution, resolved by X-ray diffraction method; (Athappilly and Hendrickson, 1995). The ClustalW™ (Thompson *et al*., 1994) alignment file obtained between the target sequence (*P. yoelii* sequences) and the template sequences were submitted to the SWISS-MODEL™ alignment interface and the resulting model was downloaded as pdb file. Quality evaluations of the models were carried out by the atomic empirical mean force potential (ANOLEA™) algorithm (Melo and Feytmans, 1998) and the Ramachandran analysis available on the SWISS-MODEL™ server. The ANOLEA™ algorithm calculates the packing qualities of the amino residues in the 3D model. The 3D models were viewed and refined (GROMOS™) with the Swiss-pdb viewer v 3.7 (downloaded from the SWISS-MODEL™ server). ProCheck™ was used validate the models for proper stereochemical conformation of the residues. Imaging was carried out with Adobe Photoshop 7.0™.

2.7.3 Phylogenetic tree construction

The acetyl-CoA carboxylase amino acid sequences were uploaded into the CLC™ free workbench (downloaded from www.clcbio.com). The sequences were aligned using the ClustalW™ (Thompson *et al*., 1994) alignment tool present in the programme. The phylogenetic tree was constructed using the slow and accurate option, 1000 bootstrap analysis and the Neighbour Joining™ tree method. The tree diagram was downloaded as a PDF file and the image edited with the Microsoft™ image editor programme.

2.7.4 Predict7™ epitope prediction

The production of synthetic peptide vaccines and synthetic peptide antigen for antibody production relies on precise prediction of the antigenic sites on a protein molecule (Stern

1991). Immunogenic regions on *P. yoelii* 17XNL acetyl-CoA carboxylase and the *P. yoelii* 17XNL lactate dehydrogenase were predicted using the Predict7™ (Cármenes *et al*., 1989) prediction programme. The programme calculates seven features of an amino acid sequence namely: antigenicity (Welling and Fries, 1985; Welling *et al*., 1985), hydrophilicity (Hopp and Woods, 1981), side chain flexibility, surface probability (Emini *et al*., 1985), hydropathy, secondary structure and N-glycosylation sites. For this study, *P. yoelii* 17XNL acetyl-CoA carboxylase and the *P. yoelii* 17XNL lactate dehydrogenase sequences (saved as text files) were uploaded in the programme and regions satisfying anitgenicity, hydrophilicity, surface probability and side chain flexibility criteria were selected. The prediction file was saved as a text file and the graphics of the four predictions were plotted using Microsoft Excel™ programme. Protein-protein BLAST were carried out on the chosen peptide to ensure that the peptide sequence is absent in *G. gallus* (antibody production host) and *M. musculus* (parasite host). Cysteine residue was added to the peptide sequence to enable conjugation to a carrier molecule.

CHAPTER 3

DETECTION OF *PLASMODIUM YOELII* (17XL) ACETYL-COA CARBOXYLASE mRNA

3.1 Introduction

The sequencing of the *P. falciparum* 3D7 genome as well as the partial sequencing of the genome of the other *Plasmodium species* has in many ways enhanced research in malaria aimed at identifying new metabolic targets or pathways for both vaccine and chemotherapeutic intervention against malaria (Di Girolamo *et al*., 2005; Gardner, 1999; Gardner *et al*., 2002a; Ginsburg, 2006; Hoffman *et al*., 1998). One metabolic pathway that has not been well explored is the *de novo* synthesis of fatty acids in the *Plasmodium* parasite (Gornicki, 2003; Tong and Harwood, 2006). Whether the *Plasmodium* parasite initiates *de novo* fatty acid biosynthesis from acetyl-CoA precursor has yet to be shown experimentally and would require the detection of the acetyl-CoA carboxylase mRNA transcript and protein. Published genome sequences of several *Plasmodium* species showed the presence of a gene, which codes for the enzyme (Plasmodb data base). However there appeared to be inconsistent annotation of the enzyme in several *Plasmodium* acetyl-CoA carboxylase orthologues as well as partial sequence of the gene in some *Plasmodium* species such as *P. berghei* and *P. chabaudi* (Plasmodb data base).

The study was designed to demonstrate (i) that the mRNA transcript that codes for acetyl-CoA carboxylase is present using reverse transcriptase PCR (RT-PCR) and (ii) that by using Northern blot analysis, the size of the transcript, which may be larger than the predicted 8.7 kb ORF due to untranslated regions, can be established. The study also looked at whether the *Plasmodium* acetyl-CoA carboxylase is a multi-enzyme-domain type acetyl-CoA carboxylase found in eukaryotes including mammals, insect, yeast and some green plants or the multi-enzyme-subunit (complex) acetyl-CoA carboxylase form found in bacteria and some dicotyledonous green plants (Jelenska *et al*., 2001; Sasaki and Nagano, 2004; Thelen *et al*., 2001).

3.2 Results

3.2.1 Primer design and detection of acetyl-CoA carboxylase mRNA by RT-PCR

PY01695, as illustrated in the Plasmodb database, is an 8.7 kb oligonucleotide open reading frame. The primary transcript is made up of two 8.5 kb and 221 bp exons separated by a

235 bp intron at the 3' end of the gene. Figure 3.1 illustrates the 18.8 kb partially sequenced chromosome 13 of *P. yoelii* strain 17XNL, which consist of PY01695, the gene coding for acetyl-CoA carboxylase. The positions of the primers relative to the ORF are as follows: PyACCBC-fwd: bp 1275 to bp 1313; PyACCBC-rev: bp 2662 to bp 2699; PyACCntCxT-fwd: bp 6729 to bp 6761; PyACCntCxT-rev: bp 7390 to bp 7426; PyACCctCxT-fwd: bp 7513 to bp 7545 and PyACCctCxT-rev: bp 8605 to bp 8640 (relative to bp 8840 to bp 8876 on the primary transcript). Table 3.1 shows the primer sequences and properties. Figure 3.2 illustrates the position of PyACCctCxT-rev on the ORF of the enzyme with respect to the acetyl-CoA carboxylase gene.

RT-PCR was carried out with Improm II™ (Promega) reverse transcriptase kit using *P. yoelii* total RNA isolated from purified parasites (Section 2.5.2). The first strand was amplified with oligodT or random oligonucleotide hexamers provided by the kit according to the manufacturer's instruction. The reverse transcriptase product from both oligodT and random oligonucleotide hexamers were subsequently used for PCR amplification using the primers in Table 3.1. The amplified PCR product was resolved by electrophoresis on a 1% agarose gel. Figure 3.3 shows the electrophoregram of the RT-PCR. PyACCBC primers (forward and reverse) amplified a product approximately 1500 bp, PyACCntCxT primers amplified a 700 bp product and PyACCctCxT primers amplified a product estimated at 1150 bp. The PCR products were purified from agarose gel and sequenced using the primers corresponding to each product. The two sequences corresponding to the 5' and 3' directions were merged and compared to the published sequence of *P. yoelii* PY01695 using the ClustalW™ algorithm (Figures 3.4 – 3.6). The results confirmed the products amplified by RT-PCR corresponded to the expected regions. However, the products appeared to be more identical to *P. berghei* acetyl-CoA carboxylase sequence by BLAST analysis.

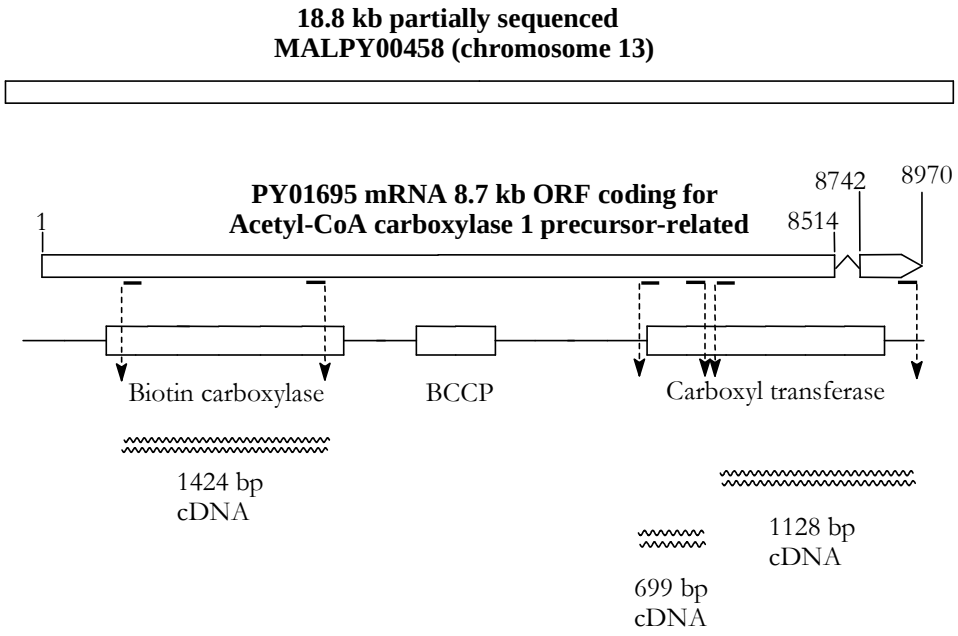

Figure 3.1 Schematic illustration of the MALPY00458 region of *P. yoelii* and PY01695 mRNA transcript. The positions of the primers (**—**) are shown to correspond to the region on the protein encoded by the amplified products. The figures above the ORF represent the length (bp) of the two exons (1 – 8514 and 8749 – 8970).

Table 3.1 Primers used to amplify the biotin carboxylase, N-terminal and C-terminal carboxyl transferase domains of *P. yoelii* acetyl-CoA carboxylase by RT-PCR

Primer	Sequence (5' → 3')	size (bp)	T_m (ºC)	Protein domain region of the amplified cDNA
PyACCBC-fwd	GCTAATAATGGTATGGCTGCATTAAAATGTATATTGTC	38	63	Biotin carboxylase
PyACCBC-rev	GCAATTTCTCTTGTTTCCCCTTTTGCAAATATATGGCC	38	71	Biotin carboxylase
PyACCntCxT-fwd	GGAAATAGGACAAAATAAAATGAGCGTAATCGG	33	64	N-terminal carboxyl transferase
PyACCntCxT-rev	GAGATATTCCATTTTTCATCATAATATTTACACCTCC	37	62	N-terminal carboxyl transferase
PyACCctCxT-fwd	GATGTTCTTGGGGAATCAACAAAATCATTTCAC	33	66	C-terminal carboxyl transferase
PyACCctCxT-rev	CTCCTTCATACATGATGATACATCATGTAGATCTGC	36	64	C-terminal carboxyl transferase

Figure 3.2 ClustalW™ alignment of MALPY00458 with PY01695 (PyACC-ORF) showing the position of PyACCctCxT-rev primer on the ORF. The position of PyACCctCxT-rev primer is highlighted (yellow) and the intron sequence is in bold. Note that the reverse complement of the primer is indicated. MALPY0048 is the Plasmodb accession number of the chromosome where the PY01695 ORF is located.

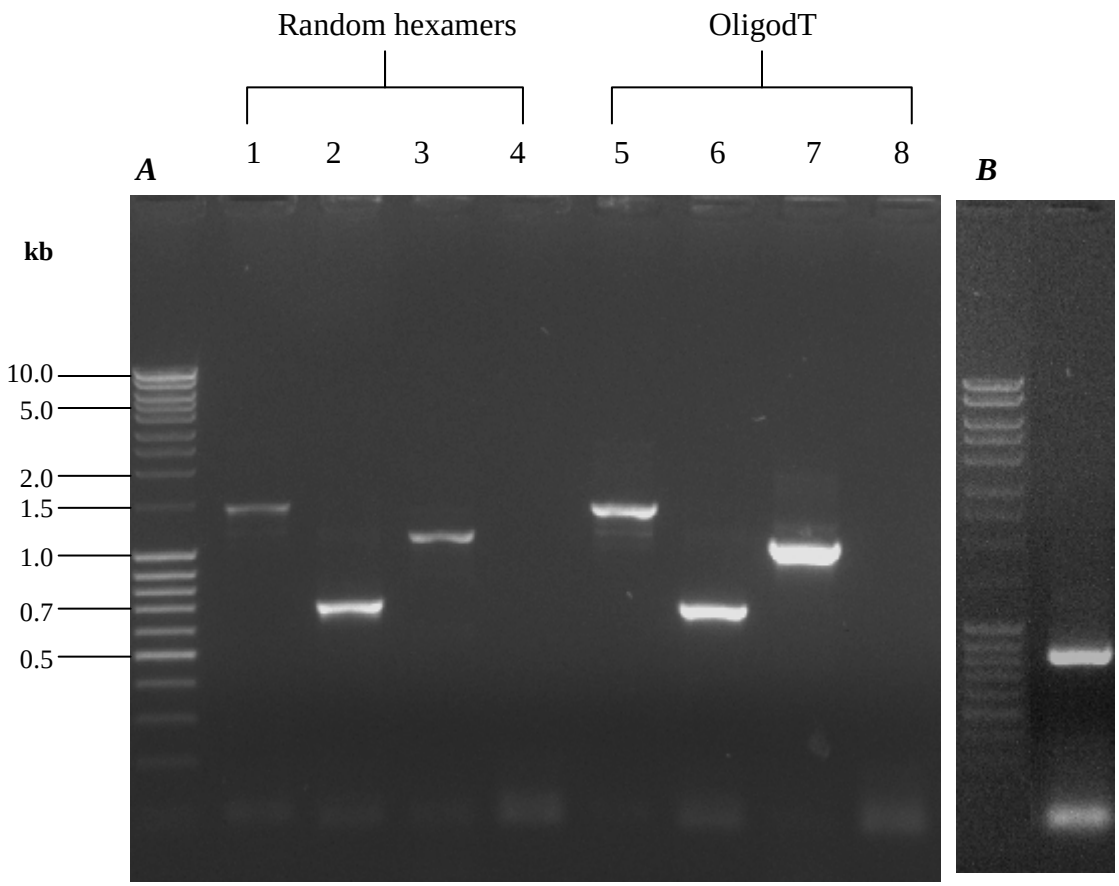

Figure 3.3 Agarose gel electrophoregram of RT-PCR products from PY01695. (*A*) Reverse transcriptase first strand synthesis was carried out using random oligonucleotide hexamers (*lanes 1 – 4*) or oligodT primers (*lanes 5 – 8*) and PCR was carried out with primer set PyACCBC (*Lane1/5*), PyACCntCxT (*lane 2/6*) and PyACCctCxT (*lane 3/7*). No template control amplified with PyACCctCxT (*lane 4/8*). (*B*) RT-PCR amplification of PyLDH cDNA (850 bp) as a control. Amplification products were resolved on a 1% (w/v) agarose gel.

Figure 3.4 Alignment of PY01695 ORF with the product of biotin carboxylase RT-PCR amplification. RT-PCR-PyBC is the merged sequences corresponding to the forward and the reverse primer sequencing products. Approximately 700 bp were sequenced in both directions.* indicates 100% conserved nucleotide.

```
PY01695.          GGAAAAAGCATCTATACGTTTAACAAAAATGATCAAATATAGAGGTGCAGGAACCATTGA 2159
RT-PCR-PyBC.      GGAAAAAGCATCTATACGTTTAACAAAAATGATCAAATATAGAGGTGCGGGAACCATTGA 841
                  ********************************************** ***********

PY01695.          ATATTTATATGATCAAGTTAATAACAAATATTATTTTTTAGAATTAAATACCCGTTTACA 2219
RT-PCR-PyBC.      ATATTTATATGATCAAGTTAATAACAAATATTATTTTTTAGAATTAAATACTCGTTTACA 901
                  ************************************************** ********

PY01695.          AGTAGAGCATCCTGTTTCAGAAGGAATAACAGATACCAATATTGTCGCTATTCAACTTCA 2279
RT-PCR-PyBC.      AGTAGAGCATCCCGTTTCAGAAGGAATAACAGATACCAACATTGTTGCTATTCAGCTTCA 961
                  ************ ************************* ***** ******** *****

PY01695.          AGTTGCTATGGGCATACCTCTTCAAAATATAGATGATATAAAAAAATTATATAAAATAGA 2339
RT-PCR-PyBC.      AGTTGCTATGGGTATACCTCTTCAAAATATAGATGATATAAAAAAATTATATAAAATAGA 1021
                  ************ ********************************************

PY01695.          AGAGAAAACAAAAAAAAACACATCGTCAAGCAGTGTTAGTATTGTAAATGATAAGTTAAA 2399
RT-PCR-PyBC.      AGAGAAAACAAAAAAAAATACATCGTCAAGCAGTGTTAGTAGTGTAAATGATAAGTTAAG 1081
                  ****************** ********************** *****************


PY01695.          ACTTCCAATAAGCGAAAAAGATAATAATAAAACAGTGAAAACTAATTTGAGTGAACAACT 2459
RT-PCR-PyBC.      ATTTCCAATAAGCGAAAAAGATAATAATAAAATAGTGAAAACTAATTTGAGTGAACAACT 1141
                  * ***************************** *************************

PY01695.          TGGCATGTTTGATTTTTACAACAACATGCCCCACACTAAAAATCATGTTATTGCTGCTCG 2519
RT-PCR-PyBC.      TGACATGTTTGATTTTTACAACAACATGCCACACACTAAAAATCATGTTATTGCTGCTCG 1201
                  ** ************************** *****************************

PY01695.          AATAACAGCCGAAAACAGTAATGATAGTTTTAAACCAACGTCAGGCTTAGTAAAAAATGT 2579
RT-PCR-PyBC.      AATAACAGCCGAAAACAGCAATGATAGTTTTAAACCGACGTCAGGCTTAGTAAAAAATGT 1261
                  ****************** ***************** ***********************

PY01695.          TAATTTTCAAAATTCGAAAGATGTATGGGGTTATTTCTCTATCAATAATGGGTTTGTTCA 2639
RT-PCR-PyBC.      TAATTTTCAAAATTCGAAAGATGTATGGGGTTATTTTTCTATCAGCAATTGGAATGAGGA 1321
                  ********************************** *******  *** **  **   *

PY01695.          TGAATTTTCAGATTCACAAATTGGCCATATATTTGCAAAAGGGGAAACAAGAGAAATTGC 2699
RT-PCR-PyBC.      CGAATATACAGAGACA-----TCGCCACAGA---------------------------- 1347
                   **** * ****  **     * **** * *
```

Figure 3.4 continued.

```
PY01695.            AACTCTTTGGAAATAGGACAAAATAAAATGAGCGTAATCGGATTGTTAATGAATGTAAAG 6780

RT-PCR-PyntCxT.     ---------------------------------------------TTATGTATGGTAAG 14
                                                                 * *** ***  ***

PY01695.            ACAGATGAATATAAAGAAGGAAGAGATATTGCTTTTATAATAAATGATATTACAACAAAT 6840
RT-PCR-PyntCxT.     ACAGATGA-TATAAAGAAGGAAGAGATATTGCTTTTATAATAAATGATATTACAACCAAT 73
                    ******** ********************************************** ***

PY01695.            GGAGGTGCATTTAGTGTTTTAGAAGACGAACTATTTTATGGAGTATCATGTTATGCGAGA 6900
RT-PCR-PyntCxT.     GGAGGTGCATTTAGTGTTTTAGAAGACGAACTATTTTATGGAGTATCATGCTATGCGAGA 133
                    ************************************************* *********

PY01695.            GAAAAAAAAATACCACGTATATGTATATCTTGCAATTCCGGAGCAAAAATTGGATTATAT 6960
RT-PCR-PyntCxT.     GAAAAAAAAATACCACGCATATACATATCTTGCAATTCCGGGGCTAAAATTGGATTATAT 193
                    ***************** ****  ***************** ** ***************

PY01695.            AATTATCTTATGGATAAAATTAAAGTATGCTGGAATGATGAAAACAAAAAAGAACTTGGA 7020
RT-PCR-PyntCxT.     AATTATCTTATGGATAAAATTAAAGTATGCTGGAATGATGAAAATAAAAAAGAACTTGGA 253
                    ****************************************** ***************

PY01695.            TATAAATATATATATATAACAGAAGAAGTAAAAGAAACAATTCCTAAAAAAGATATTATT 7080
RT-PCR-PyntCxT.     TATAAGTATATATATATAACAGAAGAAATAAAAGAAACAATTCCTAAAAAAGATATTATT 313
                    ***** ******************** ********************************

PY01695.            TATTTAAGAGAAATTTATGAAAATGGAGAAAAAAGATATATAATTGATGCTATAGTAGGA 7140
RT-PCR-PyntCxT.     TATTTAAGAGAAATTTATGAAAATGGAGAAAAAAGATATATAATTGATGCTATAGTAGGA 373
                    ************************************************************

PY01695.            AATTTAAATAATCATATAGGAGTAGAAAATTTAAGAGGTAGTGGATTAATAGCAGGAGAA 7200
RT-PCR-PyntCxT.     AATTTAAATAATCATATCGGGGTAGAAAATTTAAGAGGTAGTGGGTTAATAGCAGGAGAA 433
                    ***************** ** ********************** ***************

PY01695.            ACCTCAAAGGCTTATGATGAGATTTTTACTCTTTCATATGTCACTGGAAGAAGTGTTGGA 7260
RT-PCR-PyntCxT.     ACCTCAAAGGCCTCCGATGAGACTTTTACTCTTTCATATGTCACTGGAAGAAGTGTTGGA 493
                    *********** *  ******* ************************************

PY01695.            ATTGGTGCTTATTTAGTTAGATTAGGTAAACGAACTATTCAAAAAAAAAGGATCGTCTCTT 7320
RT-PCR-PyntCxT.     ATTGCTGCTTATTTCGTTAGATTAGGTAAACGAACTATTCAAAAAAAAAGCATCCTCTCTT 553
                    **** ********* ********************************** *** ******

PY01695.            TTACTAACTGGTTTTAATGCTTTAAATAAAATATTAGGTGAAAAGGTATATATAAGTAAT 7380
RT-PCR-PyntCxT.     TTAA-AACCGGTTATAATGCAAGCAAAACTCTTCCGGCATAATAGTCATCTTCTAACATG 612
                    ***  *** **** ******    ** *   *    *   ** **  ** *   *  *

PY01695.            GAACAATTAGGAGGTGTAAATATTATGATGAAAAATGGAATATCTCAATTAGAAGCTGAA 7440
RT-PCR-PyntCxT.     CATTAA------------------------------------------------------ 618
                     *  **
```

Figure 3.5 Alignment of PY01695 ORF with the product of N-terminal carboxyl transferase RT-PCR amplification. RT-PCR-PyntCxT is the merged sequences corresponding to the forward and the reverse primer sequencing products. * indicates 100% conserved nucleotide.

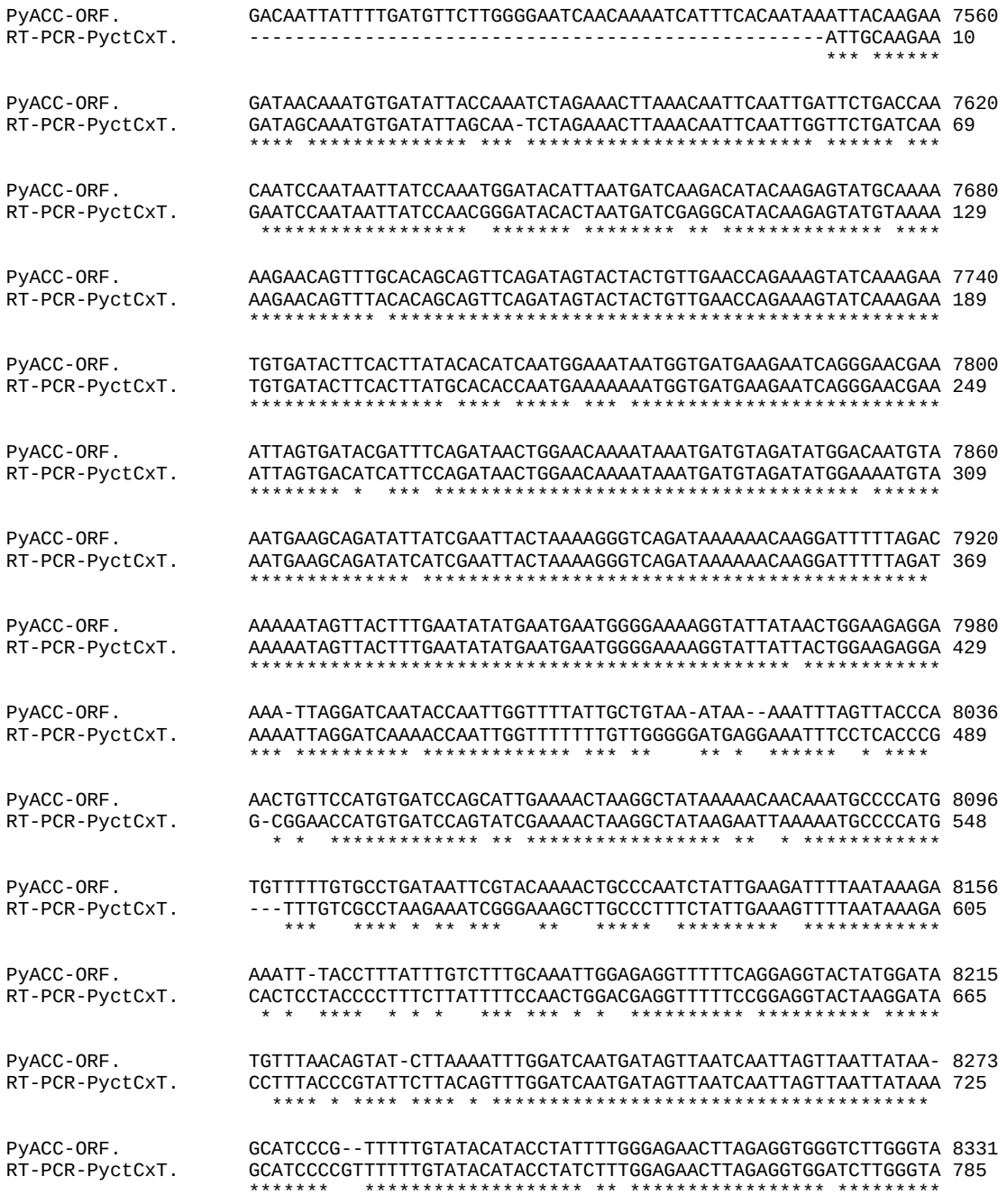

Figure 3.6 Alignment of PY01695 ORF with the product of C-terminal carboxyl transferase RT-PCR amplification. RT-PCR-PyctCxT is the merged sequences corresponding to the forward and the reverse primer sequencing products. Approximately 500 bp were sequenced in both directions.* indicates 100% conserved nucleotide. (▼) represents the splicing point of the exons.

```
PyACC-ORF.          GTAGTAGATGAAACATTGAACAGCCAAATAATAGAAATGTATGCAGATACTAATAGTAAA 8391
RT-PCR-PyctCxT.     GTAGTAGATGAAACATTGAACAGCCAAATAATAGAAATGTATGCAGATAATAATAGTAAA 845
                    ********************************************** **********

PyACC-ORF.          GGTGGAATATTAGAACCTCCAGGATTAGTAGAAGTCAAATTTAAGTTCGCAGAAATTAAG 8451
RT-PCR-PyctCxT.     GGTGGAATATTAGAACCTCCAGGATTAGTAGAAGTCAAATTTAAGTTCGCAGAAATTAAG 905
                    ************************************************************

PyACC-ORF.          AAATTAATGAATAACAGTGATCCATATATAATAGAACTAAATCAGAAACTCGCGACTCTT 8511
RT-PCR-PyctCxT.     AAATTAATGAATAACAGTGATCCATATATAATAGAACTAAATCAGAAGCTCGCGACTCTT 965
                    ********************************************** ************

                    ▼
PyACC-ORF.          CAGAATGAAGAAGAAATTTTAAGTGTAAAAAAGGAAATAGAAAAGAAGGAAAAGGAAATG 8571
RT-PCR-PyctCxT.     CAGGATGACCAATAAATATTCATAATAAGAATTGAAATAAGATTAAAATCAACGAATATG 1025
                    *** ****  ** **** ** *   *** **  ******  *   **   ** * * ***

PyACC-ORF.          CTTCCATTTTATTTACAAGTGTGTCATAAATATGCAGATCTACATGATGTATCATCATGT 8631
RT-PCR-PyctCxT.     CTTC-ATTTATTTAACAAATGAATAATAAAAGTATAGATCTACAAGATGCATGATACTCT 1084
                    **** ****  ** **** **  * *****  *  ********* **** ** **  * *

PyACC-ORF.          ATGAAGGAGAAAGGTGTTATTAGAAAAATTGTTCCATGGGAAAAATCTAGATCCTTTTTC 8691
RT-PCR-PyctCxT.     ATGAAGGAAAAAGGTGTTATTAGCAAAGTTAATATATGT-ATATTTCTGAATTCATTTTA 1143
                    ******** ************** *** **  *  ***  * *  ***  ** * ****

PyACC-ORF.          TATTATCGCTTATTAAGGAGATTGATATTACATACATTAAAGTAA 8736
RT-PCR-PyctCxT.     TGTGATCGCTTACTTAGGAAACT---------------------- 1166
                    * * ******** * **** * *
```

Figure 3.6 continued.

3.2.2 Detection of acetyl-CoA carboxylase gene transcript by Northern blot analysis

Total RNA isolated from *P. yoelii*, *T. congolense* and *PyBCCP* (Chapter 5) was resolved along side RNA standard markers by agarose gel electrophoresis. Figure 3.7*A* shows the electrophoregram prior to blotting onto a nitrocellulose membrane. *P. yoelii* total RNA (lane 1) consist of four bands; a band greater than 9 kb as well as three bands estimated at 2.8 kb, 2 kb and 0.7 kb. These three bands may correspond to *P. yoelii* large subunit ribosomal RNA (28S rRNA), small subunit ribosomal RNA (18S rRNA) and possibly the fragment of 28S rRNA (Dame and McCutchan, 1983; van Spaendonk *et al*., 2001). The band greater than 9 kb may be mRNA transcripts of large polypeptide of ± 500 kD. Four major bands were observed in lane 2 containing *T. congolense* total RNA control. These bands were estimated to be 2.2 kb, 1.4 kb, 1 kb and 0.7 kb corresponding to 18S rRNA, 28S rRNA (α-fragment), 28S rRNA (β-fragment) and the cleavage product of 28S rRNA (Hasan *et al*., 1982; Urakawa and Majiwa, 2001). A band of approximately 3 kb corresponding to the *P. yoelii* biotinoyl domain cDNA was observed in lane 3; though the cDNA appeared to be partially degraded.

The presence of *P. yoelii* acetyl-CoA carboxylase transcript in the total RNA preparation was confirmed by enhanced-chemiluminescence detection using avidin-peroxidase-*p*-iodophenol system for detecting the presence of hybridized probes on the membrane (Figure 3.7*B*). Panel *B* and *D* was exposed to X-ray film for approximately 30 min while panel *C* was exposed for less than 5 min. A band greater than 9 kb was prominent in both lanes, however the size of the bands were different. This may be due to variation in exptression level of the enzyme at various stages of the parasite debelopment (Le Roch).

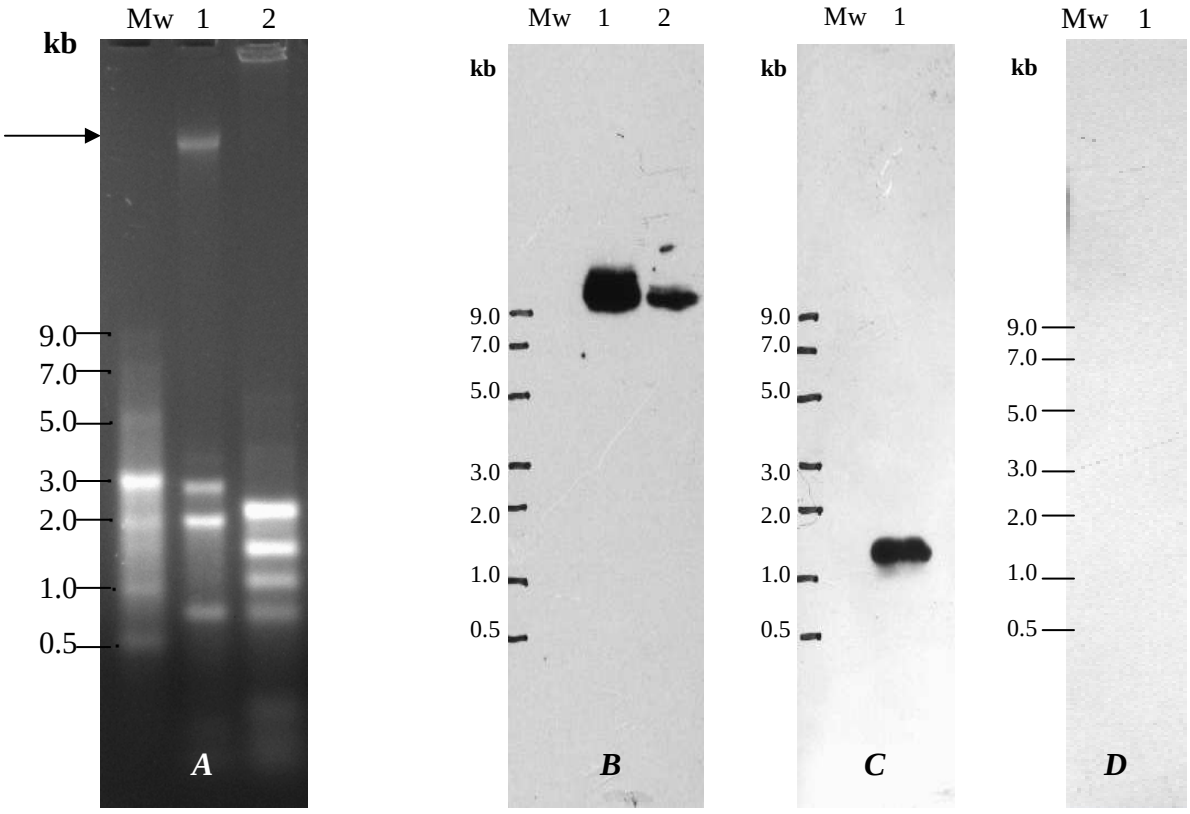

Figure 3.7 Detection of *P. yoelii* acetyl-CoA carboxylase transcript by Northern blot analysis. (*A*) Agarose gel analysis of *P. yoelii* total RNA (*lane 1*) and *T. congolense* total RNA (*lane 2*). The molecular weight standards are shown (*lane Mw*). Agarose gel concentration was 1.2%. The arrow indicates a band above the 9 kb marker. Northern blot analysis of *P. yoelii* total RNA (*B* - *C*) and *T. congolense* total RNA (*D*). *Lane 1 panel B* contains 55.0 µg total RNA from predominantly trophzoites and schizonts*; lane 2 panel B* contains 55.0 µg total RNA from ring stage. *Lane 1 panel C* contains 25 µg total RNA from mixed stage. RNA in panels *B* and *D* were hybridised with biotinylated probes prepared from *P. yoelii* biotin carboxylase-biotinoyl domain cDNA, while RNA in *panel C* was hybridised with biotinylated probes prepared from *P. yoelii* lactate dehydrogenase cDNA. Hybridization was detected with the avidin-peroxidase-*p*-iodophenol enhanced chemiluminescence detection system.

A band of size 1.25 kb was detected in panel C corresponding to *P. yoelii* lactate dehydrogenase as positive control. No RNA was detected in the negative control (panel *D*) even though a higher quantity of RNA product was resolved compared to panel *B.*

3.3 Discussion

This chapter describes the application of reverse transcriptase-PCR (RT-PCR) and Northern blot analysis to investigate the expression of the gene that codes for acetyl-CoA carboxylase by *P. yoelii* strain 17XL. Primers were designed to amplify portions of the biotin carboxylase, N-terminal and C-terminal carboxyl transferase domains of what is believed to be a gene encoding the *P. yoelii* multi-domain polypeptide acetyl-CoA carboxylase. Primers were designed based on the Plasmodb-published *P. yoelii* 17XNL PY01695 ORF sequence. The PCR products were sequenced to verify the RT-PCR results. Biotinylated probes prepared to hybridise with the region of the transcript encoding the biotinoyl domain were used to detect the presence and size of the transcript.

There is no available information on the size of the large subunit ribosomal RNA (LSU rRNA) and small subunit ribosomal RNA (SSU rRNA) transcripts in *P. yoelii*. Only partial sequences are available on the NCBI and Plasmodb (Bahl *et al*., 2003) databases. Although the pattern of resolution on an agarose gel appeared to be consistent with reports on *P. berghei* ribosomal RNA transcripts (Dame and McCutchan, 1983; van Spaendonk *et al*., 2001). Unlike in other organisms, some apicomplexan parasites produce ribosomes with structurally distinct rRNA molecules that are encoded on a single copy gene and expressed at different stages of the parasite development (Dame and McCutchan, 1983; McCutchan *et al*., 1988; McCutchan *et al*., 1995). In *Plasmodium*, the A-type ribosome is expressed at the liver and blood stages, while the O-type and S-type ribosomes are expressed at the insect stage (McCutchan *et al*., 1988; McCutchan *et al*., 1995). The transcript for the LSU rRNA in *Plasmodium* is cleaved to produce two subunits. In *P. berghei*, the sizes are 3 kb and 0.8 kb (Dame and McCutchan, 1983; van Spaendonk *et al*., 2001). The SSU rRNA is not cleaved. The results therefore suggest that *P. yoelii* strain 17XL may have a similar mechanism of post-transcriptional modification of the LSU rRNA. Thus the size of the LSU rRNA and the SSU rRNA in *P. yoelii* strain 17XL is approximately 3.5 kb (cleaved into 2.8 kb and 0.7 kb fragments) and 2 kb, respectively.

Acetyl-CoA carboxylase in *P. yoelii* strain 17XNL is encoded by a single copy gene that is located on chromosome 13 (Plasmodb database). First strand cDNA synthesis was carried out using either oligo-dT primers that annealed on the poly-A tail on the 3'untranslated region (UTR) of the transcript or random hexameric oligonucleotides. The two methods of first strand cDNA synthesis appeared to produce cDNA that was subsequently amplified by the primers positioned as illustrated on Figure 3.1. The PyACCctCxT primer pair was positioned to amplify the mRNA without the 235 bp intron at 3, end of the ORF (Figure 3.6). A proper negative control for this analysis would have involved using a reverse primer designed to anneal on the intron. However, the RNA samples were treated with DNase I to digest any residual genomic DNA before reverse transcriptase reaction. The size of the PCR products (Figure 3.3) and the sequencing data (Figures 3.4 – 3.6) clearly showed that the products were from an RNA transcript instead of genomic DNA. This therefore suggests that the blood stage *P. yoelii* transcribes the gene that encodes acetyl-CoA carboxylase. The copy number of the gene was not deduced in the study. Real time PCR could be used to quantify the amount of mRNA transcript, precisely at the various stages of the parasite life cycle. The blood samples used for the study contained a mixed stage *P. yoelii* infection; therefore stage-specific expression of the gene was not established. Previous studies (Le Roch *et al*., 2003) using *P. falciparum* as model showed that the gene is highly expressed at the gametocyte and sporozoite stages and minimally expressed at the intraerythrocytic stage of the parasite life cycle. *P. yoelii* is likely to have a similar expression profile.

The details of the synthesis of fatty acids for membrane biogenesis at the intraerythrocytic stage of the parasite still remain to be evaluated. The high rate of morphological changes within the intraerythrocytic stage of the parasite is expected to be synonymous with increased membrane biogenesis (Mitamura and Palacpac, 2003; Palacpac *et al*., 2004), therefore suggesting high expression levels of the acetyl-CoA carboxylase gene (Davis *et al*., 2000; Hasslacher *et al*., 1993). Does the expression level of acetyl-CoA carboxylase gene correlate with the expression levels of the genes encoding the enzymes of the Type II fatty acid synthase complex? Using the expression pattern derived from an array experiment (Le Roch *et al*., 2003) it was observed that a similar pattern does exist between the expression profile of acetyl-CoA carboxylase and the genes encoding enzymes of the fatty acid synthase complex (Figure 3.5) in *P. falciparum*; namely: malonyl-CoA-acyl carrier protein transacylase (FabD), beta-ketoacyl-acyl carrier protein

synthase III (FabH), 3-oxoacyl-(acyl-carrier protein) reductase (FabG) and beta-hydroxyacyl-ACP dehydratase (FabA/Z). Beta-ketoacyl-acyl carrier protein synthase III precursor is yet to be identified in *P. yoelii* and *P. vivax*, and 3-oxoacyl-(acyl-carrier protein) reductase is yet to be identified in other *Plasmodium* species. There was no data on the expression profiles of enoyl-ACP reductase (FabI) and FabB/F (Le Roch *et al*., 2003).

The pattern of expression of the genes for Type II FAS clearly suggests that the rate of *de novo* fatty acid biosynthesis is lower at the blood stage and higher at the gametocyte and sporozoite stages. Acetyl-CoA carboxylase and FabD mRNA transcripts were not detected at the ring and merozoite stages (Le Roch *et al*., 2003). Perhaps this information validates previous postulates that the parasite scavenges lipid precursors from the hosts at the intraerythrocytic stage without the need for *de novo* fatty acid biosynthesis (Beaumelle and Vial, 1988a; Beaumelle and Vial, 1988b; Beaumelle *et al*., 1988; Paula Simões *et al.*, 1993; Simões *et al.*, 1990; Van der Schaft *et al.*, 1987). To add to this, the pattern of expression of genes involved in the Type II fatty acid synthesis strongly suggests that the parasite increases *de novo* fatty acid biosynthesis at the gametocyte and sporozoite stages. These stages occur predominantly at the insect stage and thus fatty acid synthesis may be increased at these stages probably due to lack of lipid precursors in the mosquito vector. Could this be an energy saving mechanism the parasite employs at the blood stage? This question could be answered by analysing the expression levels of the genes involved in the Type II fatty acid synthase and the acetyl-CoA carboxylase gene in a lipid-free culture of synchronised *Plasmodium* parasites. The low level of expression of acetyl-CoA carboxylase at the trophozoite (blood) stage is to perhaps make up the fatty acids that the parasite may have been unable to obtain from the host. This can be explored by knocking out the acetyl-CoA carboxylase gene in the parasite and monitoring parasite survival.

Phospholipase C, glycerophosphodiester phosphodiesterase, diacylglycrol kinase, acyl-CoA synthase and diacylglycerol-O-acyltransferase are some key enzymes involved in the metabolism of imported lipid precursors (Mitamura and Palacpac, 2003; Palacpac *et al*., 2004) such as phosphatidylserine, phosphatidylcholine, diacylglycerol and fatty acids in *P. falciparum* (http://sites.huji.ac.il/malaria/maps/phserine).

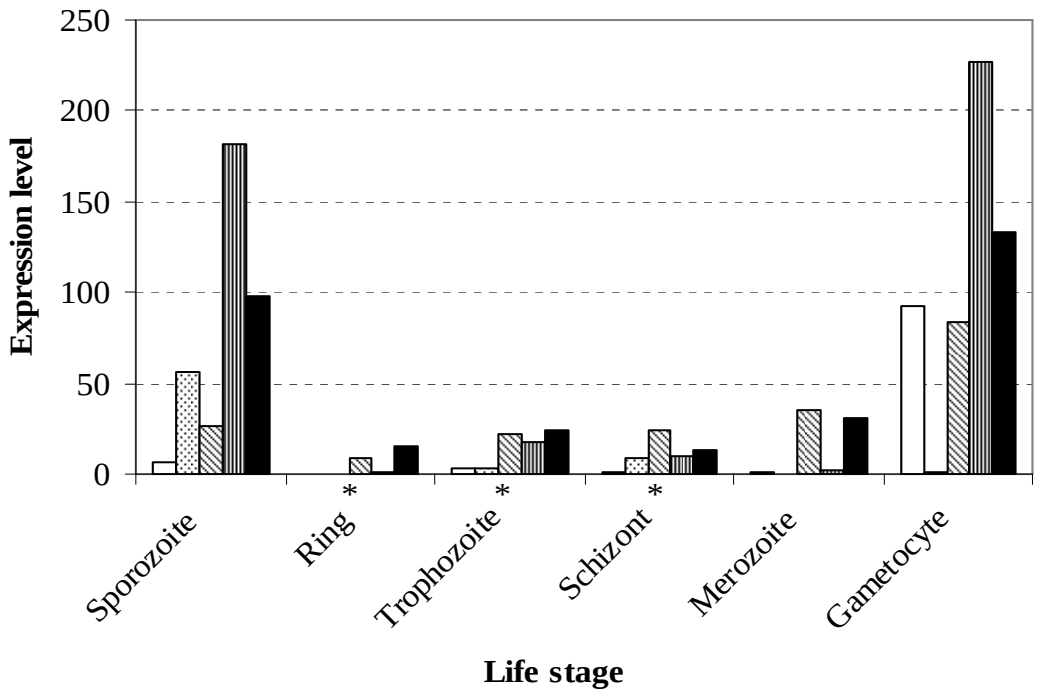

Figure 3.8 Expression profile of five genes involved in fatty acid synthesis in *P. falicparum*. The expression levels of acetyl-CoA carboxylase (□), FabD (▨), FabH (▧), FabG (▥) and FabA/Z (■) obtained by LeRoch *et al.* (2003). * represents average of the early and late stages of the parasite.

These metabolites are involved in the biosynthesis of phospholipids used in membrane biogenesis (Holtz, 1977; Ke *et al*., 2000b; Mitamura and Palacpac, 2003). The transcription profiles (data not shown) of the genes encoding these enzymes show that they are more highly expressed at the intraerythrocytic stage, than in the gametocyte and the sporozoite stages of the parasite (Le Roch *et al*., 2003). This is in contrast to the expression profiles of the acetyl-CoA carboxylase and Type II fatty acid synthase genes. As a result membrane biogenesis at the intraerythrocytic stage, which has been shown to be high at this stage (Moll *et al*., 1988; Moll *et al*., 1990; Van der Schaft *et al*., 1987; Vial *et al*., 1988), may utilize imported lipid precursors instead of those produced by a *de novo* acetyl-CoA carboxylase-Type II fatty acid synthase pathway.

The RT-PCR results were further supported by the Northern blot analysis. Biotinylated ("cold") probes were prepared with Klenow fragment (Feinberg and Vogelstein, 1983) using decanucleotide primers supplied by the manufacturer to the enhance specificity of hybridisation

between the target mRNA transcript and its corresponding probes. Enhanced chemiluminescence (ECL) used to detect presence of hybridisation using avidin-peroxidase-*p*-iodophenol-luminol system due to the high affinity between avidin and biotin; thus eliminating the need for autoradiography. ECL is a highly sensitive technique and can detect targets at femtomole (10^{-15} mole) quantity (Kricka and Thorpe, 1986a; Kricka and Thorpe, 1986b; Thorpe *et al*., 1985).

The size of the published (Plasmodb) ORF of PY10695 gene is 8.7 kb. The size detected by Northern blot was above 9 kb. The presence of 5' and 3' untranslated regions (UTR) on the transcript may account for the size observed on the luminograph. Acetyl-CoA carboxylase has been shown to be regulated at the transcription level (Barber *et al*., 2003; Mao *et al*., 2003; Thampy and Wakil, 1988a; Wakil *et al*., 1983). The expression profile of acetyl-CoA carboxylase gene suggests that the *Plasmodium* acetyl-CoA carboxylase gene is inducible, depending on the stage of the parasite development. Being an inducible gene, it is expected that the gene may contain regulatory regions upstream from the start codon or down stream from the stop codon that regulates the transcription of the gene. The presence of UTR in transcripts is not uncommon in *Plasmodium*. Several *Plasmodium* transcripts such as *rif* gene, heat shock proteins and DNA polymerase have 5'UTR ranging between 0.5 kb and 2 kb, which are transcriptionally or post-transcriptionally regulated (Militello *et al*., 2004; Porter, 2001; Tham *et al*., 2007; Watanabe *et al*., 2002).

In mammals, transcription of acetyl-CoA carboxylase genes are controlled by two to three sets of promoters upstream of the coding sequence (Barber *et al*., 2003; Mao *et al*., 2003). This results in heterogeneous populations of acetyl-CoA carboxylase transcripts in various tissues such as mammary gland, liver, adipose tissue and heart (Barber *et al*., 2003; Lopez-Casillas *et al*., 1989; Luo *et al*., 1989). This heterogeneity mostly occurs at the 5' UTR region of the transcript (Lopez-Casillas *et al*., 1989; Luo *et al*., 1989). Perhaps, the smearing effect observed on the Northern blot (Figure 3.7*B*) may be as a result of the presence of a heterogeneous population of acetyl-CoA carboxylase transcripts; though there is no other evidence to support this. However, the heterogeneity in mRNA population due to differential processing of the 5'UTR region is also observed in *Plasmodium* (Pace *et al*., 1998). The size of the 5' and 3' flanking regions of the acetyl-CoA carboxylase gene was deduced from the Plasmodb database (Figure 3.9). It was observed that the 5' flanking region between the initiation codon of the acetyl-CoA carboxylase

coding sequence and the adjacent coding sequence was consistent (~ 2.9 kb) in *P. falciparum*, *vivax* and *knowlesi*. The 5' flanking region of *P. yoelii* was spread between two unassembled contiguous fragments of Chromosome 13, therefore the complete sequence was not obtained. The consistent length on the 5' flanking region may suggest an organized structure containing transcription promoters and other regulatory elements. The *AT*-content 5' flanking region of acetyl-CoA carboxylase gene in *P. falciparum* and *yoelii* (partial) is ~ 76%. Whereas the *AT*-content of the 5'UTR flanking region of acetyl-CoA carboxylase gene in *P. vivax* and *knowlesi* is 51% and 60%, respectively, with 77% sequence identity. The 5' flanking regions of the acetyl-CoA carboxylase gene in the four *Plasmodium* species contain very long streteches of *A* and *T* nucleotides. The size of the 3' flanking regions was not consistent. Mapping of the 5' and 3' UTRs of acetyl-CoA carboxylase transcripts in *Plasmodium* by PCR may reveal the configuration of the promoter regions and possible mechanism of transcription of the gene at the various stages of the parasite development.

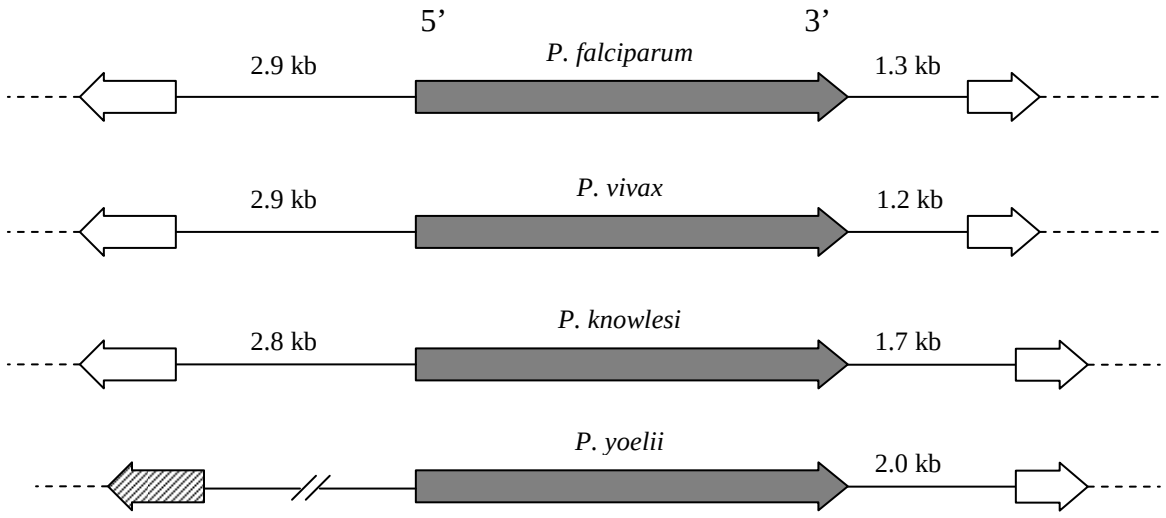

Figure 3.9 The size of the 5' and 3' flanking regions of acetyl-CoA carboxylase gene locus in four *Plasmodium* species. Arrows represent gene coding regions pointing from 5' to 3' direction. Filled arrows represent acetyl-CoA carboxylase gene coding region, open arrows represent coding regions for hypothetical proteins and stripped arrow represents coding region for TATA modulatory element in the *P. yoelii* gene sequence. The 5' and 3' acetyl-CoA carboxylase flanking regions are represented by solid lines (adapted from Plasmodb database).

CHAPTER 4

PLASMODIUM YOELII ACETYL-COA CARBOXYLASE: ANTIBODY PRODUCTION AND IMMUNODETECTION

4.1 Introduction

The *P. yoelii* acetyl-CoA carboxylase gene of strain 17XNL was identified in Plasmodb (ID: PY01695) and this study showed that the strain 17XL *P. yoelii* parasite produces an mRNA transcript that codes for the enzyme (Chapter 3). The enzyme can be detected by the presence of the biotin moiety using streptavidin or avidin-mediated detection, anti-biotin antibodies or an antibody directed against an immunogenic peptide within the enzyme. This may reveal the subcellular localisation of the enzyme that is believed to be targeted to the apicoplast.

The challenge for designing a suitable peptide for antibody production in chickens as well as other hosts is to select a region of a protein sequence that fulfils the following criteria: (i) high surface probability (ii) hydrophilicity and (iii) the region must be flexible to assume a spatial orientation that is found in the native protein. Avoiding potential N-glycosylation sites of the protein may be useful in designing effective peptides for antibody production because of possible masking of the selected region on the native protein by the polysaccharide moiety. Anti-peptide antibodies produced in chickens against *Plasmodium* protein kinases have been shown to be effective tools in characterising several malaria parasite proteins (Dorin *et al*., 2005; Nunes *et al*., 2007). A major obstacle faced in designing peptides from *Plasmodium* proteins for antibody production is the presence of multiple lysine residues in many *Plasmodium* proteins. Lysine-rich regions contribute to the high scores in the surface probability, hydrophilicity and flexibility algorithms. Antibodies made against such region may cross-react with several *Plasmodium* proteins and thus are avoided in peptide design.

By use of the Predict7™ epitope prediction algorithm (Cármenes *et al*., 1989), a peptide from an immunogenic region of PyACC was designed and synthesised to generate anti-PyACC-peptide antibodies in chickens. It was necessary to avoid choosing a peptide from conserved regions of the enzyme to prevent possible cross-reactivity with mouse acetyl-CoA carboxylase. In a similar manner, anti-peptide antibody was produced in chickens against *P. yoelii* lactate dehydrogenase

(PyLDH). PyLDH is a metabolic protein (Zhou *et al*., 2004) expressed at high levels by the parasite (Le Roch *et al*., 2003). These antibodies were used for the detection of acetyl-CoA carboxylase and lactate dehydrogenase in *P. yoelii* lysate resolved by SDS-PAGE and blotted onto nitrocellulose membrane and *P. yoelii*-infected mouse red blood cells by immunofluorescence microscopy.

4.2 Results

4.2.1 Selection of immunogenic peptide for anti-*P. yoelii* acetyl-CoA carboxylase antibody production in chickens

Following sequence alignment, a peptide from the *P. yoelii* acetyl-CoA carboxylase that appeared to be unique to *P. yoelii* and absent in chicken and mammalian acetyl-CoA carboxylases was chosen by epitope prediction analysis using the Predict7™ software . The *P. yoelii* lactate dehydrogenase (*Py*LDH) peptide was selected as a comparison for this experiment using the same epitope prediction software. This LDH peptide appeared to be conserved across all *Plasmodium* lactate dehydrogenase orthologues examined and not present in chicken and mouse lactate dehydrogenase amino acid sequences.

Figure 4.1*A* shows the ClustalW™ alignment of lactate dehydrogenase sequences from *Plasmodium*, chicken and mouse. A region (residue 55 – 135) was plotted (Figure 4.1*B*) to show the surface probability, hydrophilicity and flexibility scores of the selected peptide (residues 85 – 100) of *P. yoelii* lactate dehydrogenase. The region in the box was chosen for peptide synthesis. A cysteine residue was added at the C-terminal of the peptide to allow the conjugation to a rabbit albumin carrier owing to the higher score of surface probability and hydrophilicity towards the N-terminal compared to the C-terminal. Figure 4.2 illustrates the ClustalW™ sequence alignment data and the plot of surface probability, hydrophilicity and flexibility of residues 1460 – 1545 containing the selected region (residue 1500 – 1517) of *P. yoelii* acetyl-CoA carboxylase. This region is located between the biotin carboxyl carrier protein and the carboxyl transferase domains (Figure 4.2*A*). The region in the box was chosen for peptide synthesis. The higher score of hydrophilicity and surface probability towards the N-terminal suggested that the conjugation of the peptide to the carrier should be at the N-terminal for maximum exposure of that region. A cysteine residue was incorporated at the N-terminal of the peptide to enable the conjugation to

rabbit albumin carrier. The two peaks flanking the chosen peptide region appeared to be more attractive options. However, those regions have a number of lysine residues and therefore were avoided. Table 4.1 summarises the features of the peptides used in this study to produce anti-peptide antibodies in chickens against *P. yoelii* lactate dehydrogenase and *P. yoelii* acetyl-CoA carboxylase.

Table 4.1 Characteristics of the *P. yoelii* acetyl-CoA carboxylase and lactate dehydrogenase peptides selected for antibody production

	Anti-pLDH-IgY	**Anti-PyACC-IgY**
Name	APG (or pLDH)	TNT (or PyACC)
Sequence	APGKSDKEWNRDDL**C**	**C**RSNDDNSQSSRNRTNT
Length (amino acid residues)	15	17
Modification	C-terminal Cys	N-terminal Cys
Molecular weight	1731.9	1954
Region on parent protein	Residue 85 – 98	Residue 1500 – 1516
NCBI access number	XP_724101	XP_729490
Linker	MBS	MBS
Carrier	Rabbit albumin	Rabbit albumin

4.2.2 Anti-*P. yoelii* acetyl-CoA carboxylase peptide antibody production in chickens

Chickens were immunised with the peptide-carrier complex emulsified in FCA (week 0) or FIA (weeks 2, 4 and 6). Eggs were collected from immunised chickens daily and IgY isolated from a weekly pool of eggs per chicken. IgY isolated from eggs collected prior to immunisation (pre-immune IgY) was used as the internal control. Weekly anti-peptide-IgY titres were assessed by ELISA against the peptides in both chickens in order to monitor the progress of anti-peptide antibody levels in each chicken (Figure 4.3). The profiles show that levels of anti-peptide-IgY increased after the second immunisation at week 2 and peaked between week 7 and week 8. The anti-peptide antibody levels started falling after week 8.

Crude IgY isolated from weeks 4 – 8 and weeks 9 – 12 from each chicken was pooled and an aliquot of the pooled antibody was kept. The pooled antibody was passed over the peptide-immobilised affinity matrix as described in Section 2.3.7.

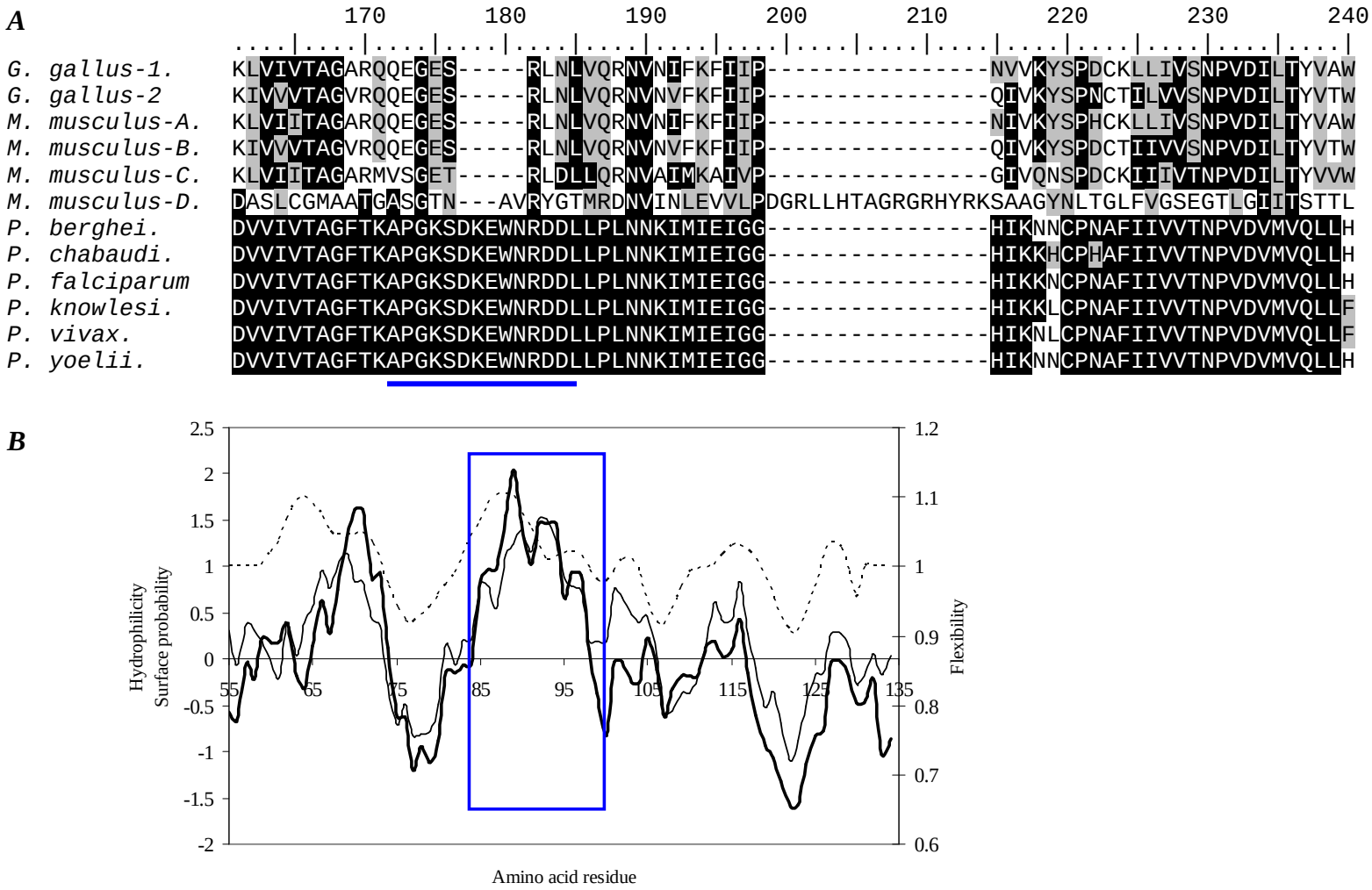

Figure 4.1 ClustalW™ alignment and selection of the *P. yoelii* lactate dehydrogenase peptide for antibody production in chickens. (*A*) ClustalW alignment showing highly conserved peptide regions of six *Plasmodium* LDH amino acid sequences (*P. berghei*, *chabaudi*, *falciparum*, *knowlesi*, *vivax* and *yoelii*) that was chosen for the production of *Plasmodium* LDH (blue underline) anti-peptide antibody. (*B*) The Predict7™ prediction plots of surface probability (—), hydrophilicity (▬), and flexibility (---) of *P. yoelii* LDH residue of the chosen peptide (55 – 135). The box represents the profile of the underlined peptide sequence in panel *A*.

A

```
                1770      1780      1790      1800      1810      1820      1830      1840
                ....|....|....|....|....|....|....|....|....|....|....|....|....|....|
M. musculus-A.  DKCVFALREENKSD----------------------------------------------------MNTVLNYIFSHAQVT
M. musculus-B.  DKCVINLREQFKPD----------------------------------------------------MTQVLDCIFSHSQVA
G. gallus.      DKCVFALREENKSD----------------------------------------------------MNAVLNYIFSHAQVT
P. chabaudi.    --TEIDA-----------------------------------------ELNFDNR-------KDKGNEFFLELSNTK
P. berghei.     ------------------------------------------------------------------------------
P. falciparum.  DESNINNITFFNNLSNNGSIRKRNNNNNSSSSNNNNNNNNNNKNNNFKHSYYMDYNNDNIYWNHVKNEKSKYLLDIPIMK
P. knowlesi.    NKEASKTSSKSSSKSSSK----SASKSASEGTFKCTSNSRTQVGGDTPGVDSPGGHPS----TAEEPRKEQFLLDIPNMK
P. vivax.       HRGSSAGASAGASAGESAGVSAGASPGASEGTSKCTSNSCTQVGGDSPGVASPSGHPSGNPNTGEDLRRNQFLLDIPNMK
P. yoelii.      --SEIDFPVNNTKDKKLDKMKIISDTEMSRSNDDNSQSSRNRTNTNYNEKIELNFDNK-------KDKENEFFLELSNMK
```

B

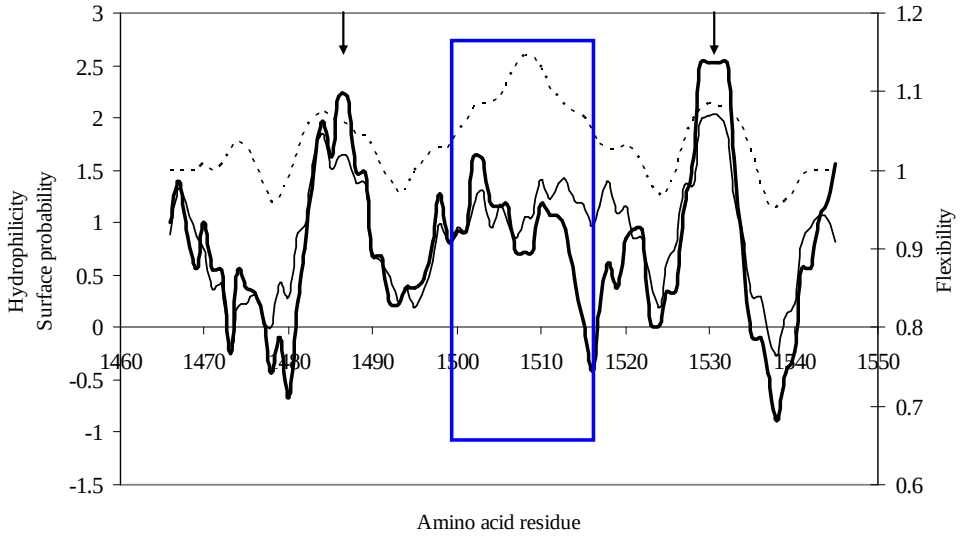

Figure 4.2 ClustalW™ alignment and selection of the anti-*P. yoelii* acetyl-CoA carboxylase peptide for antibody production in chickens. (*A*) ClustalW™ alignment showing a non-conserved peptide (blue underline) region between *P. yoelii* acetyl-CoA carboxylase and acetyl-CoA carboxylase from mouse and chicken that was chosen for the production of *P. yoelii* acetyl-CoA carboxylase anti-peptide antibodies. The degree of conservation is indicated by the shading, with black shading indication 100% conservation of the amino acid. (*B*) The Predict7^{TM} epitope prediction plots of surface probability (—), hydrophilicity (**—**) and flexibility (---) of the *P. yoelii* acetyl-CoA carboxylase amino acid residues of the chosen peptide (1465 – 1545) are indicated. The box represents the profile of the underlined peptide sequence in panel *A*. The arrows indicate other regions with high epitope prediction scores but containing tandem lysine repeats.

Figure 4.4 shows the elution profiles of anti-pLDH antibody and anti-PyACC antibody. The profile showed a similar trend for both chickens. The peak fraction for anti-pLDH eluted at 10 ml with $A_{280\ nm}$ of > 3.0 for both chickens (Figure 4.4*A*), while the peak fraction for anti-PyACC eluted at 5 ml with $A_{280\ nm}$ of 2.4 for both chickens. Fractions from the affinity matrix with $A_{280\ nm}$ between 0.3 and > 3.0 were pooled. The total yield of pooled affinity-purified anti-pLDH peptide and anti-PyACC peptide antibody was 23 mg and 25 mg respectively.

4.2.3 Detecting *P. yoelii* acetyl-CoA carboxylase in *P. yoelii*-infected mouse erythrocyte lysate with anti-peptide antibody directed against *P. yoelii* acetyl-CoA carboxylase

The anti-PyACC antibody was used to establish the *in vivo* expression of acetyl-CoA carboxylase in *P. yoelii*-infected mouse-blood cells lysate from a mixed stage infection. Anti-pLDH peptide IgY was used as a control. The antibody detected two major proteins at 35 kD and 56 kD and minor bands at 44 kD and above 116 kD (Figure 4.5). The antibody did not detect any protein in non-parasitised-mouse blood cells. The preimmune control did not detect any protein on both lanes. The anti-PyACC antibody recognised a diffuse band extending from approximately 440 kD to about 220 kD on parasitised-blood cells lysate (Figure 4.5*B*). No detectable protein was observed in non infected mouse red blood cell lysate negative control containing approximately equal amounts of blood cells as in the infected blood cells. The pre-immune IgY control did not detect any protein.

4.2.4 Detection of acetyl-CoA carboxylase in *P. yoelii*-infected red blood cells by immunofluorescence microscopy

The anti-PyLDH and anti-PyACC antibodies were used to detect the presence of lactate dehydrogenase (positive control) and acetyl-CoA carboxylase *in situ* in parasitized mouse red blood cells by immunofluorescence microscopy. The secondary antibody was FITC-conjugated donkey anti-chicken IgY. 4',6-diamidino-2-phenyl dihydrochloride (DAPI) was used as the nuclear stain to confirm the presence of parasites in a red blood cell. DAPI is a cell permeable dye that binds to minor groove of DNA double helix, preferably on the *AT*-rich region (Naimski *et al*., 1980). The excitation and emission wavelength for FITC is 492 nm and 518 nm, respectively (Harlow and Lane, 1988), while the excitation and emission wavelength for DAPI-DNA complex is 364 nm and 458 nm, respectively (Naimski *et al*., 1980).

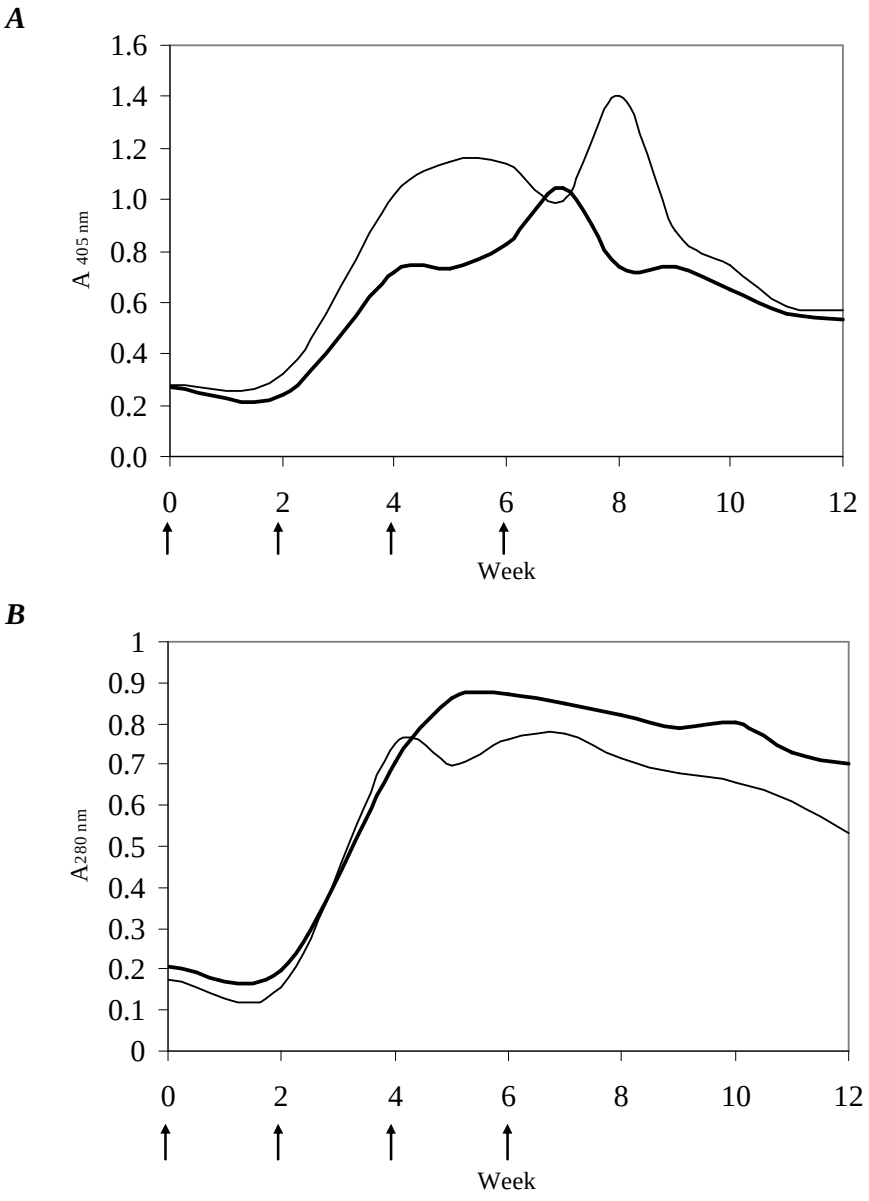

Figure 4.3 Evaluation of anti-peptide antibody production in chicken. Laying chickens were immunised at weeks 0, 2, 4 and 6 (arrows) with synthetic peptides-rabbit albumin (carrier) complex in Freund's adjuvant. IgY isolated from chickens immunised with pLDH peptide (*A*) and PyACC peptide (*B*) was evaluated by ELISA (described in Section 2.3.8) for response against the peptide antigens. Peptide concentration was 1 µg/ml (0.15 µg/well) and primary antibody (crude IgY) was 100 µg/ml (0.1 µg/well). (▬▬) chicken 1 and (—) chicken 2. Antibodies were detected with rabbit-anti-chicken IgY antibody conjugated to HRPO.

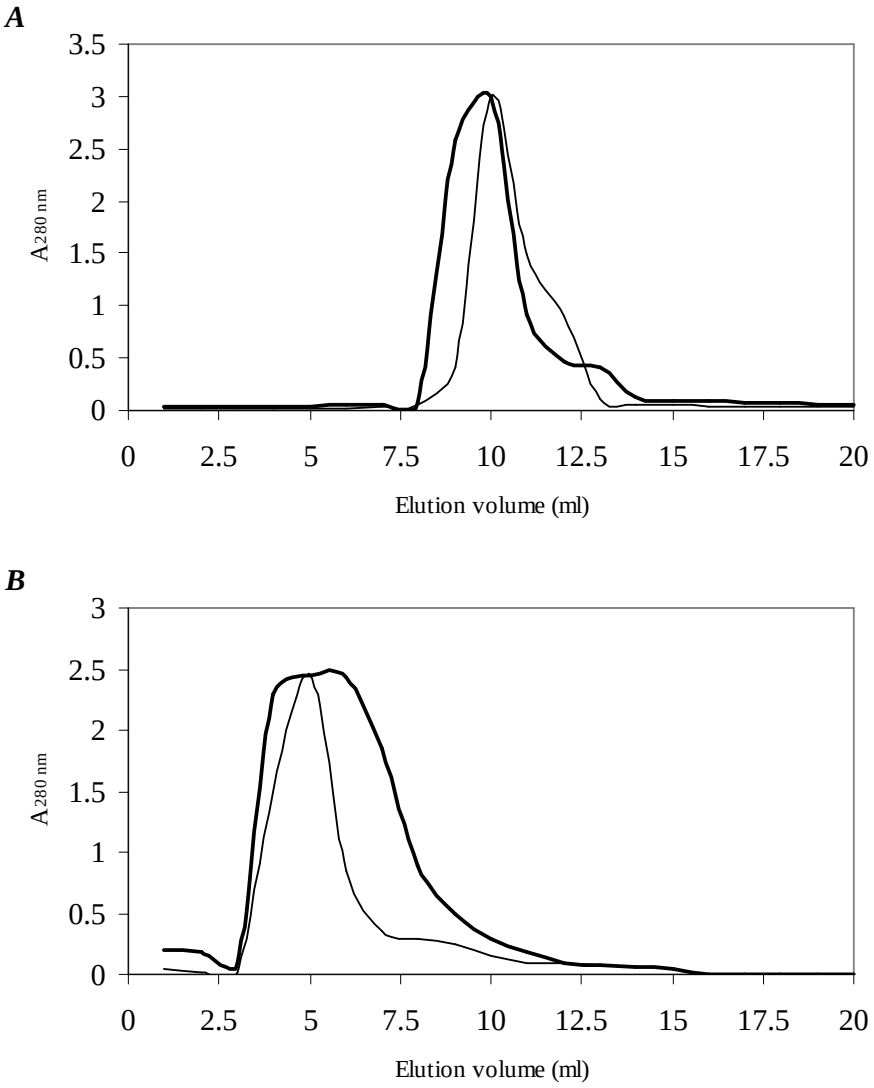

Figure 4.4 Elution profile of anti-peptide antibody from affinity matrices. Pooled weeks 4 – 8 anti-peptide antibody was passed over pLDH peptide (*A*) and PyACC-peptide (*B*) immobilised-affinity matrices, eluted with 0.1M glycine-HCl (pH 2.8). (▬▬) chicken 1 and (──) chicken 2.

The sample used was from a mixed infection. Green fluorescence was detected in parasitized RBC incubated with the anti-PyACC peptide antibodies indicating the presence of *Plasmodium* acetyl-CoA carboxylase. The green fluorescence appeared to be distributed within a specific organelle in the parasite cells at trophozoite and gametocyte ateges, sightly in the cytoplasm but absent from the RBC cytoplasm. The blue fluorescence showed that the green FITC fluorescent signal is from a parasitized RBC. No signal was detected in non-parasitised RBC. A diffrent trend was observed with the anti-PyLDH antibodies positive

control. The FITC signal was more evenly distributed in the cytoplasm of the parasite. The preimmune IgY was negative.

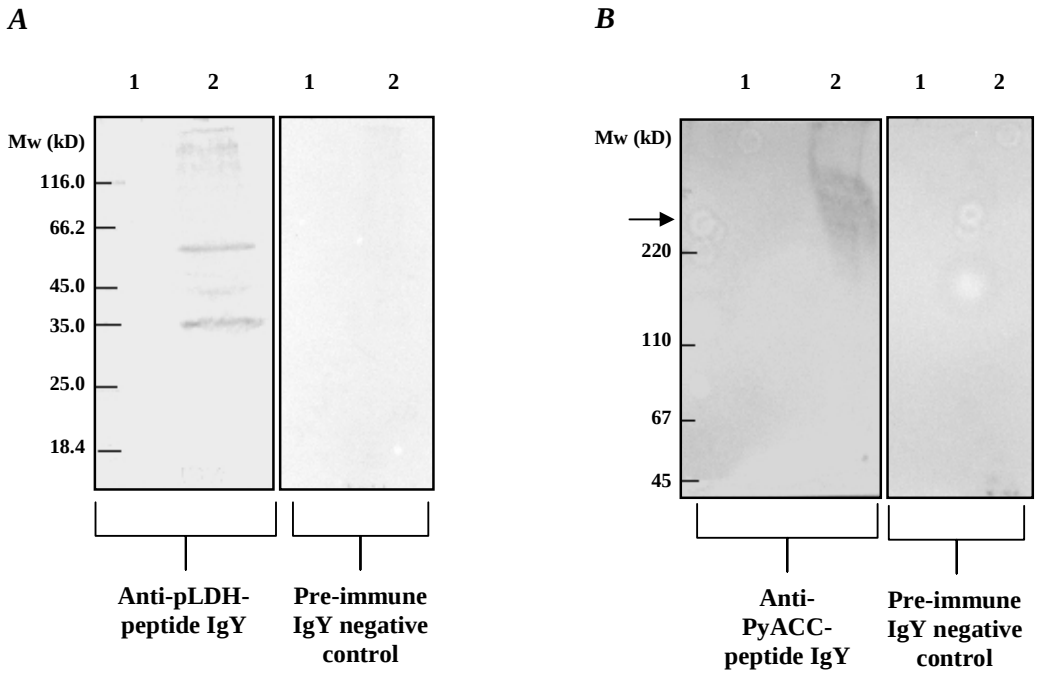

Figure 4.5 Anti-peptide antibody detection of acetyl-CoA carboxylase and lactate dehydrogenase in *P. yoelii*-infected mouse blood cell lysate by Western blot. Immuno-blotting of *P. yoelii*-infected mouse blood cells lysate (*lane 2*) from a mixed stage parasite infection or non-infected mouse blood cells (*lane 1*) with antibodies directed against peptides *P. yoelii* acetyl-CoA carboxylase and lactate dehydrogenase peptides. The lysate was resolved by SDS-PAGE on a 10% (*A*) and a 5.5% (*B*) acrylamide gel, transferred to nitrocellulose membrane and probed with 2.5 µg/ml of immune or pre-immune (negative control) antibody. Antibodies were detected with rabbit-anti-chicken IgY antibody conjugated to HRPO. Both lanes were loaded with approximately equal amounts of RBC. The position of molecular weight standards are indicated on the left hand panels. The arrow indicates the estimated position of 330 kD.

A similar study to detect the presence of acetyl-CoA carboxylase in *P. yoelii*-infected mouse RBC was carried out with FITC-conjugated avidin. The signal FITC signal was low (data not shown) but a pattern similar to anti-PyACC antibodies was observed. Avidin alone was used as a negative control, and no fluorescent signal was observed in cells incubated with avidin alone.

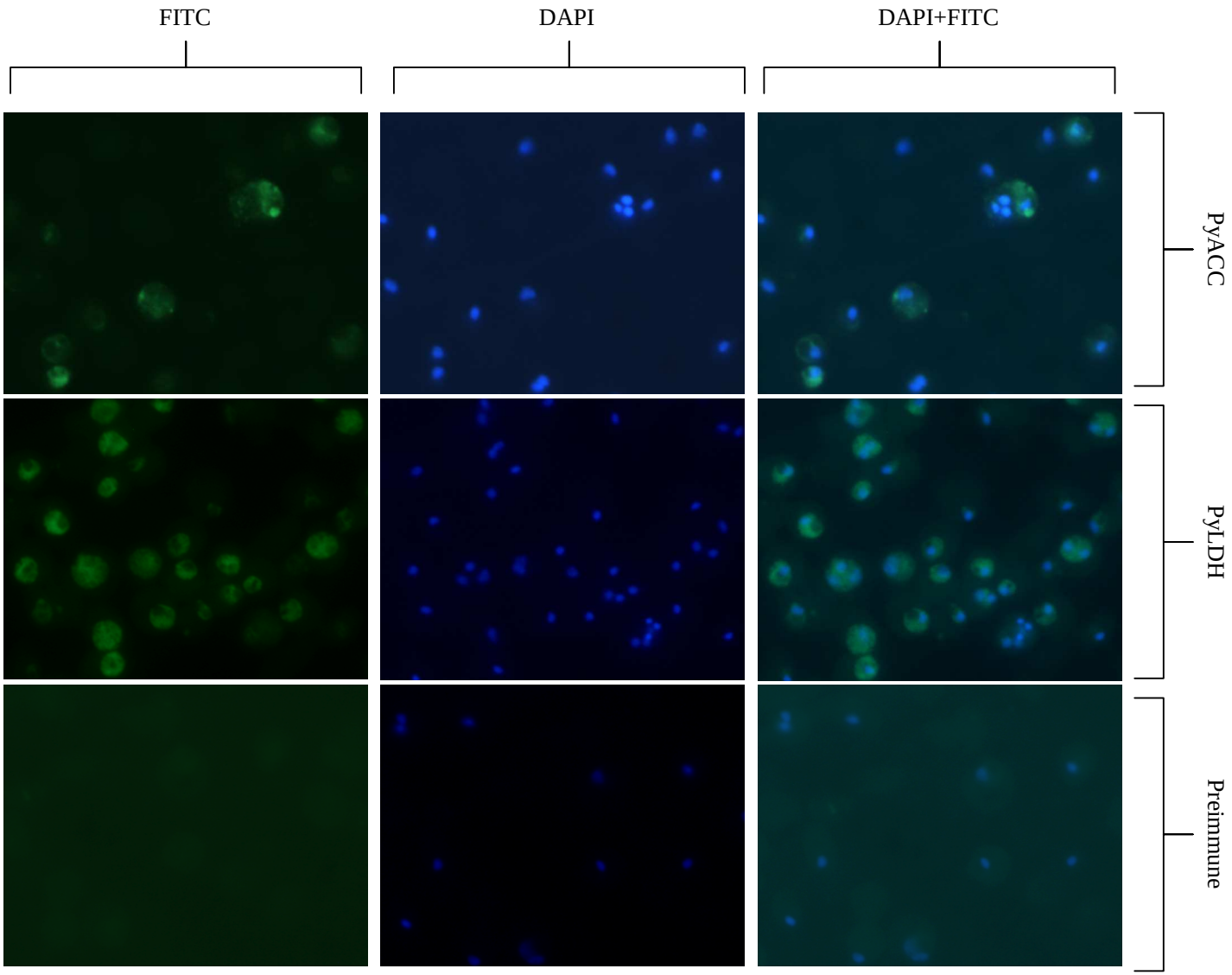

Figure 4.6 Detection of acetyl-CoA carboxylase and lactate dehydrogenase using anti-peptide antibodies. *P. yoelii*-infected mouse red blood cells (unsynchronised) were incubated with 10 µg of anti-PyLDH peptide IgY or anti-PyACC IgY or pre-immune IgY. Antibodies were detected with FITC-conjugated donkey anti-IgY IgG and cells were conterstained with DAPI. Cells were viewed at 1000× magnification with a fluorescent microscope mounted with a digital camera. Flourescent images were captured under UV and green filters, and processed with the analySIS™ software. Arrows indicate uninfected RBC.

4.3 Discussion

Having shown that the parasite transcribes the mRNA encoding *P. yoelii* acetyl-CoA carboxylase, the next step was to confirm the presence of the enzyme in parasite lysates. An immunogenic peptide was chosen from the published sequence of *P. yoelii* 17XNL acetyl-CoA carboxylase as well as lactate dehydrogenase; an "in house" protein used as a control in immunochemical assays. Several regions of the protein exhibiting high predicted surface probability, hydrophilicity, antigenicity and flexibility (Cármenes *et al.*, 1989) were identified. Rabbit albumin was chosen as the carrier because it has been shown in our laboratory to induce strong immune responses in chickens resulting in the production of high antibody titre.

The use of chickens in antibody production is very convenient because chickens naturally package antibodies against an immunogen in to their eggs to protect their unhatched chicks (Erhard and Schade, 2001; Larsson and Sjöquist, 1990). Therefore antibodies are extracted from the chicken egg yolk, which is less traumatic for the birds than having to bleed them to isolate antibodies from the serum. Chicken egg yolks have higher antibody titre than chicken serum as a result of active transport of IgY from serum into egg yolk (Larsson and Sjöquist, 1988; Larsson and Sjöquist, 1990). Chicken egg yolk IgY can retain biological activities for several years when stored at 4ºC in the presence of anti-bacterial against such as sodium azide (Goldring and Coetzer, 2003). Sometimes due to persistent freeze-thaw cycles, IgY forms insoluble precipitates. This can be avoided by storing the antibody at –20ºC in the presence of 50% glycerol (Personal observation). Antibodies directed against plasmodial proteins have been shown to be useful tools in characterising plasmodial kinases (Dorin *et al.*, 2005; Merckx *et al.*, 2003; Nunes *et al.*, 2007).

Both peptides produced peak immunogenic responses in chickens between week 6 and 8 post immunization. The free peptide was used as antigen in ELISA because antibodies directed against the carrier may produce erroneous results in the monitoring of the anti-peptide antibody titres. The length of the peptides is thought to contribute to the degree of binding. While some studies have shown that 6 – 15-mer peptides bind poorly to plastic (Muller, 1988), other studies have shown that 10 – 20-mer peptides binds effectively to plastic (Davies *et al.*, 1987).

Both affinity-purified anti-peptide antibodies recognised the native enzyme resolved by SDS-PAGE and *in situ* by immunofluorescence microscopy. This demonstrated that the anti-peptide antibodies could recognise non-conformational forms of the native protein (Davies *et al*., 1987; Dyson and Wright, 1995). The theoretical molecular weight of PyLDH is 34 kD but the enzyme may form homotetrameric complexes of approximately 120 kD (Menting *et al*., 1997; Turgut-Balik *et al*., 2004). The size of the protein was estimated (Figure 4.5*B*) corresponds to the size of the theoretical mass of the *P. yoelii* acetyl-CoA carboxylase. Northern blot analysis showed similar pattern (Figure 3.7), suggesting that there might be a relationship between the the proteins produced from the transcripts. Previous studies have shown that this diffused pattern in resolution of native *Plasmodium* proteins on SDS-PAGE gel is probably due to the size and presence of highly charged amino acid residues common in the *Plasmodium* proteome (Mattei and Scherf, 1992a; Mattei and Scherf, 1992b; Tebele *et al*., 2000).

The apicomplexa plastid is believed to be the organelle responsible for fatty acid biosynthesis since most enzymes of the Type II fatty acid synthase have apicoplast target sequences (Gornicki, 2003; Prigge *et al*., 2003; Ralph *et al*., 2004a), thus may be targeted to the plastid. The patterns of FITC signal obatained for acetyl-CoA carboxylase (Figure 4.6) suggest that the enzyme is distributed within the plastid. This was diffrent to lactate dehydrogenase, a cytoplasmic enzyme involved in the glycolytic pathway (Tomar *et al*., 2006; Winter *et al*., 2003). Using antibodies directed against a known apicoplast-targeted protein such as acyl carrier protein for co-localisation studies (Jelenska *et al*., 2001) may be useful in discerning the localisation of the enzyme in a *Plasmodium* parasite. The result of FITC-conjugated avidin was expected to show a similar trend to anti-PyACC antibody. This reagent will detect other biotinylated proteins in parasite cells. Immuno-precipitation of the native acetyl-CoA carboxylase from a parasite lysate using anti-PyACC antibodies for activity assays was not successful. Perhaps, using metabolically labelled proteins would yield a better result (McCarthy *et al*., 1983).

CHAPTER 5

PLASMODIUM YOELII ACETYL-COA CARBOXYLASE: CLONING, EXPRESSION AND CHARACTERISATION OF THE BIOTINOYL DOMAIN

5.1 Introduction

One major benefit of the sequencing of the *Plasmodium* genome is that several genes with or without any annotated function can be studied by cloning and expression of the protein encoded by such a gene. *Escherichia coli* has proved to be a valuable tool for the cloning and expression of recombinant proteins for structure and function studies aimed at novel drug design (Makrides, 1996). *Plasmodium* protein kinases (Dorin *et al*., 2005; Merckx *et al*., 2003; Nunes *et al*., 2007), glycolytic enzymes (Brady and Cameron, 2004; Turgut-Balik *et al*., 2004; Winter *et al*., 2003) and surface-related proteins (Narum *et al*., 2001; Rodrigues *et al*., 2003; Wang *et al*., 2008) have been successfully cloned and expressed using the *E. coli* expression system. In 2003, about 80% of the proteins deposited in the Protein Data Bank with resolved crystal structures were expressed in *E. coli* due to the robustness and the relative cost of using the *E. coli* expression system (Sorensen and Mortensen, 2005b). However, not every protein has been successfully expressed in *E. coli* even when correctly cloned in frame with the expression plasmid promoters and other genetic information needed for high level expression of the cloned gene (Flick *et al*., 2004; Mehlin *et al*., 2006; Narum *et al*., 2001; Withers-Martinez *et al*., 1999; Zhou *et al*., 2004). This shortcoming is often attributed to distinctive structural features of the gene to be expressed and instability and inefficiency of translation of the mRNA in *E. coli*. Susceptibility of the expressed protein to proteolytic degradation by endogenous proteases and improper folding of the expressed protein also results in insoluble recombinant proteins. The uniqueness of the *AT*-rich malaria genome is thought to contribute to problems expressing *Plasmodium* proteins (Flick *et al*., 2004; Mehlin *et al*., 2006; Withers-Martinez *et al*., 1999; Zhou *et al*., 2004).

There is a concerted effort to study acetyl-CoA carboxylase in organisms ranging from higher eukaryotes such as humans (Abu-Elheiga *et al*., 1995; Boone *et al*., 2000; Boone *et al*., 1999; Munday, 2002) to lower eukaryotes such as protozoan parasites (Gornicki, 2003; Zuther *et al*., 1999) due to the implication of this enzyme in obesity and a possible target for anti-parasitic drugs (Blanchard and Waldrop, 1998; Thampy and Wakil, 1988a; Thampy and Wakil, 1988b). However, only the *E. coli* and yeast acetyl-CoA carboxylase crystal structures of various domains and subunits of the enzyme (Al-Feel *et al*., 2003; Athappilly and

Hendrickson, 1995; Cronan, 2002; Cronan and Waldrop, 2002; Shen *et al*., 2004; Zhang *et al*., 2004) have been resolved. Human acetyl-CoA carboxylase has been recently cloned, expressed and characterised (Kim *et al*., 2007)**.** Lee *et al*. (Lee *et al*., 2008) published the structural and functional organisation of the human acetyl-CoA carboxyalse-2 biotinoyl domain and it is the only eukaryotic biotinoyl domain of a multi-enzyme-domain type acetyl-CoA carboxylase to be structurally elucidated.

The importance of carbon in energy metabolism emphasises the essential function of biotin in living systems. Biotin, also known as vitamin H, is an important cofactor for several proteins that possess diversified metabolic functions in the living system (Beckett, 2005; Chapman-Smith and Cronan, 1999b; Chapman-Smith and Cronan, 1999c; Reche and Perham, 1999). It is required by all organisms and synthesised by plants and most prokaryotes. Biotin-dependent enzymes play crucial roles in energy metabolism by mediating catalytic functions in pathways such as lipogenesis, gluconeogenesis and amino-acid metabolism (Goss and Wood, 1984). Primarily, biotin functions as an acceptor of a carboxyl group in the carbon fixation pathways of fatty acid synthesis and oxidation. Enzymes such as acetyl-CoA carboxylase, pyruvate carboxylase and transcarboxylases have covalently bound biotin in their biotin binding domains which is often referred to as the biotin carboxyl carrier protein (BCCP) or biotinoyl domain. A biotin ligase (EC 6.3.4.15) attaches the biotin molecule to an ε-amine of a lysine residue within a highly conserved biotin binding motif (Chapman-Smith *et al*., 1999). The process of covalent attachment of a biotin molecule to a biotin-dependent enzyme is called biotinylation. This reaction is a highly conserved and a specific post/co-translational modification (Chapman-Smith *et al*., 1999; Reche *et al*., 1998). The *Plasmodium* genome has been shown to contain biotin-dependent enzymes (Plasmodb database). These inferences were made by gene annotation using comparative analysis with well established biotin-bound enzymes in organisms such as human, *S. cerevisiae, E. coli* and *A. thaliana*. The genomes of *S. cerevisiae* (Piskur, 2001) and *A. thaliana* (Walbot, 2000) have been sequenced, published and are well characterised.

There is little understanding of the fate of biotin in the *Plasmodium* parasite, though the importance of this cofactor in glucose and amino-acid metabolism is evident. The biotin carboxylase and the carboxyl transferase domains (as well as subunits) of acetyl-CoA carboxylase are entirely dependent on the biotinylated biotin carboxyl carrier protein domain for their activities (Cronan, 2001; Goss and Wood, 1984; Lee *et al*., 2008; Solbiati *et al*.,

2002). Thus, it is essential to embark on the study of acetyl-CoA carboxylase by empirically characterising the biotin carboxyl carrier protein domain which is conserved in evolutionary divergent organisms. The aim of this study was to recombinantly express the regions spanning the biotin carboxyl carrier protein domain of *P. yoelii* 17XL acetyl-CoA carboxylase. Primers were designed based upon the PY01695 (Plasmodb™ ID) ORF of *P. yoelii yoelii* 17XNL annotated as "acetyl-CoA carboxylase 1 precursor-related". The recombinant protein was analysed for its potential to be biotinylated *in vivo* by the expression host, *E. coli*. Figure 5.1 is a flowchart illustrating the experimental plan used to recombinantly express and characterise *P. yoelii* 17XL acetyl-CoA carboxylase biotinoyl domain.

5.2 Results

5.2.1 PCR amplification of a 1041 bp cDNA containing the biotinoyl domain of acetyl-CoA carboxylase from *P. yoelii* 17XL genomic DNA

The High Fidelity™ PCR system was used to amplify the 1041 bp DNA fragment which includes the acetyl-CoA carboxylase biotin carboxyl carrier protein domain (*PyBCCP*) from *P. yoelii* 17XL genomic DNA. The PyBCCP-fwd and PyBCCP-rev primers with added *Eco*RI and *Not*I restriction sites (Table 2.2) were used for this process. The nucleotide sequence and the coding amino-acid sequence from the published PY01695 corresponding to the region intended to be amplified from the 17XL strain are shown in Figure 5.2. The nucleotide sequence is approximately 1041 bp, which excludes the additional nucleotides corresponding to the restriction sites. The entire sequence spans the biotin carboxyl carrier protein domain of *P. yoelii* acetyl-CoA carboxylase with 108 and 169 amino acid residues before and after the first and last amino acid residues of the biotin carboxyl carrier protein domain respectively. The VEAMKM biotin binding motif was intended to be in the centre of the 1041 bp sequence to (i) be as far removed as possible from the His-tag and GST-tag sequence on the N terminals of the recombinant proteins and (ii) include other possible residues out side the domain that may be vital for interaction with the biotin protein ligase and correct protein folding.

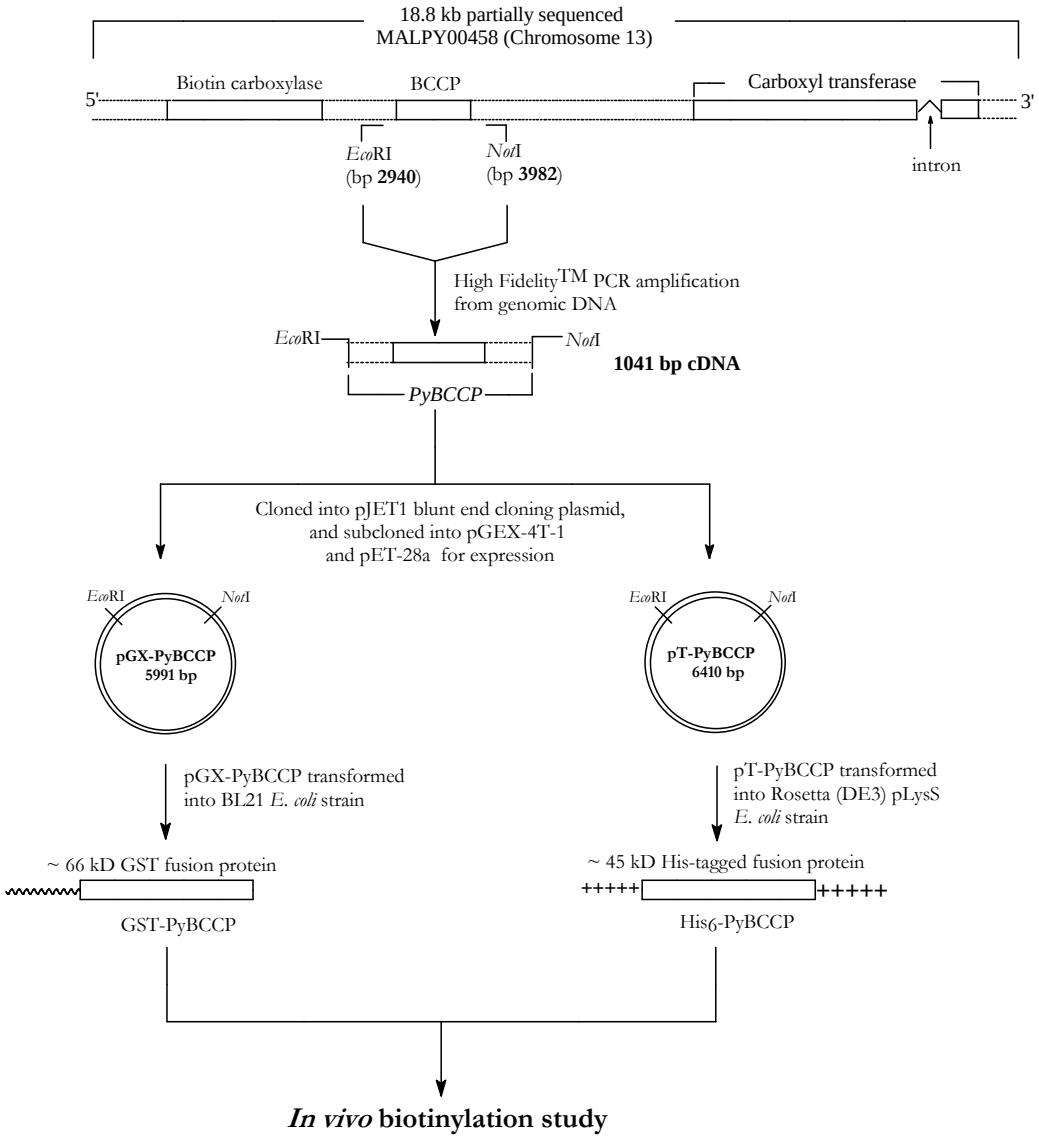

Figure 5.1 Flow chart depicting the experimental plan to clone and express *P. yoelii* 17XL biotin carboxyl carrier protein domain. A region spanning the 73 amino-acid biotin carboxyl carrier protein domain of the multi-domain gene (PY01695) encoding *P. yoelii* acetyl-CoA carboxylase was amplified, cloned into pJET1and subcloned into pET-28a and pGEX-4T-1 expression vectors using the *Eco*RI and *Not*I restriction sites. The numbers 2940 bp and 3982 bp indicate the region of the ORF amplified for the study. The entire fragment to be cloned was 1041 bp.

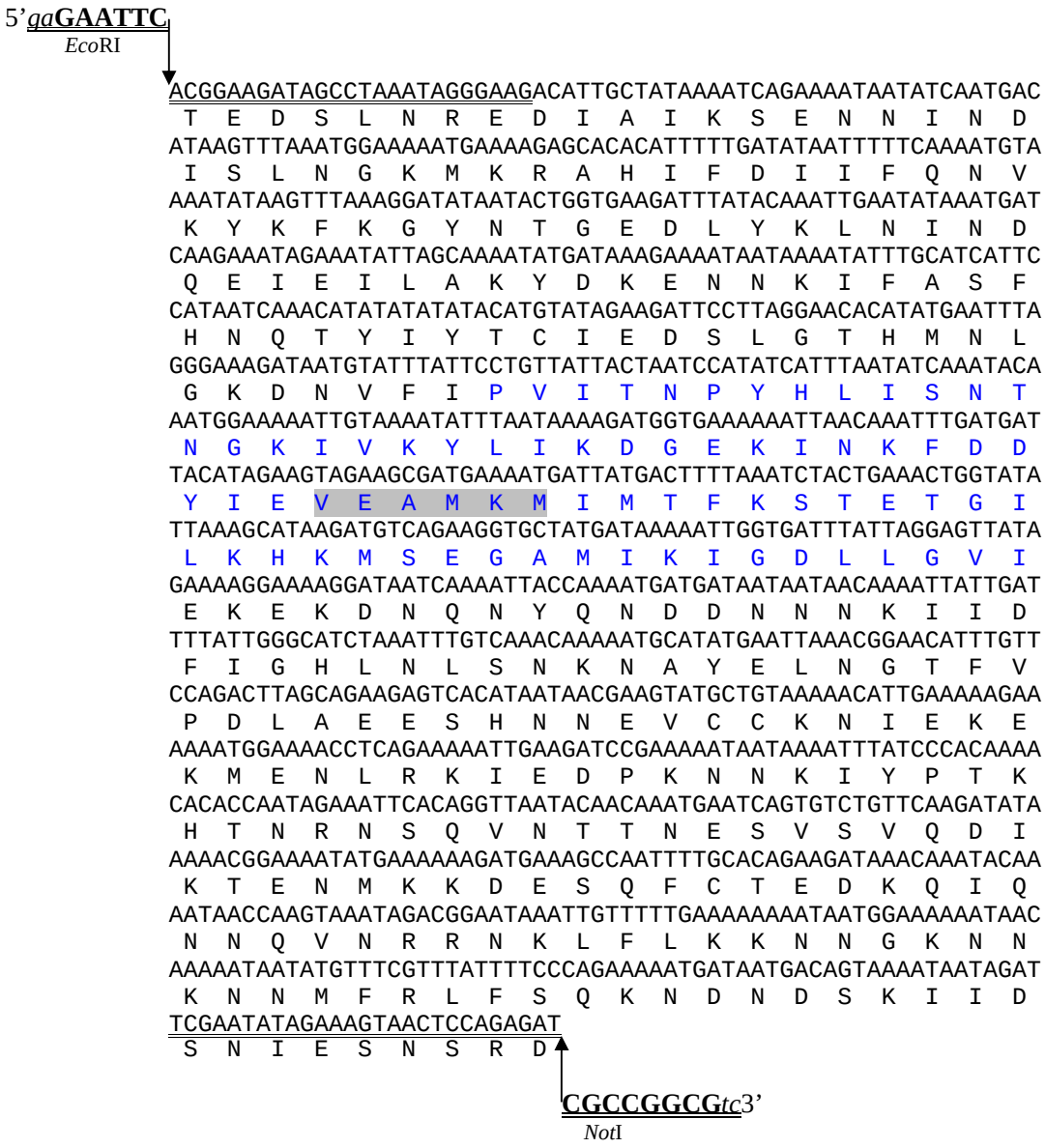

Figure 5.2 Nucleotide and predicted amino acid sequences of PY01695 region 2940 bp – 2982 bp. The entire region spanning the biotin carboxyl carrier protein domain (in blue) with the biotin binding motif (highlighted) of PY01695 ORF of MAL00458 of *P. yoelii*. The theoretical molecular weight of the polypeptide was deduced to be 40.6 kD. The double underlined sequences were used to design the primers. The bold nucleotide sequences are the added *Eco*RI and *Not*I restriction sites. The arrows points to the position where the restriction site sequences were added. The lower case italics are additional bases.

The PCR product was analysed by agarose gel electrophoresis (Figure 5.3*A*). A DNA band corresponding to the expected size of 1041 bp was observed. The 850 bp DNA band in lane 2 codes for *P. yoelii* 17XL lactate dehydrogenase (PyLDH) positive control amplified from the same sample of *P. yoelii* genomic DNA. Prior to ligation into the pJET1 plasmid, the PCR

product was purified from the agarose gel and analysed by agarose gel electrophoresis to ascertain the level of purity. A distinct band of the expected size is seen (Figure 5.3). The yield of the purified product was approximately 5 µg.

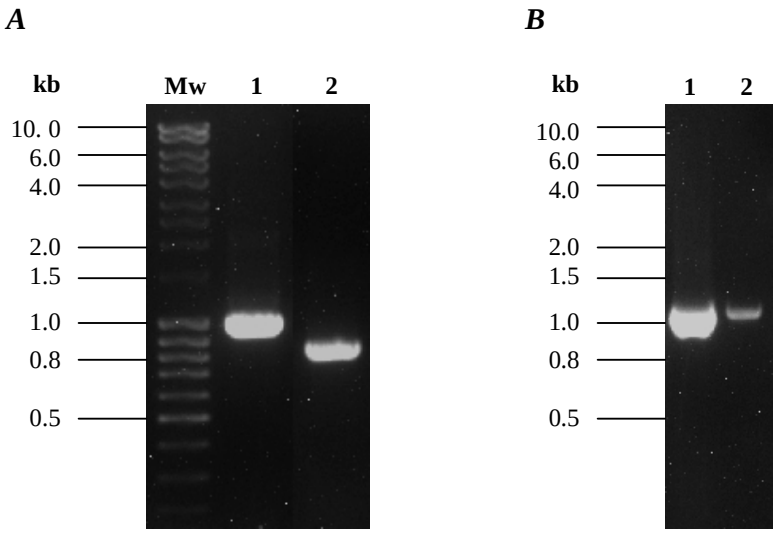

Figure 5.3 PCR amplification of the *PyBCCP* cDNA from *P. yoelii* genomic DNA and purification of the PCR product. (*A*) Agarose gel (0.5%) analysis of *PyBCCP* (*lane1*) and PyLDH DNA positive control (*lane* 2) PCR products. (*B*) *Lane* 1 is unpurified PCR product and *lane 2* is purified PCR product. The approximate amount of purified PCR product was estimated using the Fermentas MassRuler™ DNA ladder (Mw in panel *A*).

5.2.2 Cloning of the *PyBCCP* PCR product into pJET1™ blunt end cloning plasmid

The PCR product was ligated into pJET1™ blunt end cloning vector to form pJ-PyBCCP. A blunt end cloning vector was used because the PCR fragment lacked T-overhangs due to the activity of a proof reading enzyme present in the High Fidelity™ PCR system. The ligation reaction product was used to transform competent *E. coli* JM109 cells and 75 colony forming units were obtained. The presence of the *PyBCCP* insert was established by colony PCR using the insert primers (PyBCCP-fwd and PyBCCP-rev), as well as by restriction digestion of the plasmid isolated from a colony forming unit using *Eco*RI and *Not*I restriction endonucleases (Figure 5.4*A*)

Plasmids isolated from the first colony (Figure 5.4*A*, *lane 1*) were digested with *Eco*RI and *Not*I either sequentially or concurrently (double digest). The restriction digestion products were analysed by agarose gel electrophoresis (Figure 5.4*B*). Two distinct DNA bands, one at 3 kb corresponding to the pJET1 plasmid and another at 1 kb fragment corresponding to *PyBCCP* insert were obtained. The *Eco*RI and *Not*I-restricted *PyBCCP* (*PyBCCP* $_{Eco\text{-}Not}$) fragment was purified from the agarose gel and used for subcloning.

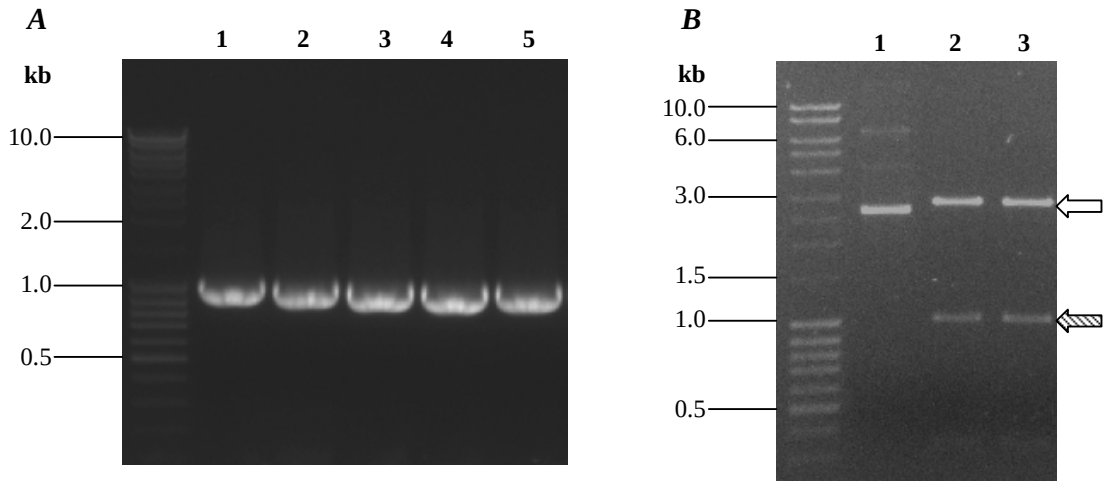

Figure 5.4 Confirmation of the presence of the *PyBCCP* insert in the plasmid of transformed *E. coli* JM109 cells. (*A*) DNA from five colonies (*lanes* 1 – 5) was amplified by PCR using the *PyBCCP* specific primers (PyBCCP-fwd and PyBCCP-rev). The 1 kb DNA band in each of the lanes corresponds to the amplified *PyBCCP* insert. (*B*) Analysis of restriction endonuclease digestion of plasmid isolated from a colony. *Lane 1* is the circular recombinant pJ-PyBCCP plasmid, *lane 2* is pJ-PyBCCP digested sequentially with *Eco*RI and *Not*I, respectively and *lane 3* is pJ-PyBCCP digested simultaneously with *Eco*RI and *Not*I. Liner pJET1 plasmid is 3 kb in size (open arrow) and *PyBCCP*$_{Eco\text{-}Not}$ fragment is 1041 bp in size (striped arrow). Agarose concentration was 0.5% (w/v).

5.2.3 Subcloning of the *PyBCCP*$_{Eco\text{-}Not}$ cDNA into pET-28a and pGEX-4T-1

The pET-28a and the pGEX-4T-1 plasmids were isolated from *E. coli* cells, digested with *Eco*RI and *Not*I restriction enzymes, and dephosphorylated with shrimp alkaline phosphatase. Figure 5.5*A* shows a single distinct band of ~ 5.5 kb (lane 2) corresponding to the size of the linear pET-28a plasmid (5.4 kb) and Figure 5.5*B* shows a single band of ~ 5 kb (lane 2) matching the size of the linear pGEX-4T-1 plasmid (4.9 kb). The three bands observed in the lane resolving the circular plasmids (lane 1) are the coiled, super coiled and nicked conformations. Approximately 1 µg/ml of pET-28a and 0.75 µg/ml of pGEX-4T-1 were obtained.

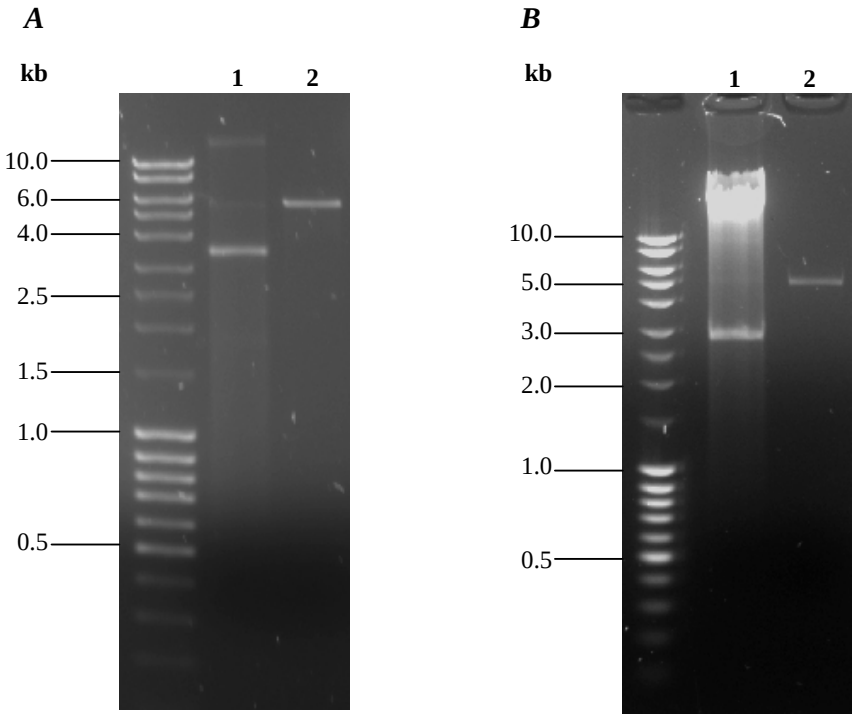

Figure 5.5 Isolation, restriction digestion and purification of expression plasmids. pET-28a (*A*) and pGEX-4T-1 (*B*) before (*lane 1*) and after (*lane 2*) double restriction digestion with *Eco*RI and *Not*I.

PyBCCP$_{Eco\text{-}Not}$ was ligated into pET-28a and pGEX-4T-1 to produce pT-PyBCCP and pGX-PyBCCP correspondingly. The recombinant pT-PyBCCP and pGX-PyBCCP plasmids were transformed into *E. coli* JM109 cells for propagation of the plasmid. Although JM109 is an expression host for pGEX-4T-1, the protease-deficient *E. coli* BL21 was subsequently used as the expression host. Approximately 100 colony forming units were obtained after transformation. A few of the colonies were screened for the presence of the *PyBCCP* $_{Eco\text{-}Not}$ insert by restriction digestion as well as by PCR using the PyBCCP-fwd and PyBCCP-rev primers and analysed by agarose gel electrophoresis (Figure 5.6). In Figure 5.6*A*, the restriction digestion with *Eco*RI yielded an intense DNA band with an estimated size of 6.5 kb (lane 2). This size corresponds to the sum of the sizes of pET-28a (5.3 kb) and the size of the cloned *PyBCCP*$_{Eco\text{-}Not}$ (~1 kb). Double digestion with *Eco*RI and *Not*I yielded two DNA bands at 5.5 kb and 1 kb (lane 3), thus confirming the presence of the cloned *PyBCCP*$_{Eco\text{-}Not}$. The PCR amplification confirmed the presence of the 1 kb *PyBCCP*$_{Eco\text{-}Not}$ (lane 4).

Similar results were obtained when plasmids isolated from an *E. coli* colony transformed with pGX-PyBCCP were analysed for the presence of the cloned $PyBCCP_{Eco\text{-}Not}$ (Figure 5.6*B*). Digestion of the plasmid with *Eco*RI resulted in a single DNA band with an approximate size of 6 kb being the sum of 1 kb cloned *PyBCCP* and 4.9 kb plasmid (lane 2). Double digestion with *Eco*RI and *Not*I produced a 1 kb insert and the plasmid that migrated at 5 kb (lane 3). The amplified PCR product also migrated at 1 kb (lane 4). The results indicated that the recombinant plasmids contained the cloned $PyBCCP_{Eco\text{-}Not}$ insert.

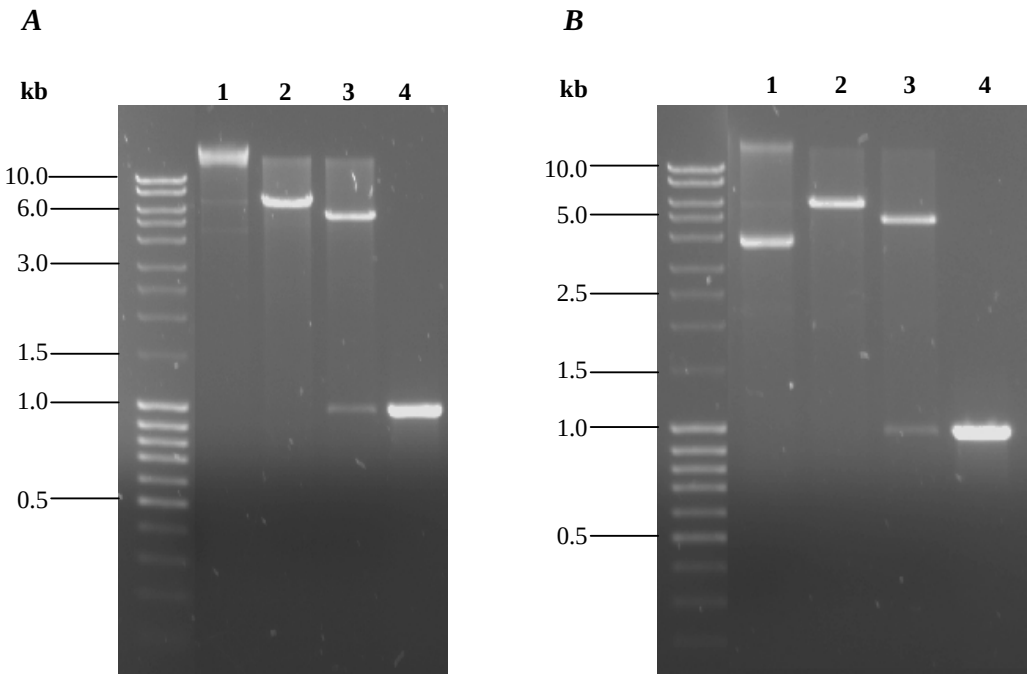

Figure 5.6 Agarose gel analysis of the subcloned of $PyBCCP_{Eco\text{-}Not}$ insert in pET-28a and pGEX-4T-1 vectors. *E. coli* transformed with pT-PyBCCP (*A*) and pGX-PyBCCP (*B*) were cultured and plasmids isolated. *Lane 1*, circular recombinant plasmid; *lane 2*, *Eco*RI-restricted plasmid; *lane 3*, *Eco*RI and *Not*I-double restricted plasmid; *lane 4*, PCR product of the plasmid amplified with *PyBCCP* sequence primers.

5.2.4 Sequencing of the pT-PyBCCP and the pGX-PyBCCP expression plasmids

To establish that the $PyBCCP_{Eco\text{-}Not}$ insert cloned into the expression vector was in the proper reading frame, the recombinant plasmids were sequenced using vector-specific primers (Table 2.2). Figure 5.7 illustrates the expression plasmid constructs showing details of the positioning of the sequencing primers with respect to the cloned $PyBCCP_{Eco\text{-}Not}$. The priming

positions of the pET-28a sequencing primers (~ 197 bp and ~ 98 bp from the *Eco*RI site and the *Not*I site, respectively) resulted in sequence data that included the start codon, stop codon, the N- and C-terminal poly-His tag, the T7 tag and the cloned *PyBCCP* as shown in Figure 5.7*A*. There was a small overlap in the sequences obtained from both primers as ~ 800 bp was sequenced from both directions. The priming positions of the pGEX-4T-1 sequencing primers (~ 188 bp and ~ 81 bp from the *Eco*RI site and the *Not*I site, respectively) resulted in sequence data that included a portion of the GST tag sequence and the stop codon as shown in Figure 5.7*B*. There was greater overlap between the two sequences (forward and reverse) than that obtained for the pT-PyBCCP construct.

The nucleotide sequences corresponding to the forward and the reverse directions of the sequencing data were merged into a single sequence that was translated into the coding amino acid sequence and aligned with the theoretical sequence (Figure 5.2) using the ClustalW™ algorithm (Figure 5.8). The sequencing data showed that the VEAMKM biotin attachment motif in the 17XL strain of *P. yoelii* was 100% identical in all published *Plasmodium* acetyl-CoA carboxylase biotinoyl domain biotin binding motifs as well as the *E. coli* BCCP biotin binding motif. Eight amino acids outside the biotinoyl domain were consistent in both constructs and different from the published sequence. These differences may be due to the different strain used for sequencing.

5.2.5 *In vitro* biotinylation of rabbit albumin as a positive control in avidin-biotin assays

Rabbit albumin was biotinylated for use as a control. *N*-Hydroxysuccinimide-biotin (NHS-biotin) was reacted with rabbit albumin, to form a stable amide bond between the ε-lysine residues on the rabbit albumin and the carboxylic acid functional group on the biotin molecule. The biotin-rabbit albumin complex was separated from unreacted NHS-biotin and NHS ester reaction product by size exclusion chromatography. Figure 5.9*A* shows the elution profile of the purification of biotin-rabbit albumin complex. Two distinct peaks were observed; the first peak corresponds to the biotin-rabbit albumin complex and the second peak corresponds to the unreacted NHS-biotin. Proteins eluting in Peak 1 (Figure 5.9*A*) were resolved along side unbiotinylated rabbit albumin on a 10% acrylamide gel. Following transfer of the protein to a nitrocellulose membrane, the presence of biotin bound to the rabbit albumin was confirmed by avidin-peroxidase and by an anti-biotin monoclonal antibody. Figures 5.9*B* and *C* illustrate the results of the SDS-PAGE of the proteins that eluted in Peak 1 and the Western blot analysis using the avidin-peroxidase detection system. The protein

band in lane 2 corresponding to the eluted proteins migrated the same distance as the unbiotinylated rabbit albumin (~ 57.7 kD). The theoretical mass of rabbit albumin used for this study is 62.8 kD. However, in a non-reducing SDS-PAGE gel, the biotin-rabbit albumin complex resolved at 66.2 kD while the unbiotinylated rabbit albumin resolved at 63.1 kD (results not shown), closer to the theoretical mass. The Western blot using avidin-peroxidase showed the presence of biotin bound to rabbit albumin molecule by detecting a band of approximately 57.7 kD in lane 2, which contains proteins eluting in Peak 1.

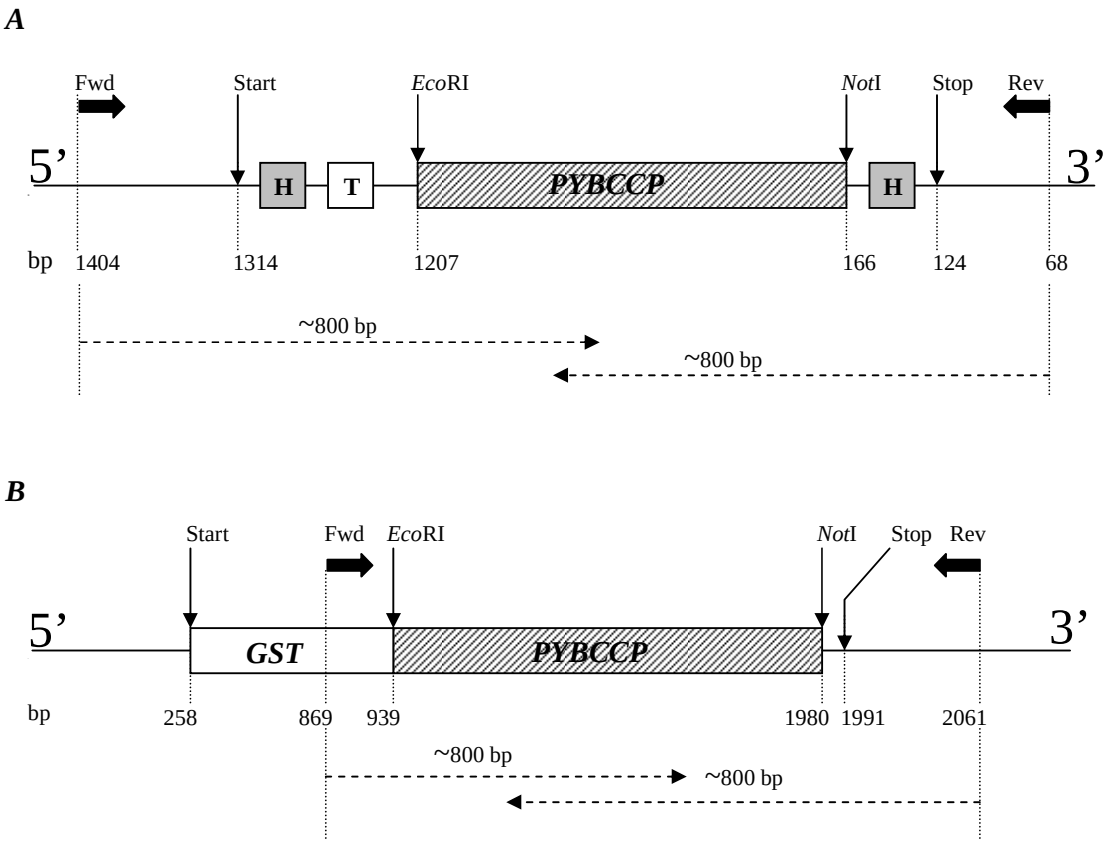

Figure 5.7 Schematic illustration of the sequencing primer positions with respect to the cloned *PyBCCP*$_{Eco\text{-}Not}$. (*A*) pT-PyBCCP construct showing the ORF (bp 124 – 1314), the cloned *PyBCCP* (striped box), the N- and C-terminal poly-His tag position (H), the T7 tag position (T) and the position of the sequencing primers (bold arrows). (*B*) pGX-PyBCCP construct showing the ORF (bp 258 – 1991), the cloned *PyBCCP* (striped box), *GST* gene (open box) and the position of the sequencing primers (bold arrows). The two sequencing directions (broken arrows) illustrate the degree of overlap in the sequencing data.

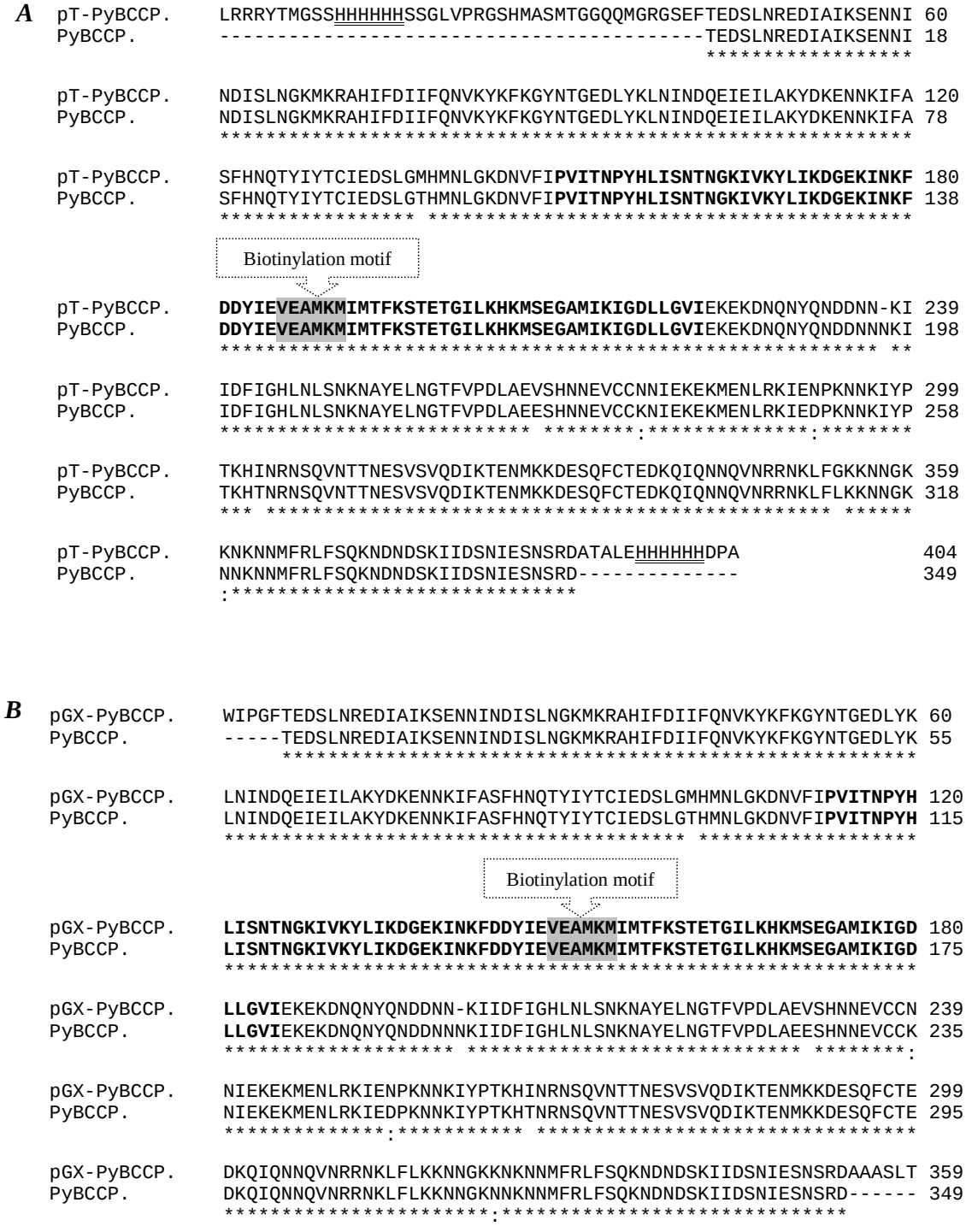

Figure 5.8 ClustalW™ alignments of the sequenced pT-PyBCCP and pGX-PyBCCP with the amino acid sequence from *P. yoelii* 17XNL obtained from the Plasmodb database. (*A*) pT-PyBCCP expression construct. The poly-His-tag on the pT-PyBCCP is double underlined (*B*) pGX-PyBCCP expression construct. For both panels, the biotinylation motif is highlighted and the biotin carboxyl carrier protein domain is in bold case. * indicates 100% conserved amino acid residue.

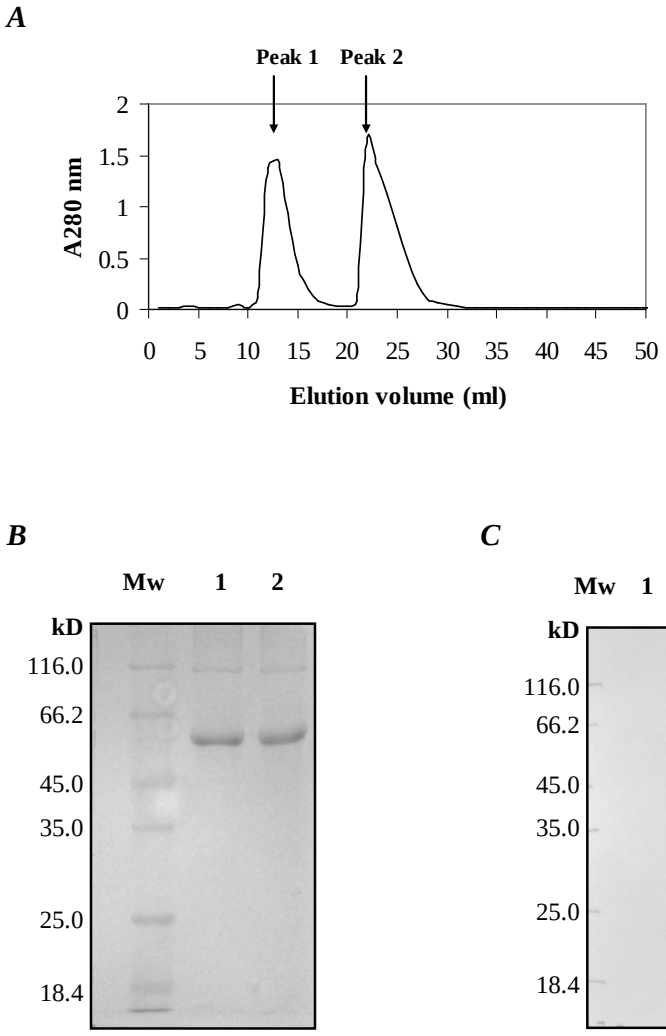

Figure 5.9 *In vitro* biotinylation of rabbit albumin using NHS-biotin. Rabbit albumin was reacted with NHS-biotin and the reaction product was purified over a Sephadex-G25 size exclusion chromatography matrix. (*A*) The elution profile of the purification process. The arrows indicate peaks corresponding to the region of the profile with significantly high absorbance at 280 nm. (*B*) Proteins eluting at peak 1 were resolved by reducing 10% SDS-PAGE; *lane 1* is unbiotinylated rabbit albumin and *lane 2* is biotinylated rabbit albumin that eluted in peak 1. (*C*) The resolved proteins were transferred onto a nitrocellulose membrane and probed for the presence on biotin with avidin-peroxidase conjugate. *Lanes 1* and *2* in Panel *C* correspond to those in Panel *B*.

5.2.6 Expression of recombinant His_6-PyBCCP and GST-PyBCCP

Recombinant *P. yoelii* biotinoyl protein (PyBCCP) was expressed at 37°C for 5 h by induction with 0.5 mM IPTG as a His-tagged (His_6-PyBCCP) or GST-tagged (GST-PyBCCP) fusion protein in *E. coli* in the presence or absence of 0.2 mM D-biotin. The expression media

was supplemented with biotin to establish whether external biotin is needed for the *in vivo* biotinylation of the expressed protein by the *E. coli* host. The total cell protein was analysed for the presence of recombinantly expressed proteins by SDS-PAGE as well as by Western blot using anti-His-tag antibody to detect His_6-PyBCCP and biotinylated-anti-GST antibody to detect GST-PyBCCP.

His_6PyBCCP was expressed as a 50 kD protein in *E. coli* cells induced with IPTG and was not prominent in lanes containing cell proteins from uninduced cells or cells expressing the parent plasmid (Figure 5.10). The supplementation of the expression medium with biotin did not appear to alter the expression of His_6PyBCCP. The size of the expressed His_6PyBCCP was 5 kD more than the theoretical mass (~ 45 kD) deduced using the ProtParam™ online tool (www.expasy.org). The 50 kD protein band contained poly-His tag as it was detected by anti-His tag antibody (Figure 5.10*B*). The anti-His-tag antibody also detected some minor protein bands below the 50 kD protein band in lanes for induced cells. These minor protein bands may be degraded or truncated products of the His_6PyBCCP. No His-tagged proteins were detected in lanes containing proteins from uninduced cells or cells expressing the parent plasmid (lanes 1 and 2).

Figure 5.11 illustrates the results of GST-PyBCCP expression in IPTG-induced/uninduced cells with or without D-biotin supplementation. GST-PyBCCP migrated as a 66 kD protein band that appears to have co-migrated with an *E. coli* protein. It is more prominent in lysates from cells induced with IPTG than in uninduced cells. The mass of the band corresponds to the sum of mass of the GST tag (26 kD) and the theoretical mass of the PyBCCP (40.5 kD) using ProParam™ (www.expasy.org). A 26 kD protein band, which is prominent in induced cells expressing the parent vector (pGEX-4T-1), which corresponds to the GST-tag. This 26 kD band was also observed in uninduced cells suggesting basal expression of GST due to a possible leaky P_{tac} promoter (Makrides, 1996).

The expression of GST-PyBCCP was further confirmed by Western blot analysis using biotinylated anti-GST-antibody. A band at 66 kD was prominent in lanes containing proteins from IPTG-induced cells as well as some minor bands below the 66 kD band, synonymous with His_6-PyBCCP expression. These minor bands may be degraded GST-PyBCCP in view of the fact that they were detected by the biotinylated anti-GST antibody.

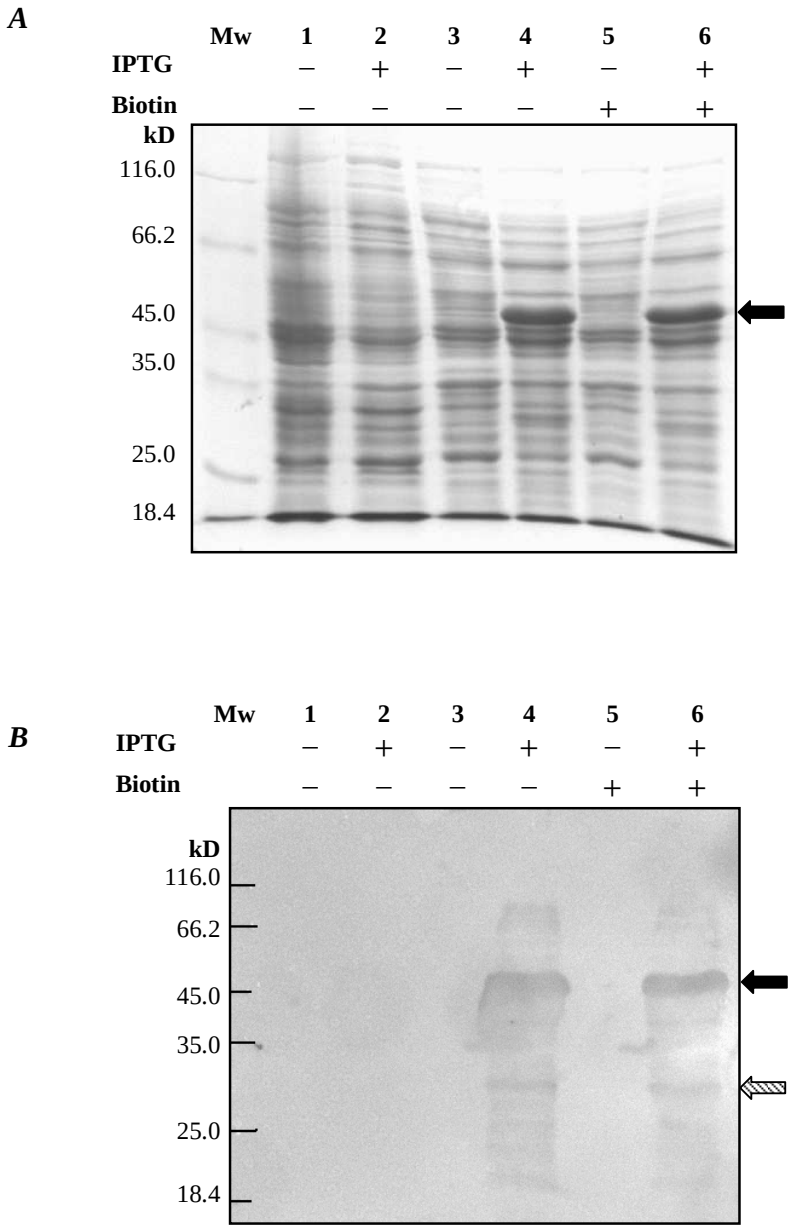

Figure 5.10 Analysis of His_6-PyBCCP expression. (*A*) SDS-PAGE (10%) analysis of total cell lysate from *E. coli* Rosetta (DE3) PLysS cells induced with IPTG (+) or uninduced (−), with (+) or without (−) biotin supplementation. *Lanes 1* and *2* contain proteins from cells expressing the parent pET-28a plasmid and *lanes 3 – 6* contain proteins from cells expressing the recombinant pT-PyBCCP plasmid. (*B*) Western blot analysis of the resolved proteins corresponding to Panel *A*, probed with anti-His-tag antibody, followed by goat anti-mouse-IgG-peroxidase. Filled arrows indicate the expressed recombinant protein while a striped arrow indicates a minor protein band detected by the anti-His-tag antibody.

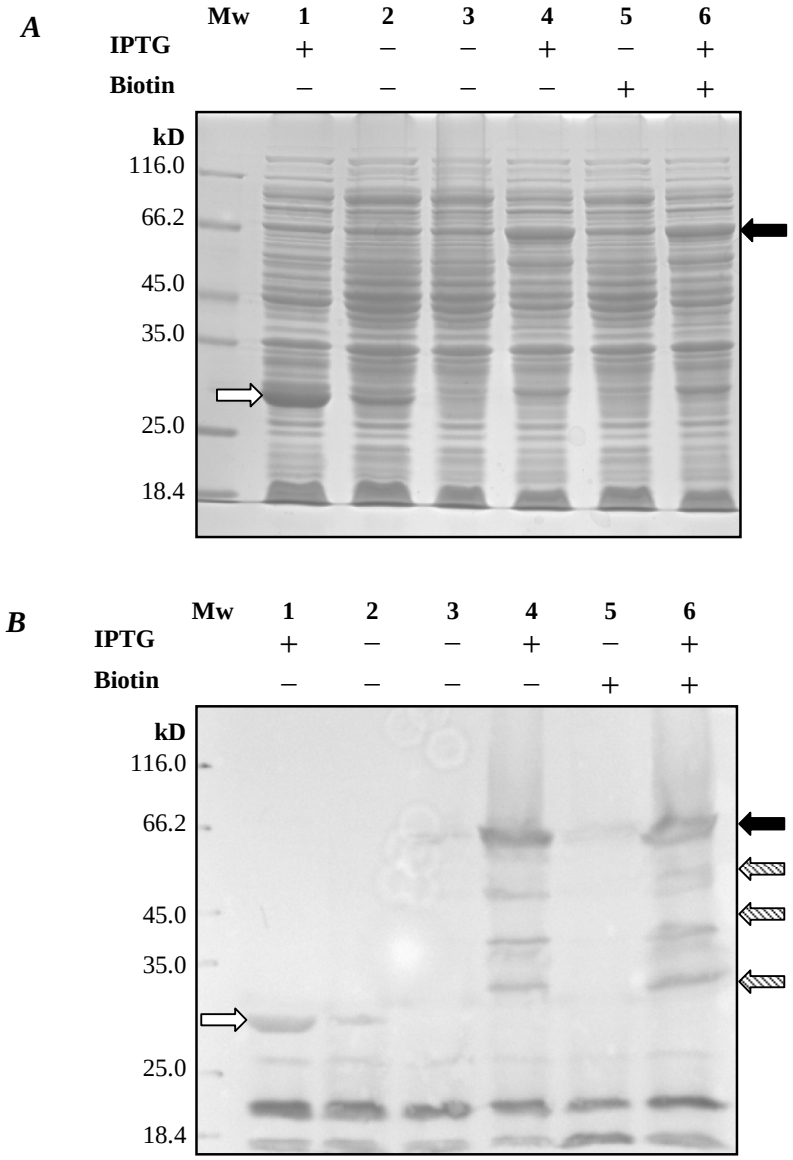

Figure 5.11 Analysis of GST-PyBCCP expression. (*A*) SDS-PAGE (10%) analysis of total cell lysate from *E. coli* BL21 cells induced with IPTG (+) or uninduced (−), with (+) or without (−) biotin supplementation. *Lanes 1* and *2* contain proteins from cells expressing the parent pGEX-4T-1 plasmid and *lanes 3 – 6* contain proteins from cells expressing the recombinant pGX-PyBCCP plasmid. (*B*) Western blot analysis of the resolved proteins corresponding to Panel *A*, probed with biotinylated anti-GST antibody, followed by avidin-peroxidase. Filled arrows indicate the expressed recombinant protein, open arrows indicate GST-tag and striped arrows indicate minor protein bands detected by the biotinylated anti-GST antibody.

The 26 kD GST was also detected in cells expressing the parent plasmid. There were conspicuous 22 kD protein bands detected in all the lanes by the avidin-peroxidase probe. These bands may be a biotinylated *E. coli* protein, possibly the biotin carboxyl carrier protein subunit of the *E. coli* acetyl-CoA carboxylase, which has a theoretical mass of 18.8 kD but due to its high alanine content, the protein has been shown to migrate higher than its actual mass in an acrylamide gel (Cronan, 2001; Cronan, 2002). The band slightly below 18.4 kD is the dye front.

5.2.7 Expression of the N-terminal region of putative *P. yoelii* copper transporter

The N-terminal region of a hypothetical *P. yoelii* surface related protein (PY00413) was expressed as a GST-fusion protein (GST-PyCTRNt) in *E. coli* BL21 strain (Choveaux and Goldring, unpublished). This was carried out as a negative control in the study of the *in vivo* biotinylation to establish that the biotinylation of PyBCCP by *E. coli* was specific owing to the presence of the biotinylation motif (VEAMKM) which is absent in the hypothetical *P. yoelii* surface related protein. This protein was preferred because it originates from *P. yoelii* and contains 14 lysine residues. The amino-acid sequence of the expressed region of the protein is shown in Figure 5.12 (lysine residues in bold). The total cell protein was analysed for the expression of GST-PyCTRNt by SDS-PAGE as well as by Western blot using biotinylated anti-GST antibody.

MNIW**K**IIYIVLIINSLFVVNVNCESNDQNDGTTSN**KK**NTGCCGGTN**K**PLP
SVN**K**PL**K**SCCSD**K**QSGDDEC**K**PILDLNHIGS**K**G**K**N**K**IPFIY**K**CCINHDIY
ESIINEHFSEENQSNTTGGPE**K**LNMMMGNLSMPMSFQNTTHTIILF**K**FWE

Figure 5.12 Predicted amino as sequence of PyCTRNt

Figure 5.13 shows SDS-PAGE and Western blot analysis of GST-PyCTRNt expression in induced/uninduced cells in the presence or absence of D-biotin. GST-PyCTRNt migrated as a 40 kD protein band, which was prominent in the lanes containing proteins from induced cells. The 40 kD protein is equivalent to the sum of the GST-tag (26 kD) and the PyCTRNt (17 kD) sequence.

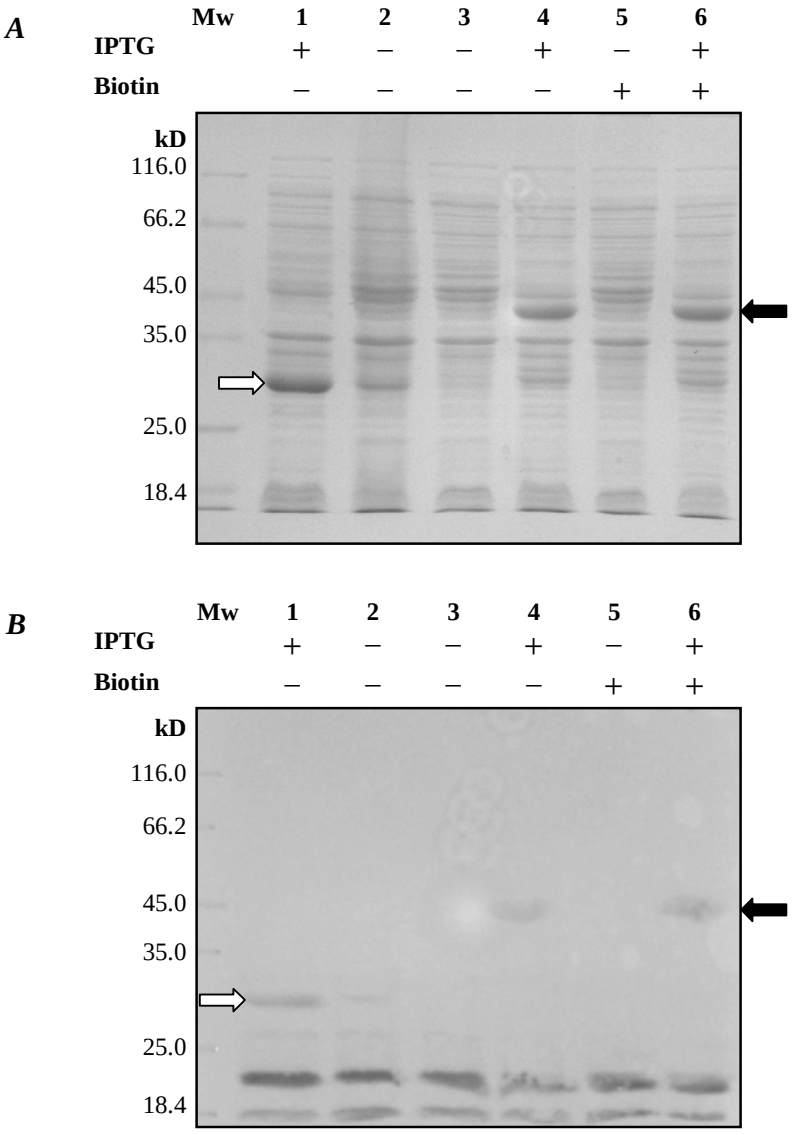

Figure 5.13 Analysis of GST-PyCTRNt expression in BL21 cells. (*A*) SDS-PAGE (10%) analysis of total cell lysate from *E. coli* BL21 cells induced with IPTG (+) or uninduced (−), with (+) or without (−) biotin supplementation. *Lanes 1* and *2* contain proteins from cells expressing the parent pGEX-4T-1 plasmid and *lanes 3 – 6* contain proteins from cells expressing the recombinant PyCTRNt-pGEX-4T-1plasmid. (*B*) Western blot analysis of the resolved proteins corresponding to Panel *A*, probed with biotinylated anti-GST antibody, followed by avidin-peroxidase. Filled arrows indicate the expressed recombinant protein and open arrows indicate GST-tag.

In cells expressing the parent vector (pGEX-4T-1), a prominent 26 kD protein band was observed in the induced cells, which corresponds to the GST tag. Basal expression of GST was also observed in uninduced cells. Expression of GST-PyCTRNt was confirmed by Western blot analysis using biotinylated anti-GST antibody. A band at 40 kD was prominent in lanes containing proteins from IPTG-induced cells. The 26 kD GST was detected in lysates of cells expressing the parent plasmid. Similar to Figure 5.11*B*, 22 kD bands were detected in all lanes by the avidin-peroxidase secondary probe.

5.2.8 Analysis of *in vivo* biotinylation of recombinant *P. yoelii* biotinoyl

To confirm that the expressed recombinant GST-PyBCCP and His_6-PyBCCP were biotinylated by the host cell, the total protein of cells induced or not induced with or without D-biotin supplementation was resolved by SDS-PAGE and blotted onto nitrocellulose membrane. The membrane was probed with avidin-peroxidase or anti-biotin antibody for the presence of biotin. Free avidin and biotin were incorporated into the assay reagents to block the biotin sites on proteins blotted onto the membrane or inhibit the binding of avidin-peroxidase and anti-biotin antibody to the biotinylated proteins as negative controls.

Recombinant His_6-PyBCCP expressed in *E. coli* resulted in the biotinylation of the recombinant protein as observed by a 50 kD major protein band and some minor bands less than 50 kD in lanes resolving total cell proteins from IPTG-induced cells (Figure 5.14), the same as Figure 5.10. An *E. coli* protein at ~ 22 kD and a protein band less than 18.4 kD (migrating with the dye front) were also detected by the avidin-peroxidase and anti-biotin antibody probes in all lanes. The supplementation of 0.2 mM D-biotin to the expression medium appeared not to have a contribution to the *in vivo* biotinylation of the recombinant His_6-PyBCCP. Incorporating free avidin or biotin into the assay system appeared to inhibit the detection of biotinylated proteins on the membrane.

The avidin-peroxidase and the anti-biotin antibody both detected protein bands at 66 kD corresponding to GST-PyBCCP as well as some minor bands less that 66 kD in lanes containing lysates from induced IPTG cells (Figure 5.15). However a faint 66 kD protein band was detected in the uninduced lanes possibly due to basal transcription as observed in the anti-GST blot (Figures 5.11 and 5.13). The 22 kD biotinylated *E. coli* protein as well as the protein band co-migrating with the dye-front were also detected in all lanes. Supplementing the expression medium with 0.2 mM D-biotin did not have any visible

enhancement of the biotinylation of GST-PyBCCP by the *E. coli* BL21 strain. The presence of free avidin or biotin in the assay medium completely abolished the interaction between the biotinylated proteins on the membrane and the avidin-peroxidase or the anti-biotin antibody probes. Once again this suggested that there was specificity towards the biotin bound to the resolved and blotted proteins.

The biotinylation carried out by the expressing *E. coli* host was shown to be specific to the presence of the VEAMKM biotinylation motif, which is not present in PyCTRNt. Total cell proteins from *E. coli* BL21 cells expressing the recombinant GST-PyCTRNt induced with IPTG or not induced, with or without biotin supplementation, were resolved by SDS-PAGE, blotted onto a nitrocellulose membrane and probed with avidin-peroxidase or anti-biotin antibody. Figure 5.16 shows that no protein bands were detected at 40 kD corresponding to the GST-PyCTRNt recombinant fusion protein in lanes containing proteins from induced cells. Supplementing the culture with external biotin did not result in any form of biotinylation of the recombinant PyCTRNt. Synonymous with previous results (Figures 5.11 and 5.13), a biotinylated *E. coli* protein of 22 kD was detected in all lanes. The results therefore support the assumption that the biotinylation of the recombinant His_6-PyBCCP and GST-PyBCCP by *E. coli* biotin protein ligase was specific and due to the presence of the biotinylation motif found on the recombinant proteins.

5.2.9 Large scale expression, purification and refolding of His_6-PyBCCP

In order to obtain a sizable amount of the recombinant His_6-PyBCCP to be used for oligomerisation studies, expression of His_6-PyBCCP was carried out on a larger scale. A culture (4.5 L) of *E. coli* cells expressing His_6-PyBCCP was induced with 0.5 mM IPTG for 5 h at 37°C. His_6-PyBCCP proteins in the inclusion bodies were separated with an immobilised-cobalt affinity matrix under denaturing conditions. Figure 5.17*A* illustrates the SDS-PAGE analysis of the purification profile of His_6-PyBCCP under denaturing conditions. Lane 1 is the insoluble fraction that was subsequently purified over the immobilised-cobalt affinity matrix and lane 2 contains the supernatant of the 2 M urea wash step prior to guanidine solubilisation (see Section 2.6.2). It can be seen that the prominent band at 50 kD corresponding to the expressed protein was predominantly in the insoluble fraction and was not solubilised by the 2 M urea wash solution. Lanes 3 – 5 contain no visible protein bands from the wash steps after binding to the immobilised-cobalt affinity matrix (prior to elution).

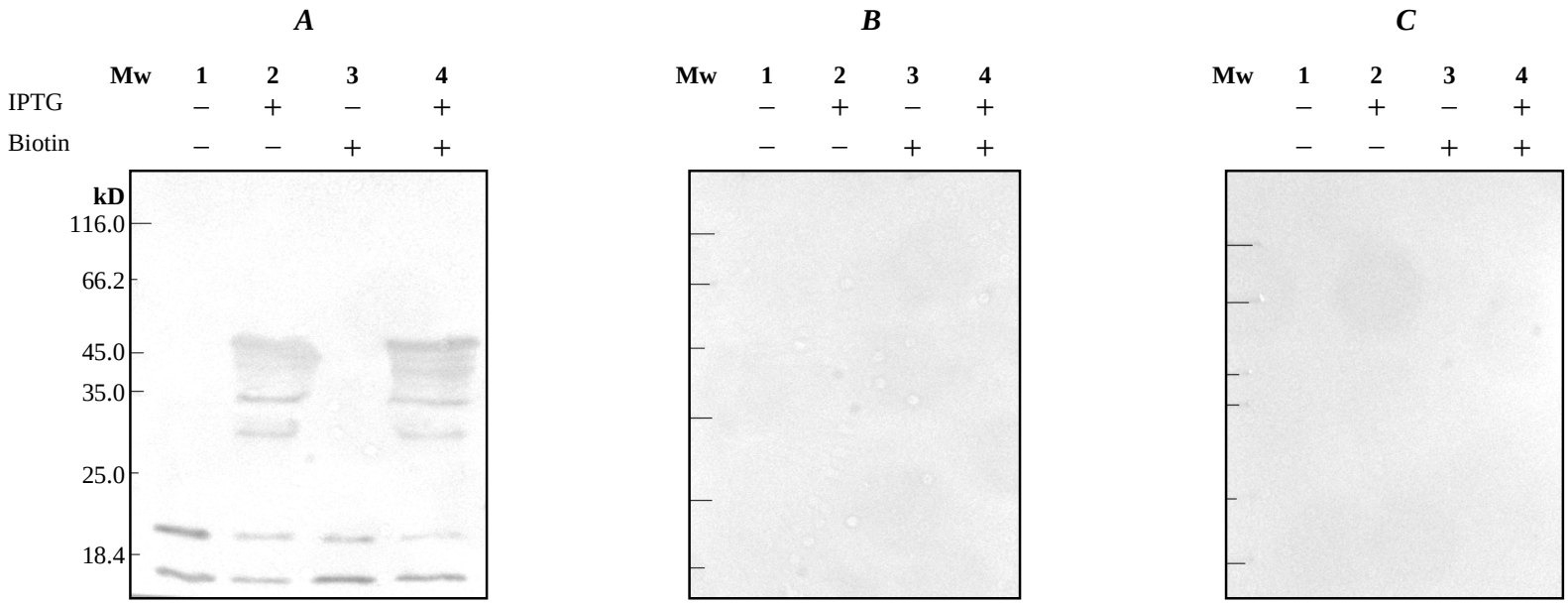

Figure 5.14 Analysis of the *in vivo* biotinylation of His_6-PyBCCP. Total cell lysate from *E. coli* cells expressing His_6-PyBCCP induced with IPTG (+) or uninduced (−), in the presence (+) or absence (−) of biotin, was resolved by SDS-PAGE (10%), blotted on a nitrocellulose membrane and probed with avidin-peroxidase alone (*A*) or incubated with free avidin followed by avidin-peroxidase conjugate (*B*) or incubated with avidin-peroxidase conjugate in the presence of free biotin (*C*).

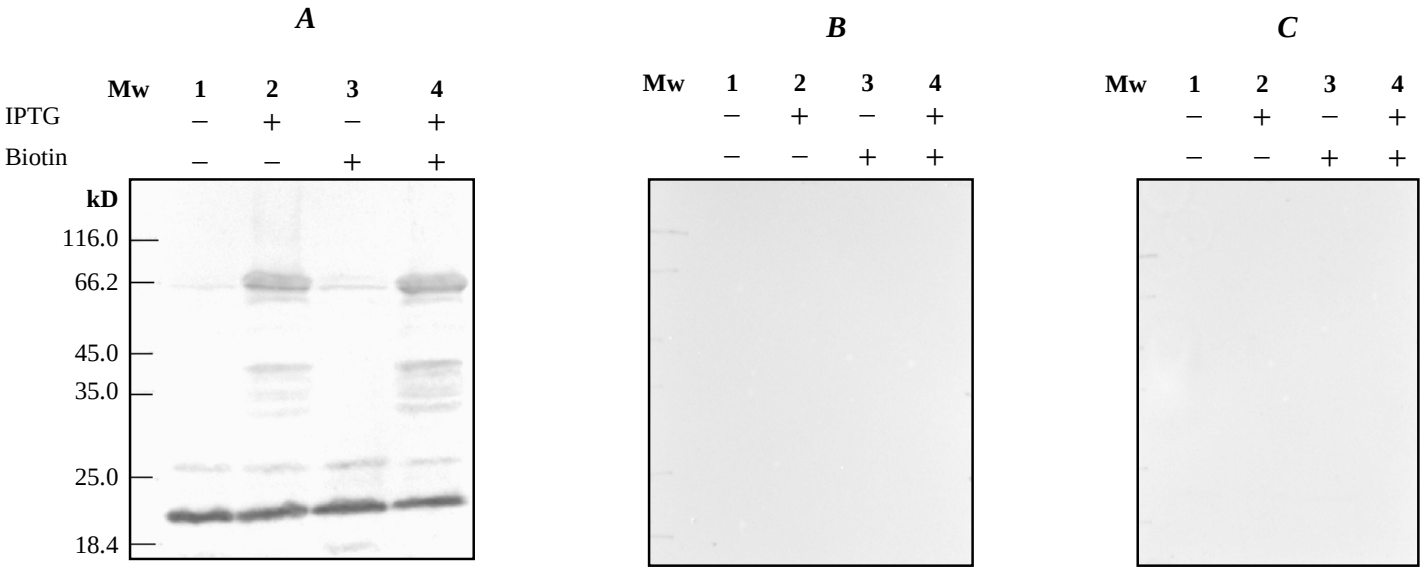

Figure 5.15 Analysis of the *in vivo* biotinylation of GST-PyBCCP. Total cell proteins from *E. coli* cells expressing GST-PyBCCP induced with IPTG (+) or uninduced (−), in the presence (+) or absence (−) of biotin, was resolved by SDS-PAGE (10%), blotted on a nitrocellulose membrane and probed with avidin-peroxidase conjugate alone (*A*) or incubated with free avidin followed by avidin-peroxidase conjugate (*B*) or incubated with avidin-peroxidase conjugate in the presence of free biotin (*C*).

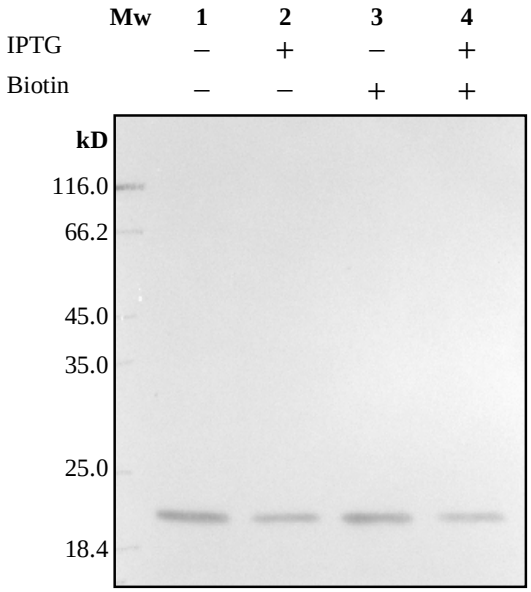

Figure 5.16 Analysis of the *in vivo* biotinylation of GST-PyCTRNt. Total cell lysate from *E. coli* cells expressing GST-PyCTRNt induced with IPTG (+) or uninduced (−), in the presence (+) or absence (−) of biotin, was resolved by SDS-PAGE (10%), blotted on a nitrocellulose membrane and probed with avidin-peroxidase conjugate.

Lane 6 contains proteins eluted with 1 M imidazole in 8 M urea buffer. The dominant protein band in lane 6 matches the 50 kD band in lane 1 corresponding to the recombinant His_6-PyBCCP. Proteins that did not bind to the immobilised-cobalt affinity matrix (before the wash steps) were not resolved on the acrylamide gel because guanidine forms an insoluble complex with SDS in the treatment buffer. Figure 5.17*B* illustrates the SDS-PAGE analysis of the purification profile of His_6-PyBCCP under native conditions using the soluble fraction obtained from cell culture (500 ml) induced with 0.5 mM IPTG (16 h, 18°C). This condition was not used because the level of expression was more than 100-fold less compared to expression at 37°C, though the expression at 18°C resulted in recombinant proteins being in the soluble fraction. Figure 5.17*B* also demonstrated that His_6-PyBCCP expressed at 18°C was capable of binding to the immobilised-cobalt affinity matrix.

The purified His_6-PyBCCP was renatured by a series of dialysis steps against decreasing concentrations of urea in 20 mM Tris-HCl buffer. At 0.5 M urea, part of the protein precipitated out of the solution. Thus, some of the recombinant protein was lost during the refolding process. The insoluble protein and the refolded protein were resolved along side

each other on 10% SDS-PAGE (Figure 5.18). The results showed that part of the refolded protein formed precipitates; however, a substantial amount of the recombinant protein was renatured and solubilised. Approximately 10 mg of recombinant purified recombinant protein per litre of culture was obtained.

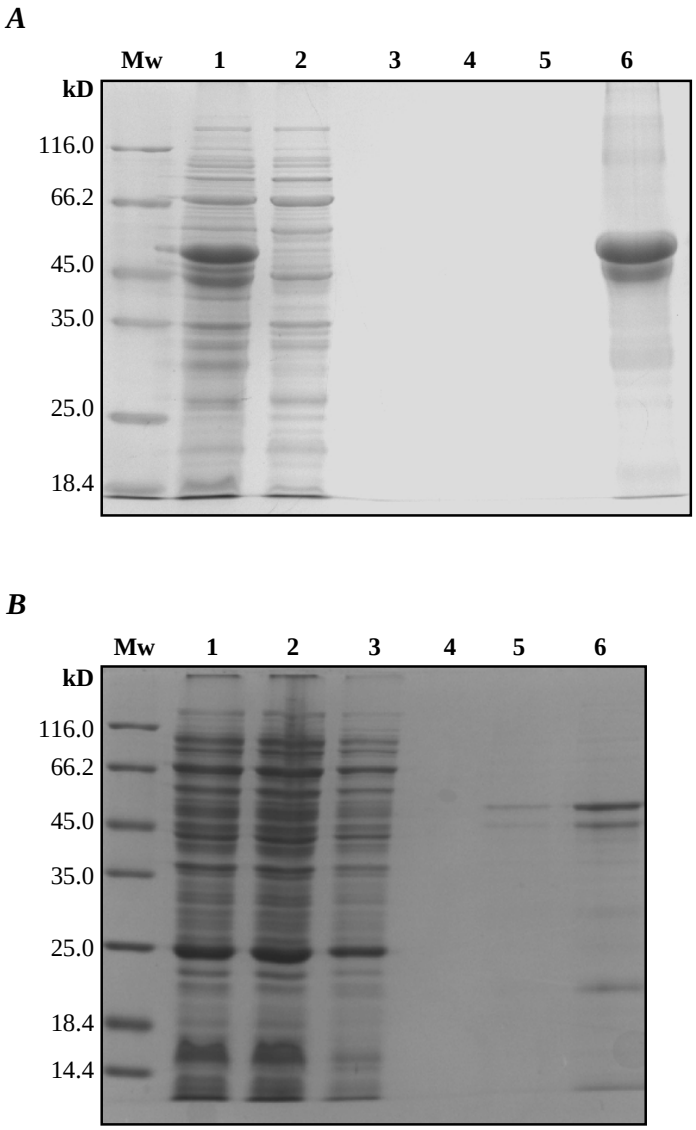

Figure 5.17 Immobilised-cobalt affinity purification of His_6-PyBCCP. The purification profile of recombinant His_6-PyBCCP was analysed by SDS-PAGE. (*A*) Under denaturing conditions (10% acrylamide gel). *Lane 1*, insoluble fraction; *lanes 2 – 5*, wash steps; *lane 6*, elution with 1 M imidazole. (*B*) Under native condition (12.5% acrylamide gel). *Lane 1*, soluble fraction of the cell lysate; *lane 2*, flow through fraction; *lanes 3* and *4* first and second wash steps, respectively; *lane 5* and *6*, elution with 50 mM and 250 mM imidazole respectively.

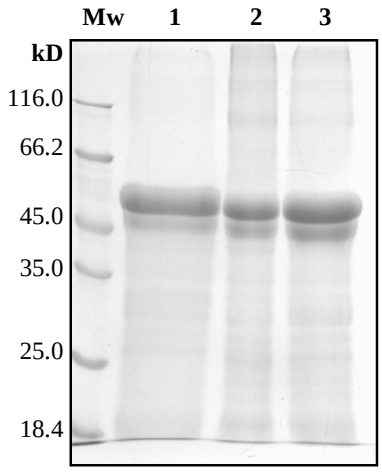

Figure 5.18 Refolding of immobilised-cobalt affinity purified-His_6-PyBCCP. The refolding of the purified recombinant His_6-PyBCCP was resolved by SDS-PAGE (10%). *Lane 1*, starting material; *lane 2*, precipitated product; *lane 3*, solubilised recombinant protein.

The refolded protein was analysed by non-reducing SDS-PAGE (10%) to ascertain if the recombinant protein formed oligomer in the absence of β-mercaptoethanol or DTT (Figure 5.19). The result showed that the recombinant protein did not form a defined quaternary structure but rather aggregated and did not resolve in the running gel (lane 2) when compared to the reduced recombinant protein sample (lane 1).

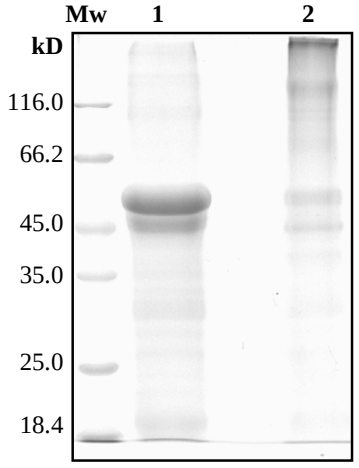

Figure 5.19 SDS-PAGE analysis of the oligomerisation of His_6-PyBCCP. Purified and refolded His6-PyBCCP was treated with reduced with β-mercpatoethanol (*lane 1*) or not reduced (*lane 2*) and resolved by SDS-PAGE (10%).

A similar result was obtained when the acrylamide concentration was reduced to 5.5%, low enough to resolve proteins between 45 kD and 350 kD (result not shown). There is no data that suggests the precise size of the polymeric form of acetyl-CoA carboxylase. Probably, the aghregation of the recombinant protein may be due to the presence of cystine residues, which is reduced in the presence of β-mercaptoethanol.

5.3 Discussion

Biotin dependent enzymes such as carboxylases and decarboxylases in several organisms ranging from prokaryotes to higher eukaryotes are strongly conserved proteins (Athappilly and Hendrickson, 1995; Gornicki and Haselkorn, 1993; Li *et al*., 2006; Reche and Perham, 1999) with a common MKM biotin binding motif (Chapman-Smith and Cronan, 1999a; Chapman-Smith and Cronan, 1999c; Reche *et al*., 1998). The interest in understanding the involvement of the biotin-dependent acetyl-CoA carboxylase in *P. yoelii* led us to clone, express and analyse the recombinant *P. yoelii* biotinoyl proteins as GST-PyBCCP and His_6-PyBCCP fusion proteins. The fusion protein was expressed in *E. coli* under the assumption that the *E. coli* biotin protein ligase would biotinylate the recombinant proteins (Chapman-Smith *et al*., 1999; Chapman-Smith *et al*., 2001; Polyak *et al*., 2001; Solbiati *et al*., 2002). Comparative sequence analysis of the enzyme revealed the presence of a biotin-binding motif, VEAMKM, within the biotinoyl domain of *Plasmodium* acetyl-CoA carboxylase. This motif is 100% identical to the *E. coli* biotinoyl protein subunit of acetyl-CoA carboxylase (Cronan, 2001; Cronan, 2002; Cronan and Waldrop, 2002).

The recognition by a biotin protein ligase of a biotin-dependent protein, such as the biotinoyl domain of acetyl-CoA carboxylase, is thought to involve residues that are outside the biotin-binding motif (Chapman-Smith and Cronan, 1999c; Chapman-Smith *et al*., 1999; Polyak *et al*., 2001; Solbiati *et al*., 2002). Therefore, it was important to consider several factors relating to the molecular structure and the dynamics of the protein such as (i) the folding of the recombinant protein expressed in a heterologous system (ii) the orientation of the VEAMKM motif on the surface for proper recognition by the *E. coli* biotin protein ligase (BirA) will be vital for the recombinant protein to be biotinylated and (iii) the role played by some residues that are far removed from the VEAMKM motif but are very crucial in the recognition by the biotin protein ligase. Previous studies on *E. coli* BCCP have shown that the extent to which a truncated BCCP is biotinylated depends on the number of amino acid residues flanking the MKM motif (Beckett *et al*., 1999).

With these factors in mind, a region between 324 – 506 bp flanking the 219 bp biotinoyl domain was cloned and expressed, thus resulting in a protein with 108 and 169 amino acid residues upstream and downstream of the biotinoyl domain. This stretch of amino acid residues outside the domain was hoped to ensure correct folding of the recombinant proteins. The presence of the highly charged poly-histidine tag and the GST-tag on the recombinant proteins are likely to hinder the activity of the *E. coli* biotin protein ligase. Studies have shown that regardless of the fact that BirA recognizes the consensus MKM motif, the recognition is based on the context of a properly folded protein (Chapman-Smith and Cronan, 1999b; Chapman-Smith and Cronan, 1999c; Chapman-Smith *et al*., 1999; Streaker and Beckett, 1999). Therefore, it is possible that improper folding of the recombinant protein may result in poor biotin attachment by BirA, which may compromise the study. Sequencing the recombinant genes from the expression plasmids confirmed the sequence of the recombinant genes. Two expression systems were chosen for this study to affirm that the biotinylation of the recombinant protein is independent of expression system. Studies have shown that the presence of enhancement tags such as MBP, poly-His and GST often do not alter the activity of the recombinant *Plasmodium* proteins (Flick *et al*., 2004; Mehlin *et al*., 2006; Pandey *et al*., 2006).

Both recombinant proteins were found to be insoluble when expressed at 37ºC. Changing the expression temperature to 20ºC produced small amounts of soluble recombinant poly-His-tag protein product. In both systems, truncated products were obtained. This may be due to the nature of the gene transcript products and the inability of the *E. coli* gene transcriptional system to properly transcribe the cloned gene (Makrides, 1996; Mehlin *et al*., 2006; Sorensen and Mortensen, 2005a). The truncations may also be as a result of proteolytic degradation of the recombinant protein. Efforts to express the protein as an MBP-fusion protein were not successful. Generally, studies have shown that *Plasmodium*-derived proteins are difficult to express heterologously in *E. coli* and most *Plasmodium* proteins expressed in *E. coli* are insoluble (Flick *et al*., 2004; Mehlin *et al*., 2006) and often truncated. These pitfalls are sometimes related to the property of the protein such as the isoelectric point pH (pI) or the gene composition (GC/AT ratio) of the recombinant transcript (Mehlin *et al*., 2006). However, the theoretical pI of the recombinant proteins (6.73 and 6.20 for His_6-PyBCCP and GST-PyBCCP, respectively) are within the range (3.6 – 6.8) that expressed as soluble proteins based on the study by Mehlin *et al*., (2006).

Due to long stretches of *A* or *T* nucleotides in the *Plasmodium* gene, expression of *Plasmodium* proteins in *E. coli* often prove to be difficult. The *PYBCCP* gene product has 76% *AT* content, with approximately 15 stretches of *AAAAA* and six stretches of *TTTT* in its sequence. The use of Rosetta (DE3) pLysS *E. coli* strain that expresses the tRNAs for rare codons not highly used by *E. coli* did not prevent the truncation of the recombinant *P. yoelii* biotinoyl protein. Although some studies have shown that *E. coli* strains engineered to express the rare codons improve the quality of the recombinant plasmodial proteins (Baca and Hol, 2000). These truncations appeared to have occurred at the C-terminal region of the protein judging by the patterns obtained when using anti-GST antibody for detection. However, it is not known whether the truncation was as a result of errors in transcription of the recombinant gene or post-translational proteolysis of the protein. This question may be answered by analysis of the mRNA transcript of the recombinant gene in the expressing *E. coli* cells; though this was not within the scope of this study.

The focus of this study was to establish the presence of biotin in the recombinant proteins. There are no reports on enzymatic cleavage of the biotin moiety from the biotinylated protein, and studies have shown that biotinylated biotin carrier protein is quite resistant to proteolytic degradation (Solbiati *et al*., 2002). The presence of biotin on the recombinant protein was established in both GST-fusion and poly-His tag recombinant *P. yoelii* biotinoyl proteins using peroxidase-conjugated avidin. This suggests that the recombinant protein folds into a conformation that is recognised by the *E. coli* BirA.

This is in contrast to an earlier study done by (Thelen *et al*., 2001) on the expression of *A. thaliana* biotinoyl protein subunit of acetyl-CoA carboxylase. A remarkable increase in the biotinylation of the recombinant protein was observed after the medium was supplemented with external D-biotin. Thelen *et al.,* (2001) did not correlate the difference between *E. coli* and *A. thaliana* biotin binding motifs as the probable cause of the poor biotinylation of the recombinant *A. thaliana* biotin carboxyl carrier protein. The consensus motif in several organisms is MKM (Chapman-Smith and Cronan, 1999c). The rate of biotinylation by the *E. coli* BirA correlates to the composition of residues around the biotinylation motif (Lee *et al*., 2008). Replacing the residues around the MKM consensus motif in human biotinoyl protein with the *E. coli* sequence improved the activity of the mutant protein compared to the wild

type (Lee *et al.*, 2008). This observation may explain why expressing recombinant *P. yoelii* biotinoyl proteins in *E. coli* resulted in the biotinylation of the recombinant protein.

The specificity of the biotinylation of the recombinant *P. yoelii* biotinoyl proteins was confirmed when the *P. yoelii* copper transport protein (PyCTRNt) was not biotinylated. PyCTRNt lacked the biotin attachment motif (VEAMKM) and contains 14 lysine residues that could have been biotinylated if the biotinylation process was not specific. The observed biotinylation of the recombinant *P. yoelii* biotinoyl proteins may be further validated by expressing the *P. yoelii* biotinoyl protein in a BirA-deficient strain of *E. coli* (Chapman-Smith *et al.*, 1994). Inhibitors of biotin synthesis pathway in bacteria may also be useful tools in validating this observation. Anti-biotin antibody used as a second detecting agent also confirmed the result from avidin-peroxidase detection. However, the results were not included due to some non-specific detection of *E. coli* proteins by the anti-biotin antibody from mouse ascites fluid.

One interesting question raised by this study is: Does the rate at which the *E. coli* biotin biosynthesis and BirA match the rate of recombinant protein synthesis? Theoretically it is thought that IPTG and chloramphenicol reduce the transcription of the *E. coli* chromosomal genes (Balbás and Bólivar, 1990; Balbás *et al*., 1986). But it appeared that the *E. coli* biotin biosynthesis and BirA may have been active in the covalent attachment of biotin on the recombinant protein. The *E. coli* biotin operon contains five structural chromosomal genes that are involved in the synthesis of biotin; thus the synthesis of biotin in *E. coli* is a tightly regulated process (Chapman-Smith and Cronan, 1999a; Streaker and Beckett, 2006). The transcription of these genes are under control of intracellular biotin-5’-AMP, BirA and the biotin acceptor substrate (Chapman-Smith and Cronan, 1999a; Chapman-Smith *et al.*, 1999). Overproduction of BirA results in the repression of the biotin operon by BirA (a bifunctional enzyme). On the other hand, over production of biotinoyl protein results in the derepression of the biotin operon (Chapman-Smith and Cronan, 1999a; Reche, 2000). In this context *P. yoelii*-biotinoyl protein is one of the biotin acceptor molecules, the other being the *E. coli* biotinoyl protein as the only biotinylated *E. coli* protein (Chapman-Smith *et al*., 2001).

The over expression of the recombinant proteins may have had a direct influence on the biotin operon, therefore leading to the derepression of the operon and consequently biotinylation of the recombinant proteins. In order to be a molecular sensor of the biotin operon, the

recombinant biotinoyl proteins must have a structural conformation recognised by the BirA (Chapman-Smith and Cronan, 1999a; Chapman-Smith and Cronan, 1999c). This is because the process of biotinylation occurs post-translationally within the context of a proper folded protein domain (Chapman-Smith and Cronan, 1999c). Therefore the tertiary conformation of *P. yoelii* biotinoyl protein may be vital for the recognition of the biotin protein ligase. This suggests that the recombinant proteins may have been folded into a proper structured conformation prior to their transformation into inclusion bodies. The interaction between BirA and its biotin-dependent substrates have been well studied (Chapman-Smith *et al.*, 1999; Reche and Perham, 1999). The three dimensional structure of *P. yoelii* biotinoyl protein with regards to interaction with BirA will be discussed in detail in the Chapter 6.

Bacteria, plants and some fungi have the ability to synthesize biotin used for the modification of biotin-dependent enzymes in these organisms (Muller and Kappes, 2007). Yeasts such as *S. pombe* and *S. cerevisiae* do have the ability to transports biotin across their cell membrane from the surrounding medium. Biotin dependent enzymes depend on biotin protein ligase for activity (Knowles, 1989). A BLAST search of the *P. falciparum* genome and the other *Plasmodium* genomes using biotin synthase from bacteria and plants reveals that the parasite lacks the gene that codes for biotin synthesis. Most *Plasmodium* species encode two copies of biotin protein ligase, in contrast with other apicomplexa parasites such as *T. gondii*, *C. parvum* and *C. hominis*, which encode one copy (Muller and Kappes, 2007).

There is no empirical evidence suggesting biotin protein ligase activities in *Plasmodium*. One possible mechanism by which the *Plasmodium* parasites obtain biotin may be by importation from the host. A search of the *P. falciparum* genome (BLAST) as well as the other *Plasmodium* genomes using putative biotin ABC transporter from *Bartonella bacilliformis* (NCBI accession number YP_989450) detected ABC-like transport protein in *P. falciparum* (Plasmodb ID: PF13_0218) and in other *Plasmodium* species. ABC transporters belong to a family of the ATP-Binding Cassette (ABC) that uses the hydrolysis of ATP to energize the transport of a wide array of substrates, ranging from ions to macromolecules, across the membrane phospho-lipid bilayer (Holland and Blight, 1999). The transport of nutrients across *Plasmodium*-infected erythrocytes has been studied. Nutrients such as vitamins and amino acids are thought to permeate the red blood cell through some form of membrane localized transporters on either the red blood cell membrane or parasitophorous vacuole membrane (Kirk, 2001). The transport of biotin is yet to be explored in the *Plasmodium* parasite. The

only vitamin that the *Plasmodium* parasite is thought to transport from the vertebrate host is pantothenic acid (vitamin B_5), due to its absolute requirement as a precursor of coenzyme-A (Kirk, 2001). It would be interesting to investigate the hypothesis that *Plasmodium* parasites imports biotin from the host using radiolabelled biotin.

The presence of biotin on the recombinant *P. yoelii* protein could further be validated by methods such as MALDI-TOF and NMR, and by Edman's degradation. Producing antibodies against the recombinant protein may be an attractive approach towards immunoprecipitation of the native enzyme for activity assays. The inability of the cells to express soluble recombinant *P. yoelii* biotinoyl protein in large quantities meant that using denaturing immobilised-metal affinity chromatography was the option for obtaining a purified recombinant *P. yoelii* biotinoyl protein. The purified recombinant *P. yoelii* biotinoyl protein was re-natured by stepwise dialysis against decreasing concentrations of urea. This resulted in solubilisation of the protein, though some the recombinant *P. yoelii* biotinoyl protein re-precipitated during this process. During the course of this study using the purified and resolubilised *P. yoelii* biotinoyl protein, it was observed that cycles of freeze-thaw of the refolded protein resulted in precipitation. However, the protein remained soluble after several cycles of free-thaws when stored in 50% glycerol. Further studies on the recombinant *P. yoelii* biotinoyl protein may be required.

CHAPTER 6

PLASMODIUM YOELII ACETYL-COA CARBOXYLASE: SEQUENCE ANALYSIS, PREDICTION OF PROTEIN KINASE PHOSPHORYLATION SITES AND HOMOLOGY MODELLING STUDIES

6.0 Introduction

With numerous genome sequencing projects, large numbers of organisms such as *Plasmodium,* humans, yeast and *Arabidopsis* have their entire genome sequenced along with their proteome and published on several databases. Important information on the evolution of protein families can be deduced by comparative amino acid sequence studies. Based on the amino acid sequences, amino acid substitutions that affect shape and stability of a protein can be studied (Knudsen and Miyamoto, 2001). Data derived from comparative studies could reveal the structure, function and it evolutionary relationship with other known protein families in a tree diagram referred to as molecular phylogenetic tree. A section of this study involved comparative analysis of the published *P. yoelii* acetyl-CoA carboxylase sequence with orthologues from other *Plasmodium* species and homologues from other organisms. The sequence alignment data was used to identify likely modification sites on *P. yoelii* acetyl-CoA carboxylase that appeared to be highly conserved across the selected set of organisms.

The three dimensional (3D) structure of a protein is primarily determined by its amino acid sequence composition; and it provides important insights into the molecular basis of protein function (Schwede *et al*., 2000; Schwede *et al*., 2003). Progress has been made, over the years, towards sequencing the genome of several organisms. This has led to large amount published protein sequences (Schwede *et al*., 2003; Sigrist *et al*., 2002). By 2003, the SWISS-PROT™ and the TrEMBL™ data bases held about 850 000 protein sequence entries, while the Protein Data Bank (PDB) held about 20 000 experimentally-determined protein 3D structures (Schwede *et al*., 2003). This indicates that two crystal structures were resolved for every 85 proteins sequenced, despite the high level of progress made in X-ray crystallography and nuclear magnetic resonance (NMR) spectroscopy. These two methods of protein crystal structure resolution are time-consuming and success is not absolutely guaranteed (Kopp and Schwede, 2004; Schwede *et al*., 2003). The shortfall in resolving 3D crystal structures of proteins has led to a lack of information on numerous proteins with published amino acid sequences (Kopp and Schwede, 2004).

Computational methods have been developed to predict 3D structures of proteins in order to close the gap between published amino acid sequences and their corresponding 3D structures (Kopp and Schwede, 2004; Schwede *et al*., 2000; Schwede *et al*., 2003; Yang and Honig, 2000a; Yang and Honig, 2000b). These methods are able to generate the 3D structure of a protein *de novo* or based upon a template of an experimentally-resolved crystal structure (Kopp and Schwede, 2004; Schwede *et al*., 2000; Schwede *et al*., 2003; Yang and Honig, 2000b). The method of predicting the 3D conformation of a protein using an existing crystal structure template is called homology or comparative protein modelling (Kopp and Schwede, 2004; Schwede *et al*., 2003). The pre-existing 3D structure must share a level of homology with the protein to be modelled (Kopp and Schwede, 2004; Schwede *et al*., 2003).

The SWISS-MODEL™ server is one of the several protein structure prediction programmes available as a downloadable or a web-based programme (Kopp and Schwede, 2004; Schwede *et al*., 2003). The server is designed to work with a minimal input from the user, sometimes limiting the input to just the amino-acid sequence (Kopp and Schwede, 2004; Schwede *et al*., 2000; Schwede *et al*., 2003). This server has three modelling modes, namely the 'first approach' mode, the 'alignment' mode and the 'project' mode. The 'first approach' mode requires only an amino acid sequence as the input data. The server automatically selects a suitable template for the protein to be modelled (the target). This mode can only work if the template and the target share at least 25% sequence identity (Kopp and Schwede, 2004; Schwede *et al*., 2003). In the alignment mode, the user is required to identify a template with a PDP coordinate for the target. The template and the target are pre-aligned. The alignment output is submitted to the server in ClustalW™, FASTA or other formats specified by the server. The 3D model of the protein is therefore built on the template. The only difference between this mode and the first approach mode is that the user has control over the choice of template sequence. The Project mode requires the user to submit a manually optimized modelling request to the server. The modelling result is evaluated by the server to verify the accuracy of the predicted model. It has been shown that conserved regions do model better than unconserved regions (Kopp and Schwede, 2004; Schwede *et al*., 2000; Schwede *et al*., 2003; Yang and Honig, 2000a; Yang and Honig, 2000b). The SWISS-MODEL™ server uses several algorithms such as ANOLEA™ (Melo and Feytmans, 1998) and GROMOS™ (van Gunsteren and Billetter, 1996) to evaluate the quality of the predicted model. The predicted model is downloaded as a PDP file containing PDB coordinates. The model can be viewed with the SWISS-PDP viewer (spdbv). The spdpv programme contains several parameters

such as energy minimization algorithms that allow the user to improve the accuracy of the model. This is because modelling algorithms introduce errors into the structure resulting in deviations in the geometry of the protein structure (Kopp and Schwede, 2004; Schwede *et al*., 2003). The root mean square deviation of the predicted 3D structure from the template is deduced from the spdv programme and expressed in Å. The refined models can be validated using the ProCheck™ algorithm found on the PDP web site for advanced deposition input tool (ADIT, http://deposit.pdb.org/adit).

Results in Chapter 5 showed that recombinant expression of the biotinoyl domain of *P. yoelii* acetyl-CoA carboxylase led to *in vivo* biotinylation of the recombinant protein by the *E. coli* host with or without an external supply of D-biotin in the culture. This suggested that the *E. coli* biotin protein ligase (Chapman-Smith *et al*., 2001; Reche, 2000) recognizes the recombinant protein as a substrate for co-translational modification (Chapman-Smith and Cronan, 1999c; Chapman-Smith *et al*., 1999). To relate this to the conformation of the recombinant protein, homology modelling of the recombinant protein was carried out with the SWISS-MODEL™ server using the *E. coli* biotinoyl domain (PDB ID: 1bdo) as the template (Athappilly and Hendrickson, 1995). The polyketide, soraphen A (Figure 6.1) has been shown to inhibit acetyl-CoA carboxylase activity by binding to 19 residues on the biotin carboxylase domain (Beckers *et al*., 2007; Shen *et al*., 2004; Weatherly *et al*., 2004). The potential of soraphen A as an inhibitor of *P. yoelii* acetyl-CoA carboxylase was examined. The 3D model of *P. yoelii* biotin carboxylase domain was modelled using *S. cerevisiae* (PDB ID: 1w93) as a template. Positive control 3D model of the *E. coli* biotinoyl subunit and the *S. cerevisiae* biotin carboxylase domain were generated using their coordinates (1bdo and 1w93) as templates. For the sake of convenience, the predicted *P. yoelii* biotinoyl model and the *E. coli* positive control model will be referred to as *Py*BCCP-model and *Ec*BCCP+, respectively. The predicted biotin carboxylase models for *P. yoelii, P. falciparum, H. sapiens* and the *S. cerevisiae* positive control will be referred to as *Py*BC-model, *Pf*BC-model, *Hs*BC-model and *Sc*BC+, respectively.

6.2 Results

6.2.1 Identification of conserved sequence motifs using ClustalW™ analysis

The amino acid sequence coding for the acetyl-CoA carboxylase 1 precursor in *P. yoelii yoelii* strain 17XNL and its orthologues from *P. falciparum, P. vivax, P. berghei, P. chabaudi* and *P. knowlesi w*ere retrieved from NCBI and/or Plasmodb database (www.plasmodb.org). These

sequences were analysed with the ClustalW™, ProSiteScan™ (Proscan™) and InterProScan™ algorithms for alignment and identification of predicted protein domains in each polypeptide. The results obtained were compared to published acetyl-CoA carboxylase amino-acid sequences from several organisms. Table 6.1 is the list of the amino-acid sequences of acetyl-CoA carboxylase from four *Plasmodium* species and eight eukaryotic organisms ranging from unicellular photosynthetic organism (*O. lucimarinus*) to humans. *P. berghei* and *chabaudi* were excluded from this study due to incomplete amino acid sequences.

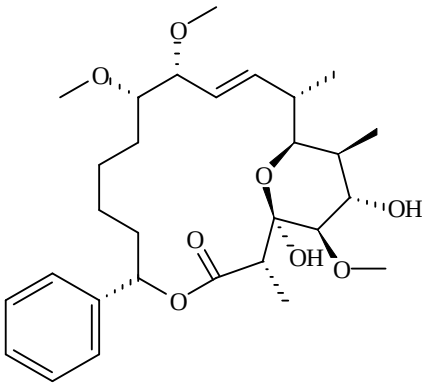

Figure 6.1 Structure of soraphen A (Shen *et al*., 2004).

In four orthologues of *Plasmodium* acetyl-CoA carboxylase, the domain closest to the N-terminus is the biotin carboxylase domain, followed by the biotin carboxyl carrier protein and the carboxyl transferase domains with two (N-terminal and C-terminal) sub-domains. The Proscan™ motif and sequence domain prediction programme showed that *P. berghei* (XP_679544) was wrongly annotated in the Plasmodb and NCBI databases as biotin carboxylase subunit instead of as a carboxyl transferase domain. *P. berghei* (PB000685.01.0) and *P. chabaudi* (XP_743705) hypothetical proteins were identified to be fragments containing the biotin carboxylase and the biotin carboxyl carrier protein domains, respectively. Using the NCBI BLAST, it was observed that *P. yoelii* acetyl-CoA carboxylase shares 45% identity and 68% similar in amino acid sequence with *Oestreococcus lucimarinus* predicted protein (with acetyl-CoA carboxylase sequence motifs). Proscan™ analysis revealed that all organisms listed in Table 6.1 all have the same array of sequence motifs with the same order. This confirms that *P. yoelii* and other *Plasmodium* species express the multi-enzyme-domain type acetyl-CoA carboxylase because the four domains form part of a long

polypeptide structure with a single ORF. This is in contrast to the multi-enzyme-subunit (complex) acetyl-CoA carboxylase consisting of four separate enzymes found in *E. coli* and plastids of some dicotyledonous green plants (Cronan and Waldrop, 2002; Sasaki and Nagano, 2004; Zhang *et al*., 2004). However some plants encode the multi-enzyme-domain type acetyl-CoA carboxylase targeted to their chloroplast, in addition to the multi-enzyme-subunit (complex) type in their cytoplasm (Sasaki and Nagano, 2004; Zhang *et al*., 2004).

Table 6.1 Acetyl-CoA carboxylase from the respective organisms used for bioinformatics

Organism	NCBI or Plasmodb access number	Sequence length	Number of predicted domains
P. yoelii	XP_729490	2911	4
P. falciparum	XP_001348838	3336	4
P. vivax	XP_001615692	3061	4
P. knowlesi	PKH_123560[a]	2921	4
H. sapiens-1	NP_942131	2346	4
H. sapiens-2	ABF48723	2458	4
M. musculus-1	AAS13686	2354	4
M. musculus-2	NP_579938	2448	4
A. thaliana-1	AAG40563	2254	4
A. thaliana-2	AAF18638	2257	4
O. lucimarinus[p]	XP_001415874	2012	4
S. cerevisiae	NP_014413	2233	4
G .gallus	NP_990836	2324	4
T. brucei	XP_847540	2181	4
T. gondii	AAF04493	2564	4
D. melanogaster	NP_610342	2323	4
C. parvum	XP_667901	2725	4

[a] Plasmodb access number,
[p] predicted protein (not annotated),

6.2.2 Phylogenetic analysis of *P. yoelii* acetyl-CoA carboxylase

A molecular phylogenetic tree was constructed from acetyl-CoA carboxylase sequences listed in Table 6.1using the CLC Free Workbench™ software. Aligned sequences were used to construct the phylogenetic tree (Figure 6.2) with the option of the neighbour joining-algorithm and 1000 bootstrap analysis (replicates); thus enabling the construction of a reliable phylogenetic tree (Brinkman and Weissig, 2001; Felsenstein, 1985). The bootstrap value for each node was attached as a measure of confidence for each branch. Thus 1000 bootstrap value indicated a perfect cluster. The phylogenetic analysis showed two major clusters shown by the arrows on the diagram. Cluster 1 (arrow 1) represents plastid-encoded organisms including *O. lucimarinus* (a unicellular photosynthetic organism), *T. gondii*, *C. parvum* and

Plasmodium. *Plasmodium* acetyl-CoA carboxylase sequences clustered to a single orthologue group with a perfect cluster (1000 bootstrap value). *P. yoelii* acetyl-CoA carboxylase clustered with *P. falciparum* with slightly lower bootstrap value (675), which is probably due to multiple asparagine repeats in the *falciparum* sequence. *T. gondii* and *O. lucimarinus* both formed a cluster with a bootstrap value of 633.

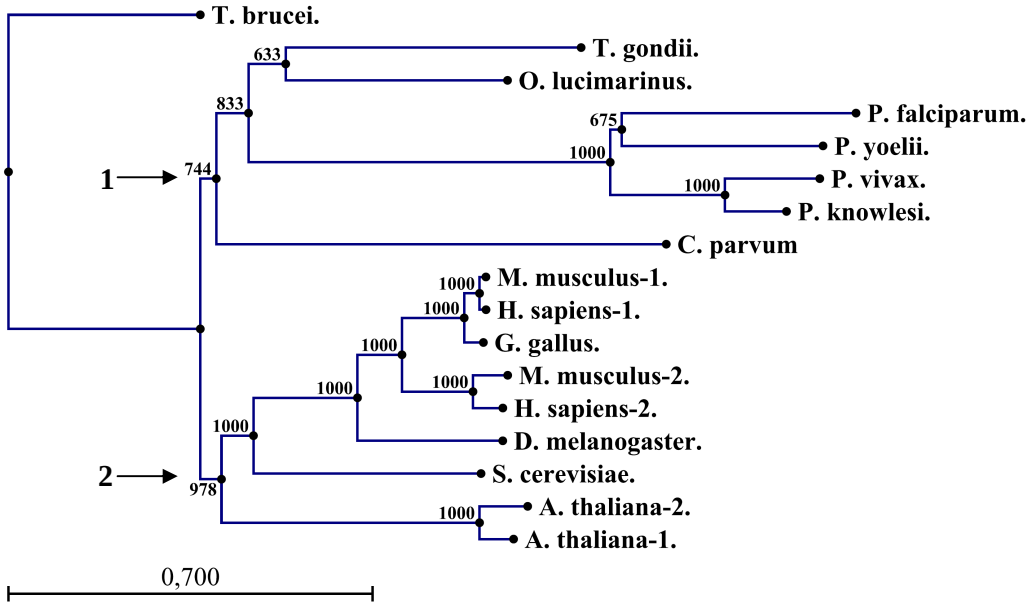

Figure 6.2 Phylogenetic tree of 17 eukaryotic acetyl-CoA carboxylase sequences. A Neighbour joining tree was built from acetyl-CoA carboxylase amino acid sequences aligned by the ClustalW™ alignment algorithm in CLC Free Workbench™ software. The numbers indicates bootstrap (replicates) values corresponding to each branch. The scale bar represents 0.7 mutational changes per amino acid residue. The access number for each sequence examined is listed on Table 6.1. Arrows 1 and 2 show two major clusters corresponding to apicomplexans and other eukaryotes, respectively.

Acetyl-CoA carboxylases sequences from other organisms formed a single cluster with a bootstrap score of 978 in cluster 2 (arrow 2). *T. brucei* acetyl-CoA carboxylase formed an outlier. By and large, the phylogenetic study depicted that *Plasmodium* acetyl-CoA carboxylase is closely related to *T. gondii*, *C. parvum* and *O. lucimarinus*, but fairly divergent from the other organisms examined. There was no explanation on why *T. brucei* did not cluster in either group.

6.2.3 Sequence length variation in regions of the selected acetyl-CoA carboxylase sequences

To examine how much the length of the amino acid sequence in the multi-enzyme-domain type acetyl-CoA carboxylase varies from one organism to another, the Proscan™ tool was used to assemble the lengths of the sequence in each region of the 17 acetyl-CoA carboxylases listed in Table 6.1. Figure 6.3 illustrates the comparison of the lengths of amino-acid sequence of the regions of the acetyl-CoA carboxylase enzymes examined. The regions of the polypeptide with no predicted functional sequence domains are I, II, III and IV as depicted in Figure 6.3. Generally, the results showed that the total length of the polypeptide chain changes from one organism to another. Regions I and IV showed the most variation in sequence length with approximately ±2 residues per 3-mer (three monomeric amino acid unit) and ±2 residues per 7-mer respectively. The variation in length of the region III was ±1 amino acid per 5-mer. The sequence length of region II varied by ±1 amino acid per 26-mer. The biotin carboxylase domain varied with ±2 amino acid residues per 29-mer while the carboxyl transferase domain varied the most amongst the predicted functional sequence domains with ±1 amino acid residue per 11-mer. The biotin carboxyl carrier protein domain is the most conserved sequence length with ±1 amino acid per 28-mer. The most significant point of note of this result is the consistent sequence length of the biotin carboxyl carrier protein domain with 73 amino acid residues in all *Plasmodium* species and 67 amino acid residues in the other organisms. This perhaps suggests high degree of evolutionary conservation in sequence length and structure of the biotin carboxyl carrier protein, thus indicating the importance of this domain to the structure and function of acetyl-CoA carboxylase.

6.2.4 Assignment of phosphorylation sites in *P. yoelii* acetyl-CoA carboxylase using predictive algorithms

Using ClustalW™ alignment (Figure 6.4*A*), the positions of possible phosphorylation sites that appeared to be highly conserved across all the organisms and *Plasmodium* species were mapped using the Proscan™ motif prediction tool. This program is similar to the InterProScan™ tool, except that it displays the amino acid sequence corresponding to a signature sequence motif as well as the confidence level for each identified motif on a polypeptide. The basis of this study hinges on the premise that important amino acid sequence motifs involved in the functioning or structural architecture of a protein are often maintained regardless of evolutionary divergence.

	I	Biotin carboxylase	II	Biotin carboxyl carrier protein	III	Carboxyl transferase	IV
Organism	**Length**	**Length**	**Length**	**Length**	**Length**	**Length**	**Length**
P. yoelii	418	530	140	73	1131	583	35
P. falciparum	467	643	155	73	1272	609	118
P. vivax	447	543	139	73	1214	530	117
P. knowlesi	407	553	139	73	1105	529	117
H. sapiens-1	116	502	134	67	880	497	152
H. sapiens-2	258	502	134	67	848	497	153
M. musculus-1	115	502	134	67	880	497	161
M. musculus-2	248	503	134	67	848	497	153
A. thaliana-1	35	508	134	67	788	579	144
A. thaliana-2	36	508	135	67	792	579	144
O. lucimarinus[pp]	-	485	136	67	742	484	118
S. cerevisiae	57	510	134	67	836	491	132
G. gallus	116	502	134	67	857	497	135
T. brucei	28	497	138	67	813	527	113
T. gondii	338	497	138	67	953	500	74
D. melanogaster	99	497	133	67	873	499	155
C. parvum	25	491	147	67	1402	503	95

Figure 6.3 Quantitative evaluation of the variation in the number amino acid residue of 17 acetyl-CoA carboxylase sequences. Full length or fragments of acetyl-CoA carboxylases were scanned by web-based Proscan™. The programme identified the three domains and the number of amino acid residues corresponding to each of the three domains. The number of amino acid residues corresponding to all the regions of the enzyme was subsequently deduced based on the Scan ProSite data. [pp] is partially predicted protein.

Figure 6.4*B* shows a schematic representation of predicted enzyme modification sites on *P. yoelii* acetyl-CoA carboxylase based upon the ClustalW™ multiple sequence alignment data combined with the Proscan™ analysis.

The results predicted five potential phosphorylation sites; one (P1) on the biotin carboxylase domain and four (P1 to P5) on the carboxyl transferase domain (Figure 6.4). The predicted protein kinase C (PKC) phosphorylation site (P1) on the biotin carboxylase domain appeared to be conserved across the 10 acetyl-CoA carboxylase sequences. The PKC phosphorylation site has a consensus sequence SL/IK in *Plasmodium* and SIR in the other organisms looked at. The putative phosphorylation serine (S) residue and a C-terminal tryptophan (W) are conserved across all the acetyl-CoA carboxylase analysed (P1).

The first phosphorylation site (P2) on the carboxyl transferase domain is predicted to be a PKC phosphorylation site with the consensus sequence TSK. This site is not present in other organisms, but the phospho-serine residue is highly conserved. P3 is a conserved predicted PKC phosphorylation site with the sequence, TGR, in *Plasmodium*, the sequence, TCR, in mammals, and the sequence, SGR, in *A. thaliana*. This suggests that threonine is a likely phosphorylation residue in all the examined organisms at this site, except *A. thaliana*, which has a serine as the possible phosphorylation residue. *P. yoelii* and other *Plasmodium* species acetyl-CoA carboxylases may be phosphorylated at P4 by either cAMP-dependent protein kinase (PKA) or cGMP-dependent protein kinase (PKG) with the KGS sequence 100% conserved in *Plasmodium*. At P5 is a potential PKC site with TGR consensus sequence synonymous with P3. This site is not present in the human and mouse α-acetyl-CoA carboxylases. This site also encodes a phosphate-binding consensus sequence GXGXXG (Kleiger and Eisenberg, 2002; Kleiger *et al.*, 2002) as GRGKLG, on the C-terminal end preceding the phosphorylation site.

The Proscan™ analysis data on protein kinase phosphorylation sites was compared to the NetPhos 2.0™ (Blom *et al.*, 1999) prediction algorithm for eukaryotic protein kinase phosphorylation site. Using ClustalW™-aligned sequences, conserved positions of possible protein kinase sites were identified (Figure 6.5). The programme indicates the possible phosphorylation residue flanked by four amino acid residues, but does not indicate the possible phosphorylating enzyme. The NetPhos 2.0™ programme predicted a highly conserved protein kinase site (N1) on the biotin carboxylase, synonymous with the P1 site

generated by Proscan™ analysis in Figure 6.4. The phospho-serine residue is highly conserved and flanked by conserved sequences, with a 100% conserved lysine and tryptophan at positions –4 and +4 respectively (the phospho-serine residue is at position 0). The serine residue at position +5 in *H. sapiens* 1 and *M. musculus* is most favoured with a score of 99.7%.

The only modification site that appeared to be conserved on the BCCP domain is the biotin attachment motif. The N-myristoylation sites predicted to be conserved by the Proscan™ tool does not precede the N-terminal methionine, and therefore ingnored. N-glycosylation sites identified by the Proscan™ analysis were not conserved and were not included in the results.

A threonine phosphorylation site at N2 was identified by the programme on the carboxyl transferase domain, which appeared to be highly conserved. Except that the phospho-threonine residue is not at a conserved position across the sequences examined. The phospho-threonine residue is flanked by a 100% conserved lysine at position – 4 and + 4 (the phospho-serine residue is at position 0), in *Plasmodium*. A phospho-serine protein kinase site that was only conserved in *Plasmodium* was identified by NetPhos 2.0™ algorithm. This site has a consensus sequence KTAQ**S**IEDF (phospho-serine in bold), with a 100% conserved lysine and phenylalanine residues at – 4 and + 4 positions, respectively.

6.2.5 Homology modelling of the biotinoyl domain of *P. yoelii* acetyl-CoA carboxylase

Of the 347 amino-acid sequence of the *P. yoelii* recombinant biotin carboxyl carrier protein (Chapter 5) submitted to the SWISS-MODEL™ sever in an alignment with 1bdo (template), 80 residues corresponding to the region with significant identity (20%) with the template (1bdo) was modelled by the server. Eighty residues on the target were modelled because the template is made up of 80 amino acid residues, which are closely related to the 80 amino acid resides on the target model. The total energy of *Py*BCCP-model before energy minimization was –163.072 kJ/mol, which was 5.5% of the total energy of *Ec*BCCP+ (–2866.027 kJ/mol). The final energy of *Py*BCCP-model reduced to –937.229 kJ/mol; resulting in about 82.6% improvement on the packaging quality (Kopp and Schwede, 2004; Melo and Feytmans, 1998) after energy minimization. The positive control improved by 3.2% (from –2866.027 kJ/mol to –2959.852 kJ/mol).

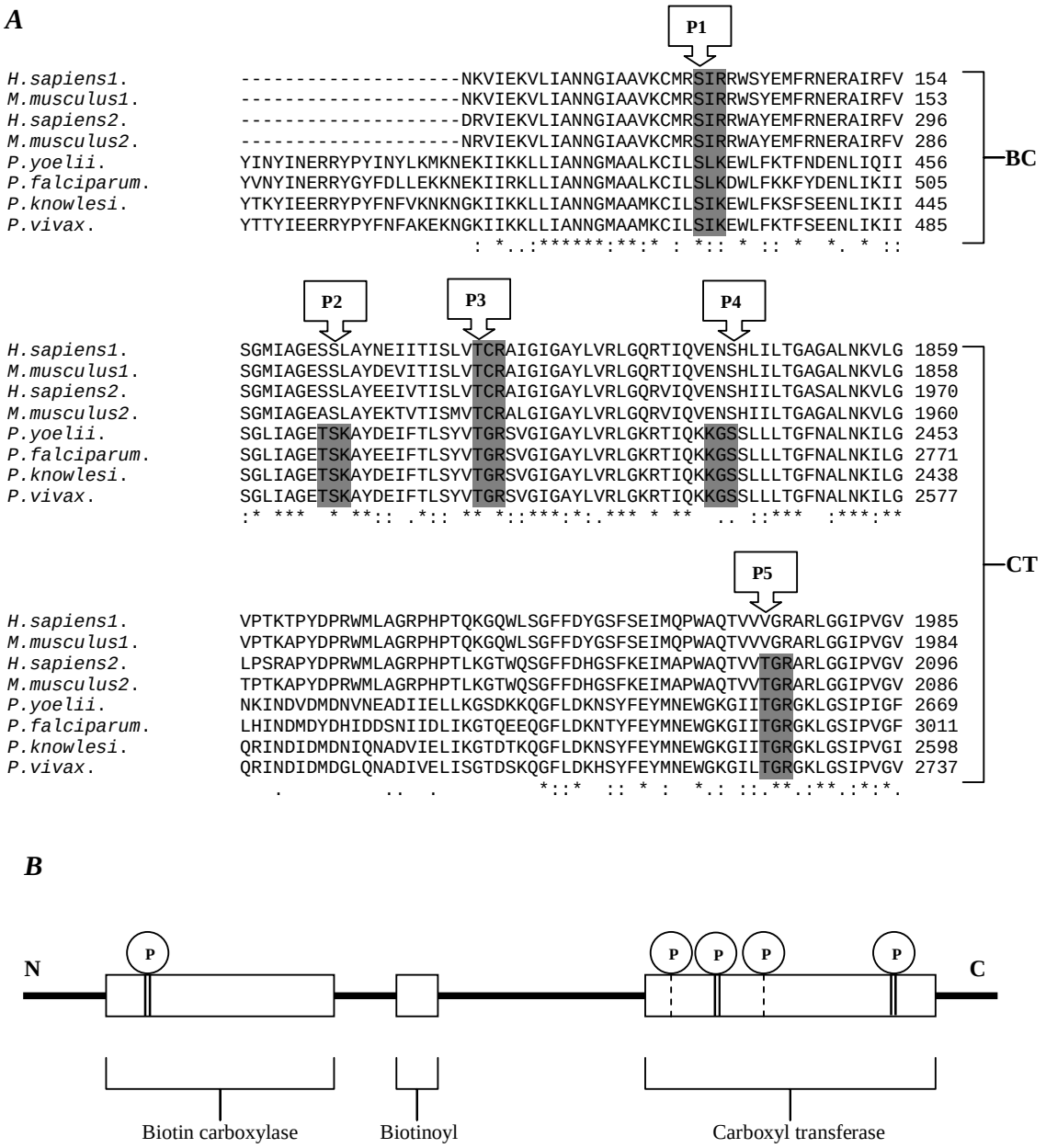

Figure 6.4 Prosite™ prediction of protein kinase phosphorylation sites on enzyme domains of mammals and *Plasmodium* acetyl-CoA carboxylases. (*A*) Alignment produced by the ClustalW™ algorithm showing the predicted sites residues (highlighted) in the biotin carboxylase (BC) and the carboxyl transferase (CT) domains. (*B*). Cartoon structure of the multi-domain acetyl-CoA carboxylase illustrating the positions of the predicted phosphorylation sites. Double line indicates position fully or partially conserved across all organisms examined, broken line indicates position conserved only in *Plasmodium*.* indicates 100% conserved residue.

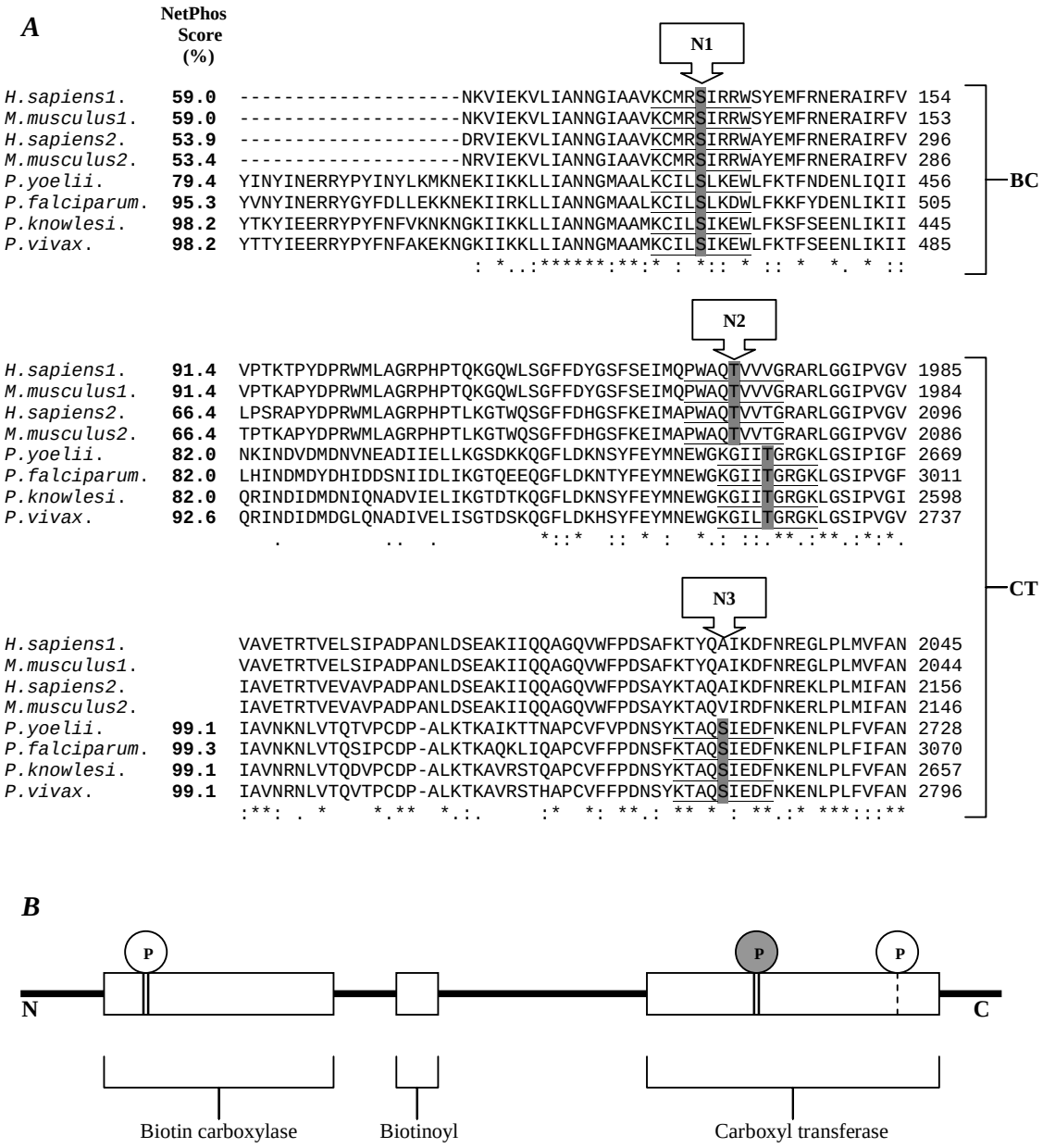

Figure 6.5 NetPhos 2.0™ prediction of protein kinase phosphorylation sites on enzyme domains of mammals and *Plasmodium* acetyl-CoA carboxylases. (*A*) Alignment produced by ClustalW™ algorithm showing phosphorylated residues (highlighted) in the biotin carboxylase (BC) and the carboxyl transferase (CT) domains. The residue between the +4 and –4 positions of the phosphorylated residues are underlined. The numbers in bold represents the probability score (%). (*B*). Cartoon structure of the multi-domain acetyl-CoA carboxylase illustrating the positions of the predicted phosphorylation sites. Broken and double lines indicate a position 100% conserved in *Plasmodium* and across all organisms, respectively. Open and closed circles indicate a serine and a threonine protein kinase sites, respectively. * indicates 100% conserved residue.

The Ramachandran analysis showed that 83.3% of non-glycine and non-proline residues in *Py*BCCP-model have conformational angles (ϕ and ψ) in the most favoured regions of the Ramachandran plot (Figure 6.6). This is comparable to *Ec*BCCP+ with 86.6%. 2.8% of the residues in *Py*BCCP-model fall in the disallowed region of the Ramachandran plot, while no residues in *Ec*-BCCP+ falls in the disallowed region.

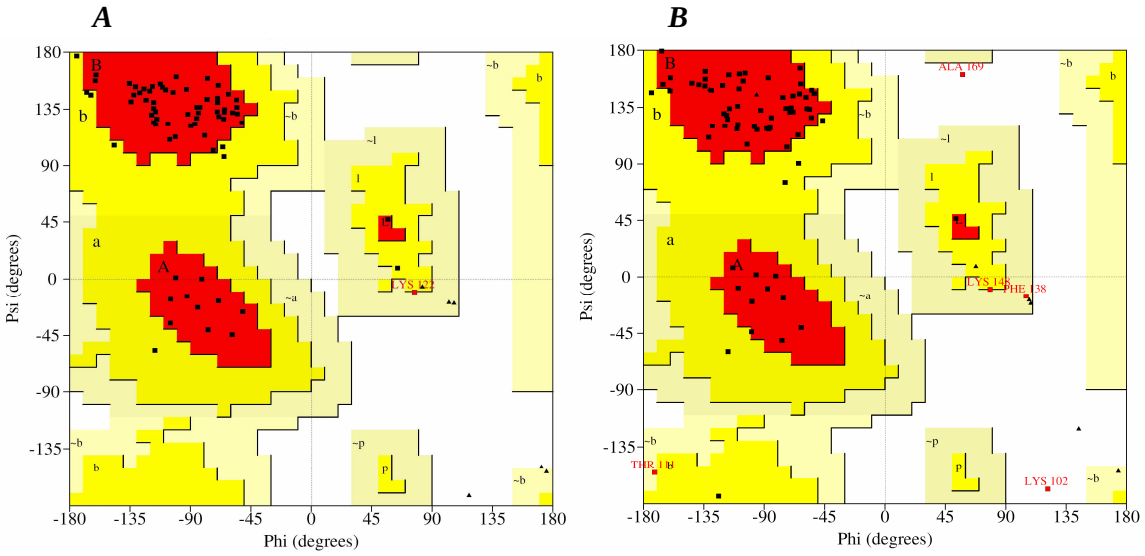

Figure 6.6 Ramachandran analyses of the homology modelling of the biotinoyl proteins by ProCheck™. The Ramachandran plots were derived after energy minimization of (*A*) *Ec*BCCP+ (*B*) *Py*BCCP-model. The different coloured regions indicate "most favoured" (red), "additionally allowed' (yellow), "generously allowed" (light yellow) and "disallowed' (white).

The *Py*BCCP-model is made of seven β-sheets, one turn and five loops, while *Ec*BCCP+ has an extra β-sheet (eight β-sheet), six loops and one turn. The predicted secondary structure can be classified as a β-sheet because it lacked α-helix secondary structures (Figure 6.7). *Ec*BCCP+ has the "protruding thumb" structure connecting β_2 to β_3; this is consistent with the experimentally resolved structure (Athappilly and Hendrickson, 1995) as well as previously determined computer models of the *E. coli* biotinoyl protein (Chapman-Smith *et al*., 2001; Cronan, 2001; Reche *et al*., 1998; Reche and Perham, 1999; Streaker and Beckett, 2006). A similar structure is also present in *Py*BCCP-model. Figure 6.8 shows that the β-sheets in *Py*BCCP-model and *Ec*BCCP+ are completely superimposable, except the extra β-sheet on the *Ec*BCCP+.

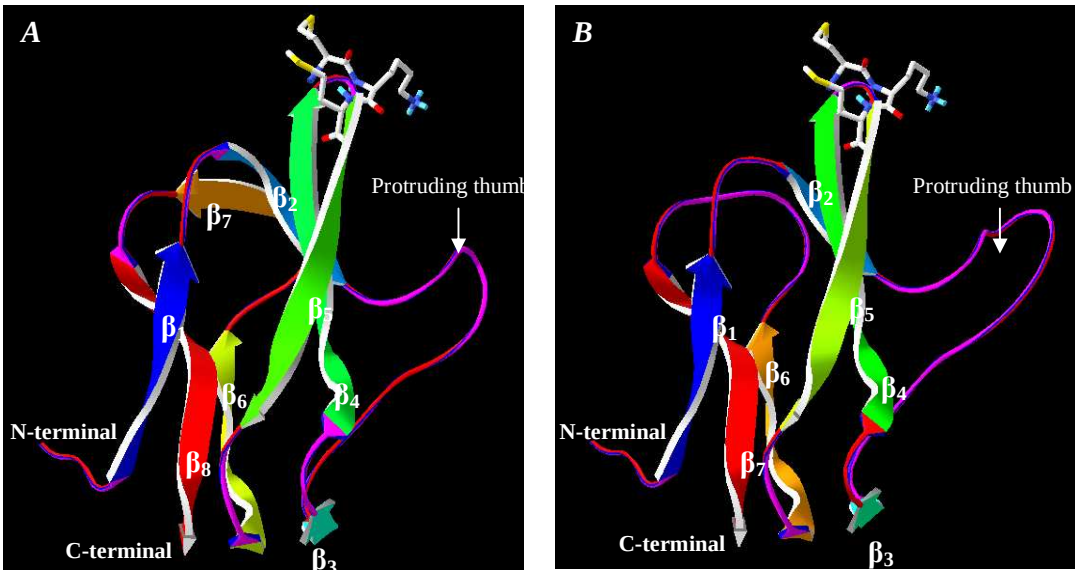

Figure 6.7 Predicted three dimensional molecular models of biotinoyl protein. (*A*) *Ec*BCCP+ and (*B*) *Py*BCCP-model. The structure is coloured according to secondary structure succession using the spdbv programme. Blue secondary structure is at the N-terminus and red secondary structure is at the C-terminus of the protein. The residues represent the conserved MKM biotinylation motifs situated at $\beta_4 \rightarrow \beta_5$ turn.

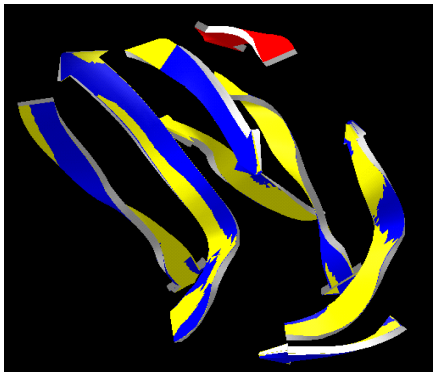

Figure 6.8 Superimposed image *Py*BCCP-model and *Ec*BCCP+ β-sheets. The β-sheets with yellow (*Ec*BCCP+) and blue (*Py*BCCP-model) coloured β-sheets are completely superimposed, while the red β-sheet is the *Ec*BCCP+ extra sheet

The *Py*BCCP-model was superimposed (Figure 6.9) on *Ec*BCCP+, and the root mean square deviation of the α-carbon was deduced to be 0.22 Å. Figure 6.9 shows that the two models are

virtually super-imposable. Although the "protruding thumb" loop structure connecting β_2 to β_3 of the *Py*BCCP-model protrudes out side the molecular surface of the positive control 3D model, as shown (arrow) in Figure 6.9*A*.

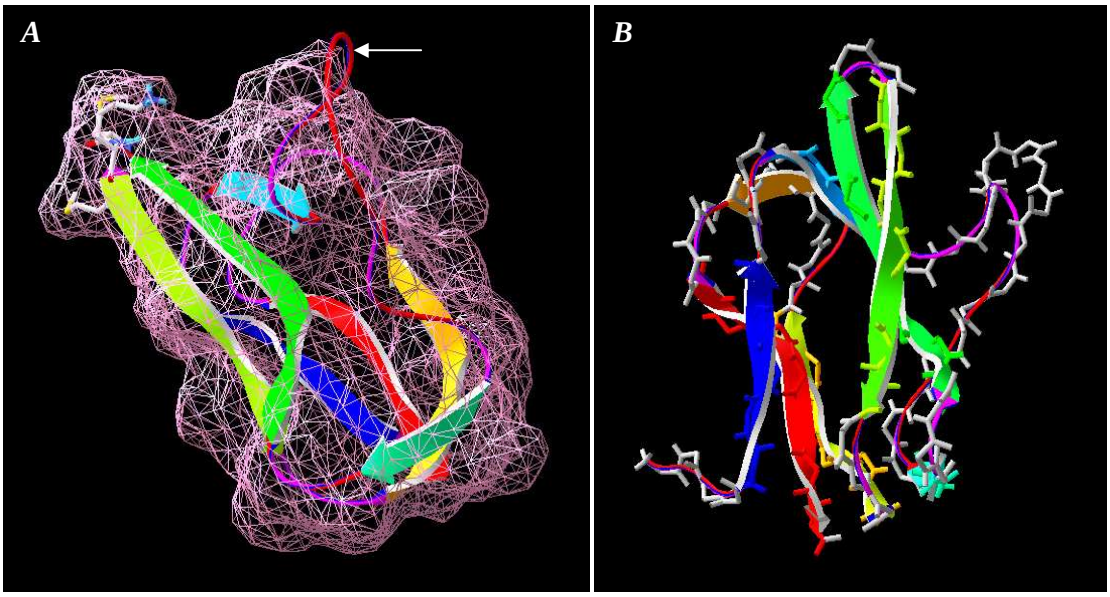

Figure 6.9 Superimposed image of *E. coli* biotinoyl protein positive control model and *P. yoelii* biotinoyl domain model. (*A*) Ribbon structure of *Py*BCCP-model superimposed in the molecular surface map of *Ec*BCCP+. (*B*) Ribbon structure of *Ec*BCCP+ superimposed with the backbone strcurure of *Py*BCCP-model.

The *E. coli* biotin-binding motif is identical to the *Plasmodium* acetyl-CoA carboxylase biotin-binding motif with a consensus sequence, VEAMKM. The lysine residue is the biotinoyl lysine (Beckett *et al*., 1999; Blanchard *et al*., 1999a; Chapman-Smith *et al*., 1999; Cronan, 2002). Studies have shown that the *E. coli* biotin protein ligase interacts with the glutamic acid residue (Glu^{115}) within the consensus sequence, as well as Glu^{147} (Chapman-Smith *et al*., 1999; Chapman-Smith *et al*., 2001; Polyak *et al*., 2001; Solbiati *et al*., 2002; Streaker and Beckett, 2006). In *P. yoelii*, Lys^{1152} is at the equivalent position of the *E. coli* Glu^{147}. Figure 6.10 shows that the side chain of Glu^{147} sticks out of the surface of *Ec*BCCP+ (Figure 6.10*A*), with a similar orientation to Lys^{1152} in the *Py*BCCP-model (Figure 6.10*B*). However Glu^{115} as well its equivalent in the *Py*BCCP-model is buried inside the structure. The consensus biotinylation motif MKM forms a knob-like structure on the molecular surface

of both predicted biotinoyl 3D structures. This is consistent with previous studies on the orientation of the MKM motif with respect to the whole molecule (Cronan, 2001; Reche and Perham, 1999; Solbiati *et al*., 2002; Yao *et al*., 1999). The VEAMKM and E^{115}/K^{1152} residues are super-imposable (Figure 6.11) with a root mean square deviation (between *Py*BCCP-model and *Ec*BCCP+) of 0.03 Å and 0.31 Å of equivalent α-carbon atoms and equivalent side chains, respectively.

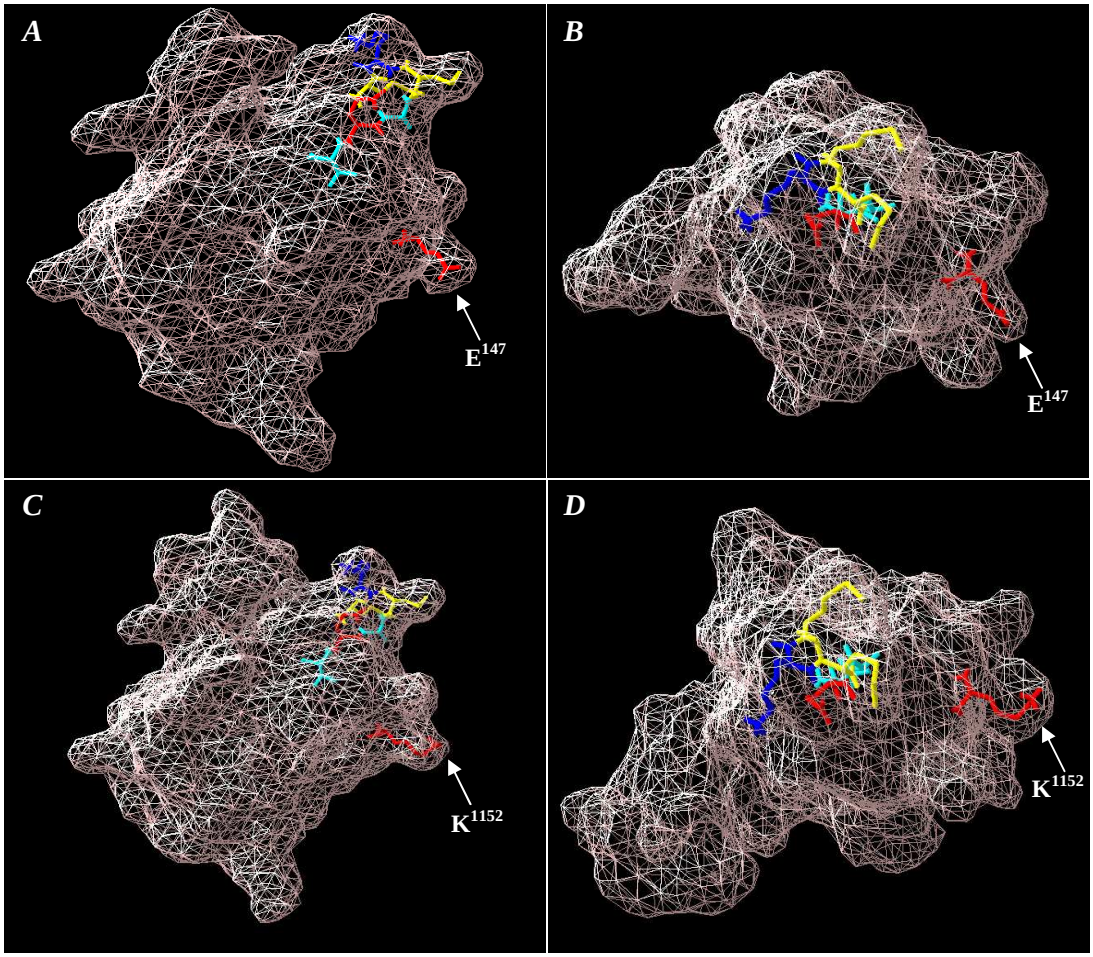

Figure 6.10 Position of the biotinylation motif with respect to the molecular surface of the biotinoyl protein models. (*A* and *B*) *Ec*BCCP+ and (*C* and *D*) *Py*BCCP-model. The backbone and side chain structures of the amino-acid residues are coloured green. *A* and *C* are in a similar orientation. *B* and *D* are in a similar orientation. The selected residues are coloured as follows: Val and Ala (cyan), Glu and Lys^{1152} (red), Met (yellow), biotinyl-Lys (blue).

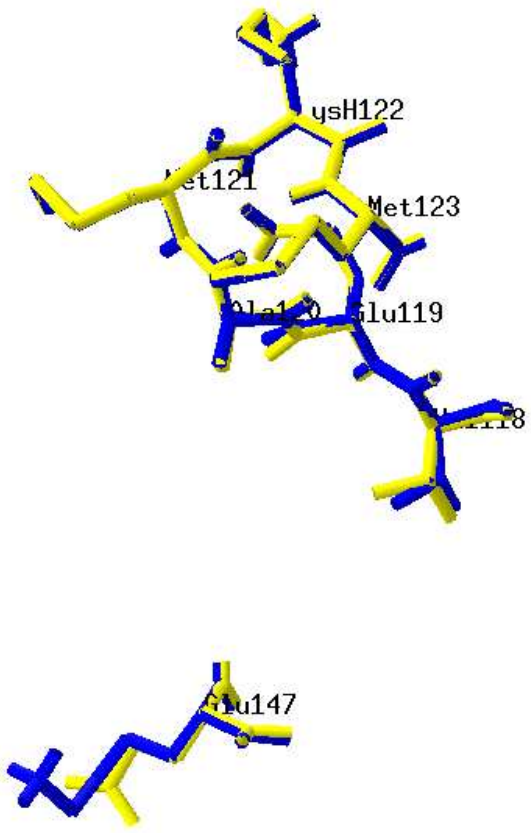

Figure 6.11 Superimposed image of the *E. coli* and the *P. yoelii* VEAMKM biotinylation motif sequence residues. The residues were coloured by selection (*Ec*BCCP+ residues are yellow; *P. yoelii* residues are blue) using the spdbv programme. The *E. coli* residues are labelled.

6.2.6 Homology modelling of mutant forms of the biotinoyl domain of *P. yoelii* acetyl-CoA carboxylase

The models obtained by the homology modelling using the SWISS-MODEL™ server were verified by carrying out a comparative modelling with modified *P. yoelii* biotinoyl sequence (Figure 6.12). We deliberately made adjustments to the amino acid sequence on the target to verify the models. The sequence was modified by deletion as well as by insertion of glycine residue(s) at positions within or around the VEAMKM biotin-binding motif. Glycine was chosen because it is not charged and lacks a side chain residue. The modified sequence was aligned with the *E. coli* biotinoyl sequence (PDP ID: 1bdo) and submitted to the SWISS-MODEL™ server for homology modelling. The mutant models generated from the modified sequences will be referred to as *Py*BCCP-mut1 and *Py*BCCP-mut2. These correspond to

M1127G and M1129G double mutation (Figure 6.12 *A*) and K1128G single mutation (Figure 6.12 *B*), respectively.

A

```
TEDSLNREDIAIKSENNINDISLNGKMKRAHIFDIIFQNVKYKFKGYNTGEDLYKLNIND
QEIEILAKYDKENNKIFASFHNQTYIYTCIEDSLGTHMNLGKDNVFIPVITNPYHLISNT
NGKIVKYLIKDGEKINKFDDYIEVEAGKGIMTFKSTETGILKHKMSEGAMIKIGDLLGVI
EKEKDNQNYQNDDNNNKIIDFIGHLNLSNKNAYELNGTFVPDLAEESHNNEVCCKNIEKE
KMENLRKIEDPKNNKIYPTKHTNRNSQVNTTNESVSVQDIKTENMKKDESQFCTEDKQIQ
NNQVNRRNKLFLKKNNGKNNKNNMFRLFSQKNDNDSKIIDSNIESNSRD
```

B

```
TEDSLNREDIAIKSENNINDISLNGKMKRAHIFDIIFQNVKYKFKGYNTGEDLYKLNIND
QEIEILAKYDKENNKIFASFHNQTYIYTCIEDSLGTHMNLGKDNVFIPVITNPYHLISNT
NGKIVKYLIKDGEKINKFDDYIEVEAMGMIMTFKSTETGILKHKMSEGAMIKIGDLLGV
IEKEKDNQNYQNDDNNNKIIDFIGHLNLSNKNAYELNGTFVPDLAEESHNNEVCCKNIEK
EKMENLRKIEDPKNNKIYPTKHTNRNSQVNTTNESVSVQDIKTENMKKDESQFCTEDKQI
QNNQVNRRNKLFLKKNNGKNNKNNMFRLFSQKNDNDSKIIDSNIESNSRD
```

Figure 6.12 Modified amino acid sequences used to generate the mutant models. (*A*) Sequence used to produce *Py*BCCP-mut1. (*B*) Sequence used to produce *Py*BCCP-mut2. The mutated residues (in red) are shown.

These alterations in the amino acid sequence of the biotinoyl domain of *P. yoelii* acetyl-CoA carboxylase severely or slightly altered the alignment with the *E. coli* biotinoyl protein (1bdo). The total energy after energy minimisation by GROMOS was 14 991 kJ/mol and −963 kJ/mol for *Py*BCCP-mut1 and *Py*BCCP-mut2, respectively. The quality of *Py*BCCP-mut1 was poor due to the severe perturbation on the sequence alignment. Figure 6.13 shows the predicted secondary structure prediction of the residues spanning the VEAMKM motif of the mutant models. The overall predicted 3D structure (Figures 6.14 *A* and *B*) of *Py*BCCP-mut1 cannot be superimposed on *Ec*BCCP+, while PyBCCP-mut2 can be super imposed with *Ec*BCCP+. This shows that the modifications resulted in erroneous prediction of the position of the biotinyl lysine using the *E. coli* biotinoyl protein (1bdo) as a template for alignment and for secondary structure prediction. The root mean square deviation of the mutant models and *Ec*BCCP+ were 12.5 Å (for 26 α-carbons) and 0.8 Å (for 75 α-carbons) for *Py*BCCP-mut1 and *Py*BCCP-mut2, The VEAMKM and the K^{1152} backbone structure of the mutant models

also deviated from the *Ec*BCCP+ with root mean square deviation of 6.45 Å and 0.6 Å for *Py*BCCP-mut1 and *Py*BCCP-mut2, respectively (Figures 6.14 *C* and *D*).

(***A***) ***Ec*BCCP+**: DTLCITLCI**VEAMKM**MNQIE
SSSSSSSSSSS..SSSSSS

(***B***) ***Py*BCCP-model**: NKFDDYIE**VEAMKM**IMTFKS
SSSSSSSSSS..SSSSSSS

(***C***) ***Py*BCCP-mut1**: NKFDDYIE**VEAGKG**IMTFKS
SSSSS..SSSSS.SSSSSSS

(***D***) ***Py*BCCP-mut2**: NKFDDYIE**VEAMGM**IMTFKS
SSSSSSSSSS..SSSSSSS

Figure 6.13 Secondary structure predictions around the biotinylation motif. (*A*) *Ec*BCCP+ (*B*) *Py*BCCP-model (*C*) *Py*BCCP-mut1 and (*D*) *Py*BCCP-mut2. (*S*) denotes residues forming a β-sheet, while (.) represents residues forming a loop or a turn. The glycine residues in red were added sequence.

6.2.7 Homology modelling of the biotin carboxylase domains of *P. yoelii, P. falciparum* and *H. sapiens* acetyl-CoA carboxylases

A homology-base approach was also used to predict the 3D structures of the biotin carboxylase domain of *P. yoelii* (*Py*BC-model), *P. falciparum* (*Pf*BC-model) and *H. sapiens* (*Hs*BC-model) acetyl Co-A carboxylases using the *S. cerevisiae* (1w93) as template (Shen *et al*., 2004). The sequence identity between *Py*BC-model, *Pf*BC-model and *Hs*BC-model and the templates were 48%, 44% and 68% respectively. The *S. cerevisiae* biotin carboxylase sequence was modelled on itself (1w93) to generate a positive control (*Sc*BC+) 3D model. The total energy of the models before energy minimisation were −16 440 kJ/mol (82.4% of *Sc*BC+), −10 421 kJ/mol (52.2% of *Sc*BC+) and −13 567 kJ/mol (68 % of *Sc*BC+) for *Py*BC-model, *Pf*BC-model and *Hs*BC-model, respectively. After energy minimisation carried out using the GROMOS™ algorithm the final energy of the models reduced to −20 602 kJ/mol, −26 393 kJ/mol, −18 070 kJ/mol and −22 944 kJ/mol for *Py*BC-model, *Pf*BC-model, *Hs*BC-model and *Sc*BC+, respectively, showing an improvement of the models. The Ramachandran plots of the models (Figure 6.15) showed that the conformational angles (ϕ and ψ) of non-proline and non-glycine are within the sterically allowed regions of the Ramachandran plot.

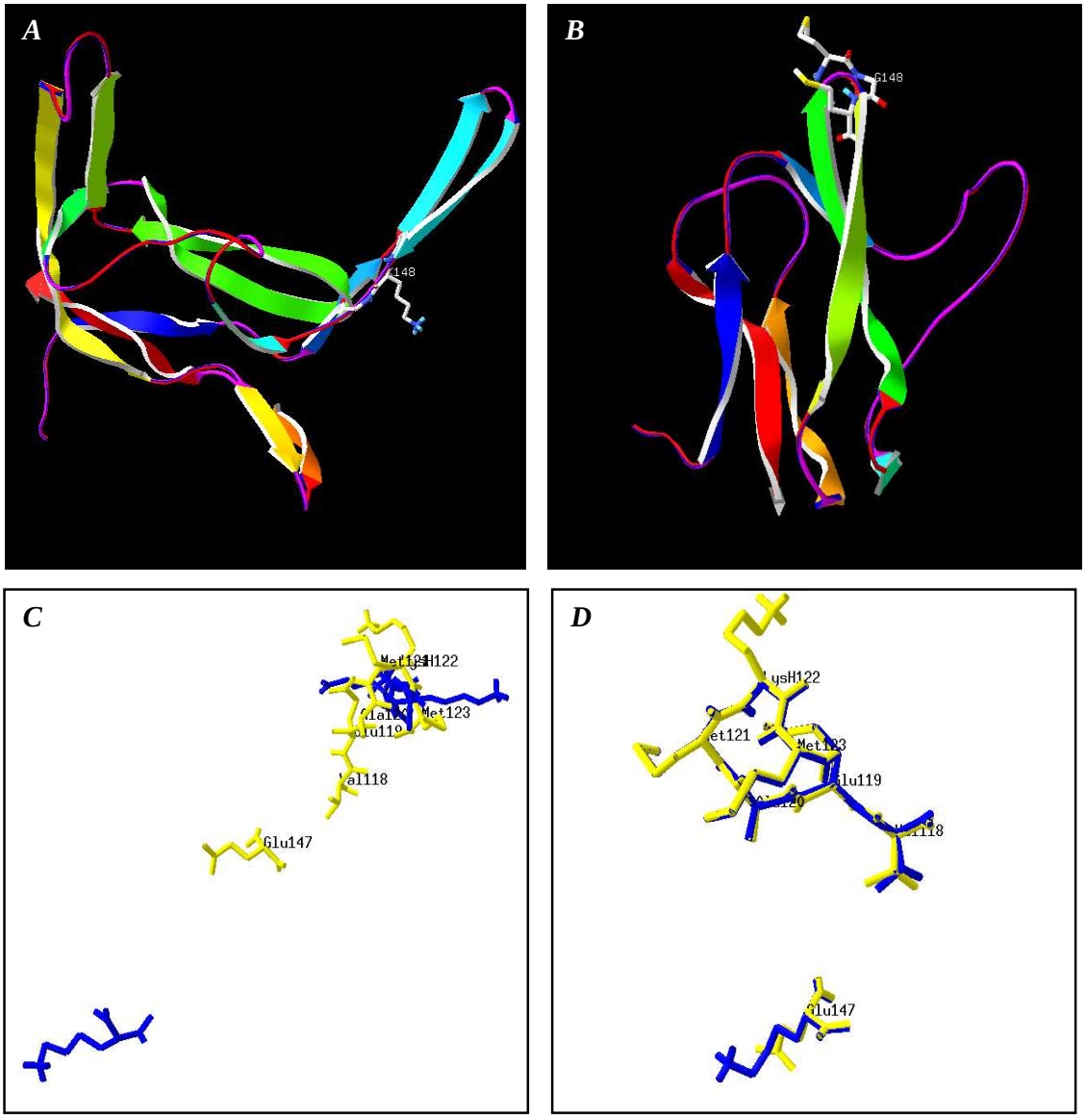

Figure 6.14 Structures predicted from mutated sequences of the *P. yoelii* biotinoyl protein. (*A* and *C*) *Py*BCCP-mut1, (*B* and *D*) *Py*BCCP-mut2. The side chains represent the MKM biotinylation motif. The structure is coloured according to secondary structure succession using the spdbv programme. *C* and *D* are superimposed images of the *E. coli* and the mutant models of *P. yoelii* VEAMKM biotinylation motif residues. The residues were coloured by selection using the spdbv programme (*E. coli* residues are yellow; *P. yoelii* residues are blue). The *E. coli* residues are labelled.

Although, few residues fall outside the allowed region of the Ramachandran plot as defined by ProCheck™. Generally, the Ramachandran analysis of *Py*BC-model, *Pf*BC-model and *Hs*BC-model showed a similar pattern with *Sc*BC+. Table 6.2 illustrates the Ramachandran analyses derived from the ProCheck™ algorithm.

Table 6.2 Ramachandran scores for the predicted biotin carboxylase models of *P. yoelii, P. falciparum, H. sapiens* and *S. cerevisiae* using ProCheck™

Ramachandran analysis	*Py*BC-model	*Pf*BC-model	*Hs*BC-model	*Sc*BC+ (1w93[b])
Number of proline residues	18	18	28	24
Number of glycine residues	28	30	38	46
Number of non-proline and non-glycine residues	481	592	433	481
Residues in the most favoured region[a] (%)	70.7	71.3	70.2	69.6
Residues in the additional allowed region[a] (%)	28.5	24.4	26.6	27.7
Residues in the generously allowed region[a] (%)	3.1	3.7	2.5	2.7
Residues in the disallowed region[a] (%)	0.4	0.5	0.7	0

[a] non-proline and non-glycine residues
[b] PDB identity number for crystal structure of *S. cerevisiae* (Shen *et al*., 2004).

The overall 3D topology of the models (Figure 6.16) can be classified as α+β conformation with a mix of β sheets and α helices in α→α, α→β and β→β super secondary structure topology. The secondary structures are connected with loops of varying lengths. Most of these loops are conserved between the targets and the templates. The signature motif of the biotin carboxylase is the carbamoyl phosphate synthatase signature (Blanchard *et al*., 1999b; Galperin and Koonin, 1997). The carbamoyl phosphate synthetase signature strands are situated on a loop structure in the four predicted models. The carbamoyl phosphate synthetase signature of *Py*BC-model, *Pf*BC-model and *Hs*BC-model (Figure 6.17) are completely super-imposable with the *Sc*BC+ with a root mean square deviation of equivalent α-carbons was 0.04 Å, for *Py*BC-model and *Pf*BC-model, and 0.03 Å for *Hs*BC-model. The 3D structures were superimposed using the spdbv programme. The root means deviation between the entire predicted 3D structure and *Sc*BC+ is 0.27 Å (for 493 α-carbons), 0.32 Å (492 α-carbons) and 0.15 Å (for 493 α-carbons) for *Py*BC-model, *Pf*BC-model and *Hs*BC-model, respectively. The minimum deviation between the *Hs*BC-model model and *Sc*BC+ model could be due to the higher amino-acid sequence identity compared to the *Plasmodium* models.

Nineteen amino acid residues have been shown to interact with soraphen A (Shen *et al*., 2004; Weatherly *et al*., 2004) in *S. cerevisiae* biotin carboxylase (PDB ID: 1w93 and 1w96). These residues and their equivalent in *P. yoelii, P. falciparum* and *H. sapiens* are highlighted in Figure 6.18. The 3D models showed that these residues in *Py*BC-model, *Pf*BC-model and *Hs*BC-model are completely superimposable with *Sc*BC+ (Figure 6.19).

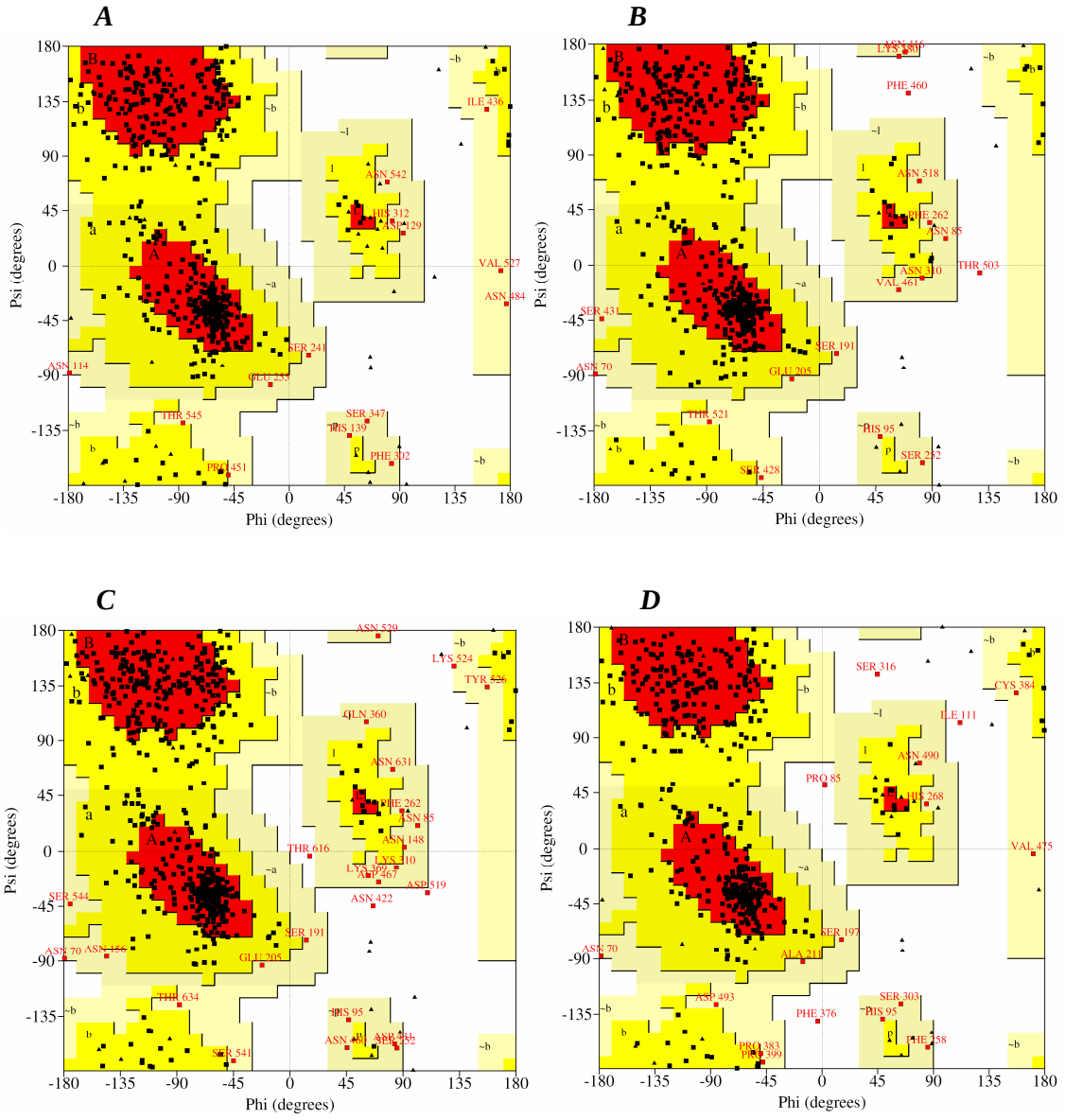

Figure 6.15 Ramachandran analysis of the homology modelling of the biotin carboxylase domains by ProCheck™. The Ramachandran plots were derived after energy minimization of (*A*) *S. cerevisiae* positive control (*B*) *P. yoelii* (*C*) *P. falciparum* and (*D*) *H. sapiens* (acetyl-CoA carboxylase-β). The different coloured regions indicate "most favoured" (red), "additionally allowed' (yellow), "generously allowed" (light yellow) and "disallowed' (white).

The root mean square deviations are 0.04 Å (for *Py*BC-model and *Pf*BC-model) and 0.03 Å (for *Hs*BC-model). The positions of the 20 soraphen-interacting residues on the 3D structure revealed that they are situated on the surface of the molecule rather than buried inside the structure (Figure 6.20). This result is consistent with the study carried out by Shen *et al.* (2004) who suggested that the soraphen-A binds at the dimer interface of the crystallised

biotin carboxylase. Although 47% of these residues are completely identical while 73.7% are similar by ClustalW™ alignment.

6.3 Discussion

Bioinformatics tools were used to study the structure and assign protein kinase phosphorylation sites on *P. yoelii* acetyl-CoA carboxylase based upon comparative analysis with acetyl-CoA carboxylases from several organisms that encodes the multi-domain acetyl-CoA carboxylase. It was necessary to compare *P. yoelii* acetyl-CoA carboxylase with orthologues from other *Plasmodium* parasites and homologues from other eukaryotic organisms in order to be confident with inferences that were drawn from the results.

The ClustalW™ alignment data (data not shown) involving 17 acetyl-CoA carboxylase sequences enable the accurate prediction of the structural organisation of *P. yoelii* acetyl-CoA carboxylase as well as other *Plasmodium* acetyl-CoA carboxylases. The biotin carboxylase and the carboxyl transferase protein domains with a fairly high degree of conservation were the points of focus. By and large, *P. yoelii* acetyl-CoA carboxylase appears to be a multi-domain type enzyme like that found in other eukaryotes.

The phylogenetic analysis derived from aligned sequences showed that there was evolutionary divergence of *Plasmodium* acetyl-CoA carboxylase from other species. The *Plasmodium* acetyl-CoA orthologues clustered with *T. gondii* and the primitive unicellular photosynthetic diatom, *O. lucimarinus* (Lanier *et al.*, 2008), suggesting that *Plasmodium* acetyl-CoA carboxylase is closely related *T. gondii* (an apicomplexa) and *O. lucimarinus* acetyl-CoA carboxylases. *T. gondii* is a plastid encoding organism (Jelenska *et al.*, 2001; Jelenska *et al.*, 2002; Zuther *et al.*, 1999) with a plastid genome of ~ 35 kb (Ralph *et al.*, 2004a; Ryall *et al.*, 2003; Waller *et al.*, 2003; Zuegge *et al.*, 2001), a size synonymous with the size of the *Plasmodium* plastid (Gleeson, 2000; Ralph *et al.*, 2004a; Waller *et al.*, 2003; Wilson, 2002).

During analysis of the 17 acetyl-CoA carboxylase sequences using PrositeScan™ to establish the amino acid sequence corresponding to the various domains of the enzyme, it was discovered that all organisms examined have 67 amino acid residues in their biotinoyl domain, except *Plasmodium*, which has 73 residues.

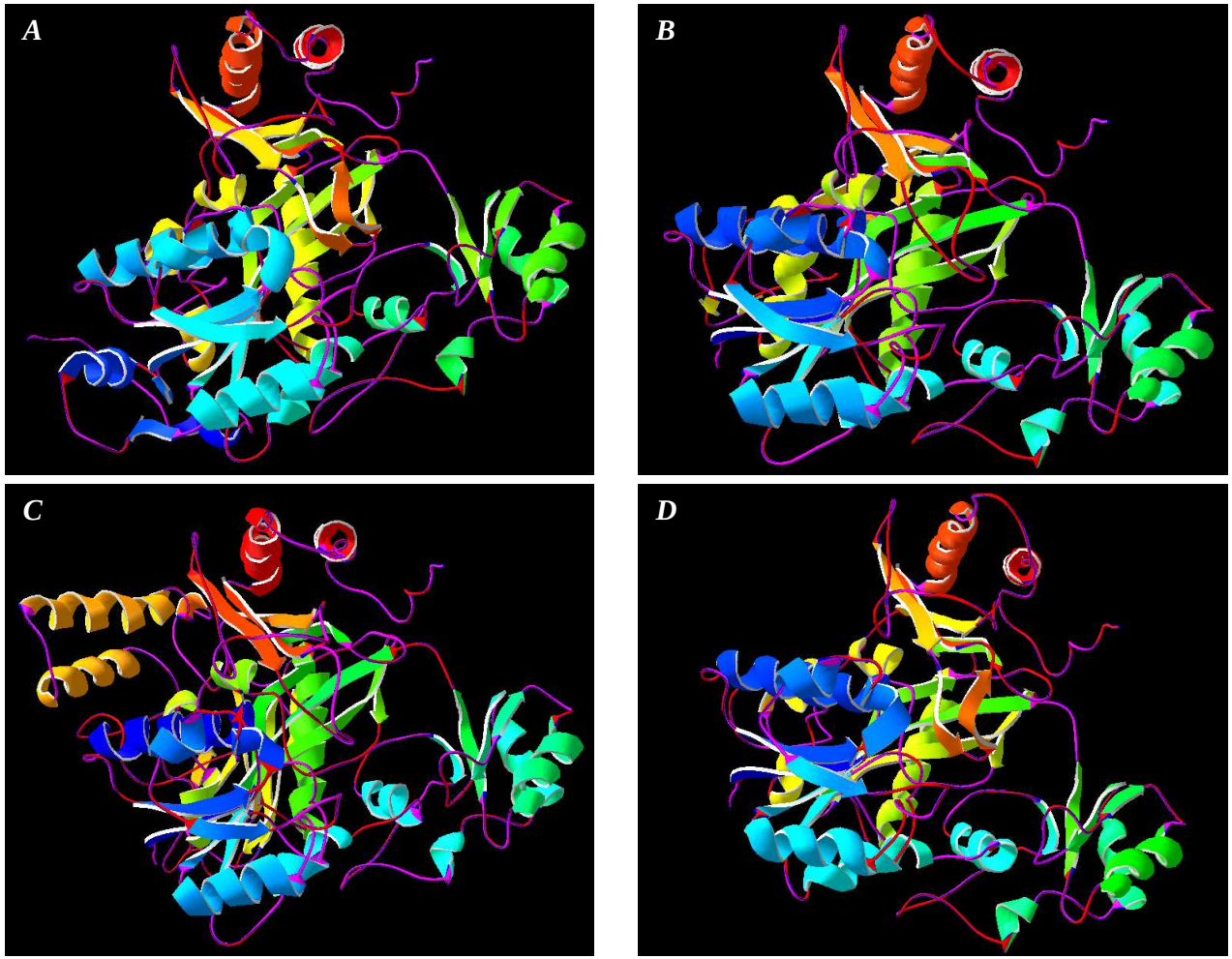

Figure 6.16 Predicted 3D molecular models of biotin carboxylase domain. (*A*) *S. cerevisiae* positive control model, (*B*) *P. yoelii*, (*C*) *P. falciparum* and (*D*) *H. sapiens*. The structure is coloured according to secondary structure succession using the spdbv programme. Blue secondary structure is at the N-terminal and red secondary structure is at the C-terminal of the protein.

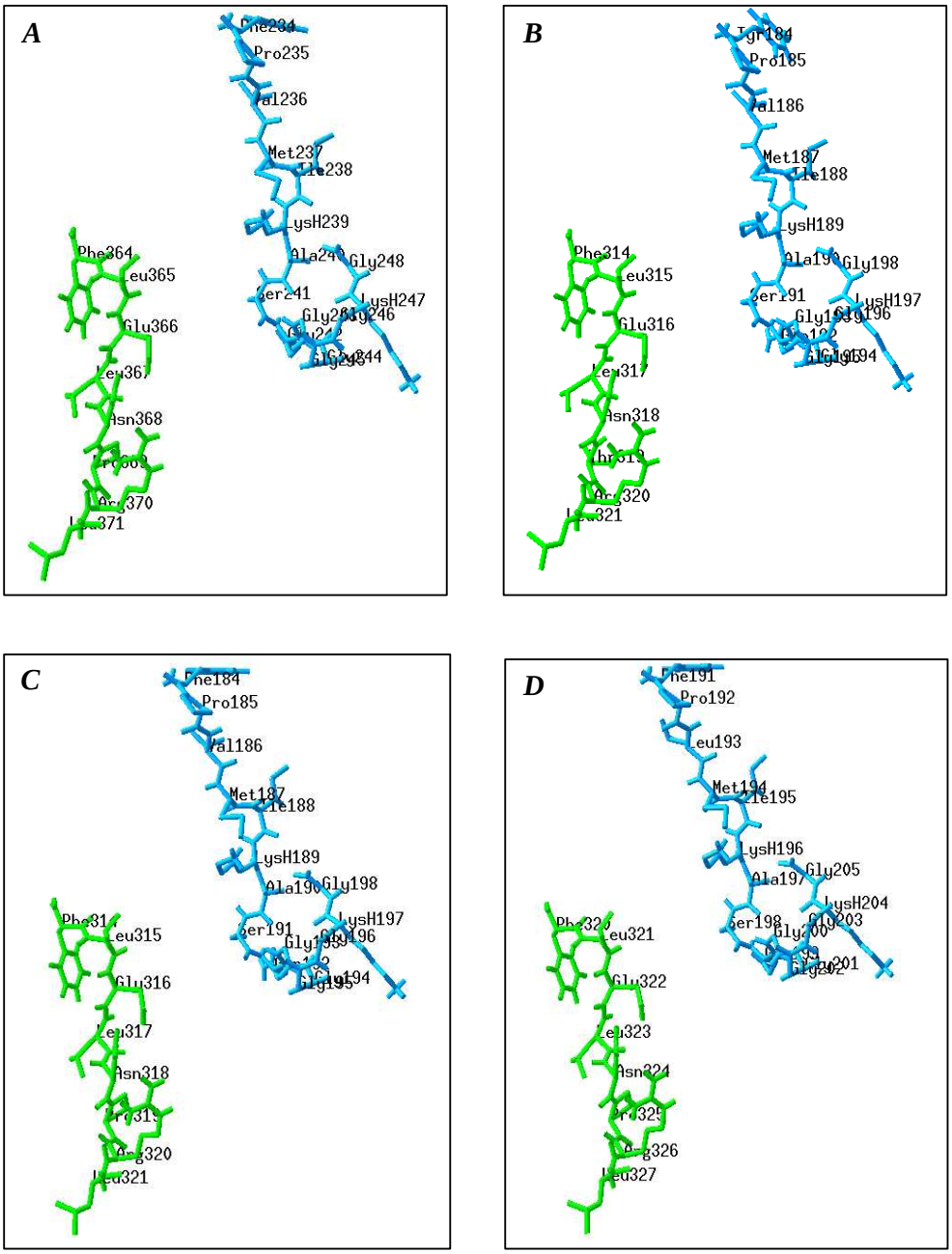

Figure 6.17 Structural comparison of the biotin carboxylase carbamoyl phosphate synthetase signature structures. (*A*) *Sc*BC+, (*B*) *Py*BC-model (*C*) *Pf*BC-model and (*D*) *Hs*BC-model. The long chain (blue) and the short chain (green) are coloured by selection using the spdbv programme.

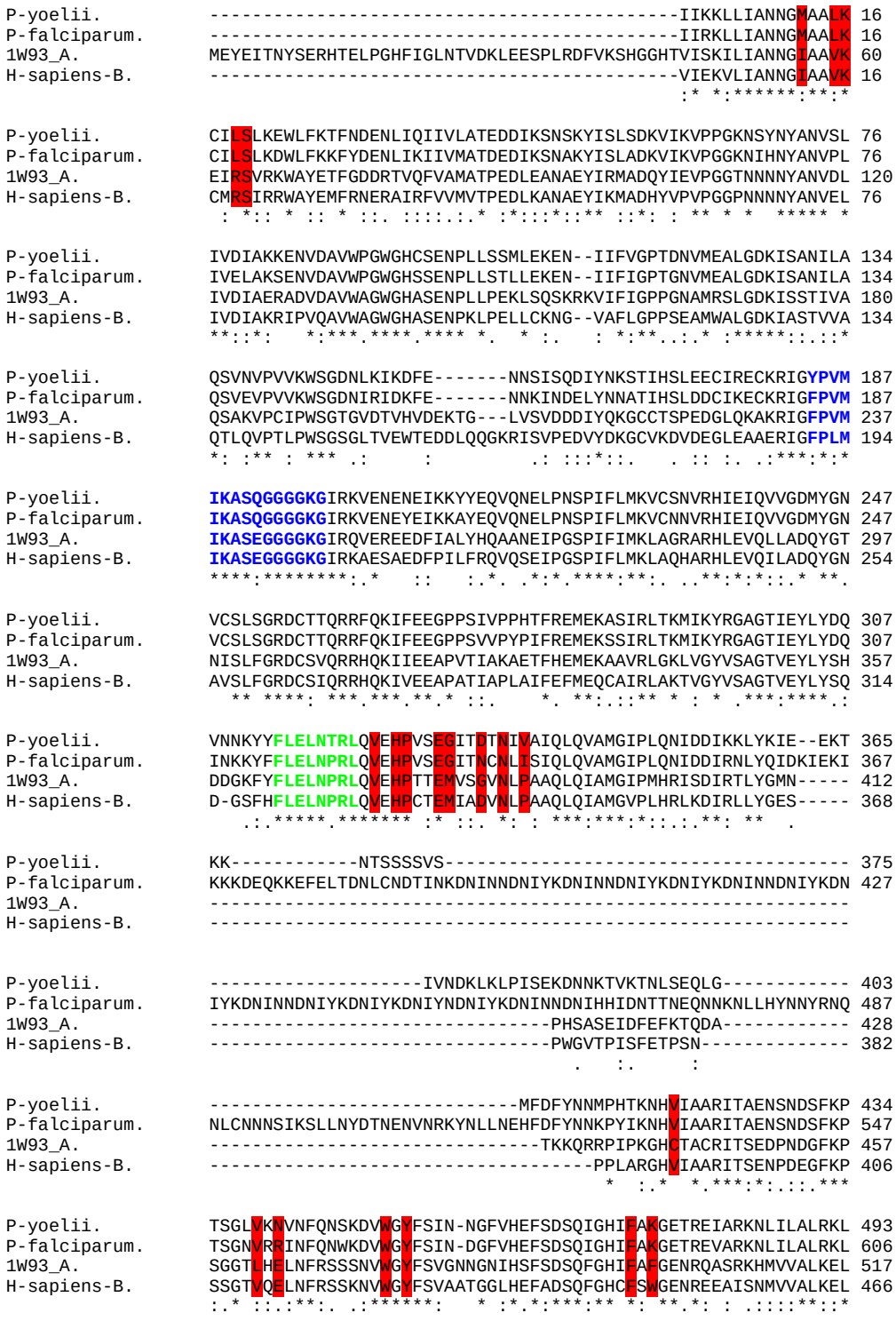

Figure 6.18 Sequence alignment of the biotin carboxylase domains of *S. cerevisiae, P. yoelii, P. falciparum* and *H. sapiens*. Residues involved in binding soraphen A are highlighted red; residues corresponding to the carbamoyl phosphate synthetase signature are coloured blue (long) and green (short). 1w93 represents the PDB-deposited amino acid sequences.

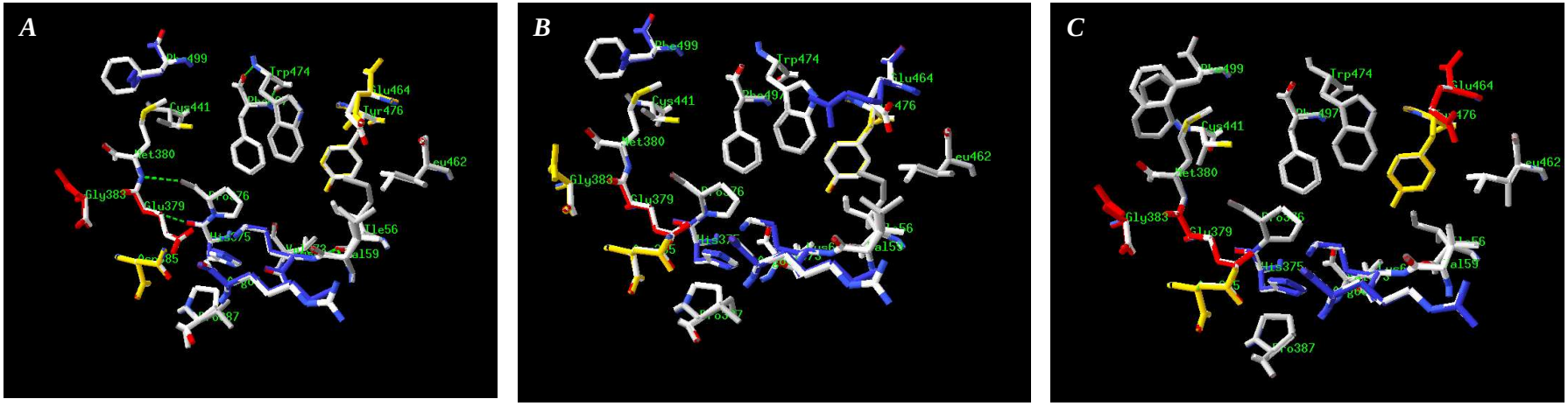

Figure 6.19 Superimposition of the residues at the equivalent positions with the *S. cerevisiae* biotin carboxylase soraphen A-binding residues. (*A*) *Py*BC-model (*B*) *Pf*BC-model (*C*) *Hs*BC-model. Labelled residues correspond to the ScBC+ residues.

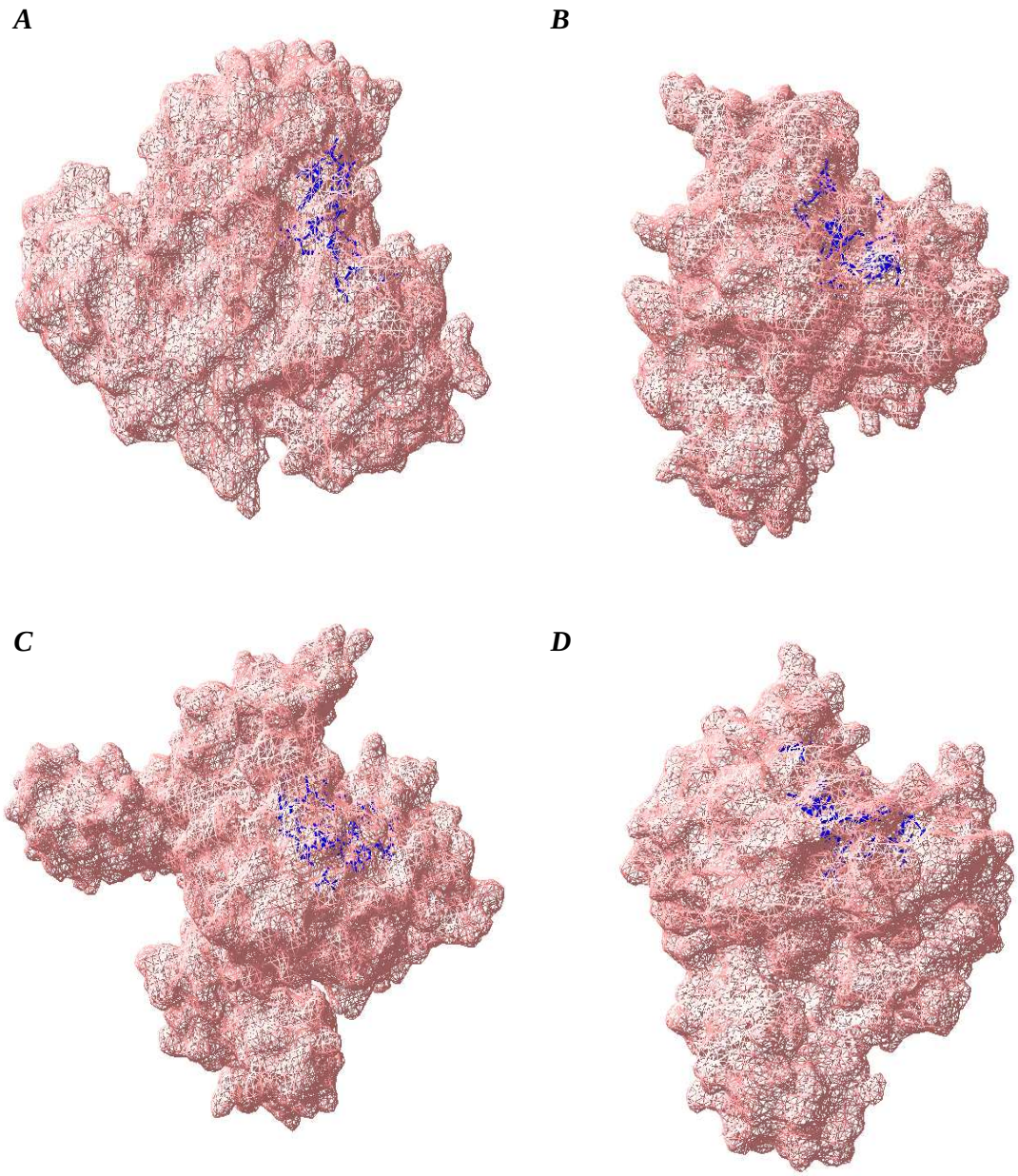

Figure 6.20 Molecular surface representation showing positions of the soraphen A-binding residues. (*A*) *Sc*BC+, (*B*) *Py*BC-model, (*C*) *Pf*BC-model and (*D*) *Hs*BC-model. The soraphen A-binding residues are coloured blue using the spdbv programme.

The additional six amino acid residues at the N-terminal region (Figure 6.21) of *Plasmodium* may be as a result of gene insertion since *T. gondii* (a close relative of *Plasmodium*) has 67 amino acid residues in its biotinoyl domain. This observation strongly suggested that regardless of the evolutionary divergence of the enzymes in the various organisms, the biotinoyl domain maintained a consistent number of residues. The reason for this consistency

is not understood, though it may be related to the functional relevance of this domain to the structure and function of the enzyme as well as the biotin protein ligase, an enzyme that attaches biotin moiety on biotin-dependent proteins as a form of post/co-translational modification. This domain was studied in Chapter 5 by recombinant protein expression and analysis for the presence of biotin.

Mapping phosphorylation sites either by experiment of by prediction algorithm is a crucial step towards understanding the catalytic mechanism of an enzyme and the resulting effects this enzyme exerts on other enzymes or metabolic pathways (Blom *et al*., 1999). Protein kinase mediated phosphorylation of acetyl-CoA carboxylase has been well studied (Boone *et al*., 2000; Hamilton *et al.*, 2002; Hardie, 2003; Hardie and Pan, 2002; Munday, 2002; Pan and Hardie, 2002), however, there are conflicting results on the actual phosphorylation sites from both *in vivo* and *in vitro* studies (Boone *et al*., 1999; Locke *et al.*, 2008; Munday, 2002). Prediction algorithms are fast, reproducible and have been shown to be accurate in terms of optimizing experiments (Doytchinova *et al*., 2006; Flower, 2003).

This study focused on identifying putative phosphorylation sites that are conserved in each of the domains of the enzyme. It was thought that the catalytic activities of the two enzyme domains may be regulated by a protein kinase; and that the phosphorylation sites will be conserved across several eukaryotes including *Plasmodium*. Biotin carboxylase is a member of the ATP-dependent carbamoyl phosphate synthetase family of enzymes (Blanchard *et al*., 1999b; Galperin and Koonin, 1997). These enzymes catalyse the phosphorylation of a carboxylate ion and the transfer of carbamoyl phosphate to an amino receptor on a protein substrate (Blanchard *et al*., 1999b; Galperin and Koonin, 1997). The carbamoyl phosphate synthatase family depends on Mg^{2+} and consists of a phosphate binding signature (Javid-Majd *et al*., 1996; Stapleton *et al*., 1996). Previous studies on protein kinase phosphorylation sites did not identify any phosphorylated residue on the biotin carboxylase as well as the carboxyl transferase domains of acetyl-CoA carboxylase. This may not imply that these enzyme domains may not be phosphorylated. Moreover, these studies were based upon enzymes that were recombinanatly expressed in a system not native to the enzyme (Boone *et al*., 1999; Locke *et al.*, 2008; Munday, 2002).

Two predictive algorithms were used to identify possible protein kinase modification sites on *P. yoelii* acetyl-CoA carboxylase by comparative analysis with *P. falciparum*, *vivax*,

knowlesi and mammalian acetyl-CoA carboxylase sequences. The Proscan™ algorithm (Bairoch *et al*., 1997) and NetPhos 2.0™ (Blom *et al*., 1999) algorithm designed to predict putative protein kinase sites on a protein sequence with sensitivities of 69% to 96% (Blom *et al*., 1999). The Proscan™ algorithm is the most widely used method for predicting protein kinase phosphorylation sites (Blom *et al*., 1999). The NetPhos 2.0™ is superior to the Proscan™ algorithm because the NetPhos 2.0™ neural network used to train its algorithm caters for a proteome wide prediction ability (Blom *et al*., 1999). This algorithm recognizes up to nine residues ±4 residues around the phosphorylation residue. This is because there is a general consensus that the protein kinase physically interacts with a stretch of 7 – 12 residues surrounding the phosphate acceptor residue (Alessi *et al*., 1996; Blom *et al*., 1999; Obata *et al*., 2000; Songyang *et al*., 1994).

Other species of *Plasmodium* including *P. berghei* and *P. chabaudi* were excluded from the study due to unavailability of the complete enzyme sequence (Plasmodb). However, the observations made in this study could be extrapolated to other species of *Plasmodium* not included in the study. Previous studies had employed the use of peptides containing phosphorylation motifs (Boone *et al*., 1999; Hardie *et al*., 1998; Munday, 2002). Some of these peptides are in an unconserved region of the protein (data not shown). Human α-acetyl-CoA carboxylase has been previously shown to be phosphorylated at Ser 79, the residue that has been implicated in the regulation of the enzyme (Boone *et al*., 1999; Hardie *et al*., 1998; Munday, 2002). This residue and its equivalent in β-acetyl-CoA carboxylase are not conserved in *Plasmodium*, though the NetPhos 2.0™ algorithm identified these sites with a probability of 99.1% (data not shown).

The Proscan™ algorithm predicted PKC, PKG and PKA phosphorylation sites; though only two of these sites corresponded to the NetPhos 2.0™ algorithm-predicted sites (P1/N1 and P5/N2, in Figures 6.4 and 6.5). cGMP-dependent protein kinase (PKG) and cAMP-dependent protein kinase (PKA) have being identified and characterised in *Plasmodium* (Deng and Baker, 2002; Diaz *et al*., 2006). The P1/N1 site is located at the N-terminal region of the biotin carboxylase domain, shown to be ATP dependent (Blanchard *et al*., 1999b; Galperin and Koonin, 1997; Javid-Majd *et al*., 1996; Stapleton *et al*., 1996). Although, the NetPhos 2.0™ score for mammalian acetyl-CoA carboxylase was less than 55% at this site. Some of these sites may be false positive results due to errors in the neural network used to train the

algorithms (Blom *et al.*, 1999). However, there is a possibility that these sites may be phosphorylation sites yet to be experimentally established (Blom *et al.*, 1999).

In the NetPhos-predicted serine phosphorylation sites, lysine appeared to be the predominant residue at position – 4, while tryptophan or phenylalanine (both are aromatic amino acids) are at the + 4 positions. These amino acids at positions + 4 and – 4 were 100% conserved. This suggests that these residues may be involved with the interaction of the *Plasmodium* protein kinase. The two serine phosphorylation sites predicted by NetPhos 2.0™ appear to be attractive options for the study of the protein kinase regulation of *Plasmodium* acetyl-CoA carboxylase. With site-directed mutagenesis on a recombinant *Plasmodium* biotin carboxylase domain or peptides derived from regions corresponding to these phosphorylation sites, the predicted sites could be experimentally validated, using recombinant *Plasmodium* protein kinases (Deng and Baker, 2002; Diaz *et al*., 2006; Dorin *et al*., 1999; Dorin *et al*., 2005; Nunes *et al*., 2007).

In this study, homology modelling was used to model the structures of the biotinoyl protein and the biotin carboxylase domains of *P. yoelii* acetyl-CoA carboxylase. Homology is widely used for predicting the possible function of a protein and for drug design (Brown *et al*., 2004; Keenan and Welsh, 2004; Singh *et al*., 2006). The predicted models of *P. yoelii* biotinoyl protein and biotin carboxylase were derived from the crystal structures of the *E. coli* biotinoyl protein (Athappilly and Hendrickson, 1995) and the *S. cerevisiae* biotin carboxylase domain of acetyl-CoA carboxylase (Shen *et al*., 2004; Waldrop *et al*., 1994). The models were refined using various algorithms provided by the spdbv v3.7 programme and validated by the ProCheck™ algorithm (Laskowski *et al*., 1996). This study supported the experimental data where the recombinant protein was biotinylated in an *E. coli* expression system. The study identified the potential interaction of the biotin carboxylase domain of *P. yoelii* acetyl-CoA carboxylase with soraphen A, a fungicide that inhibits acetyl-CoA carboxylase (Beckers *et al*., 2007; Shen *et al*., 2004; Shirra *et al*., 2001; Weatherly *et al*., 2004).

In most homology modelling studies, it is crucial to evaluate the structure predicted by the modelling programme used (Kleywegt, 1997; Kleywegt and Jones, 1996; Schwede *et al*., 2000; Schwede *et al*., 2003). This evaluation often requires a control structure for comparative assessments. Therefore the amino acid sequence (submitted to PDB) of the

protein used as a template for the study was modelled on its 3D structure in an attempt to produce a 'predicted' control model. Visual comparison (Schwede *et al*., 2000; Schwede *et al*., 2003) between the control model and the predicted protein was carried out as the first evaluation step. The total energy (kJ/mol) of the models were negative, suggesting highly relaxed structures (Melo and Feytmans, 1998). The refinement of the models carried out with an incremental energy reduction steps using GROMOS™ (van Gunsteren and Billetter, 1996) showed differences between the original model and the refined model in terms of total energy. This resulted in an improvement on the number of amino acid residues in the core regions of the Ramachandran plot. The minute differences in energy of the control models before and after refinement by GROMOS™ authenticated the modelling algorithm. The root mean square deviation (RMSD) of the predicted model from the experimental control model is another parameter that was used to assess the quality of the models (Chothia and Lesk, 1986; Wells *et al*., 2006). It is expected that there should be a minimal deviation between the back bone structure of the predicted model and its experimental control. A model could be declared inaccurate if its atomic coordinates are more than 0.5 Å RMSD of an experimental control (Chothia and Lesk, 1986; Lesk, 1997). In this study, the RMSD between the predicted models and their respective model controls were well within this limit.

The measure of the stereochemical properties of residues in a protein or peptide is the definitive means of validating a protein structure (Kleywegt, 1997; Kleywegt and Jones, 1996; Schwede *et al*., 2000; Schwede *et al*., 2003). The main chain of a polypeptide assumes a preferred energetically favourable conformation, which is characterised by the value of two torsion angles, ϕ and ψ; the third angle, ω, is largely restricted to 180º and 0º for *trans*-peptides and *cis*-peptides, respectively (Kleywegt and Jones, 1996; Ramakrishnan and Ramachandran, 1965). The plot of the torsion angles of the residues in a polypeptide, often referred to as the Ramachandran plot (Ramakrishnan and Ramachandran, 1965), is widely used in protein prediction algorithms. The protein structure validation algorithm, ProCheck™ (Laskowski *et al*., 1996) uses Ramachandran analysis to evaluate the quality of predicted protein models. This algorithm is used for protein structure quality assessment when depositing a protein structure into the Protein Data Bank (http://deposit.pdb.org/adit). The ProCheck™ algorithm further divided the original Ramachandran plot from three to four regions namely: "most favoured", "additional allowed", "generously allowed" and "disallowed". The predicted models in this study showed the majority of residues to lie in the

most favoured regions and a small fraction in the disallowed regions. Typically, a good model should not only have very many residues in the allowed regions, but very few in the disallowed regions (Kleywegt, 1997; Kleywegt and Jones, 1996). Some published predicted models confirmed the presence of few residues in the disallowed regions (Choubey *et al*., 2006; Joshi *et al*., 2008; Singh *et al*., 2006; Wells *et al*., 2006). By and large, the stereochemical properties of the predicted models were comparable to the controls structures used to generate the models.

The SWISS-MODEL™ homology modelling algorithm was further tested using mutations introduced to the *P. yoelii* biotinoyl protein region. Given that the modelling algorithm is typically based on sequence identity and proper alignment (Schwede *et al*., 2000; Schwede *et al*., 2003), it was expected that major alterations such as deletion, insertion or replacement of residues at regions conserved between the target and the template will result in major perturbations in the overall structure predicted by the algorithm, while minor alterations such as substituting an amino acid with a similar one will result in minor perturbations. The mutant models generated by the modelling algorithm showed major alterations on the 3D structure when the residues forming the loop structure between β_3 and β_4 were deleted before alignment, and when the methionine residues flanking the biotinyl-lysine were replaced with glycine. No alteration on the structure compared to the predicted *Py*BCCP-model was observed when the biotinyl lysine was replaced with glycine, arginine and glutamic acid (data not shown). This was because the sequences maintained a proper alignment with these minor alterations in amino acid sequence.

The *E. coli* biotinoyl protein, though a separate subunit polypeptide of the acetyl-CoA carboxylase complex, shares structural similarity with the *P. yoelii* biotinoyl protein domain. Alignment of the biotinoyl protein domain of *P. yoelii* with the *E. coli*-1bdo sequence used to resolve its crystal structure (PDB-deposited sequence) showed 20% identity and 52% similarity. Although the percentage identity is lower than the 25% threshold stipulated by the SWISS-MODEL™ algorithm (Schwede *et al*., 2000; Schwede *et al*., 2003), studies have shown that residues at an environmentally or evolutionarily conserved position on two similar proteins with dissimilar residues play similar structural roles (Kleiger *et al*., 2000). The predicted 3D model of *P. yoelii* biotinoyl was found to be similar to both experimentally resolved (Athappilly and Hendrickson, 1995) and algorithm-predicted (Chapman-Smith *et al*., 1999; Chapman-Smith *et al*., 2001; Reche *et al*., 1998) 3D structures of *E. coli* biotinoyl

protein. The structural relationship between the two proteins could have led to the biotinylation of *P. yoelii* biotinoyl protein expressed in *E. coli* by the *E. coli* biotin protein ligase. Both structures are made up of β-sheets without an α-helix and the consensus MKM motif in both structures is located at a tight β-turn joining two sheets. This conformation is consistent with the resolved crystallographic structures of the human acetyl-CoA carboxylase biotinoyl domain (Lee *et al*., 2008) and *P. shermanii* transcarboxylase biotin carboxyl carrier domain (Reddy *et al*., 2000).

Site directed mutagenesis studies aimed at determining the residues on BirA involved with the interaction with *E. coli* biotinoyl protein showed that E147K mutation on the biotinoyl protein minimally affected its biotinylation by BirA (Chapman-Smith *et al*., 2001). A lysine residue (K^{1152}) is at an equivalent position on the *P. yoelii* biotinoyl domain (Figure 6.22), and 100% conserved across *P. falciparum*, *vivax*, *berghei*, *chabaudi* and *knowlesi* domains. This residue is orientated on the surface of the structure in the model, comparable to E^{147} of the *E. coli* biotinoyl protein. Conversely, E119K mutation resulted in significant alteration in the activity of BirA activity on the biotinoyl protein (Chapman-Smith *et al*., 2001). This glutamic acid residue is conserved in *P. yoelii* and other *Plasmodium* biotinoyl protein domain of acetyl-CoA carboxylase. The observations made from these studies clearly indicated that, while residue charge is essential in the recognition process, an interaction between single amino acids residues is not sufficient enough for the interaction between BirA and its biotin-dependent substrate (Chapman-Smith *et al*., 2001; Reche *et al*., 1998; Reche and Perham, 1999; Reche, 2000). The negligible RMSD between the back bone α-carbon atoms of the VEAMKM-$(X)_n$-E/K (147/1152) residues clearly suggested that it is a conserved pattern common between the two structures and may be involved in conserving the conformation vital for biotin protein ligase interaction (Kleiger *et al*., 2000; Yang and Honig, 2000a; Yang and Honig, 2000b). This conformation may be the determining factor for the interaction between the recombinant *P. yoelii* biotinoyl protein and the *E. coil* BirA (Reche *et al*., 1998; Reche and Perham, 1999; Reche, 2000). A significant contribution made by the homology modelling study is that site directed mutagenesis on key amino acid residues on *P. yoelii* biotinoyl protein can be carried out based on the spatial organisation of the residues on the surface of the 3D structure.

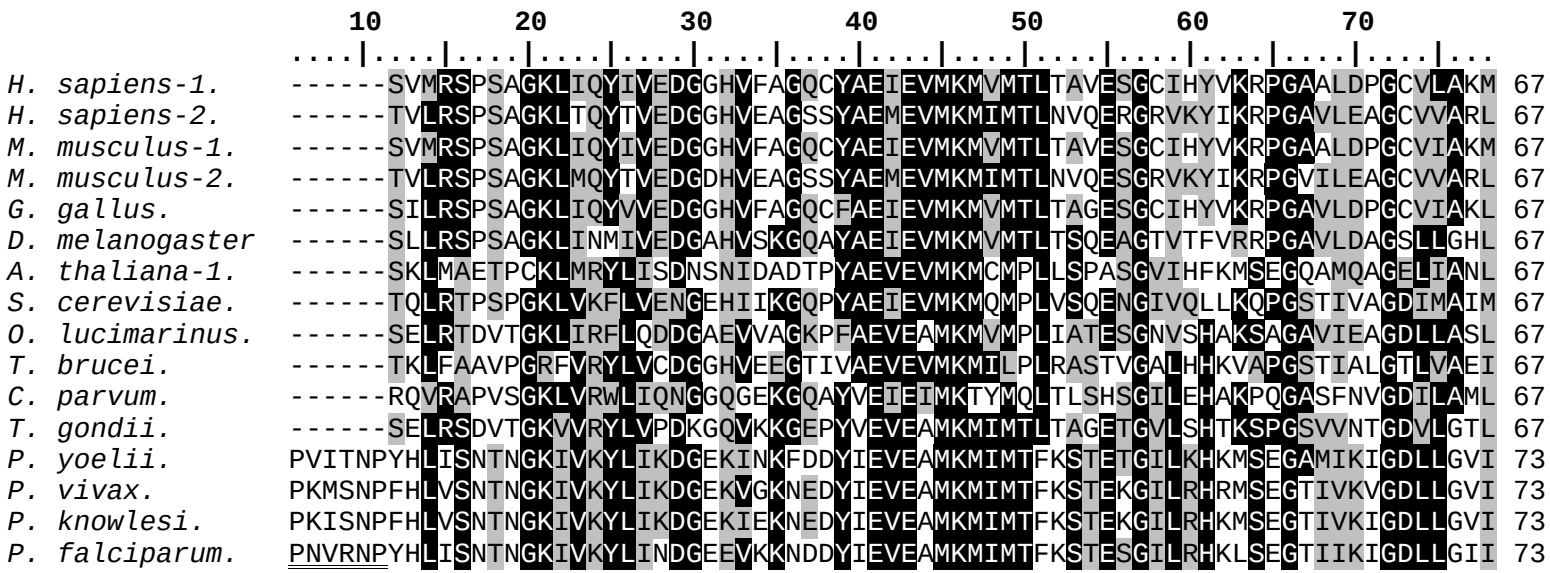

Figure 6.21 Sequence conservation in the biotinoyl domain of the multi-enzyme-domain type acetyl-CoA carboxylase. Acetyl-CoA carboxylase sequences (16) from various organisms were submitted to the ScanProsite™ database to identify the amino-acid sequence corresponding to the biotinoyl domain. The sequences were extracted and aligned with the ClustalW™ algorithm (1000 bootstrap analysis). Residues are shaded based on the degree of conservation, with black shading indicating 100% conservation. The double underline indicates the five amino-acid residues that may have been inserted into the *Plasmodium* sequence by evolution. *A. thaliana 1 and 2* shares 100% sequence identity in their biotinoyl domain, hence *A. thaliana-2* was excluded.

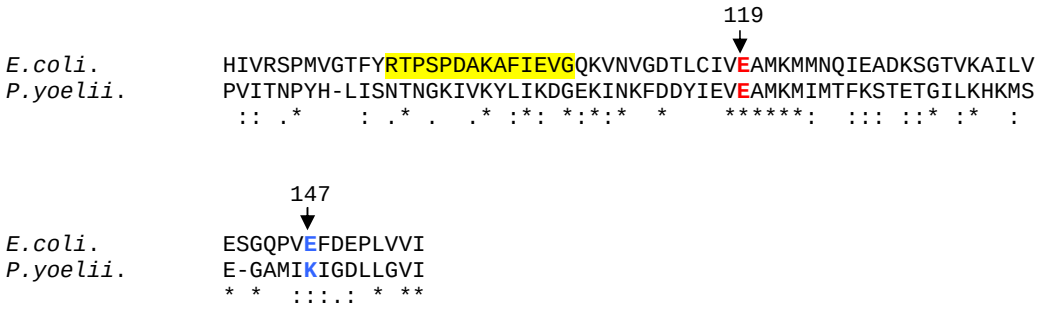

Figure 6.22 ClustalW™ alignment of *E. coli* biotinoyl protein and *P. yoelii* biotinoyl protein domain. Residues in red and blue are at equivalent positions, corresponding to the previously studied BirA interacting residues (Chapman-Smith *et al*., 2001). The residues highlighted yellow corresponds to the "thumb" structure on the *E. coli* protein (Cronan, 2001; Lee *et al*., 2008).

One key observation made from the predicted structure of *E. coli* biotinoyl protein is the presence of the "thumb" structure connecting β_2 and β_3 (see Figure 6.7). This structure is also found in both the experimentally-resolved crystal structure as well as the predicted structures of *E. coli* biotinoyl protein (Cronan, 2001; Lee *et al*., 2008). The residues involved in the "thumb" structure are 64% similar with *P. yoelii* biotinoyl protein (highlighted residues in Figure 6.21). A ClustalW™ alignment between the *E. coli* biotinoyl protein and human biotinoyl protein domain revealed a gap (data not shown) at an equivalent position, indicating the absence of this structure in the human protein, as recently suggested (Lee *et al*., 2008). This structure is also absent in the biotinoyl protein domain of *P. shermani* transcarboxylase (Lee *et al*., 2008; Reddy *et al*., 2000). The relevance of this structure to the protein is still not clear. A number of studies have shown that the "thumb" structure contributes to the overall stability of the biotinoyl protein to proteolysis (Solbiati *et al*., 2002). Other studies have also shown that it contributes to the stability of the transient biotinylated structure of the holo enzyme by interacting with the biotin moiety (Roberts *et al*., 1999; Yao *et al*., 1999). The deletion of the thumb structure in *E. coli* leads to a decrease in fatty acid biosynthesis hence growth of the cells (Cronan, 2001). However, lack of the "thumb" structure in some other biotinoyl subunits or domains of acetyl-CoA carboxylase (Lee *et al*., 2008; Reddy *et al*., 2000) and the long half life of carboxy-biotin (Knowles, 1989) contradicts these suggestions about the involvement of the "thumb" structure in the stability of the holo-biotinoyl protein (Solbiati *et al*., 2002). The biotinoyl domain of the human acetyl-CoA carboxylase β crystal structure would have been a good template to model the *P. yoelii* protein considering the

evolutionary relationship between the two enzymes. It may be important to use the 2dn8 (deposited in the PDB by Ruhul Momone *et al*., 2006) template for more comparative studies of the *P. yoelii* biotinoyl protein domain with regards to its structural evolution.

The inhibition of acetyl-CoA carboxylase activity by soraphen A has been studied in humans and yeast (Beckers *et al*., 2007; Shen *et al*., 2004; Shirra *et al*., 2001). This compound has been shown to inhibit the activity of biotin carboxylase by interacting with 20 residues within the domain (Shen *et al*., 2004). The crystal structure of *S. cerevisiase* (Shen *et al*., 2004) provided a good template to model the *P. yoelii* acetyl-CoA carboxylase biotin carboxylase domain, in an effort to investigate the structural organisation of this domain and the possibility of inhibiting the enzyme with soraphen A or close analogues. The structures of the *P. falciparum* orthologue, as well as the human version of the enzyme domain were also predicted for comparison. Although, there is a resolved crystal structure of the *S. cerevisiase* biotin carboxylase (PDB ID: 1w96) in complex with soraphen A (Shen *et al*., 2004), the coordinates of the domain without the inhibitor was preferred. This was to prevent errors that may be introduced in the models due to the influence of the inhibitor interaction with the general conformation of the protein structure (Schwede *et al*., 2003). Generally, the high sequence identity between the target and the template sequence correlated to the good quality of the predicted models (Joshi *et al*., 2008; Keenan and Welsh, 2004; Schwede *et al*., 2003). The GROMOS™ refinement data suggested good quality structures based upon the total energy (kJ/mol) before and after the energy minimisation processes. This was also evident in the marginal RMSD of the α-carbon backbone structures between predicted models and the control model. Therefore, it was vital to carry out energy minimisation before subsequent studies on the predicted structure, such as inhibitor or ligand interactions.

The key enzyme subdomain in the biotin carboxylase is the carbamoyl phosphate synthetase signature (Galperin and Koonin, 1997). Enzymes belonging to this super family have been well studied (Blanchard *et al*., 1999b; Javid-Majd *et al*., 1996; Stapleton *et al*., 1996) and they catalyse the phosphorylation of the carboxylate anion (COO^-) and subsequent transfer of the carbamoyl phosphate to an amine acceptor molecule, in this case a biotin molecule attached to the biotin carrier protein. This reaction forms part of the commited step of acetyl-CoA carboxylase (Brownsey *et al*., 2006; Hardie and Pan, 2002). The predicted models revealed similarity in the conformation of the carbamoyl phosphate synthetase signatures, with negligible RMSD of the α-carbon backbone conformation between the models and the

control model. This observation structurally characterised this domain, and suggested a possible similarity in the enzyme function of the biotin carboxylase domains of *S. cerevisiae* and *Plasmodium*.

The Ramachandran analysis using the ProCheck™ algorithm showed a lower percentage of the non-glycine and non-proline residues in the most favoured region; however, this appeared to be consistent with the control model. In addition, very few residues were in the disallowed region of the Ramachandran plot. This shortfall in the stipulated percentage (Laskowski *et al*., 1996) of residues in the most favoured region may be traced to the original structure deposited in the PDB database (Kleywegt and Jones, 1996). When the crystal structure of *S. cerevisiae* biotin-carboxylase in complex with soraphen A (1w96) was used as a template to build a control model and a *P. yoelii* biotin carboxylase model, ProCheck™ analysis revealed that 90.6% and 86.7% of the residues in the control and *P. yoelii* models, respectively, were in the most favoured region of the Ramachandran plot (results not shown). However, the *P. yoelii* models derived from the different templates of *S. cerevisiae* biotin carboxylase (PDB ID: 1w93 and 1w96) deviated by 0.7 Å (RMSD of the backbone α-carbon atoms), despite an equal number of residues between the two models. Besides, the control models generated from the two crystal structures also deviated by 0.6 Å. The differences in the resolution of the crystals (2.5 Å for 1w93 and 1.8 Å for 1w96) may have influenced the observed constraints in the predicted models (Kleywegt and Jones, 1996). The interaction of the protein with the inhibitor may have resulted in the more relaxed conformation of the 1w96 crystal structure compared to the 1w93 crystal structure. The biotin carboxylases consist of a highly conserved ATP-binding subdomain that is characteristics of this class of enzymes (Galperin and Koonin, 1997). Perhaps, the binding of ATP stabilises the structure, which may occur with soraphen A binding; though soraphen A is not a structural analogue of ATP. Studies have shown that ligand interaction stabilises the structure of a protein. For example, the interaction between apo-haemoglobin and the porphyrin ring results in stability of haemoglobin (Fontana *et al*., 1997) and the structural stability of ATP-sulfurylase increases with ATP-binding (Ullrich *et al*., 2001; Yu *et al*., 2007).

The residues at equivalent positions involved in soraphen A binding were superimposeable with negligible RMSD. None of these residues are in the disallowed regions of the Ramachandran plot as determined by the ProCheck™ algorithm (data not shown). Four out of these 19 residues were not conserved. Such structural dissimilarities may prove to be

advantageous in designing soraphen A analogues that may interact with higher specificity with *Plasmodium* biotin carboxylase (Keenan and Welsh, 2004). However, the interaction of soraphen A with apicomplexa biotin carboxylase is experimentally characterised. It would be interesting to investigate the inhibition of *Plasmodium* acetyl-CoA carboxylase using *in vitro Plasmodium* culture. The observation made from this predicted models can be further evaluated using automated molecular docking algorithms such as *GOLD* (Genetic Optimisation for Ligand Docking) (Jones *et al*., 1997) to examine hydrogen bonding formations between these 19 residues and the soraphen A molecule. Molecular docking studies in combination with protein structure prediction is widely applied in drug design and synthesis (Bjelic and Åqvist, 2004; Keenan and Welsh, 2004; Singh *et al*., 2006). The inference made from this study could be strengthened by applying other homology modelling programmes and compare the models generated from two or more different homology modelling algorithms.

CHAPTER 7
FINAL DISCUSSION

7.1 Introduction

The clinical manifestations of malaria in humans, which occurs only when infected by one of the four species of the human malaria parasites, remain a major health and economic burden in most tropical regions of the world, where the disease is highly endemic. To date there is no effective malaria vaccine and the parasite has developed resistance to most drugs available for the treatment of malaria (Gregson and Plowe, 2005; Wainwright and Amaral, 2005; White, 2004). This has led to a search for new drug targets against malaria, enhanced by the complete sequencing of the genome of the *falciparum* species in addition to other species of the parasite. Although the malaria parasite has been studied for several decades, the parasite's biochemistry and interactions with the immune system in humans is not clearly understood (McKean, 2002). This may be as a result of the unique nature of the parasite's genome, which is the only organism with an *AT*-rich genome identified so far. Besides, more than 60% of the predicted proteins in the parasite proteome do not have any functional similarity with proteins in many other organisms (Gardner *et al*., 2002a).

The first port of call when investigating preliminary anti-malaria drug effectiveness and immune response towards vaccine candidates are the rodent malaria models (Carlton *et al*., 2002). These species of *Plasmodium* parasites, originally isolated from African thicket rats, are laboratory-adapted and can be established efficiently in rodents (Sanni *et al*., 2002). Nevertheless, the usefulness of the rodent malaria models as a study alternative to the human malaria parasites is still debatable (Carlton *et al*., 2002). This is because different species have been shown to develop different mechanisms of drug resistance, regardless of a similar mechanism of action of the particular drug (Carlton *et al*., 2001). In addition, different species of the parasite display different modes of immune invasion in the host. By and large studies have shown that regions, where a gene is involved in house keeping, are highly conserved between *P. falciparum* and *P. yoelii*, but regions where a gene is involved in antigenic variation and immune invasion are located are not conserved (Carlton *et al*., 2002; Carlton *et al*., 2001). This may be interpreted as a pitfall in using rodent malaria parasites to model vaccine efficacy; while on the other hand, it shows that malaria models could be selected based on genes that best fits the phenotypic trait under study (Kaiser *et al*., 2004). Therefore identifying a protein or enzyme mediating an important pathway for study as a

drug target should be based on the presence of orthologues of the protein in other species and the degree of sequence identity between the orthologues of the protein under study.

The "post-genomics" era has witnessed major milestones in malaria research based upon deductions made from *"in silico"* analyses of the published genomes of the parasite. Several genes encoding proteins that were previously thought to be lacking in the *Plasmodium* parasite have been identified as a result of the malaria genome sequencing projects. Genome-wide studies on the expression profile of the *P. falciparum* transcriptome (Le Roch *et al*., 2003) has revealed the pattern of expression of several genes encoding potential drug targets. This has contributed to understanding the importance of a potential drug or vaccine target to the stage of the parasite life cycle based on the expression level of protein at the particular stage of the parasite development. Generally, it is believed that only genes encoding proteins essential for the survival and progression of the parasite at a particular stage are expressed (Kaiser *et al*., 2004; Le Roch *et al*., 2004). However, care must be taken when making deductions from these gene transcriptions profile data, because these data were derived from a *P. falciparum* isolate grown *in vitro* (Le Roch *et al*., 2003). There have been recent efforts to establish the expression profile of *P. falciparum* transcriptome from field isolates (Daily *et al*., 2007; Siau *et al*., 2007).

Fatty acid biosynthesis is vital in any organism for membrane biogenesis and survival. The ability of the *Plasmodium* parasite to synthesise fatty acid precursors *de novo* has been a subject of controversy. Initial studies showed the parasite synthesises or imports fatty acid based on the dramatic elevation of lipid metabolism in *Plasmodium*-infected erythrocytes, which is almost absent in uninfected erythrocytes (Mitamura and Palacpac, 2003). Central to fatty acid metabolism in most organisms is acetyl-CoA carboxylase. This enzyme, which catalyses the commitment step in fatty acid biosynthesis, has been shown to be inhibited by herbicides and fungicides (Gornicki, 2003; Shen *et al*., 2004). These observations have led to increased attention on this enzyme as a possible drug target for anti-parasite and anti-obesity chemotherapy. The presence of this enzyme in the *Plasmodium* parasite was, until now, based upon comparative sequence analysis with characterised acetyl-CoA carboxylases from other organism (Plasmodb database).

7.2 RT-PCR and Northern blotting analysis of *P. yoelii* acetyl-CoA carboxylase mRNA

This is the first study to specifically verify the presence of acetyl-CoA carboxylase and characterise the highly conserved biotin-binding domain of the enzyme in a *Plasmodium* parasite. This was demonstrated in this study using *P. yoelii* propagated in mice by employing RT-PCR analysis to show that the parasite expresses the enzyme at the erythrocytic stage of the parasite life cycle. The results were further confirmed by sequencing of the RT-PCR products. Although the quantitative levels of expression of this gene at the blood stage of *P. yoelii* was not determined. Northern blot analysis using total RNA isolated from infected mouse blood confirmed the presence and size of the transcript, which was greater than the published size of the ORF. This perhaps suggests that the extended 5' and 3' untranslated regions may be involved in the regulation of the gene translation. This observation shows that the parasite is capable of *de novo* fatty acid biosynthesis. Studies have shown that acetyl-CoA carboxylase is transcriptionally regulated (Barber *et al*., 2003; Munday, 2002), therefore studying the transcription profile and the UTR of this gene transcript could to be important for understanding the regulation of acetyl-CoA carboxylase activity.

Analysis of the transcription profile of the genes encoding acetyl-CoA carboxylase and fatty acid synthase complex in *P. falciparum* suggests that these enzymes, though very crucial in fatty acid synthesis, are down regulated in the blood stage of the parasite cycle and up regulated in (the predominant insect stages) the gametocyte and sporozoite stages (Plasmodb database). Conversely, enzymes possibly involved in the trafficking and processing of imported lipid precursors are up regulated at the erythrocyte stages and down regulated at the gametocyte and sporozoite stages. This is an important observation that suggests that *de novo* fatty acid biosynthesis in the parasite may be stage-specific. In other words: why make fatty acid when it can easily be extracted from the host? This remains to be investigated.

7.3 Production of anti-PyACC peptide antibodies used for the detection of *P. yoelii* acetyl-CoA carboxylase

The availability of the published amino acid sequence of *P. yoelii* acetyl-CoA carboxylase enabled the selection of immunogenic peptides from the enzyme for antibody production in chickens using an epitope prediction algorithm. The use of synthetic peptides for the production of antibodies is a useful approach when the whole protein cannot be easily isolated and/or purified to homogeneity. Studies carried out in our laboratory have showed

that synthetic peptides coupled to a carrier induce immunogenic response in chickens to produce up to 30 mg of affinity purified anti-peptide antibodies. These antibodies have been used to successfully characterise several novel *Plasmodium* protein kinases (Dorin *et al*., 2005; Merckx *et al*., 2003). The anti-peptide IgY directed against *P. yoelii* acetyl-CoA carboxylase detected the enzyme in parasite lysates obtained from a mixed stage *P. yoelii*-infection. The enzyme was also detected *in situ* by immunofluorescence microscopy. The detection of the enzyme in both lysate and *in situ* is a clear indication of the ability of the parasite to synthesise acetyl-CoA carboxylase for *de novo* fatty acid metabolism. The precise localisation of the enzyme in the parasite needs to be established by either immunotransmission electron microscopy or confocal microscopy. This would confirm previous speculations that fatty acid biosynthesis in apicomplexans occurs in the plastid.

7.4 Expression of the biotinoyl domain *P. yoelii* acetyl-CoA carboxylase in *E. coli*

A major observation drawn from the *in silico* characterisation of *P. yoelii* acetyl-CoA carboxylase by comparative sequence analysis is the consistency in the number of amino acid residues in the biotin-binding domain in all organisms examined. This consistency in the number of amino acid residues, coupled with the 100% sequence identity in the biotinylation motif of *E. coli* and *Plasmodium*, led to the possibility that expressing the *P. yoelii* acetyl-CoA carboxlase biotin-binding domain in *E. coli* may result in the attachment of biotin to the recombinant protein by the *E. coli* biotin protein ligase (Chapman-Smith and Cronan, 1999c; Chapman-Smith *et al*., 1994; Lee *et al*., 2008). The biotinylation of the recombinant *P. yoelii* protein suggested a structural feature of the enzyme. The expression of *P. yoelii* biotinoyl protein in *lon*-protease deficient *E. coli* strains using two different expression systems yielded full protein products, in addition to some truncated recombinant protein products. This is not uncommon when *Plasmodium* proteins are expressed in heterologous systems, including yeast (Mehlin *et al*., 2006). Studies on improving the quality of recombinant *Plasmodium* proteins expressed have led to the use of synthetic codon-optimised genes due to the bias in codon usage between the *AT*-rich-genome *Plasmodium* and heterologous protein expression cells such as yeast and *E. coli*. The use of synthetic codon-optimised genes for the expression of *Plasmodium* proteins have so far improved the quality and quantity of recombinant *Plasmodium* proteins expressed heterologously in different expression systems (Flick *et al*., 2004; Nagata *et al*., 1999; Narum *et al*., 2001; Yadava and Ockenhouse, 2003; Zhou *et al*., 2004). The use of synthetic codon-optimised genes was not applied in this study. One major benefit of this approach is that a plasmodial protein can be

effectively expressed and characterised without the need to culture parasites. Secondly, RT-PCR-mediated cloning of an intron-rich gene is bypassed when using the synthetic codon-optimised gene approach.

7.5 Characterisation of recombinant *P. yoelii* biotinoyl proteins

Biotin was enzymatically attached *in vivo* on the recombinant *P. yoelii* biotinoyl protein in *E. coli* as shown by a peroxidase-conjugated avidin detection system. Several controls were included to ensure that the reaction between the avidin and the biotinylated proteins were specific. The distinguishing feature of the avidin-biotin detection system is the extraordinary affinity (K_a=10^{15} M^{-1}) and specificity that characterises the complex formed between biotin and avidin or streptavidin (Bayer *et al*., 1979). Peroxidase-conjugated streptavidin was the choice for detection in a recent study on the activity of *E. coli* BirA on recombinantly expressed biotinoyl protein of human acetyl-CoA carboxylase (Lee *et al*., 2008). The absence of biotin in recombinant *P. yoelii* putative copper transporter supported the specificity of the biotinylation reaction in *E. coli*. An effort made to renature the recombinant protein was successful, though cycles of freeze-thaw of the refolded protein resulted in re-precipitation of the protein.

7.6 Prediction of protein kinase phosphorylation sites on the biotin carboxylase and carboxyltransferase domains of *P. yoelii* acetyl-CoA carboxylase

Protein kinases have been shown to regulate the activity of acetyl-CoA carboxylase in yeast, and mammals. Although, the actual protein kinases involved in the "phospho-regulation" of acetyl-CoA carboxylase are yet to be established (Locke *et al*., 2008; Munday, 2002). Two algorithms designed to predict potential phosphorylation sites and the potential protein kinases identified three sites in the enzyme domains based on evolutionary conservation across several organisms. However, these sites were not identified in previous studies, which appeared to focus on phosphorylation motifs conserved in the mammalian and insect acetyl-CoA carboxylases. 5'-AMP-activated protein kinase has been shown to be involved in the regulation acetyl-CoA carboxylase and other enzymes in higher eukaryotes (Hardie and Pan, 2002). The only protein kinase found in the *Plasmodium* kinome that is similar to AMPK and SNF1 (the yeast version of AMPK) is PF14_0516, which has orthologues in other *Plasmodium* species (Personal observation). Remarkably, the expression profile of this gene (PF14_0516) is similar to the expression profile of acetyl-CoA carboxylase gene (PF14_0664). The genes encoding acetyl-CoA carboxylase and this putative protein kinase

are located on the same chromosome (chromosome-14 in *P. falciparum* and chromosome-13 in *P. yoelii*). Although this may be inconsequential, the involvement of this protein kinase in the regulation of acetyl-CoA carboxylase and other enzymes in *Plasmodium* should not be overlooked. Efforts made to recombinantly express the *P. yoelii* orthologue, PY06885 in *E. coli* and *P. pastoris* were not successful in this study.

7.7 Homology modelling of the biotinoyl and biotin carboxylase domains of *P. yoelii* acetyl-CoA carboxylase

Predicting the 3D structure of a protein by homology modelling typically proceeds in an ordered sequence of well defined steps, namely: amino acid sequence alignment between the target and the modelling template, building the preliminary model, refining the preliminary model and validating the refined model (Kopp and Schwede, 2004). Prior to this study, there were no reported crystal structures of any parasitic protozoan acetyl-CoA carboxylase. In fact, the biotinoyl domain of the human acetyl-CoA carboxylase was the first domain of the multi-domain acetyl-CoA carboxylase to be resolved by NMR (Lee *et al*., 2008), which was "in press" by the time this study was concluded. Nevertheless, reasonable inferences were made from the work by Lee *et al*. (2008). This study has revealed an insight to the likely structural conformations of biotin carboxylase and the biotinoyl protein domains of *P. yoelii* acetyl-CoA carboxylase. The amino acids within the active sites are conserved between the target and their respective templates. Model refinement and validations studies indicated that the stereochemical attributes of the residues in the models were satisfactory to make valid deductions from the predicted structures. The structure of the carboxyltransferase domain of *P. yoelii* acetyl-CoA carboxylase was not predicted for this study because the amino acid sequence does not completely align with a single PDB template. This may require more computational adjustment to model both ends of the protein to derive a single structure, similar to the study by de Matos Guedes *et al*., (2007). By and large, the predicted models showed prospects on the possibilities of extending the study towards structure-based designs to develop effective inhibitors against the enzyme for testing *in vitro* on malaria parasites.

7.8 Conclusion and future directions

A classical approach towards understanding the functions of a protein that is not established in an organism is to demonstrate that (i) the gene responsible for the expression of the protein is present in the genome (ii) the gene is transcribed into mRNA, (iii) the mRNA transcript is translated into the protein and (iv) the protein displays features common to that class of

proteins or enzymes. The first approach was established by the sequencing of the *Plasmodium* parasites genomes. This study has empirically demonstrated steps two to four, therefore confirming the ability of *P. yoelii*, and perhaps other *Plasmodium* species, to synthesise fatty acids *de novo* via acetyl-CoA carboxylase-mediated metabolic pathway. Nevertheless, further characterisation employing the native enzyme or recombinantly expressed enzyme domains (biotin carboxylase and carboxyltransferase) may be required.

Two major questions that present possible future directions about *P. yoelii* acetyl-CoA carboxylase and the prospects of targeting this enzyme for anti-plasmodial chemotherapy were raised by this study.

(1) *What is the fate of biotin in the Plasmodium parasite?* The relevance of biotin as a cofactor to several enzymes including acetyl-CoA carboxylase and transcarboxylase is evident. A BLAST study of the *Plasmodium* proteome and genome showed that biotin synthetase and biotinidase, an enzyme that recycles biotin in the mammalian system (Kothapalli *et al*., 2005; Wolf, 2005) appear not to be present (Personal observation). No *Plasmodium* proteins have been annotated for biotin transport at present. The likely explanation is that *Plasmodium* derives its biotin from the host. Previous studies stated that the only vitamin that the *Plasmodium* parasite imports is B_5 (pantothenic acid) due to its involvement with Coenzyme-A synthesis (Kirk, 2001). Establishing the fate of biotin in the parasite is important to understanding the role of acetyl-CoA carboxylase in the life cycle of the *Plasmodium* parasite. In addition, it would be useful to characterise the *Plasmodium* biotin protein ligase.

(2) *Is acetyl-CoA carboxylase a good target for anti-plasmodial chemotherapy?* One of the criteria for choosing a protein target for anti-plasmodial drug design is that the target must be relevant to the survival of the parasite (White, 2004; White *et al*., 1999). Besides, the protein must be expressed at all stages of the parasite life cycle, especially the asexual blood stage where the parasite exerts its pathological features. The expression profile of the gene that codes for acetyl-CoA carboxylase suggests that the parasite may not absolutely require the enzyme at the blood stage, but rather at the gametocyte and sporozoite stages. The importance of this enzyme in the initiation of fatty acid biosynthesis makes it a good target for chemotherapy. However, the need for acetyl-CoA carboxylase at the blood stage of the parasite life cycle needs to be investigated.

REFERENCES

Abu-Elheiga, L., Brinkley, W. R., Zhong, L., Chirala, S. S., Woldegiorgis, G. and Wakil, S. J. (2000). The subcellular localization of acetyl-CoA carboxylase 2. *Proc Natl Acad Sci U S A* **97**, 1444-9.

Abu-Elheiga, L., Jayakumar, A., Baldini, A., Chirala, S. S. and Wakil, S. J. (1995). Human acetyl-CoA carboxylase: characterization, molecular cloning, and evidence for two isoforms. *Proc Natl Acad Sci U S A* **92**, 4011-5.

Al-Feel, W., Chirala, S. S. and Wakil, S. J. (1992). Cloning of the yeast FAS3 gene and primary structure of yeast acetyl-CoA carboxylase. *Proc Natl Acad Sci U S A* **89**, 4534-8.

Al-Feel, W., DeMar, J. C. and Wakil, S. J. (2003). A Saccharomyces cerevisiae mutant strain defective in acetyl-CoA carboxylase arrests at the G2/M phase of the cell cycle. *Proc Natl Acad Sci U S A* **100**, 3095-100.

Alessi, D. R., Barry Caudwell, F., Andjelkovic, M., Hemmings, B. A. and Cohen, P. (1996). Molecular basis for the substrate specificity of protein kinase B; comparison with MAPKAP kinase-1 and p70 S6 kinase. *FEBS Lett* **399**, 333-338.

Altschul, S. F., Madden, T. L., Schäffer, A. A., Zhang, J., Zhang, Z., Miller, W. and Lipman, D. J. (1997). Gapped BLAST and PSI-BLAST: a new generation of protein database search programs. *Nucleic Acids Res* **25**, 3389-402.

AmershamBiosciences. (2002). GST Gene Fussion System: Handbook Uppsala Sweden: Amersham Biosciences.

Atha, D. H. and Ingham, K. C. (1981). Mechanism of precipitation of proteins by polyethylene glycols. Analysis in terms of excluded volume. *J Biol Chem* **256**, 12108-17.

Athappilly, F. K. and Hendrickson, W. A. (1995). Structure of the biotinyl domain of acetyl-coenzyme A carboxylase determined by MAD phasing. *Structure* **3**, 1407-19.

Baca, A. M. and Hol, W. G. J. (2000). Overcoming codon bias: A method for high-level overexpression of *Plasmodium* and other AT-rich parasite genes in Escherichia coli. *Int J Parasitol* **30**, 113-118.

Bahl, A., Brunk, B., Crabtree, J., Fraunholz, M. J., Gajria, B., Grant, G. R., Ginsburg, H., Gupta, D., Kissinger, J. C., Labo, P. *et al*. (2003). PlasmoDB: the *Plasmodium* genome resource. A database integrating experimental and computational data. *Nucleic Acids Res* **31**, 212-5.

Bairoch, A., Bucher, P. and Hofmann, K. (1997). The PROSITE database, its status in 1997. *Nucleic Acids Res* **25**, 217-21.

Balbás, P. and Bólivar, F. (1990). Design and construction of expression plasmid vectors in *Escherichia coli*. *Methods Enzymol* **185**, 14-37.

Balbás, P., Soberon, X., Merino, E., Zurita, M., Lomeli, H., Valle, F., Flores, N. and Bólivar, F. (1986). Plasmid vector pBR322 and its special-purpose derivatives-a review. *Gene* **50**, 3-40.

Banoo, S., Bell, D., Bossuyt, P., Herring, A., Mabey, D., Poole, F., Smith, P. G., Sriram, N., Wongsrichanalai, C., Linke, R. *et al*. (2006). Evaluation of diagnostic tests for infectious diseases: general principles. *Nat Rev Microbiol* **4**, S21-31.

Barber, M. C., Vallance, A. J., Kennedy, H. T. and Travers, M. T. (2003). Induction of transcripts derived from promoter III of the acetyl-CoA carboxylase-alpha gene in mammary gland is associated with recruitment of SREBP-1 to a region of the proximal promoter defined by a DNase I hypersensitive site. *Biochem J* **375**, 489-501.

Bayer, E. A., Skutelsky, E. and Wilchek, M. (1979). The avidin-biotin complex in affinity cytochemistry. *Methods Enzymol* **62**, 308-15.

Beaumelle, B. D. and Vial, H. J. (1988a). Correlation of the efficiency of fatty acid derivatives in suppressing *Plasmodium falciparum* growth in culture with their inhibitory effect on acyl-CoA synthetase activity. *Mol Biochem Parasitol* **28**, 39-42.

Beaumelle, B. D. and Vial, H. J. (1988b). Uninfected red cells from malaria-infected blood: alteration of fatty acid composition involving a serum protein: an in vivo and in vitro study. *In Vitro Cell Dev Biol* **24**, 711-8.

Beaumelle, B. D., Vial, H. J. and Bienvenue, A. (1988). Enhanced transbilayer mobility of phospholipids in malaria-infected monkey erythrocytes: a spin-label study. *J Cell Physiol* **135**, 94-100.

Beckers, A., Organe, S., Timmermans, L., Scheys, K., Peeters, A., Brusselmans, K., Verhoeven, G. and Swinnen, J. V. (2007). Chemical Inhibition of Acetyl-CoA Carboxylase Induces Growth Arrest and Cytotoxicity Selectively in Cancer Cells, vol. 67 (ed., pp. 8180-8187.

Beckett, D. (2005). The *Escherichia coli* biotin regulatory system: a transcriptional switch. *J Nutr Biochem* **16**, 411-5.

Beckett, D., Kovaleva, E. and Schatz, P. J. (1999). A minimal peptide substrate in biotin holoenzyme synthetase-catalyzed biotinylation. *Protein Sci* **8**, 921-9.

Bell, A. S. and Ranford-Cartwright, L. C. (2002). Real-time quantitative PCR in parasitology. *Trends Parasitol* **18**, 337-42.

Bell, D. and Peeling, R. W. (2006). Evaluation of rapid diagnostic tests: malaria. *Nat Rev Microbiol* **4**, S34-8.

Bell, D., Wongsrichanalai, C. and Barnwell, J. W. (2006). Ensuring quality and access for malaria diagnosis: how can it be achieved? *Nat Rev Microbiol* **4**, S7-20.

Bjelic, S. and Åqvist, J. (2004). Computational prediction of structure, substrate binding mode, mechanism, and rate for a malaria protease with a novel type of active site. *Biochemistry* **43**, 14521-8.

Blanchard, C. Z., Chapman-Smith, A., Wallace, J. C. and Waldrop, G. L. (1999a). The biotin domain peptide from the biotin carboxyl carrier protein of *Escherichia coli* acetyl-CoA carboxylase causes a marked increase in the catalytic efficiency of biotin carboxylase and carboxyltransferase relative to free biotin. *J Biol Chem* **274**, 31767-9.

Blanchard, C. Z., Lee, Y. M., Frantom, P. A. and Waldrop, G. L. (1999b). Mutations at four active site residues of biotin carboxylase abolish substrate-induced synergism by biotin. *Biochemistry* **38**, 3393-400.

Blanchard, C. Z. and Waldrop, G. L. (1998). Overexpression and kinetic characterization of the carboxyltransferase component of acetyl-CoA carboxylase. *J Biol Chem* **273**, 19140-5.

Blom, N., Gammeltoft, S. and Brunak, S. (1999). Sequence and structure-based prediction of eukaryotic protein phosphorylation sites. *J Mol Biol* **294**, 1351-1362.

Boone, A. N., Chan, A., Kulpa, J. E. and Brownsey, R. W. (2000). Bimodal activation of acetyl-CoA carboxylase by glutamate. *J Biol Chem* **275**, 10819-25.

Boone, A. N., Rodrigues, B. and Brownsey, R. W. (1999). Multiple-site phosphorylation of the 280 kDa isoform of acetyl-CoA carboxylase in rat cardiac myocytes: evidence that cAMP-dependent protein kinase mediates effects of beta-adrenergic stimulation. *Biochem J* **341 (Pt 2)**, 347-54.

Brady, R. L. and Cameron, A. (2004). Structure-based approaches to the development of novel anti-malarials. *Curr Drug Targets* **5**, 137-49.

Brasseur, P., Guiguemde, R., Diallo, S., Guiyedi, V., Kombila, M., Ringwald, P. and Olliaro, P. (1999). Amodiaquine remains effective for treating uncomplicated malaria in west and central Africa. *Trans R Soc Trop Med Hyg* **93**, 645-50.

Brinkman, F. and Weissig, H. (2001). Phylogenetic analysis. In *Bioinformatics: A practical guide to the analysis of genes and protein* (ed. A. Baxevanis and B. Ouellette), pp. 323-357. Toronto: Wiley-Interscience.

Brown, W. M., Yowell, C. A., Hoard, A., Vander Jagt, T. A., Hunsaker, L. A., Deck, L. M., Royer, R. E., Piper, R. C., Dame, J. B., Makler, M. T. *et al.* (2004). Comparative structural analysis and kinetic properties of lactate dehydrogenases from the four species of human malarial parasites. *Biochemistry* **43**, 6219-29.

Brownsey, R. W., Boone, A. N., Elliott, J. E., Kulpa, J. E. and Lee, W. M. (2006). Regulation of acetyl-CoA carboxylase. *Biochem Soc Trans* **34**, 223-7.

Carlton, J. M., Angiuoli, S. V., Suh, B. B., Kooij, T. W., Pertea, M., Silva, J. C., Ermolaeva, M. D., Allen, J. E., Selengut, J. D., Koo, H. L. *et al.* (2002). Genome sequence and comparative analysis of the model rodent malaria parasite *Plasmodium yoelii yoelii*. *Nature* **419**, 512-9.

Carlton, J. M., Fidock, D. A., Djimde, A., Plowe, C. V. and Wellems, T. E. (2001). Conservation of a novel vacuolar transporter in *Plasmodium* species and its central role in chloroquine resistance of *P. falciparum*. *Curr Opin Microbiol* **4**, 415-20.

Cármenes, R. S., Freije, J. P., Molina, M. M. and Martín, J. M. (1989). Predict7, a program for protein structure prediction. *Biochem Biophys Res Commun* **159**, 687-693.

Carter, K. C., Phillips, R. S. and Roberts, C. W. (1998). Protozoan Parasites: Familiar Faces, New Directions. *Parasitol Today* **14**, 341-342.

Chapman-Smith, A. and Cronan, J. E., Jr. (1999a). The enzymatic biotinylation of proteins: a post-translational modification of exceptional specificity. *Trends Biochem Sci* **24**, 359-63.

Chapman-Smith, A. and Cronan, J. E., Jr. (1999b). In vivo enzymatic protein biotinylation. *Biomol Eng* **16**, 119-25.

Chapman-Smith, A. and Cronan, J. E., Jr. (1999c). Molecular biology of biotin attachment to proteins. *J Nutr* **129**, 477S-484S.

Chapman-Smith, A., Morris, T. W., Wallace, J. C. and Cronan, J. E., Jr. (1999). Molecular recognition in a post-translational modification of exceptional specificity. Mutants of the biotinylated domain of acetyl-CoA carboxylase defective in recognition by biotin protein ligase. *J Biol Chem* **274**, 1449-57.

Chapman-Smith, A., Mulhern, T. D., Whelan, F., Cronan, J. E., Jr. and Wallace, J. C. (2001). The C-terminal domain of biotin protein ligase from *E. coli* is required for catalytic activity. *Protein Sci* **10**, 2608-17.

Chapman-Smith, A., Turner, D. L., Cronan, J. E., Jr., Morris, T. W. and Wallace, J. C. (1994). Expression, biotinylation and purification of a biotin-domain peptide from the biotin carboxy carrier protein of *Escherichia coli* acetyl-CoA carboxylase. *Biochem J* **302 (Pt 3)**, 881-7.

Chiodini, P. L., Bowers, K., Jorgensen, P., Barnwell, J. W., Grady, K. K., Luchavez, J., Moody, A. H., Cenizal, A. and Bell, D. (2007). The heat stability of Plasmodium lactate dehydrogenase-based and histidine-rich protein 2-based malaria rapid diagnostic tests. *Trans R Soc Trop Med Hyg* **101**, 331-7.

Chothia, C. and Lesk, A. M. (1986). The relation between the divergence of sequence and structure in proteins. *Embo J* **5**, 823-6.

Choubey, V., Guha, M., Maity, P., Kumar, S., Raghunandan, R., Maulik, P. R., Mitra, K., Halder, U. C. and Bandyopadhyay, U. (2006). Molecular characterization and localization of *Plasmodium falciparum* choline kinase. *Biochim Biophys Acta* **1760**, 1027-38.

Chun, P. W., Fried, M. and Ellis, E. F. (1967). Use of water-soluble polymers for the isolation and purification of human immunoglobulins. *Anal Biochem* **19**, 481-97.

Coleman, R. E., Sattabongkot, J., Promstaporm, S., Maneechai, N., Tippayachai, B., Kengluecha, A., Rachapaew, N., Zollner, G., Miller, R. S., Vaughan, J. A. *et al*. (2006). Comparison of PCR and microscopy for the detection of asymptomatic malaria in a *Plasmodium falciparum*/*vivax* endemic area in Thailand. *Malar J* **5**, 121.

Cronan, J. E., Jr. (2001). The biotinyl domain of *Escherichia coli* acetyl-CoA carboxylase. Evidence that the "thumb" structure id essential and that the domain functions as a dimer. *J Biol Chem* **276**, 37355-64.

Cronan, J. E., Jr. (2002). Interchangeable enzyme modules. Functional replacement of the essential linker of the biotinylated subunit of acetyl-CoA carboxylase with a linker from the lipoylated subunit of pyruvate dehydrogenase. *J Biol Chem* **277**, 22520-7.

Cronan, J. E., Jr. and Waldrop, G. L. (2002). Multi-subunit acetyl-CoA carboxylases. *Prog Lipid Res* **41**, 407-35.

Curtis, C. and Mnzava, A. (2000). Comparison of house spraying and insceticide-treated nets for malaria control. *Bulletin of the World Health Organization* **78**, 1389-1393.

Daily, J. P., Scanfeld, D., Pochet, N., Le Roch, K., Plouffe, D., Kamal, M., Sarr, O., Mboup, S., Ndir, O., Wypij, D. *et al*. (2007). Distinct physiological states of *Plasmodium falciparum* in malaria-infected patients. *Nature* **450**, 1091-5.

Dame, J. B. and McCutchan, T. F. (1983). Cloning and characterization of a ribosomal RNA gene from *Plasmodium berghei*. *Mol Biochem Parasitol* **8**, 263-79.

Davies, A., Meeran, K., Cairns, M. T. and Baldwin, S. A. (1987). Peptide-specific antibodies as probes of the orientation of the glucose transporter in the human erythrocyte membrane. *J Biol Chem* **262**, 9347-52.

Davies, S. P., Sim, A. T. and Hardie, D. G. (1990). Location and function of three sites phosphorylated on rat acetyl-CoA carboxylase by the AMP-activated protein kinase. *Eur J Biochem* **187**, 183-90.

Davis, M. S., Solbiati, J. and Cronan, J. E., Jr. (2000). Overproduction of acetyl-CoA carboxylase activity increases the rate of fatty acid biosynthesis in Escherichia coli. *J Biol Chem* **275**, 28593-8.

de Castro, E., Sigrist, C. J., Gattiker, A., Bulliard, V., Langendijk-Genevaux, P. S., Gasteiger, E., Bairoch, A. and Hulo, N. (2006). ScanProsite: detection of PROSITE signature matches and ProRule-associated functional and structural residues in proteins. *Nucleic Acids Res* **34**, W362-5.

de Matos Guedes, H. L., Carneiro, M. P., Gomes, D. C., Rossi-Bergmanmn, B. and Giovanni de Simone, S. (2007). Oligopeptidase B from *L. amazonensis*: molecular cloning, gene expression analysis and molecular model. *Parasitol Res* **101**, 853-63.

Deng, W. and Baker, D. A. (2002). A novel cyclic GMP-dependent protein kinase is expressed in the ring stage of the *Plasmodium falciparum* life cycle. *Mol Microbiol* **44**, 1141-51.

Di Girolamo, F., Raggi, C., Bultrini, E., Lanfrancotti, A., Silvestrini, F., Sargiacomo, M., Birago, C., Pizzi, E., Alano, P. and Ponzi, M. (2005). Functional genomics, new tools in malaria research. *Ann Ist Super Sanita* **41**, 469-77.

Diaz, C. A., Allocco, J., Powles, M. A., Yeung, L., Donald, R. G., Anderson, J. W. and Liberator, P. A. (2006). Characterization of *Plasmodium falciparum* cGMP-dependent protein kinase (PfPKG): antiparasitic activity of a PKG inhibitor. *Mol Biochem Parasitol* **146**, 78-88.

Dorin, D., Alano, P., Boccaccio, I., Ciceron, L., Doerig, C., Sulpice, R., Parzy, D. and Doerig, C. (1999). An atypical mitogen-activated protein kinase (MAPK) homologue expressed in gametocytes of the human malaria parasite *Plasmodium falciparum*. Identification of a MAPK signature. *J Biol Chem* **274**, 29912-20.

Dorin, D., Semblat, J. P., Poullet, P., Alano, P., Goldring, J. P., Whittle, C., Patterson, S., Chakrabarti, D. and Doerig, C. (2005). PfPK7, an atypical MEK-related protein kinase, reflects the absence of classical three-component MAPK pathways in the human malaria parasite Plasmodium falciparum. *Mol Microbiol* **55**, 184-96.

Doytchinova, I. A., Guan, P. and Flower, D. R. (2006). EpiJen: a server for multistep T cell epitope prediction. *BMC Bioinformatics* **7**, 131.

Dyson, H. J. and Wright, P. E. (1995). Antigenic peptides. *Faseb J* **9**, 37-42.

Emini, E. A., Schleif, W. A., Jameson, B. A. and Wimmer, E. (1985). The immune response to poliovirus-specific synthetic peptides: effects of adjuvants and test animal species. *J Virol Methods* **10**, 163-70.

Erhard, M. and Schade, R. (2001). Short introduction to hen's humoral immune system. In *Chicken egg yolk antibodies,* (ed. R. Schade I. Behn M. Erhard A. Hlinak and C. Staak). Berlin: Springer-Verlag.

Falquet, L., Pagni, M., Bucher, P., Hulo, N., Sigrist, C. J., Hofmann, K. and Bairoch, A. (2002). The PROSITE database, its status in 2002. *Nucleic Acids Res* **30**, 235-8.

Färber, P. M., Arscott, L. D., Williams, C. H., Becker, K. and Schirmer, R. H. (1998). Recombinant *Plasmodium falciparum* glutathione reductase is inhibited by the antimalarial dye methylene blue. *FEBS Letters* **422**, 311-314.

Feinberg, A. P. and Vogelstein, B. (1983). A technique for radiolabeling DNA restriction endonuclease fragments to high specific activity. *Anal Biochem* **132**, 6-13.

Felsenstein, J. (1985). Confidence Limits on Phylogenies: An Approach Using the Bootstrap, vol. 39 (ed., pp. 783-791: Society for the Study of Evolution.

Fermentas. (2006). Molecular Biology Catalogue & Product Application Guide.

Flick, K., Ahuja, S., Chene, A., Bejarano, M. T. and Chen, Q. (2004). Optimized expression of *Plasmodium falciparum* erythrocyte membrane protein 1 domains in Escherichia coli. *Malar J* **3**, 50.

Flower, D. R. (2003). Towards in silico prediction of immunogenic epitopes. *Trends Immunol* **24**, 667-74.

Fontana, A., Zambonin, M., Polverino de Laureto, P., De Filippis, V., Clementi, A. and Scaramella, E. (1997). Probing the conformational state of apomyoglobin by limited proteolysis. *J Mol Biol* **266**, 223-230.

Galperin, M. Y. and Koonin, E. V. (1997). A diverse superfamily of enzymes with ATP-dependent carboxylate-amine/thiol ligase activity. *Protein Sci* **6**, 2639-43.

Gardner, M. J. (1999). The genome of the malaria parasite. *Curr Opin Genet Dev* **9**, 704-8.

Gardner, M. J., Hall, N., Fung, E., White, O., Berriman, M., Hyman, R. W., Carlton, J. M., Pain, A., Nelson, K. E., Bowman, S. *et al.* (2002a). Genome sequence of the human malaria parasite Plasmodium falciparum. *Nature* **419**, 498-511.

Gardner, M. J., Shallom, S. J., Carlton, J. M., Salzberg, S. L., Nene, V., Shoaibi, A., Ciecko, A., Lynn, J., Rizzo, M., Weaver, B. *et al.* (2002b). Sequence of *Plasmodium falciparum* chromosomes 2, 10, 11 and 14. *Nature* **419**, 531-4.

Gasteiger, E., Hoogland, C., Gattiker, A., Duvaud, S., Wilkins, M., RD, A. and Bairoch, A. (2005). Protein identification and analysis toos on expasy server. In *The proteomics protocols handbook,* (ed. J. Walker), pp. 571-607: Humana Press.

Gattiker, A., Gasteiger, E. and Bairoch, A. (2002). ScanProsite: a reference implementation of a PROSITE scanning tool. *Appl Bioinformatics* **1**, 107-8.

Gilles, H. (1997). Pathology of Malaria. In *Handbook of malaria infection in the tropics*, vol. 15 (ed. G. Carosi and F. Castelli), pp. 73-78. Bologna: Organizzazione per la Cooperazione Sanitaria Internazionale.

Ginsburg, H. (2006). Progress in in silico functional genomics: the malaria Metabolic Pathways database. *Trends Parasitol* **22**, 238-40.

Gleeson, M. T. (2000). The plastid in Apicomplexa: what use is it? *Int J Parasitol* **30**, 1053-70.

Goldring, J. and Coetzer, T. (2003). Isolation of Chicken Immunoglobulins (IgY) from Egg Yolk. *Biochemistry and Molecular Biology Education* **31**, 185-187.

Goldring, J. D., Padayachee, T. and Ismail, I. (1999). *Plasmodium falciparum* malaria: rosettes are disrupted by quinine, artemisinin, mefloquine, primaquine, pyrimethamine, chloroquine and proguanil. *Mem Inst Oswaldo Cruz* **94**, 667-74.

Goldring, J. P. and Nemaorani, S. (1999). Antimalarial drugs modulate the expression of monocyte receptors. *Int J Immunopharmacol* **21**, 599-607.

Gornicki, P. (2003). Apicoplast fatty acid biosynthesis as a target for medical intervention in apicomplexan parasites. *Int J Parasitol* **33**, 885-96.

Gornicki, P. and Haselkorn, R. (1993). Wheat acetyl-CoA carboxylase. *Plant Mol Biol* **22**, 547-52.

Goss, N. H. and Wood, H. G. (1984). Formation of N epsilon-(biotinyl)lysine in biotin enzymes. *Methods Enzymol* **107**, 261-78.

Gregson, A. and Plowe, C. V. (2005). Mechanisms of resistance of malaria parasites to antifolates. *Pharmacol Rev* **57**, 117-45.

Günther, S., Wallace, L., Patzewitz, E. M., McMillan, P. J., Storm, J., Wrenger, C., Bissett, R., Smith, T. K. and Muller, S. (2007). Apicoplast Lipoic Acid Protein Ligase B Is Not Essential for *Plasmodium falciparum*. *PLoS Pathog* **3**, e189.

Ha, J., Lee, J. K., Kim, K. S., Witters, L. A. and Kim, K. H. (1996). Cloning of human acetyl-CoA carboxylase-beta and its unique features. *Proc Natl Acad Sci U S A* **93**, 11466-70.

Hamilton, S. R., O'Donnell, J. B., Jr., Hammet, A., Stapleton, D., Habinowski, S. A., Means, A. R., Kemp, B. E. and Witters, L. A. (2002). AMP-activated protein kinase kinase: detection with recombinant AMPK alpha1 subunit. *Biochem Biophys Res Commun* **293**, 892-8.

Hammarton, T. C., Mottram, J. C. and Doerig, C. (2003). The cell cycle of parasitic protozoa: potential for chemotherapeutic exploitation. *Prog Cell Cycle Res* **5**, 91-101.

Hanada, K., Palacpac, N. M., Magistrado, P. A., Kurokawa, K., Rai, G., Sakata, D., Hara, T., Horii, T., Nishijima, M. and Mitamura, T. (2002). Plasmodium falciparum phospholipase C hydrolyzing sphingomyelin and lysocholinephospholipids is a possible target for malaria chemotherapy. *J Exp Med* **195**, 23-34.

Hardie, D. G. (2003). Minireview: the AMP-activated protein kinase cascade: the key sensor of cellular energy status. *Endocrinology* **144**, 5179-83.

Hardie, D. G., Carling, D. and Carlson, M. (1998). The AMP-activated/SNF1 protein kinase subfamily: metabolic sensors of the eukaryotic cell? *Annu Rev Biochem* **67**, 821-55.

Hardie, D. G. and Pan, D. A. (2002). Regulation of fatty acid synthesis and oxidation by the AMP-activated protein kinase. *Biochem Soc Trans* **30**, 1064-70.

Harlow, E. and Lane, D. (1988). Antibodies: A Laboratory Manual, pp. 353-355. New York: Cold Spring Habour.

Hasan, G., Turner, M. J. and Cordingley, J. S. (1982). Ribosomal RNA genes of Trypanosoma brucei. Cloning of a rRNA gene containing a mobile element. *Nucleic Acids Res* **10**, 6747-61.

Hasslacher, M., Ivessa, A. S., Paltauf, F. and Kohlwein, S. D. (1993). Acetyl-CoA carboxylase from yeast is an essential enzyme and is regulated by factors that control phospholipid metabolism. *J Biol Chem* **268**, 10946-52.

Hermanson, G. (1996). Bioconjugate Techniques. California: Academic Press.

Hoffman, S. L., Rogers, W. O., Carucci, D. J. and Venter, J. C. (1998). From genomics to vaccines: malaria as a model system. *Nat Med* **4**, 1351-3.

Holland, I. and Blight, A. (1999). ABC-ATPases, adaptable energy generators fuelling transmembrane movement of a variety of molecules in organisms from bacteria to humans. *J Mol Biol* **293**, 381-399.

Holtz, G. (1977). Lipids and the malaria parasite. *Bulletin of the World Health Organization* **55**, 237-248.

Hopp, T. P. and Woods, K. R. (1981). Prediction of protein antigenic determinants from amino acid sequences. *Proc Natl Acad Sci U S A* **78**, 3824-8.

Hopwood, D. A. and Sherman, D. H. (1990). Molecular genetics of polyketides and its comparison to fatty acid biosynthesis. *Annu Rev Genet* **24**, 37-66.

Hulo, N., Bairoch, A., Bulliard, V., Cerutti, L., De Castro, E., Langendijk-Genevaux, P. S., Pagni, M. and Sigrist, C. J. (2006). The PROSITE database. *Nucleic Acids Res* **34**, D227-30.

Hunt, N. H., Golenser, J., Chan-Ling, T., Parekh, S., Rae, C., Potter, S., Medana, I. M., Miu, J. and Ball, H. J. (2006). Immunopathogenesis of cerebral malaria. *Int J Parasitol* **36**, 569-582.

Ingham, K. C. (1984). Protein precipitation with polyethylene glycol. *Methods Enzymol* **104**, 351-6.

Iritani, N. (1992). Nutritional and hormonal regulation of lipogenic-enzyme gene expression in rat liver. *Eur J Biochem* **205**, 433-42.

Javid-Majd, F., Stapleton, M. A., Harmon, M. F., Hanks, B. A., Mullins, L. S. and Raushel, F. M. (1996). Comparison of the functional differences for the homologous residues within the carboxy phosphate and carbamate domains of carbamoyl phosphate synthetase. *Biochemistry* **35**, 14362-9.

Jelenska, J., Crawford, M. J., Harb, O. S., Zuther, E., Haselkorn, R., Roos, D. S. and Gornicki, P. (2001). Subcellular localization of acetyl-CoA carboxylase in the apicomplexan parasite *Toxoplasma gondii*. *Proc Natl Acad Sci U S A* **98**, 2723-8.

Jelenska, J., Sirikhachornkit, A., Haselkorn, R. and Gornicki, P. (2002). The carboxyltransferase activity of the apicoplast acetyl-CoA carboxylase of Toxoplasma gondii is the target of aryloxyphenoxypropionate inhibitors. *J Biol Chem* **277**, 23208-15.

Johnson, D. R., Knoll, L. J., Levin, D. E. and Gordon, J. I. (1994). *Saccharomyces cerevisiae* contains four fatty acid activation (FAA) genes: an assessment of their role in regulating protein N-myristoylation and cellular lipid metabolism. *J Cell Biol* **127**, 751-62.

Jones, G., Willett, P., Glen, R. C., Leach, A. R. and Taylor, R. (1997). Development and validation of a genetic algorithm for flexible docking. *J Mol Biol* **267**, 727-48.

Joshi, S., Singh, A. R., Kumar, A., Misra, P. C., Siddiqi, M. I. and Saxena, J. K. (2008). Molecular cloning and characterization of *Plasmodium falciparum* transketolase. *Mol Biochem Parasitol* **160**, 32-41.

Kaiser, K., Matuschewski, K., Camargo, N., Ross, J. and Kappe, S. H. (2004). Differential transcriptome profiling identifies *Plasmodium* genes encoding pre-erythrocytic stage-specific proteins. *Mol Microbiol* **51**, 1221-32.

Ke, J., Behal, R. H., Back, S. L., Nikolau, B. J., Wurtele, E. S. and Oliver, D. J. (2000a). The role of pyruvate dehydrogenase and acetyl-coenzyme A synthetase in fatty acid synthesis in developing *Arabidopsis* seeds. *Plant Physiol* **123**, 497-508.

Ke, J., Wen, T. N., Nikolau, B. J. and Wurtele, E. S. (2000b). Coordinate regulation of the nuclear and plastidic genes coding for the subunits of the heteromeric acetyl-coenzyme A carboxylase. *Plant Physiol* **122**, 1057-71.

Keenan, S. M. and Welsh, W. J. (2004). Characteristics of the *Plasmodium falciparum* PK5 ATP-binding site: implications for the design of novel antimalarial agents. *J Mol Graph Model* **22**, 241-7.

Kim, K. W., Yamane, H., Zondlo, J., Busby, J. and Wang, M. (2007). Expression, purification, and characterization of human acetyl-CoA carboxylase 2. *Protein Expr Purif* **53**, 16-23.

Kirk, K. (2001). Membrane transport in the malaria-infected erythrocyte. *Physiol Rev* **81**, 495-537.

Kleiger, G., Beamer, L. J., Grothe, R., Mallick, P. and Eisenberg, D. (2000). The 1.7 Å crystal structure of BPI: a study of how two dissimilar amino acid sequences can adopt the same fold. *J Mol Biol* **299**, 1019-1034.

Kleiger, G. and Eisenberg, D. (2002). GXXXG and GXXXA motifs stabilize FAD and NAD(P)-binding Rossmann folds through C^{α}-H... O hydrogen bonds and van der waals interactions. *J Mol Biol* **323**, 69-76.

Kleiger, G., Grothe, R., Mallick, P. and Eisenberg, D. (2002). GXXXG and AXXXA: common alpha-helical interaction motifs in proteins, particularly in extremophiles. *Biochemistry* **41**, 5990-7.

Kleywegt, G. J. (1997). Validation of protein models from C^{α} coordinates alone. *J Mol Biol* **273**, 371-6.

Kleywegt, G. J. and Jones, T. A. (1996). Phi/psi-chology: Ramachandran revisited. *Structure* **4**, 1395-400.

Knowles, J. R. (1989). The mechanism of biotin-dependent enzymes. *Annu Rev Biochem* **58**, 195-221.

Knudsen, B. and Miyamoto, M. M. (2001). A likelihood ratio test for evolutionary rate shifts and functional divergence among proteins. *Proc Natl Acad Sci U S A* **98**, 14512-7.

Konishi, T., Shinohara, K., Yamada, K. and Sasaki, Y. (1996). Acetyl-CoA carboxylase in higher plants: most plants other than gramineae have both the prokaryotic and the eukaryotic forms of this enzyme. *Plant Cell Physiol* **37**, 117-22.

Kooij, T. W., Janse, C. J. and Waters, A. P. (2006). *Plasmodium* post-genomics: better the bug you know? *Nat Rev Microbiol* **4**, 344-57.

Kopp, J. and Schwede, T. (2004). The SWISS-MODEL Repository of annotated three-dimensional protein structure homology models. *Nucleic Acids Res* **32**, D230-4.

Kothapalli, N., Camporeale, G., Kueh, A., Chew, Y. C., Oommen, A. M., Griffin, J. B. and Zempleni, J. (2005). Biological functions of biotinylated histones. *J Nutr Biochem* **16**, 446-8.

Kricka, L. J. and Thorpe, G. H. (1986a). Enhanced chemiluminescent enzyme immunoassays. *Parasitol Today* **2**, 123-5.

Kricka, L. J. and Thorpe, G. H. (1986b). Photographic detection of chemiluminescent and bioluminescent reactions. *Methods Enzymol* **133**, 404-20.

Lack, G., Homberger-Zizzari, E., Folkers, G., Scapozza, L. and Perozzo, R. (2006). Recombinant expression and biochemical characterization of the unique elongating beta-ketoacyl-acyl carrier protein synthase involved in fatty acid biosynthesis of *Plasmodium falciparum* using natural and artificial substrates. *J Biol Chem* **281**, 9538-46.

Laemmli, U. K. (1970). Cleavage of structural proteins during the assembly of the head of bacteriophage T4. *Nature* **227**, 680-5.

Lanier, W., Moustafa, A., Bhattacharya, D. and Comeron, J. M. (2008). EST Analysis of *Ostreococcus lucimarinus*, the Most Compact Eukaryotic Genome, Shows an Excess of Introns in Highly Expressed Genes. *PLoS ONE* **3**, e2171.

Larsson, A. and Sjöquist, J. (1988). Chicken antibodies: a tool to avoid false positive results by rheumatoid factor in latex fixation tests. *J Immunol Methods* **108**, 205-8.

Larsson, A. and Sjöquist, J. (1990). Chicken IgY: utilizing the evolutionary difference. *Comp Immunol Microbiol Infect Dis* **13**, 199-201.

Laskowski, R. A., Rullmannn, J. A., MacArthur, M. W., Kaptein, R. and Thornton, J. M. (1996). AQUA and PROCHECK-NMR: programs for checking the quality of protein structures solved by NMR. *J Biomol NMR* **8**, 477-86.

Lauer, S. A., Ghori, N. and Haldar, K. (1995). Sphingolipid synthesis as a target for chemotherapy against malaria parasites. *Proc Natl Acad Sci U S A* **92**, 9181-5.

Le Roch, K. G., Johnson, J. R., Florens, L., Zhou, Y., Santrosyan, A., Grainger, M., Yan, S. F., Williamson, K. C., Holder, A. A., Carucci, D. J. *et al.* (2004). Global analysis of transcript and protein levels across the Plasmodium falciparum life cycle. *Genome Res* **14**, 2308-18.

Le Roch, K. G., Zhou, Y., Blair, P. L., Grainger, M., Moch, J. K., Haynes, J. D., De La Vega, P., Holder, A. A., Batalov, S., Carucci, D. J. *et al.* (2003). Discovery of gene function by expression profiling of the malaria parasite life cycle. *Science* **301**, 1503-8.

Lee, C. K., Cheong, H. K., Ryu, K. S., Lee, J. I., Lee, W., Jeon, Y. H. and Cheong, C. (2008). Biotinoyl domain of human acetyl-CoA carboxylase: Structural insights into the carboxyl transfer mechanism. *Proteins*.

Lesk, A. M. (1997). Extraction of well-fitting substructures: root-mean-square deviation and the difference distance matrix. *Fold Des* **2**, S12-4.

Li, Y. Q., Sueda, S., Kondo, H. and Kawarabayasi, Y. (2006). A unique biotin carboxyl carrier protein in archaeon *Sulfolobus tokodaii*. *FEBS Lett* **580**, 1536-40.

Locke, G. A., Cheng, D., Witmer, M. R., Tamura, J. K., Haque, T., Carney, R. F., Rendina, A. R. and Marcinkeviciene, J. (2008). Differential activation of recombinant human acetyl-CoA carboxylases 1 and 2 by citrate. *Arch Biochem Biophys* **475**, 72-79.

Lopez-Casillas, F., Luo, X. C., Kong, I. S. and Kim, K. H. (1989). Characterization of different forms of rat mammary gland acetyl-coenzyme A carboxylase mRNA: analysis of heterogeneity in the 5' end. *Gene* **83**, 311-9.

Lu, J. Z., Lee, P. J., Waters, N. C. and Prigge, S. T. (2005). Fatty Acid synthesis as a target for antimalarial drug discovery. *Comb Chem High Throughput Screen* **8**, 15-26.

Luo, X. C., Park, K., Lopez-Casillas, F. and Kim, K. H. (1989). Structural features of the acetyl-CoA carboxylase gene: mechanisms for the generation of mRNAs with 5' end heterogeneity. *Proc Natl Acad Sci U S A* **86**, 4042-6.

Macreadie, I., Ginsburg, H., Sirawaraporn, W. and Tilley, L. (2000). Antimalarial drug development and new targets. *Parasitol Today* **16**, 438-44.

Maegraith, B. (1968). Liver involvement in acute mammalian malaria: with special reference to *Plasmodium knowlesi*. In *Advances in Parasitology*, vol. 6 (ed. B. Dawes), pp. 89-127. London: Academic Press.

Makrides, S. C. (1996). Strategies for achieving high-level expression of genes in *Escherichia coli*. *Microbiol Rev* **60**, 512-38.

Mao, J., Chirala, S. S. and Wakil, S. J. (2003). Human acetyl-CoA carboxylase 1 gene: presence of three promoters and heterogeneity at the 5'-untranslated mRNA region. *Proc Natl Acad Sci U S A* **100**, 7515-20.

Matteelli, A., Castelli, F. and Caligaris, S. (1997). Life Cycle of malaria parasites. In *Handbook of malaria infection in the tropics*, vol. 15 (ed. G. Carosi and F. Castelli), pp. 17-24. Bologna: Associazione Italiana "Amici di R. Follereau" Organizzazione per la Cooperazione Sanitaria Internazionale.

Mattei, D. and Scherf, A. (1992a). The Pf332 gene codes for a megadalton protein of *Plasmodium falciparum* asexual blood stages. *Mem Inst Oswaldo Cruz* **87 Suppl 3**, 163-8.

Mattei, D. and Scherf, A. (1992b). The Pf332 gene of *Plasmodium falciparum* codes for a giant protein that is translocated from the parasite to the membrane of infected erythrocytes. *Gene* **110**, 71-9.

McCarthy, A. D., Dean Goldring, J. P. and Grahame Hardie, D. (1983). Evidence that the multifunctional polypeptides of vertebrate and fungal fatty acid synthases have arisen by independent gene fusion events. *FEBS Lett* **162**, 300-304.

McCutchan, T. F., de la Cruz, V. F., Lal, A. A., Gunderson, J. H., Elwood, H. J. and Sogin, M. L. (1988). Primary sequences of two small subunit ribosomal RNA genes from *Plasmodium falciparum*. *Mol Biochem Parasitol* **28**, 63-8.

McCutchan, T. F., Li, J., McConkey, G. A., Rogers, M. J. and Waters, A. P. (1995). The cytoplasmic ribosomal RNAs of *Plasmodium* spp. *Parasitol Today* **11**, 134-8.

McGarry, J. D. (2002). Banting lecture 2001: dysregulation of fatty acid metabolism in the etiology of type 2 diabetes. *Diabetes* **51**, 7-18.

McKean, P. (2002). New hope for the neglected diseases. *Microbiology TodayMicrobiology Today* **29**, 129-131.

Mehlin, C., Boni, E., Buckner, F. S., Engel, L., Feist, T., Gelb, M. H., Haji, L., Kim, D., Liu, C., Mueller, N. *et al.* (2006). Heterologous expression of proteins from *Plasmodium falciparum*: results from 1000 genes. *Mol Biochem Parasitol* **148**, 144-60.

Meis, J. and Verhave, J. (1988). Erythrocytic development of malaria parasite. In *Advances in Parasitology*, vol. 27 (ed. J. Baker and R. Muller), pp. 1-50. London: Academic Press.

Melo, F. and Feytmans, E. (1998). Assessing protein structures with a non-local atomic interaction energy. *J Mol Biol* **277**, 1141-52.

Menard, R. (2007). Apicomplexa research. *Current Opinion in Microbiology* **10**, 346-348.

Mens, P. F., Schoone, G. J., Kager, P. A. and Schallig, H. D. (2006). Detection and identification of human *Plasmodium* species with real-time quantitative nucleic acid sequence-based amplification. *Malar J* **5**, 80.

Menting, J. G., Tilley, L., Deady, L. W., Ng, K., Simpson, R. J., Cowman, A. F. and Foley, M. (1997). The antimalarial drug, chloroquine, interacts with lactate dehydrogenase from *Plasmodium falciparum*. *Mol Biochem Parasitol* **88**, 215-24.

Merckx, A., Le Roch, K., Nivez, M. P., Dorin, D., Alano, P., Gutierrez, G. J., Nebreda, A. R., Goldring, D., Whittle, C., Patterson, S. *et al.* (2003). Identification and initial characterization of three novel cyclin-related proteins of the human malaria parasite *Plasmodium falciparum*. *J Biol Chem* **278**, 39839-50.

Militello, K. T., Dodge, M., Bethke, L. and Wirth, D. F. (2004). Identification of regulatory elements in the *Plasmodium falciparum* genome. *Mol Biochem Parasitol* **134**, 75-88.

Mitamura, T. and Palacpac, N. M. (2003). Lipid metabolism in Plasmodium falciparum-infected erythrocytes: possible new targets for malaria chemotherapy. *Microbes Infect* **5**, 545-52.

Moll, G. N., Vial, H. J., Ancelin, M. L., Op den Kamp, J. A., Roelofsen, B. and van Deenen, L. L. (1988). Phospholipid uptake by Plasmodium knowlesi infected erythrocytes. *FEBS Lett* **232**, 341-6.

Moll, G. N., Vial, H. J., Bevers, E. M., Ancelin, M. L., Roelofsen, B., Comfurius, P., Slotboom, A. J., Zwaal, R. F., Op den Kamp, J. A. and van Deenen, L. L. (1990). Phospholipid asymmetry in the plasma membrane of malaria infected erythrocytes. *Biochem Cell Biol* **68**, 579-85.

Monti, D., Vodopivec, B., Basilico, N., Olliaro, P. and Taramelli, D. (1999). A novel endogenous antimalarial: Fe(II)-protoporphyrin IX alpha (heme) inhibits hematin polymerization to beta-hematin (malaria pigment) and kills malaria parasites. *Biochemistry* **38**, 8858-63.

Moody, A. (2002). Rapid diagnostic tests for malaria parasites. *Clin Microbiol Rev* **15**, 66-78.

Moody, A. H. and Chiodini, P. L. (2002). Non-microscopic method for malaria diagnosis using OptiMAL IT, a second-generation dipstick for malaria pLDH antigen detection. *Br J Biomed Sci* **59**, 228-31.

Moule, S. K., Edgell, N. J., Borthwick, A. C. and Denton, R. M. (1992). Coenzyme A is a potent inhibitor of acetyl-CoA carboxylase from rat epididymal fat-pads. *Biochem J* **283 (Pt 1)**, 35-8.

Mulder, N. J., Apweiler, R., Attwood, T. K., Bairoch, A., Bateman, A., Binns, D., Biswas, M., Bradley, P., Bork, P., Bucher, P. *et al*. (2002). InterPro: an integrated documentation resource for protein families, domains and functional sites. *Brief Bioinform* **3**, 225-35.

Muller, S. (1988). Peptide-carrier conjugation. In *Synthetic peptides as antigens*, vol. 19 (ed. R. Burdon and P. Van Knippenberg), pp. 131-141. Amsterdam: Elservier.

Muller, S. and Kappes, B. (2007). Vitamin and cofactor biosynthesis pathways in *Plasmodium* and other apicomplexan parasites. *Trends Parasitol* **23**, 112-21.

Munday, M. R. (2002). Regulation of mammalian acetyl-CoA carboxylase. *Biochem Soc Trans* **30**, 1059-64.

Nagata, T., Uchijima, M., Yoshida, A., Kawashima, M. and Koide, Y. (1999). Codon optimization effect on translational efficiency of DNA vaccine in mammalian cells: analysis of plasmid DNA encoding a CTL epitope derived from microorganisms. *Biochem Biophys Res Commun* **261**, 445-51.

Naimski, P., Bierzynski, A. and Fikus, M. (1980). Quantitative fluorescent analysis of different conformational forms of DNA bound to the Dye, 4',6-diamidine-2-phenylindole, and separated by gel electrophoresis. *Anal Biochem* **106**, 471-5.

Nakamura, R., Voller, A. and Bidwell, D. (1986). Enzyme immuno assays: heterogenous and homogenous systems. In *Handbook of experimental immunology*, vol. 1 (ed. D. Weir L. Herzenberg and C. Blackwell): Blackwell Scientific Publications.

Narum, D. L., Kumar, S., Rogers, W. O., Fuhrmann, S. R., Liang, H., Oakley, M., Taye, A., Sim, B. K. and Hoffman, S. L. (2001). Codon optimization of gene fragments encoding *Plasmodium falciparum* merzoite proteins enhances DNA vaccine protein expression and immunogenicity in mice. *Infect Immun* **69**, 7250-3.

Nunes, M. C., Goldring, J. P., Doerig, C. and Scherf, A. (2007). A novel protein kinase family in *Plasmodium falciparum* is differentially transcribed and secreted to various cellular compartments of the host cell. *Mol Microbiol* **63**, 391-403.

Obata, T., Yaffe, M. B., Leparc, G. G., Piro, E. T., Maegawa, H., Kashiwagi, A., Kikkawa, R. and Cantley, L. C. (2000). Peptide and Protein Library Screening Defines Optimal Substrate Motifs for AKT/PKB, vol. 275 (ed., pp. 36108-36115.

Ohlrogge, J., Pollard, M., Bao, X., Focke, M., Girke, T., Ruuska, S., Mekhedov, S. and Benning, C. (2000). Fatty acid synthesis: from CO2 to functional genomics. *Biochem Soc Trans* **28**, 567-73.

Olliaro, P. L. and Yuthavong, Y. (1999). An overview of chemotherapeutic targets for antimalarial drug discovery. *Pharmacol Ther* **81**, 91-110.

Pace, T., Birago, C., Janse, C. J., Picci, L. and Ponzi, M. (1998). Developmental regulation of a *Plasmodium* gene involves the generation of stage-specific 5' untranslated sequences. *Mol Biochem Parasitol* **97**, 45-53.

Palacpac, N. M., Hiramine, Y., Mi-ichi, F., Torii, M., Kita, K., Hiramatsu, R., Horii, T. and Mitamura, T. (2004). Developmental-stage-specific triacylglycerol biosynthesis, degradation and trafficking as lipid bodies in *Plasmodium falciparum*-infected erythrocytes. *J Cell Sci* **117**, 1469-80.

Pan, D. A. and Hardie, D. G. (2002). A homologue of AMP-activated protein kinase in Drosophila melanogaster is sensitive to AMP and is activated by ATP depletion. *Biochem J* **367**, 179-86.

Pandey, A. V., Tekwani, B. L., Singh, R. L. and Chauhan, V. S. (1999). Artemisinin, an endoperoxide antimalarial, disrupts the hemoglobin catabolism and heme detoxification systems in malarial parasite. *J Biol Chem* **274**, 19383-8.

Pandey, K. C., Singh, N., Arastu-Kapur, S., Bogyo, M. and Rosenthal, P. J. (2006). Falstatin, a cysteine protease inhibitor of *Plasmodium falciparum*, facilitates erythrocyte invasion. *PLoS Pathog* **2**, e117.

Paula Simões, A., Fiebig, S., Wunderlich, F., Vial, H., Roelofsen, B. and Op den Kamp, J. A. F. (1993). *Plasmodium chabaudi*-parasitized erythrocytes: phosphatidylcholine species of parasites and host cell membranes. *Mol Biochem Parasitol* **57**, 345-348.

Pearson, P. (1972). The use of new staining techniques for human chromosome identification. *J Med Genet* **9**, 264-75.

Pélle, R. and Murphy, N. B. (1993). Northern hybridization: rapid and simple electrophoretic conditions. *Nucleic Acids Res* **21**, 2783-4.

Perozzo, R., Kuo, M., Sidhu, A. S., Valiyaveettil, J. T., Bittman, R., Jacobs, W. R., Jr., Fidock, D. A. and Sacchettini, J. C. (2002). Structural elucidation of the specificity of the antibacterial agent triclosan for malarial enoyl acyl carrier protein reductase. *J Biol Chem* **277**, 13106-14.

pET-28a-c(+) and Vectors. (1998). Novagen TB074/98.

Peters, W. (1974). Recent advances in antimalaria chemotherapy and drug resistance. In *Advances in Parasitology*, vol. 12 (ed. B. Dawes), pp. 69-106. London: Academic Press.

Peters, W. (1998). Drug resistance in malaria. In *Advances in Parasitology*, vol. 41 (ed. J. Baker and R. Muller), pp. 1-62. San Diego: Academic Press.

Piskur, J. (2001). Origin of the duplicated regions in the yeast genomes. *Trends in Genetics* **17**, 302-303.

Polson, A., Coetzer, T., Kruger, J., von Maltzahn, E. and van der Merwe, K. J. (1985). Improvements in the isolation of IgY from the yolks of eggs laid by immunized hens. *Immunol Invest* **14**, 323-7.

Polyak, S. W., Chapman-Smith, A., Mulhern, T. D., Cronan, J. E., Jr. and Wallace, J. C. (2001). Mutational analysis of protein substrate presentation in the post-translational attachment of biotin to biotin domains. *J Biol Chem* **276**, 3037-45.

Porter, M. E. (2001). The DNA polymerase delta promoter from *Plasmodium falciparum* contains an unusually long 5' untranslated region and intrinsic DNA curvature. *Mol Biochem Parasitol* **114**, 249-55.

Prigge, S. T., He, X., Gerena, L., Waters, N. C. and Reynolds, K. A. (2003). The initiating steps of a type II fatty acid synthase in *Plasmodium falciparum* are catalyzed by pfACP, pfMCAT, and pfKASIII. *Biochemistry* **42**, 1160-9.

Ralph, S. A., Foth, B. J., Hall, N. and McFadden, G. I. (2004a). Evolutionary pressures on apicoplast transit peptides. *Mol Biol Evol* **21**, 2183-94.

Ralph, S. A., van Dooren, G. G., Waller, R. F., Crawford, M. J., Fraunholz, M. J., Foth, B. J., Tonkin, C. J., Roos, D. S. and McFadden, G. I. (2004b). Tropical infectious diseases: metabolic maps and functions of the Plasmodium falciparum apicoplast. *Nat Rev Microbiol* **2**, 203-16.

Ramakrishnan, C. and Ramachandran, G. N. (1965). Stereochemical Criteria for Polypeptide and Protein Chain Conformations: II. Allowed Conformations for a Pair of Peptide Units. *Biophysical Journal* **5**, 909-933.

Reche, P., Li, Y. L., Fuller, C., Eichhorn, K. and Perham, R. N. (1998). Selectivity of post-translational modification in biotinylated proteins: the carboxy carrier protein of the acetyl-CoA carboxylase of *Escherichia coli*. *Biochem J* **329 (Pt 3)**, 589-96.

Reche, P. and Perham, R. N. (1999). Structure and selectivity in post-translational modification: attaching the biotinyl-lysine and lipoyl-lysine swinging arms in multifunctional enzymes. *Embo J* **18**, 2673-82.

Reche, P. A. (2000). Lipoylating and biotinylating enzymes contain a homologous catalytic module. *Protein Sci* **9**, 1922-9.

Reddy, D. V., Shenoy, B. C., Carey, P. R. and Sonnichsen, F. D. (2000). High Resolution Solution Structure of the 1.3S Subunit of Transcarboxylase from *Propionibacterium shermanii*. *Biochemistry* **39**, 2509-2516.

Ridley, R. G. (2002). Chemotherapeutic hope on the horizon for *Plasmodium vivax* malaria? *Proc Natl Acad Sci U S A* **99**, 13362-4.

Rietveld, A. and Kouznetsov, R. (1997). Epidemiology of human malaria. In *Handbook of malaria infection in the tropics*, vol. 15 (ed. G. Carosi and F. Castelli), pp. 39-52. Bologna: Associazione Italiana "Amici di R. Follereau" Organizzazione per la Cooperazione Sanitaria Internazionale.

Roberts, E. L., Shu, N., Howard, M. J., Broadhurst, R. W., Chapman-Smith, A., Wallace, J. C., Morris, T., Cronan, J. E., Jr. and Perham, R. N. (1999). Solution structures of apo and holo biotinyl domains from acetyl coenzyme A carboxylase of *Escherichia coli* determined by triple-resonance nuclear magnetic resonance spectroscopy. *Biochemistry* **38**, 5045-53.

Rodrigues, M. H., Cunha, M. G., Machado, R. L., Ferreira, O. C., Jr., Rodrigues, M. M. and Soares, I. S. (2003). Serological detection of *Plasmodium vivax* malaria using recombinant proteins corresponding to the 19-kDa C-terminal region of the merozoite surface protein-1. *Malar J* **2**, 39.

RSA, N. D. o. H. (2004). Guidelines for the prevention of malaria in South Africa, (ed. Health): National Department of Health

Ryall, K., Harper, J. T. and Keeling, P. J. (2003). Plastid-derived Type II fatty acid biosynthetic enzymes in chromists. *Gene* **313**, 139-48.

Sachs, J. and Malaney, P. (2002). The economic and social burden of malaria. *Nature* **415**, 680-5.

Sachs, J. D. (2002). A new global effort to control malaria. *Science* **298**, 122-4.

Sambrook, J., Fritsch, E. F., and Maniatis, T. (1989a). Enzymes used in molecular cloning. In *Molecular cloning: A laboratory manual* vol. 1 (ed. C. Nolan), pp. 5.3 - 5.90. New York: Cold Spring Harbor Laboratory Press

Sambrook, J., Fritsch, E. F., and Maniatis, T. (1989b). Plasmid vectors. In *Molecular cloning: A laboratory manual*, vol. 1 (ed. C. Nolan), pp. 1.3 - 1.105. New York: Cold Spring Harbor Laboratory Press.

Sanni, L., Fonseca, L. and Langhorne, J. (2002). Mouse Models for Erythrocytic-Stage Malaria. In *Malaria Methods and Protocols*, (ed. D. Doolan), pp. 57-76. New Jersey: Humana Press

Sasaki, Y., Hakamada, K., Suama, Y., Nagano, Y., Furusawa, I. and Matsuno, R. (1993). Chloroplast-encoded protein as a subunit of acetyl-CoA carboxylase in pea plant. *J Biol Chem* **268**, 25118-23.

Sasaki, Y. and Nagano, Y. (2004). Plant acetyl-CoA carboxylase: structure, biosynthesis, regulation, and gene manipulation for plant breeding. *Biosci Biotechnol Biochem* **68**, 1175-84.

Schwede, T., Diemand, A., Guex, N. and Peitsch, M. C. (2000). Protein structure computing in the genomic era. *Res Microbiol* **151**, 107-12.

Schwede, T., Kopp, J., Guex, N. and Peitsch, M. C. (2003). SWISS-MODEL: An automated protein homology-modeling server. *Nucleic Acids Res* **31**, 3381-5.

Sharma, S. K., Kapoor, M., Ramya, T. N., Kumar, S., Kumar, G., Modak, R., Sharma, S., Surolia, N. and Surolia, A. (2003). Identification, characterization, and inhibition of *Plasmodium falciparum* beta-hydroxyacyl-acyl carrier protein dehydratase (FabZ). *J Biol Chem* **278**, 45661-71.

Shen, Y., Volrath, S. L., Weatherly, S. C., Elich, T. D. and Tong, L. (2004). A mechanism for the potent inhibition of eukaryotic acetyl-coenzyme A carboxylase by soraphen A, a macrocyclic polyketide natural product. *Mol Cell* **16**, 881-91.

Sherman, I. W. (1979). Biochemistry of Plasmodium (malarial parasites). *Microbiol Rev* **43**, 453-95.

Shirra, M. K., Patton-Vogt, J., Ulrich, A., Liuta-Tehlivets, O., Kohlwein, S. D., Henry, S. A. and Arndt, K. M. (2001). Inhibition of acetyl coenzyme A carboxylase activity restores expression of the INO1 gene in a snf1 mutant strain of *Saccharomyces cerevisiae*. *Mol Cell Biol* **21**, 5710-22.

Siau, A., Touré, F. S., Ouwe-Missi-Oukem-Boyer, O., Ciceron, L., Mahmoudi, N., Vaquero, C., Froissard, P., Bisvigou, U., Bisser, S., Coppee, J. Y. *et al*. (2007). Whole-transcriptome analysis of Plasmodium falciparum field isolates: identification of new pathogenicity factors. *J Infect Dis* **196**, 1603-12.

Sigrist, C. J., Cerutti, L., Hulo, N., Gattiker, A., Falquet, L., Pagni, M., Bairoch, A. and Bucher, P. (2002). PROSITE: a documented database using patterns and profiles as motif descriptors. *Brief Bioinform* **3**, 265-74.

Simões, A. P., Moll, G. N., Beaumelle, B., Vial, H. J., Roelofsen, B. and Op den Kamp, J. A. F. (1990). *Plasmodium knowlesi* induces alterations in phosphatidylcholine and phosphatidylethanolamine molecular species composition of parasitized monkey erythrocytes. *Biochimica et Biophysica Acta (BBA) - Biomembranes* **1022**, 135-145.

Singh, N., Chévë, G., Avery, M. A. and McCurdy, C. R. (2006). Comparative protein modeling of 1-deoxy-D-xylulose-5-phosphate reductoisomerase enzyme from *Plasmodium falciparum*: a potential target for antimalarial drug discovery. *J Chem Inf Model* **46**, 1360-70.

Solbiati, J., Chapman-Smith, A. and Cronan, J. E., Jr. (2002). Stabilization of the biotinoyl domain of *Escherichia coli* acetyl-CoA carboxylase by interactions between the attached biotin and the protruding "thumb" structure. *J Biol Chem* **277**, 21604-9.

Song, C. S. and Kim, K. H. (1981). Reevaluation of properties of acetyl-CoA carboxylase from rat liver. *J Biol Chem* **256**, 7786-8.

Songyang, Z., Blechner, S., Hoagland, N., Hoekstra, M. F., Piwnica-Worms, H. and Cantley, L. C. (1994). Use of an oriented peptide library to determine the optimal substrates of protein kinases. *Current Biology* **4**, 973-982.

Sorensen, H. P. and Mortensen, K. K. (2005a). Advanced genetic strategies for recombinant protein expression in Escherichia coli. *J Biotechnol* **115**, 113-28.

Sorensen, H. P. and Mortensen, K. K. (2005b). Soluble expression of recombinant proteins in the cytoplasm of Escherichia coli. *Microb Cell Fact* **4**, 1.

Stapleton, M. A., Javid-Majd, F., Harmon, M. F., Hanks, B. A., Grahmann, J. L., Mullins, L. S. and Raushel, F. M. (1996). Role of conserved residues within the carboxy phosphate domain of carbamoyl phosphate synthetase. *Biochemistry* **35**, 14352-61.

Streaker, E. D. and Beckett, D. (1999). Ligand-linked structural changes in the *Escherichia coli* biotin repressor: the significance of surface loops for binding and allostery. *J Mol Biol* **292**, 619-32.

Streaker, E. D. and Beckett, D. (2006). Nonenzymatic biotinylation of a biotin carboxyl carrier protein: unusual reactivity of the physiological target lysine. *Protein Sci* **15**, 1928-35.

Suguna, K., Surolia, A. and Surolia, N. (2001). Structural basis for triclosan and NAD binding to enoyl-ACP reductase of *Plasmodium falciparum*. *Biochem Biophys Res Commun* **283**, 224-8.

Surolia, A., Ramya, T. N., Ramya, V. and Surolia, N. (2004). 'FAS't inhibition of malaria. *Biochem J* **383**, 401-12.

Surolia, N. and Surolia, A. (2001). Triclosan offers protection against blood stages of malaria by inhibiting enoyl-ACP reductase of *Plasmodium falciparum*. *Nat Med* **7**, 167-73.

Tebele, N., Skilton, R. A., Katende, J., Wells, C. W., Nene, V., McElwain, T., Morzaria, S. P. and Musoke, A. J. (2000). Cloning, characterization, and expression of a 200-kilodalton diagnostic antigen of *Babesia bigemina*. *J Clin Microbiol* **38**, 2240-7.

Teklehaimanot, A., Sachs, J. D. and Curtis, C. (2007). Malaria control needs mass distribution of insecticidal bednets. *Lancet* **369**, 2143-6.

Tham, W. H., Payne, P. D., Brown, G. V. and Rogerson, S. J. (2007). Identification of basic transcriptional elements required for rif gene transcription. *Int J Parasitol* **37**, 605-15.

Thampy, K. G. (1989). Formation of malonyl coenzyme A in rat heart. Identification and purification of an isozyme of A carboxylase from rat heart. *J Biol Chem* **264**, 17631-4.

Thampy, K. G. and Wakil, S. J. (1988a). Regulation of acetyl-coenzyme A carboxylase. I. Purification and properties of two forms of acetyl-coenzyme A carboxylase from rat liver. *J Biol Chem* **263**, 6447-53.

Thampy, K. G. and Wakil, S. J. (1988b). Regulation of acetyl-coenzyme A carboxylase. II. Effect of fasting and refeeding on the activity, phosphate content, and aggregation state of the enzyme. *J Biol Chem* **263**, 6454-8.

Thelen, J. J., Mekhedov, S. and Ohlrogge, J. B. (2001). *Brassicaceae* express multiple isoforms of biotin carboxyl carrier protein in a tissue-specific manner. *Plant Physiol* **125**, 2016-28.

Thompson, J. D., Higgins, D. G. and Gibson, T. J. (1994). CLUSTAL W: improving the sensitivity of progressive multiple sequence alignment through sequence weighting, position-specific gap penalties and weight matrix choice. *Nucleic Acids Res* **22**, 4673-80.

Thorpe, G. H., Kricka, L. J., Moseley, S. B. and Whitehead, T. P. (1985). Phenols as enhancers of the chemiluminescent horseradish peroxidase-luminol-hydrogen peroxide reaction: application in luminescence-monitored enzyme immunoassays. *Clin Chem* **31**, 1335-41.

Tomar, D., Biswas, S., Tripathi, V. and Rao, D. N. (2006). Development of diagnostic reagents: raising antibodies against synthetic peptides of PfHRP-2 and LDH using microsphere delivery. *Immunobiology* **211**, 797-805.

Tong, L. and Harwood, H. J., Jr. (2006). Acetyl-coenzyme A carboxylases: versatile targets for drug discovery. *J Cell Biochem* **99**, 1476-88.

Towbin, H., Staehelin, T. and Gordon, J. (1979). Electrophoretic transfer of proteins from polyacrylamide gels to nitrocellulose sheets: procedure and some applications. *Proc Natl Acad Sci U S A* **76**, 4350-4.

Turgut-Balik, D., Akbulut, E., Shoemark, D. K., Celik, V., Moreton, K. M., Sessions, R. B., Holbrook, J. J. and Brady, R. L. (2004). Cloning, sequence and expression of the lactate dehydrogenase gene from the human malaria parasite, *Plasmodium vivax*. *Biotechnol Lett* **26**, 1051-5.

Ullrich, T. C., Blaesse, M. and Huber, R. (2001). Crystal structure of ATP sulfurylase from *Saccharomyces cerevisiae*, a key enzyme in sulfate activation. *Embo J* **20**, 316-29.

Urakawa, T. and Majiwa, P. A. (2001). Physical and transcriptional organization of the ribosomal RNA genes of the savannah-type *Trypanosoma congolense*. *Parasitol Res* **87**, 431-8.

Van den Ende, J. and Van Gompel, A. (1997). Clinical aspects of malaria. In *Handbook of malaria infection in the tropics* vol. 15 (ed. G. Carosi and F. Castelli), pp. 79-96. Bologna: Organizzazione per la Cooperazione Sanitaria Internazionale.

Van der Schaft, P. H., Beaumelle, B., Vial, H., Roelofsen, B., Op den Kamp, J. A. and Van Deenen, L. L. (1987). Phospholipid organization in monkey erythrocytes upon Plasmodium knowlesi infection. *Biochim Biophys Acta* **901**, 1-14.

van Gunsteren, W. and Billetter, S. (1996). Biomolecular Simulations: The GROMOS96 Manual and User Guide. Zurich: VdF Hochschulverlag ETHZ.

van Spaendonk, R. M., Ramesar, J., van Wigcheren, A., Eling, W., Beetsma, A. L., van Gemert, G. J., Hooghof, J., Janse, C. J. and Waters, A. P. (2001). Functional equivalence of structurally distinct ribosomes in the malaria parasite, *Plasmodium berghei*. *J Biol Chem* **276**, 22638-47.

Vial, H. J., Ancelin, M. L., Thuet, M. J. and Philippot, J. R. (1988). Differential effects of chloroquine on the phospholipid metabolism of *Plasmodium*-infected erythrocytes. *Biochem Pharmacol* **37**, 3139-47.

Vial, H. J., Philippot, J. R. and Wallach, D. F. (1984). A reevaluation of the status of cholesterol in erythrocytes infected by *Plasmodium knowlesi* and *P. falciparum*. *Mol Biochem Parasitol* **13**, 53-65.

Voss, T. (2002). Extraction and purification of *Plasmodium* total RNA. In *Malaria methods and protocols*, (ed. D. L. Doolan), pp. 151 - 157 New Jersey: Humana Press.

Wainwright, M. and Amaral, L. (2005). The phenothiazinium chromophore and the evolution of antimalarial drugs. *Trop Med Int Health* **10**, 501-11.

Wakil, S. J., Stoops, J. K. and Joshi, V. C. (1983). Fatty acid synthesis and its regulation. *Annu Rev Biochem* **52**, 537-79.

Walbot, V. (2000). *Arabidopsis thaliana* genome. A green chapter in the book of life. *Nature* **408**, 794-5.

Waldrop, G. L., Rayment, I. and Holden, H. M. (1994). Three-dimensional structure of the biotin carboxylase subunit of acetyl-CoA carboxylase. *Biochemistry* **33**, 10249-56.

Waller, R. F., Ralph, S. A., Reed, M. B., Su, V., Douglas, J. D., Minnikin, D. E., Cowman, A. F., Besra, G. S. and McFadden, G. I. (2003). A type II pathway for fatty acid biosynthesis presents drug targets in Plasmodium falciparum. *Antimicrob Agents Chemother* **47**, 297-301.

Waller, R. F., Reed, M. B., Cowman, A. F. and McFadden, G. I. (2000). Protein trafficking to the plastid of *Plasmodium falciparum* via the secretory pathway. *Embo J* **19**, 1794-1802.

Wang, L., Webster, D. E., Campbell, A. E., Dry, I. B., Wesselingh, S. L. and Coppel, R. L. (2008). Immunogenicity of *Plasmodium yoelii* merozoite surface protein 4/5 produced in transgenic plants. *Int J Parasitol* **38**, 103-10.

Watanabe, J., Sasaki, M., Suzuki, Y. and Sugano, S. (2002). Analysis of transcriptomes of human malaria parasite *Plasmodium falciparum* using full-length enriched library: identification of novel genes and diverse transcription start sites of messenger RNAs. *Gene* **291**, 105-13.

Weatherly, S. C., Volrath, S. L. and Elich, T. D. (2004). Expression and characterization of recombinant fungal acetyl-CoA carboxylase and isolation of a soraphen-binding domain. *Biochem J* **380**, 105-10.

Welling, G. W. and Fries, H. (1985). Choice of peptide and peptide length for the generation of antibodies reactive with the intact protein. *FEBS Lett* **182**, 81-4.

Welling, G. W., Weijer, W. J., van der Zee, R. and Welling-Wester, S. (1985). Prediction of sequential antigenic regions in proteins. *FEBS Lett* **188**, 215-8.

Wells, G. A., Birkholtz, L. M., Joubert, F., Walter, R. D. and Louw, A. I. (2006). Novel properties of malarial S-adenosylmethionine decarboxylase as revealed by structural modelling. *J Mol Graph Model* **24**, 307-18.

White, N. J. (1992). Pathophysiology of malaria. In *Advances in Parasitology*, vol. 31 (ed. J. Baker and S. Muller), pp. 83-173. London: Academic Press.

White, N. J. (2004). Antimalarial drug resistance. *J Clin Invest* **113**, 1084-92.

White, N. J., Nosten, F., Looareesuwan, S., Watkins, W. M., Marsh, K., Snow, R. W., Kokwaro, G., Ouma, J., Hien, T. T., Molyneux, M. E. *et al*. (1999). Averting a malaria disaster. *Lancet* **353**, 1965-7.

WHO. (2003). The Africa malaria report, (ed.: World Health Organization/UNICEF.

WHO. (2005a). Rolling Back malaria; The World Bank Global Strategy and Booster Program, (ed.

WHO. (2005b). World Malaria Report, (ed.: World Health Organzation, UNICEF.

Wilson, R. J. (2002). Progress with parasite plastids. *J Mol Biol* **319**, 257-74.

Winter, V. J., Cameron, A., Tranter, R., Sessions, R. B. and Brady, R. L. (2003). Crystal structure of *Plasmodium berghei* lactate dehydrogenase indicates the unique structural differences of these enzymes are shared across the *Plasmodium* genus. *Mol Biochem Parasitol* **131**, 1-10.

Withers-Martinez, C., Carpenter, E. P., Hackett, F., Ely, B., Sajid, M., Grainger, M. and Blackman, M. J. (1999). PCR-based gene synthesis as an efficient approach for expression of the A+T-rich malaria genome. *Protein Eng* **12**, 1113-20.

Wolf, B. (2005). Biotinidase: its role in biotinidase deficiency and biotin metabolism. *J Nutr Biochem* **16**, 441-445.

Yadava, A. and Ockenhouse, C. F. (2003). Effect of codon optimization on expression levels of a functionally folded malaria vaccine candidate in prokaryotic and eukaryotic expression systems. *Infect Immun* **71**, 4961-9.

Yang, A. S. and Honig, B. (2000a). An integrated approach to the analysis and modeling of protein sequences and structures. II. On the relationship between sequence and structural similarity for proteins that are not obviously related in sequence. *J Mol Biol* **301**, 679-89.

Yang, A. S. and Honig, B. (2000b). An integrated approach to the analysis and modeling of protein sequences and structures. III. A comparative study of sequence conservation in protein structural families using multiple structural alignments. *J Mol Biol* **301**, 691-711.

Yao, X., Soden, C., Jr., Summers, M. F. and Beckett, D. (1999). Comparison of the backbone dynamics of the apo- and holo-carboxy-terminal domain of the biotin carboxyl carrier subunit of *Escherichia coli* acetyl-CoA carboxylase. *Protein Sci* **8**, 307-17.

Yu, Z., Lansdon, E. B., Segel, I. H. and Fisher, A. J. (2007). Crystal Structure of the Bifunctional ATP Sulfurylase - APS kinase from the Chemolithotrophic Thermophile Aquifex aeolicus. *J Mol Biol* **365**, 732-743.

Zhang, H., Tweel, B. and Tong, L. (2004). Molecular basis for the inhibition of the carboxyltransferase domain of acetyl-coenzyme-A carboxylase by haloxyfop and diclofop. *Proc Natl Acad Sci U S A* **101**, 5910-5.

Zhang, H., Yang, Z., Shen, Y. and Tong, L. (2003). Crystal structure of the carboxyltransferase domain of acetyl-coenzyme A carboxylase. *Science* **299**, 2064-7.

Zhou, Z., Schnake, P., Xiao, L. and Lal, A. A. (2004). Enhanced expression of a recombinant malaria candidate vaccine in *Escherichia coli* by codon optimization. *Protein Expr Purif* **34**, 87-94.

Zhu, G. (2004). Current progress in the fatty acid metabolism in Cryptosporidium parvum. *J Eukaryot Microbiol* **51**, 381-8.

Zhu, G., Li, Y., Cai, X., Millership, J. J., Marchewka, M. J. and Keithly, J. S. (2004). Expression and functional characterization of a giant Type I fatty acid synthase (CpFAS1) gene from Cryptosporidium parvum. *Mol Biochem Parasitol* **134**, 127-35.

Zhu, G., Marchewka, M. J., Woods, K. M., Upton, S. J. and Keithly, J. S. (2000). Molecular analysis of a Type I fatty acid synthase in Cryptosporidium parvum. *Mol Biochem Parasitol* **105**, 253-60.

Zuegge, J., Ralph, S., Schmuker, M., McFadden, G. I. and Schneider, G. (2001). Deciphering apicoplast targeting signals-feature extraction from nuclear-encoded precursors of *Plasmodium falciparum* apicoplast proteins. *Gene* **280**, 19-26.

Zuther, E., Johnson, J. J., Haselkorn, R., McLeod, R. and Gornicki, P. (1999). Growth of Toxoplasma gondii is inhibited by aryloxyphenoxypropionate herbicides targeting acetyl-CoA carboxylase. *Proc Natl Acad Sci U S A* **96**, 13387-92.